National Library of Canada
Acquisitions and Bibliographic Services Branch
395 Wellington Street
Ottawa, Ontario
K1A 0N4

Bibliothèque nationale du Canada
Direction des acquisitions et des services bibliographiques
395, rue Wellington
Ottawa (Ontario)
K1A 0N4

Your file Votre référence

Our file Notre référence

NOTICE

The quality of this microform is heavily dependent upon the quality of the original thesis submitted for microfilming. Every effort has been made to ensure the highest quality of reproduction possible.

If pages are missing, contact the university which granted the degree.

Some pages may have indistinct print especially if the original pages were typed with a poor typewriter ribbon or if the university sent us an inferior photocopy.

Reproduction in full or in part of this microform is governed by the Canadian Copyright Act, R.S.C. 1970, c. C-30, and subsequent amendments.

AVIS

La qualité de cette microforme dépend grandement de la qualité de la thèse soumise au microfilmage. Nous avons tout fait pour assurer une qualité supérieure de reproduction.

S'il manque des pages, veuillez communiquer avec l'université qui a conféré le grade.

La qualité d'impression de certaines pages peut laisser à désirer, surtout si les pages originales ont été dactylographiées à l'aide d'un ruban usé ou si l'université nous a fait parvenir une photocopie de qualité inférieure.

La reproduction, même partielle, de cette microforme est soumise à la Loi canadienne sur le droit d'auteur, SRC 1970, c. C-30, et ses amendements subséquents.

Canada

National Library of Canada
Acquisitions and Bibliographic Services Branch
395 Wellington Street
Ottawa, Ontario
K1A 0N4

Bibliothèque nationale du Canada
Direction des acquisitions et des services bibliographiques
395, rue Wellington
Ottawa (Ontario)
K1A 0N4

Your file Votre référence

Our file Notre référence

THE AUTHOR HAS GRANTED AN IRREVOCABLE NON-EXCLUSIVE LICENCE ALLOWING THE NATIONAL LIBRARY OF CANADA TO REPRODUCE, LOAN, DISTRIBUTE OR SELL COPIES OF HIS/HER THESIS BY ANY MEANS AND IN ANY FORM OR FORMAT, MAKING THIS THESIS AVAILABLE TO INTERESTED PERSONS.

L'AUTEUR A ACCORDE UNE LICENCE IRREVOCABLE ET NON EXCLUSIVE PERMETTANT A LA BIBLIOTHEQUE NATIONALE DU CANADA DE REPRODUIRE, PRETER, DISTRIBUER OU VENDRE DES COPIES DE SA THESE DE QUELQUE MANIERE ET SOUS QUELQUE FORME QUE CE SOIT POUR METTRE DES EXEMPLAIRES DE CETTE THESE A LA DISPOSITION DES PERSONNE INTERESSEES.

THE AUTHOR RETAINS OWNERSHIP OF THE COPYRIGHT IN HIS/HER THESIS. NEITHER THE THESIS NOR SUBSTANTIAL EXTRACTS FROM IT MAY BE PRINTED OR OTHERWISE REPRODUCED WITHOUT HIS/HER PERMISSION.

L'AUTEUR CONSERVE LA PROPRIETE DU DROIT D'AUTEUR QUI PROTEGE SA THESE. NI LA THESE NI DES EXTRAITS SUBSTANTIELS DE CELLE-CI NE DOIVENT ETRE IMPRIMES OU AUTREMENT REPRODUITS SANS SON AUTORISATION.

ISBN 0-315-95969-X

Canada

UNIVERSITÉ D'OTTAWA
UNIVERSITY OF OTTAWA

TO MY FATHER YOU HAOZHANG

献给我的父親游豪章

PREFACE

The present manuscript consists of five chapters which deal with complementary aspects of the kinetics and mechanisms of anodic bromine formation and the role of adsorbed species in the reaction. Descriptions of new experimental results obtained in the course of the research, and their theoretical interpretation and discussion, form an important part of the work.

Chapter 1 provides an introduction which presents an overview of previous works, and the importance of the bromide/bromine system in various applications. Chapter 2 presents the objectives of the present work. Chapter 3 covers experimental aspects of the work, including the electrochemical systems and the measurement techniques employed. In chapter 4, the theoretical approaches employed in interpretation of results are outlined and cover topics such as the thermodynamics and kinetics of the reaction. Chapter 5 describes and discusses results based on voltammograms, Tafel relations, potential-decay relations, and the experimental and simulated a.c. impedance behaviour.

Part of the work in this dissertation was presented at an international symposium in Honolulu, Hawaii, USA in May, 1993 (organized by the American Electrochemical Society, and co-sponsored by the Japanese Electrochemical Society). The title

of the paper was: Kinetics and Mechanisms of the Anodic Bromine Formation Reaction. A principal paper on the research has been submitted for publication in J. Chem. Soc., Faraday Trans., as follows,

1. B.E. Conway and Youyu Phillips, The Surface Electrochemistry and Kinetics of Anodic Br_2 Formation at Pt.

Other papers in preparation for publications are:

2. Youyu Phillips, B.E Conway and Shiyuan Qian, Equivalent Circuits of the A.C. Impedance Spectroscopy for the Simulation of Behaviours of Adsorbed Intermediates in the Anodic Br_2 Formation Reaction.
3. Youyu Phillips and B.E. Conway, Theoretical Approaches for Study of the Kinetics and Mechanism of Electrochemical Radical Recombination-type Reactions Exemplified by the Anodic Bromine Formation Reaction.

ACKNOWLEDGEMENTS

I am greatly indebted to the world-leading electrochemist, Dr. Brian E. Conway, who supervised this research project, offered enlightened guidance and provided stimulating suggestions and criticisms. I feel truly honoured to have worked under such a devoted researcher and professor; his dedication will undoubtably benefit my future research and teaching.

I also wish to thank my colleagues, especially Mr. Shiyuan Qian and Dr. Lijun Bai for their invaluable assistance with experimental techniques. Thanks are also due to many other staff in the Department, particularly Mr. Egon Kristoff for his skillful glassblowing work on the electrodes and cells.

Special gratitude is due for my husband, Mr. Andrew Phillips, for his understanding and encouragement during the course of the work.

I would also like to express gratitude to my parents, brothers and in-laws for their unfailing support. Finally, I want to thank Ms. Susan Lee for her help in the editing of this dissertation.

Youyu Phillips

INDEX OF CONTENTS

CHAPTER 4
ELECTROCHEMICAL KINETICS AND THE ROLE OF ADSORBED INTERMEDIATES

CHAPTER 5
RESULTS AND DISCUSSION

LIST OF FIGURES

LIST OF TABLES

LIST OF ABBREVIATIONS AND SYMBOLS

SERS	Surface Enhanced Raman Spectroscopy
a.p.c.	anodic polarization curve
r.d.s.	rate-determining reaction step
CV	Cyclic Voltammetry
WE	Working Electrode
ER	Electroreflectance
i	current density (A cm^{-2})
AUX	Auxiliary Electrode
RDE	Rotating Disc Electrode
RHE	Reversible Hydrogen Electrode
NHE	Normal Hydrogen Electrode
b	coefficient in Tafel relationship
C	Concentration
C	Coulomb
E	Electrode Potential
F	Faraday
SCE	Saturated Calomel Electrode
NCE	Normal Calomel Electrode
q	electron charge density (μC cm^{-2})
θ	Fractional Surface Coverage
Δ	Ellipsometric Phase Shift
χ	Ellipsometric Amplitude

RPE	Rotating Platinum Electrode
ob	observed
R_1	Faradaic Charge Transfer Resistance
R_s	Solution Resistance
R_u	Uncompensated Solution Resistance
σ	Charge density
a_i^b	Activity of substance i in bulk solution
C_ϕ	Adsorption pseudocapacity
CPA	Constant Phase Angle
TFA	Trifluoroacetic Acid
GCS	Gouy-Chapman-Stern
IP	Ionization Potential
WE	Working Electrode
CE	Counter Electrode
RE	Reference Electrode
TEAB	Tetraethylammonium Bromide
g	interaction parameter in isotherms
η	Overpotential
DSA	Dimensionally Stable Anode
UPD	Underpotential Deposition
IP's	Ionization Potentials
h.e.r.	Hydrogen evolution reaction
i_0	Exchange Current Density
C_{dl}	Double Layer Capacitance
Γ	Gibbs Surface Excess Function
ϵ	Complex Dielectric Constant

ABSTRACT

Batteries are the most practical and, historically, the earliest applications of electrochemistry. The zinc/bromine flow battery (in aqueous or nonaqueous embodiments) has received considerable attention in recent years as a durable, rechargeable storage device for applications such as vehicle propulsion and levelling of peak electricity usage. It is therefore important to understand the kinetics and mechanisms of the anodic and cathodic reactions of the bromine/bromide couple. Among the halide/halogen systems, the electrochemical kinetics and mechanisms of the bromide/bromine system have particular interest since this couple sometimes behaves like the chloride/chlorine couple while at other times like the iodide/iodine system. The effect of adsorbed halide ions at solid electrodes such as chloride adsorption at Pt has been the subject of a number of investigations.

In the present research, new experimental results on the role of adsorbed bromide ion in the kinetics of anodic Br_2 formation at platinum electrodes, using mainly electrochemical measurements, are reported. The anodic peak currents in cyclic voltammetry associated with the processes of surface oxidation of Pt and bromine formation, during an anodic sweep, decrease as the concentration of bromide in solution increases (NaBr or HBr

in 0.1 M aqueous perchloric acid solution, cobalt bromide or R_4NBr where R is CH_3, C_2H_5, C_3H_7 in nonaqueous acetonitrile). This is due to competitive adsorption between adsorbed Br and electrodeposited OH or O species at platinum.

Changes in rotation rate of a Pt rotating disc electrode in Tafel polarization experiments have little influence on the limiting currents that are observed in the Tafel plots; such currents are therefore due to activation-controlled recombination of discharged $Br^{\cdot}$. Rotation does, however, eliminate some residual diffusion effect compared with the behaviour in the complete absence of rotation.

The results from potential relaxation and a.c. impedance measurements indicate that an adsorption process is involved. For most cases, the theoretically appropriate mechanisms involving a three-step process for bromide ion adsorption, $Br^{\cdot}$ electrosorption and adsorbed $Br^{\cdot}$ combination are introduced and their applicability to the observed kinetics tested.

Most experimental a.c. impedance complex-plane plots are in the form of two semicircles, showing that the anodic Br_2 formation reaction is a two-step process involving $Br^{\cdot}$ adsorption and $Br^{\cdot}$ combination. However, some experimental complex-plane plots exhibit three semicircles which can be related to participation of the tribromide ion in the process; this suggests more complicated kinetics and mechanisms. Two alternative new equivalent circuits are proposed for the purpose of simulation of the frequency-response behaviour involving the

role of Br_3^-/Br^- adsorption, leading to the three semicircles in complex-plane plots.

The anodic bromine formation reaction is found to depend on the concentration of the bromide solution, the type of electrode and, certainly, the applied electrode potential, as expected. Correspondingly, the type of information obtained depends on the electrochemical measurement techniques employed; several complementary ones have been used in the present work, as will be explained in chapter 3.

The idea that "bromide" adsorption involves both adsorbed $Br^{\cdot}$ and $Br_3^{\cdot}$ intermediates, as well as Br^- and Br_3^- ions, provides a fuller basis for the understanding of the anodic formation reaction of Br_2 than has hitherto been given, and of the mechanisms and kinetics of the reaction that obtain in more concentrated Br^- solutions after elemental Br_2 has been generated at the electrode surface following significant passage of anodic charge. This introduction of the role of tribromide species is required because of the known appreciable stability of the tribromide ion. The results of the present research by electrochemical methods provide qualitative and quantitative evidence for these suggestions.

Chapter 1. INTRODUCTION

1.1. Significance of the Br^-/Br_2 Reaction

1.1.1. Introduction

Electrode processes are chemical reactions at the metal-electrolyte (solution or ionic melt) interface accompanied by the transfer of electric charge between the phases in contact.

The pioneer work of Nicholson (1800), Faraday (1833), and later Kohlrausch and others on the phenomena of electrolysis, led to some of the first studies of electrode processes during the nineteenth century, together with the research of Tafel (1905) in the early twentieth.

During the past four decades, the dynamics and mechanisms of electron-transfer processes have been studied extensively by numerous groups and new advances made. Such research has been made possible by the development of new experimental techniques employing modern instrumentation, complemented by application of transition-state theory to electrochemical kinetic processes. As a result, both the kinetics of the electron-transfer process (from solid electrode to or from the solution species) as well as of pre- and post-electrochemical heterogeneous or homogeneous chemical processes, can be characterized quantitatively. This has resulted in a more profound understanding of heterogeneous electron-transfer mechanisms.

In general, three types of electrode processes can be involved: a) electron transfer in a redox reaction at the electrode where both the reactant and product are stable solvated ions, e.g. as in the cases of the $Fe(CN)_6^{3-}/Fe(CN)_6^{4-}$ or $Fe(H_2O)_6^{3+}/Fe(H_2O)_6^{2+}$ couples. Such reactions are often rapid and therefore diffusion-controlled; b) electron transfer producing a radical-type intermediate that is chemisorbed at the electrode surface and then, by a following heterogeneous chemical or electrochemical step, a final, stable product is formed, e.g. as for Br_2 formation studied in the present work and for the model reaction of H_2 evolution; and c) reactions in which an heterogeneous chemical step, e.g. dissociative chemisorption at the electrode, *precedes* one or more electron transfer steps as in electro-oxidation of H_2, some hydrocarbons or methanol. Such a process is involved in the electrochemical *reduction* of molecular Br_2.

Processes that involve more than one step, with one or more chemisorbed intermediates involved (process b above), are often referred to as "electrocatalytic reactions"; their rate constants and mechanisms depend on the electrode metal and the state of its surface. Reactions of type (a) above usually do not, but the Br_2 formation reaction studied in the present work is a process of the electrocatalytic type.

Detailed examination of the mechanisms of electrocatalytic reactions have been limited to only a few reactions studied especially at the noble metals [1] or their congeners Ni,Co,Fe.

Under conditions of "good electrocatalysis", faradaic reactions proceed at practical high current-densities of the order of 100 mA cm^{-2} or more at an overvoltage of only 100 mV while H_2 evolution at Hg requires 1 V of overpotential to pass 1 mA cm^{-2}!

By the use of various transient methods, electrochemistry has found extensive new applications for the study of fast chemical reactions and adsorption phenomena. Thus, a combination of thermodynamic and kinetic measurements has made it possible for electrochemists to characterize the chemistry of heterogeneous electron-transfer reactions in quantitative ways and with detailed interpretations. Indeed, the 1992 Nobel Prize was awarded to R.A. Marcus for this kind of work. Furthermore, heterogeneous adsorption processes (liquid-solid) have also been the subject of intensive investigations, as well as mechanisms of metal-ion complexation reactions through the use of various electrochemical impulse techniques.

In the case of electrode reactions involving chemisorption, added complications are caused by the presence of the solvent and ionic specific adsorption in comparison with metal-gas chemisorption. Nevertheless, the availability, through electrochemical techniques, of the controllable variables, charge or potential, provides important opportunities for modulation of the adsorption and kinetic processes, not available in gas/solid experimentation.

Although the anodic Cl_2 evolution reaction has received much attention, due in part to its great commercial significance in

the "chlor-alkali" process, and has been the subject of several review articles, much less information is available on the anodic Br_2 formation process. Hence, it is both appropriate and necessary here, as the first section of this thesis, to present a fairly detailed review of this subject for the first time in the electrochemical literature, except for an encyclopaedia type article [2].

The word "Halogen" means "salt former". All halogens, with the exception of At_2, were first discovered in the period 1774-1886. The fifth halogen element, At (Astatine), was found as an highly radioactive substance (two isotopes, ^{210}At and ^{211}At) with limited stability and too unstable to occur freely in nature. Bromides are less common than the widely distributed chlorides, but sources are widely available; for example, sea water is less than 10^{-4} M in bromides, but bromide can be also found in underground brine, halide salts and the Dead Sea.

Bromine is commercially prepared mainly by the oxidation of bromide ion, e.g. by chlorine:

$$Br^-(aq) + Cl_2(g) \rightarrow Br_2(l) + 2Cl^-(aq) \qquad (1)$$

According to the ease of oxidation, in the order $F^- < Cl^- < Br^- < I^-$, chlorine is a stronger oxidizing agent than bromine, and the equilibrium for this reaction lies well to the right in eqn. 1. Essentially all bromine is produced commercially by chlorine oxidation of bromide ions obtained from underground brine, e.g. as found in Arkansas.

The larger scale winning of bromine from brine that

contains less than 0.2% of bromine as bromide requires an industrial chemical process involving chemical engineering, process control and a close study of various means to improve overall efficiency. When the process was originally established in 1889, bleaching powder was added to large batches of brine, which enabled the liberated bromine to be carried off as vapour in a strong current of air and subsequently condensed. The introduction of electrolytic oxidation of Br^- ion allowed this batch process to be superseded by a more economically continuous one. Over-oxidation, leading to contamination of the bromine with chlorine or bromate can, however, arise but is minimized by sampling, chemical analysis and subsequent adjustment either of the brine flow rate or of the electrolysis current.

Bromine is used to produce certain dyes, light-sensitive silver bromide for photographic film, and sodium and potassium bromides for sedatives and soporifics, as well as formation of a variety of organo-bromine compounds. In recent years, an electrochemical printing process was developed by IBM involving anodic Br_2 formation from a Br^--salt which was reacted *in situ* with a leuco-dye in the paper. Also, over the past 20 years or so, an important rechargeable battery system involving Zn and Br_2 has been commercialized and demonstrated in electric-vehicle applications. This aspect of Br_2 electrochemistry is described in more detail below.

1.1.2. Role of the Br_2/Br^- Reaction in Zn/Br_2 Battery Operation

Batteries constitute one of the most direct applications of electrochemistry. The zinc/bromine flow battery, involving aqueous or nonaqueous electrolytes, has received considerable attention [3—5] in recent years as a durable, rechargeable storage battery, i.e., a secondary battery that can be recharged and used again over many cycles. Some applications such as vehicle propulsion and levelling of peak electricity usage are important at the present time. An analysis of a back-fed porous electrode for the Br_2/Br^- redox reaction has been made by Zee and White [3]. A flow-by, back-fed porous electrode, in which the reactant flows outside rather than through the electrode, is referred to as a diffusion electrode [3].

The $Zn/ZnBr_2(aq.)/Br_2$ cell behaves as a secondary battery for energy storage. The Zn metal electrode is consumed when energy is withdrawn form the cell and the $ZnBr_2$ electrolyte is formed during the discharge reaction of the cell [3—7]. The bromine and the metal is fed into the cell initially but thereafter this type of battery is highly rechargeable. The main purpose of this cell is to store energy, e.g., for load-levelling, or to make it available from certain small mobile units.

As uses of the zinc/bromine battery are increasing, more extensive studies of the Br^-/Br_2 reaction system are required, especially at macro-electrodes. Therefore, the significance of

the present work is not only in relation to understanding the kinetics and mechanisms of anodic bromine formation, but it is also helpful for cell design and electrolyte selection in rechargeable zinc/bromine battery technology.

In the process of charge or recharge of the Zn/Br_2 battery, it is the reaction of formation of Br_2 that is involved and Zn metal is redeposited from $ZnBr_2$ in solution. The Br_2 formation (on charge) or reduction (on discharge) reaction normally takes place on an high-area C-matrix cathode. However, for practical reasons, in order to diminish its volatility and rate of diffusion to the Zn anode material, and thus to diminish self-discharge of the anode, the Br_2 formed anodically on recharge is combined with morpholine as a donor-acceptor complex (cf. pyridine/I_2 complexes). In most other respects the electrochemical reactions involving bromine are the same as in regular aqueous bromide ion solutions.

In Zn/Br_2 batteries the Br_2 electrode is not required to operate above 50 mA cm^{-2} because of zinc dendrite formation which otherwise occurs at the zinc counter-electrode, leading to internal shorting. Since the design principles for flow-by, back-fed porous electrodes were not well known, an analysis of this electrode design has been presented [3] for the bromine/bromide reaction:

$$Br_2 + 2e \rightleftharpoons 2Br^- \qquad (2)$$

Zee and White [3] conducted such a study as follows: first, a mechanistic model of the steady-state process at the Br_2

cathode of the cell was developed; next, an experimental study of the bromine/bromide redox reaction was made; then, least-squares regression techniques were used to fit the model to experimental data in order to obtain physically meaningful estimates of the parameters; finally, the regression results and the mechanistic model were used to analyze the physical behaviour of a flow-by, back-fed porous Br_2 electrode [3].

In an actual Zn/Br_2 cell/battery in the charged state, the Br_2 is complexed with morpholine; however, much of the bromine is present in the forms of complex tribromide and pentabromide ions:

$$Br_2 + Br^- \rightleftharpoons Br_3^- \qquad K_{1/3} = 16$$

$$2Br_2 + Br^- \rightleftharpoons Br_5^- \qquad K_{1/5} = 40$$

depending on the bromide ion concentration.

A different kind of rechargeable battery embodiment of a new and interesting type involves a cell employing the rechargeable bromine-bromide electrochemical couple but in a 1-methyl-3-ethylimidazolium chloride/aluminum chloride low-temperature, molten-salt mixture. Experiments show that the electrochemistry of the bromine-bromide couple is complex, possibly due to halide exchange in the chloroaluminate melt that is used as the electrolyte.

Electrochemical investigations on 1-methyl-5-ethylimidazolium bromide/aluminum bromide molten salt systems for rechargeable batteries have been made by Boon, Wilkes and Lanning [8]. They find that the oxidation of bromide in the

low-temperature bromoaluminate melts is more complex than chloride oxidation in the analogous chloroaluminate melts and occurs in two steps involving tribromide ion, as also found in nonaqueous solvents e.g. acetonitrile. Otherwise, the melts behave similarly to the analogous chloroaluminate system.

1.1.3. Role of Br^- Ions in Base-Metal Corrosion Processes

The bromide/bromine system is also important in studies of corrosion of iron and various alloys, e.g., bromide (halide) ion adsorption has been reported to affect pitting corrosion of Al alloys. Dallek and Foley [9] reported that, following the initiation of the pit, the current rises rapidly and is then a measure of the faradaic reactions associated with the pit growth. The influence of Cl^-, Br^-, I^- and F^- on the initiation and kinetics of pitting of an Al alloy (such as type 7075) was studied over a wide range of temperature and concentration.

The adsorption of anions, especially halides, is also known to affect the electrochemical dissolution of iron in a complicated way. Under certain conditions, the anodic overpotential is almost completely eliminated because upon adsorption of anions on the iron surface, the latter becomes depassivated. On a non-regenerated surface, however, the adsorption of bromide ions from a 0.01 M solution already exerts an inhibiting effect on the corrosion. Schwabe and Voigt [10] showed, surprisingly, that the corrosion of iron in acidic solutions is not only retarded by Br^- but also by Cl^- ions (although Cl^- ion usually acts as an activator). However, if the

concentration of halide ions becomes increased in solutions of constant pH, the rate of corrosion passes through a minimum (the overpotential for hydrogen evolution goes through a maximum) [10]. The rate-determining process at high anodic current-densities is convective diffusion rather than an electrochemical reaction step, and this process transports iron ions away from the surface and carries anions to it.

1.1.4. Types of Processes Involving Br_2 in Relation to the Mechanisms of the H_2 and Cl_2 Reactions

Liquid bromine has a high vapour pressure and the reddish vapor can easily be seen in a bottle containing the liquid. It is a deep reddish-brown liquid, three times as dense as water, and is only slightly soluble in water with which it undergoes the hydrolytic reaction:

$$Br_2 + H_2O \rightleftharpoons H^+ + Br^- + HOBr \qquad (3)$$

In weak sunlight:

$$2HOBr \rightharpoonup 2H^+ + Br^- + O_2(g) \qquad (4)$$

At room temperature, HBr is a gas. BrO^- may also disproportionate:

$$3BrO^- \rightarrow 2Br^- + BrO_3^- \qquad (5)$$

Like the anodic Cl_2 evolution process, the Br_2 formation reaction has the following interesting and significant features:

(a) it is a simple anodic reaction requiring the discharge of two Br^- ions leading to the formation of the diatomic Br_2 molecule after a chemical or electrochemical "combination"

type of reaction (see chapter 5);

(b) it proceeds with high coulombic yields except in dilute Br^- solutions where some O_2 and bromine oxides may be involved;

(c) the overall anodic reaction leading to Br_2 formation formally has mechanistic features similar to those of the cathodic H_2 evolution reaction for which much fundamental kinetic and electrocatalytic information exists;

(d) according to Novak, Tilak and Conway [11], the reaction kinetics should be sensitive to the electrocatalytic and adsorptive properties of the anode electrode material, both for the reactant ion Br^- and the intermediate $Br^{\cdot}$, as found for the Cl_2 reaction; and

(e) depending on Br^- concentration, the reaction can proceed in aqueous solutions at electrode surfaces that are partially covered with an electrolytically generated oxide film or a specifically (thermally) formed oxide film, as with proprietary "dimensionally stable anodes" (DSA electrodes) of RuO_2/TiO_2 on Ti of the type used for anodic Cl_2 production.

1.2. Overview

1.2.1. Thermodynamic Aspects of the Br_2 Reaction and Related Processes

Prior to considering kinetic and mechanistic aspects of the Br_2 formation process it will be logical to outline some

thermodynamic aspects of the reaction in so far as they bear on to the experimental kinetic studies conducted in the present work.

Reversible, Standard Electrode Potential, E°

At 298 K, the bromine-bromide reaction at equilibrium is

$$2Br^-_{(aq)} \rightleftharpoons Br_2(aq.) + 2e \qquad E° = 1.087 \text{ V } (\underline{vs} \text{ NHE})$$

having the indicated standard electrode potential, E°.

At the same temperature, the $Ag/AgBr/Br^-$ reference electrode, as used in the present work (see chapter 3), involves processes corresponding to the equilibrium reaction

$Ag + Br^- \rightleftharpoons AgBr + e$ having an E° value of 0.071 V.

Then, thermodynamically, Br_2 can be formed at potentials more positive than:

$$E°_{Br^-/Br_2} \underline{vs} \text{ Ag/AgBr} = 1.087 - 0.071 = 1.016 \text{ V}$$

and oxygen will be evolved at or beyond a thermodynamic potential:

$$E°_{O_2,H^+} \underline{vs} \text{ Ag/AgBr} = 1.23 - 0.07 = 1.16 \text{ V}$$

For an undisturbed overall electrode reaction, the following conditions obtain:

1) the Nernst equation holds for the zero-current potential;
2) stirring of the electrolyte has no influence on the zero-current potential;
3) the zero-current potential is independent of the state of the electrode, provided the electrode material(s) remain(s) pure.

Calculated equilibrium potentials for bromine formation at

various concentrations, based on

$$E = E^\circ - (RT/2F) \ln [Br^-]^2$$

at 298 K, with $E = 1.016 - 0.059 \log [Br^-]$ vs $E_{Ag/AgBr}$, are the following, assuming unit activity of Br_2:

TABLE 1. Formal Potentials (vs Ag/AgBr) for Br_2 Formation

C_{Br^-} (M)	10^{-2}	10^{-3}	10^{-4}	10^{-5}	10^{-6}	10^{-7}	10^{-8}
E (V)	1.13	1.19	1.25	1.31	1.37	1.43	1.49

In practice, of course, the Br_2/Br^- electrode must be established in an electrolyte of either an acid (HBr) or a bromide salt (e.g. NaBr, KBr). Then the formal E values of Table 1 have to be corrected to small extents for the mean activity coefficients of the electrolyte at various concentrations listed. However, even for higher Br^- concentrations, the activity coefficient correction for say KBr electrolyte would be only ca. 10 mV in the above table of E values.

These data are important for giving, in the kinetic work, an indication of the respective potentials above which, in solutions having various Br^- concentrations, Br_2 will just begin to be, or expected to be, anodically generated.

The state of the electrode can vary depending upon its pretreatment; this is important for the *kinetics* of the process involved. Despite this, the equilibrium potential must be *independent* of this state for thermodynamic reasons, since the

state of the electrode manifests itself only in the velocity of the equilibrium adjustment, i.e. on the exchange current-density, i_0, or the limiting reaction current density, but not on the equilibrium value itself. A mixed potential, whose value arises from coupling of the current-potential curve of the reaction under investigation with that of an interfering or alternative electrode process, e.g. as in corrosion of the electrode metal, will, in general, depend on the state of the electrode.

Common reactions involving Br^- and molecular Br_2, relevant to processes investigated in the present work, are as follows, with their standard potentials E° as listed below:

$Br_2(aq) + 2e \rightleftharpoons 2Br^-$	1.087 V
$Br_2(l) + 2e \rightleftharpoons 2Br^-$	1.065 V
$HBrO + H^+ + e \rightleftharpoons \frac{1}{2}Br_2 + 3H_2O$	1.59 V
$HBrO + H^+ + 2e \rightleftharpoons Br^- + H_2O$	1.6 V
$BrO_3^- + 6H^+ + 5e \rightleftharpoons \frac{1}{2}Br_2 + 3H_2O$	1.52 V
$BrO_3^- + 6H^+ + 6e \rightleftharpoons Br^- + 3H_2O$	1.44 V
$Ag + Br^- \rightarrow AgBr + e$	0.071 V

Studies on the electrochemistry of Br_2 and its formation are complicated by Br_2 and water being partially miscible; the slightly soluble bromine in water makes two layers, where the water layer is light brown, while pure bromine should be deep orange. As the elemental Br_2 experimentally formed in anodic kinetic work is normally a small quantity, it might be assumed that electro-generated Br_2 remains in the solution homogeneously.

However, the elemental Br_2 must initially be formed on the electrode surface as a thin liquid film and subsequently pass into solution, depending on the mass-transfer conditions that obtain. In the present work, such conditions have been controlled in some of the experiments by use of a rotating-disc electrode.

Since how bromide becomes oxidized to bromine anodically is the major aspect of interest, cyclic voltammetry experiments in the present work were usually run with an upper limit of potential substantially less than 1.5 V (RHE) [12] in order to minimize elemental Br_2 formation in the liquid form.

1.2.2. Anion Adsorption in the Reaction Related to the Anion as the Reagent

1.2.2.a) Introduction

The effect of adsorbed substances at solid electrodes has been the subject of numerous investigations because of its interest fundamentally and the technical implications of such adsorption effects. According to Woods [13], this is especially true for noble metals that are used as electrodes or electrocatalysts in fuel-cells and other applications. Also, quite generally, the effects of specifically adsorbed ions, e.g. as studied in the electrode kinetics of H_2 evolution at Hg by the Frumkin School and by Gierst [14] in earlier years, are usually of major significance in electrode kinetics as account of their modification of the structure of the interphasial double-layer and the potential profile across the latter.

Since experiments at Pt are usually performed in aqueous H_2SO_4 solutions, it is interesting also to know the degree of adsorption of HSO_4^- ions at Pt surfaces. The specific adsorption of HSO_4^- ions is, however, found to be much weaker than that of the halide ions Cl^-, Br^- or I^-.

The necessity for considering adsorption effects that cannot be interpreted in terms of simple electrostatic interactions of the type analyzed by Gouy [15] (1910) and Chapman [16] (1913), is now well recognized. Stern [17] introduced the concept of "specific" or chemisorption and gave it a mathematical basis using a Langmuir-type isotherm (1924). Also, adsorption of uncharged substances was already treated by Frumkin [18] in pioneering work in 1926 and onwards by assuming that a Langmuir-type configurational function in fractional coverage is valid at constant electrode potential provided particle-particle interactions are introduced much in the same way as in the equation of state for real gases. Such concepts have been applied to anion adsorption. Butler [19] also treated electrical effects in organic molecule adsorption (1929) in a related way.

Adsorption processes at electrodes can be broadly divided into two groups according to the type of adsorption involved:

a) physical adsorption and

b) chemisorption.

Physical adsorption does not involve bonding to the electrode of the kind that prevails in chemisorption and usually

requires the introduction of an electrical variable (potential or charge on the electrode) in description of the adsorption in terms of an isotherm based on electrostatic polarization energies. Conversely, bonding of a chemisorbed species with the electrode is usually strong (< ca. -40 kJ mol^{-1}) and, if sufficiently strong, may not be much influenced by the electrical variable in the isotherm. The intermediate situation of chemisorption with some significant influence of the electrical variable on the isotherm parameters is more usual.

Randles [20] (1947) studied the influence of adsorbed ions on the kinetics of various electrode processes and found that they may either accelerate or retard the reaction, depending on the conditions. According to Randles, the overpotentials of metal deposition on amalgams are decreased by added anions in the order PO_4^{3-}, NO_3^-, ClO_3^-, Cl^-, Br^-, I^-, i.e., to an increasing extent related to their order of specific adsorption. Since the overpotentials for deposition of numerous base metals are usually relatively small for appreciable current-densities (10~100 mA cm^{-2}), the overpotential decreasing (retardation) effect of anions is weak for such cases. Based on Randles' interpretation of transient responses to electrical perturbation of electrodes, he concluded that the simple activation-controlled charge-transfer step was rate-determining in such metal deposition processes.

1.2.2.b) Halide Adsorption at Noble Metals: Competitive Effects with H and OH or O Electrosorption

According to the early work of Slygin and Frumkin [21] (1934), "capillary-active"[1] anions competitively decrease the adsorption energy of H-atoms, their effects increasing in the order $SO_4^{2-} < Cl^- < Br^- < I^-$. Br^- ions are found to be significantly "capillary-active" in changing the surface tension of Hg (see section 1.2.2.d and the footnote below) from the data of Lawrence, etc. [22].

The state of adsorbed halide ions at noble metal electrodes has been studied by means of:

(1) cyclic-voltammetry for study of changes in H adsorption and surface oxidation, due to competitive halide coverage;

(2) relative reflectivity changes and

(3) a direct method, using radioactively labelled ions, as referred to in section 1.2.2.e.

Breiter [23] suggested that adsorbed halide ions practically replace electrodeposited oxide species at noble metal surfaces, but such an effect depends very much on the halide ion concentration and potential. However, in the cathodic direction of the sweep, adsorbed halide ions can be desorbed in the H adsorption region at Pt if their concentration is not too high, $< 10^{-3}$ M. Since Br_2 formation occurs at less

---

[1]This term originated from the use of the Lippmann capillary electrometer for study of adsorption effects at the liquid Hg interface in a capillary tube, with ionic solutions — the so-called "electrocapillary effect", cf. Butler's monograph (1940) titled "Electrocapillarity".

positive potentials than those for Cl_2 evolution, Breiter concluded that Cl_2 evolution most probably occurs in parallel with oxide formation processes while, in the case of Br_2 formation, it proceeds initially on free Pt-metal surface sites. Thus, when anodic bromine formation becomes significant, the Pt is not appreciably covered by oxide species (depending on the Br^- concentration), as demonstrated in the present work.

In the presence of Br^- or I^- ions, as well as of Cl^- ions at higher concentrations, formation of OH and O species, constituting the initial monolayer oxide film at Pt, is inhibited.

Adsorption of Br^- ions on platinized Pt electrodes in 0.5 M H_2SO_4 has been studied by Bagotskii [24]. The aim of the work was to investigate the effects of Br^- ion adsorption on both H and surface oxide coverage at Pt electrodes. In order to determine surface coverage of the electrode upon adsorption of Br^- ion, they used three complementary techniques:

(a) measurement of decreases in oxide coverage;

(b) observation of redistribution of states of adsorbed H and

(c) measurement of decrease in methanol adsorption (see section 1.2.2.c) caused by competitive adsorption of Br^-.

The first technique, if used above 1.1 V E_H, leads to oxidation of adsorbed Br^-, to Br_2, and thus can be employed only for the potential range 0.5 V to 1.1 V E_H, depending on concentration (see Table 1).

In the second method, the amount of H strongly bonded to

the Pt surface decreases as a result of Br^- adsorption but the amount of weakly bonded H apparently increases; the distribution of the extent of adsorption of H with potential is changed by the presence of co-adsorbed Br^- ion.

At relatively high concentrations of halide ion in solution (> 0.1 M), Pt electrode surfaces undergo significant anodic dissolution by forming complexes of the type PtX_4^{2-} or PtX_6^{2-}, especially at elevated temperatures and depending on the anode potential. Such processes do not, however, occur in experiments where the halide ion concentrations are relatively low in comparison with the concentration of the supporting electrolyte ($HClO_4$ or H_2SO_4) and if ordinary temperatures are involved.

The redistribution of adsorption states and blocking effects caused by very small concentrations (down to 10^{-8} M) of various anions (Cl^-, Br^- and I^-) on the profile for underpotential deposition of H at Pt, and the surface oxidation profiles at Au and Pt, have been investigated by Breiter [25] and by Conway and Novak [26]. These experiments were carried out by titrating into a dilute supporting electrolyte of H_2SO_4 or $HClO_4$ very small, but controlled, quantities of a standard solution of salt of the desired additive anion by means of a micrometer syringe.

In the case of the H UPD profile at Pt, studied by Breiter [27] (1963), it was shown that the two principal peaks observed in 1 M H_2SO_4, i.e., at relatively high HSO_4^- concentration, were shifted to less positive potentials as the halide ion concentration was increased. The sensitivity of the effects was

larger in the order Cl^- < Br^- < I^- and were confirmed by Stonehart's results [28] later.

Frumkin, Balashova and Kazarinov [29] (1966) had found that the adsorption of anions at Pt increases in the sequence SO_4^{2-} < Cl^- < Br^- < I^-, the maximum charge associated with the adsorption of these anions in this sequence being from 15 to 140 $\mu C\ cm^{-2}$. The developments concerning effects of anions on anodic oxidation of hydrogen on Pt electrodes have been surveyed by Frumkin, Sobol and Dmitrieva [30] (1967).

Bagotskii, Vassilyév, Weber and Pirtskhalava [31] (1970) established that the adsorption of Cl^-, Br^-, I^-, SCN^-, ClO_4^-, BrO_3^-, NO_3^-, ClO_3^- and HSO_4^- anions at Pt could be described by a logarithmic isotherm. These workers had also observed similar behaviour to that in Breiter's study, i.e., the sensitivity of the effects is larger in the order Cl^- < Br^- < I^-, a not unexpected result, based on the order of donicities and hydration energies of these ions.

Adsorptivity of ions can also be determined from the potential shift that arises upon their introduction, under isoelectric conditions, into a solution containing only weakly, or non-, specifically adsorbable ions. Such "adsorption" potentials of anions (Cl^-, Br^-, I^-) were determined on platinized and smooth platinum in work by Frumkin [32]. A related scale of "adsorptivity" also follows from the hierarchy of effects of anions, at a given concentration, on the potential of zero charge of a Hg electrode (see 1.2.2.d and chapter 5).

1.2.2.c) Competitive Effect of Br^- on CH_3OH Adsorption at Pt

It was mentioned in 1.2.2.b that Bagotskii et al [24] had proposed that anion adsorption effects could be characterized not only by their competition versus the elementary steps of surface oxide film formation but also by their interference with methanol adsorption and its electro-oxidation at Pt. Such effects are not, of course, involved in the Br_2 formation reaction studied in the present work but they illustrate, in another context, the affinity of the Br^- ion for noble metal electrode surfaces and resulting effects on electrode processes thereat. The processes involved will therefore be only briefly referred to here.

The procedure used in their experiments was based on the observation [24] that a monolayer of CH_3OH (or derived chemisorbed species) become adsorbed only on that fraction of the surface not occupied by Br^- ions.

The coverage by chemisorbed species derived from CH_3OH, determined in all three methods (a), (b) and (c) referred to in section 1.2.2.b, can be determined by the fast anodic or cathodic pulse technique [24] in which the decrease in total charge for either oxide or hydrogen adsorption is measured. A limiting coverage by Br^- ions is found to be reached at concentrations of $Br^- \geq 10^{-6}$ M in the potential range 0.3—1.0 V E_H at smooth Pt electrodes in the case of competitive adsorption with CH_3OH. When the limiting coverage of Br^- ions was attained, there could be 40% of a monolayer of oxide co-adsorbed on the

surface. At potentials higher than 1.0 V E_H, a decrease in surface coverage by Br^- ions occurs due to oxidation of Br^- ion to Br_2. These observations are relevant to those made in the present work on the competition between surface-oxide film formation and Br^- ion adsorption (see 1.2.2.b).

An interesting difference between the state of adsorbed Cl^- ion at Pt and that of Br^- or I^- was determined by Sobkowski and Wieckowski [33] in their studies on competitive adsorption with CH_3OH. The rate of adsorption of CH_3OH at 0.5 V E_H was decreased in the presence of halide ions when simultaneous adsorption of a given ion and the molecule was taking place. The differences in behaviour of the halide ions were attributed:

(a) to the greater electrostatic interaction of the Cl^- ion than that of Br^- or I^-, with Pt and

(b) in the case of Br^- and I^-, to some supposed reactions of these ions with the species derived from dissociative chemisorption of CH_3OH.

1.2.2.d) Adsorption of Bromide and Other Halide Ions at Hg

While the chemisorptive properties of Hg are substantially different from those of Pt (since the latter is a transition metal having an incomplete d-band), much useful absolute and comparative information has been obtained by studies of adsorption of halide ions including Br^-, at the Hg electrode using the classical techniques of surface tension γ and double-layer capacitance (C_{dl}) measurement. Hg is thus to be regarded as a kind of "reference system" for ion adsorption information,

especially in a comparative way for a series of chemically analogous anions such as the halides. Additionally, evaluations of shifts of potential of zero charge (cf. Fig. 1, [22]) from electrocapillary or C_{dl} measurements in dilute solutions provide information on relative strengths of ion chemisorption at Hg.

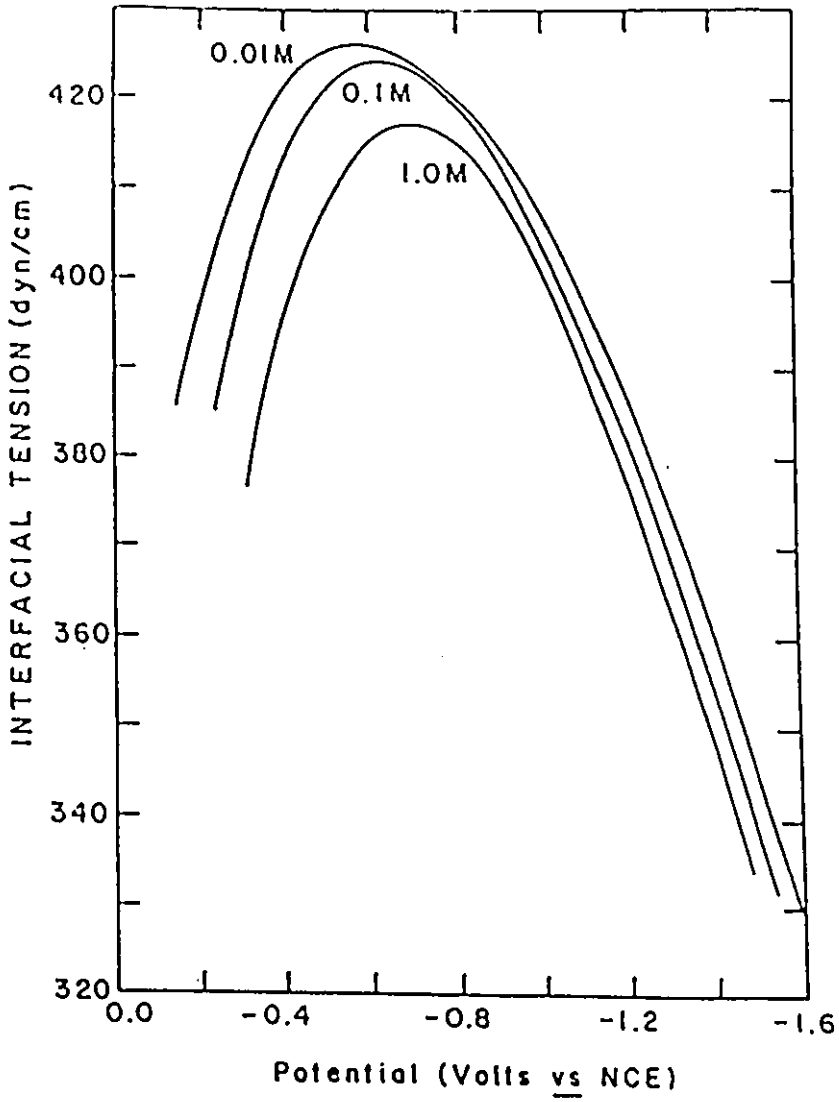

Fig. 1. Electrocapillary curves for KBr solutions on the Hg electrode [22]

Bromide ion adsorption has been studied by the

electrocapillary method using the cell

Cu | Pt | Hg | KBr solution | Hg_2Br_2 | Hg| Pt | Cu'

for which potentials were measured for a series of polarizations of the Hg capillary electrode on the left-hand side of the above cell. Typical behaviour is exemplified by the electrocapillary curves for KBr adsorption at Hg shown in Fig. 1. The resulting changes of γ of the Hg in aq. KBr are given by the Gibbs-Lippmann equation

$$d\gamma = -q^M dE^- - \Gamma_{K^+} d\mu_{KBr} \qquad (6)$$

where E^- is the potential of the reference electrode (here Hg/Hg_2Br_2) reversible to the relevant anion.

The behaviour is related to q^M by the Lippmann equation (cf. eqn. 6)

$$q^M = - (\partial\gamma/\partial E^-)_{T,P,\mu_{KBr}} \qquad (7)$$

Γ_{K^+} at a given point on the curve is determined by differentiating graphically a plot of γ, at constant E^-, versus log $a_\pm^2$, where $a_\pm$ is the mean activity of KBr in the solution. From the thermodynamics of surface tension changes at electrodes [6], the value of Γ_{Br^-} is given [noting that $q^M = -F(\Gamma_{K^+} + \Gamma_{Br^-})$] by

$$\Gamma_{Br^-} = (q^M/F) + \Gamma_{K^+} \qquad (8)$$

which is then the value of the relative surface excess of bromide ion at given values of E^- and $a_\pm$. A useful pictorial representation, summarizing the various integral and differential relationships between γ, q, Γ and C, is shown in Fig. 2.

At every point along each electrocapillary curve in Figure

1, the corresponding values of the excess charge density, q^M, on the metal and thence from eqn. 8 and eqn. 6 the relative surface excesses of potassium and of bromide ions can be determined. The experimental results quoted here were those obtained by Grahame, Poth and Cummings [34] for KBr solution.

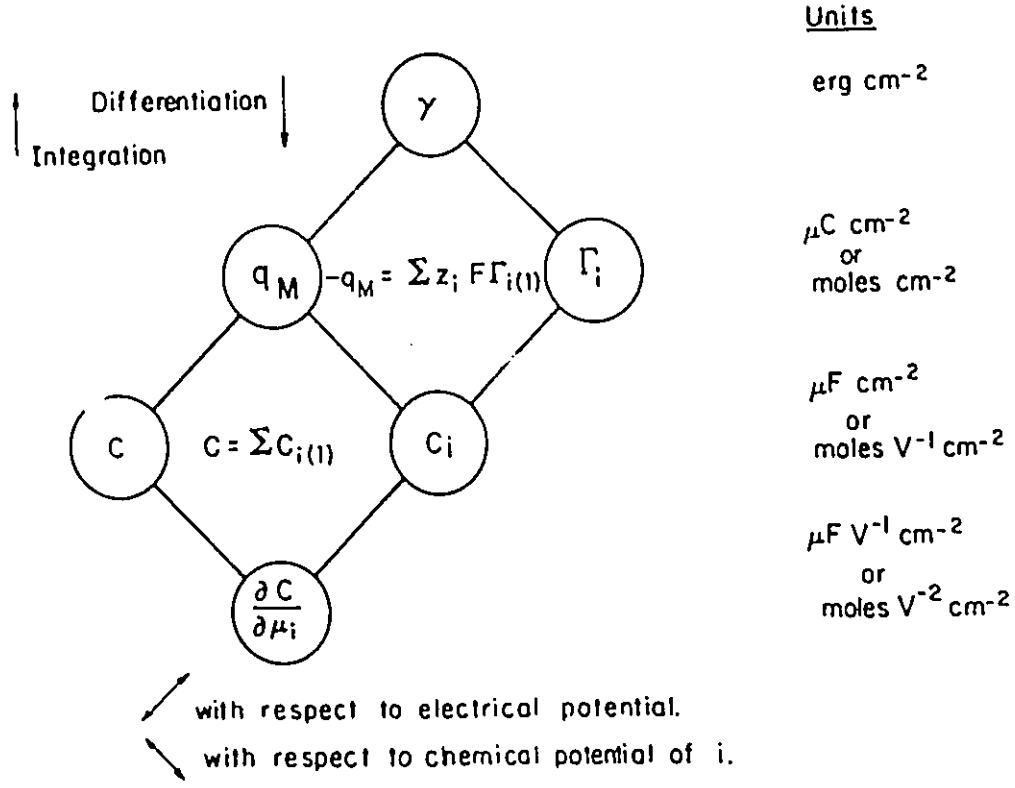

Fig. 2. Fundamental relations in electrocapillary thermodynamics [6]

Lawrence, Parsons and Payne [22] (1968) also determined electrocapillary curves for KBr solutions (Fig. 1), as in the works of Devanathan and Peries [35], and Grahame, Poth and Cummings [34]. Specific adsorption of the Br^- anion caused a marked decrease in γ at all potentials on the positive branch of the electrocapillary curve, and the potential of zero charge was

shifted in the negative direction, as expected for anion adsorption.

Some comparative data on values of p.z.c. at Hg are listed in Table 2 which illustrate the dependence of the p.z.c. on a) the type of halide anion and b) its concentration in solution.

TABLE 2. Potentials of Zero Charge of Hg in Various Halide Electrolytes [36]

Electrolyte	Concentration (M)	E_z (V) vs NCE
NaF	1.0	-0.472
	0.1	-0.472
	0.01	-0.480
	0.001	-0.482
NaCl	1.0	-0.556
	0.3	-0.524
	0.1	-0.505
KBr	1.0	-0.65
	0.1	-0.58
	0.01	-0.54
KI	1.0	-0.82
	0.1	-0.72
	0.01	-0.66
	0.001	-0.59

The data in Table 2 demonstrate that chloride, bromide and iodide are all specifically adsorbed at Hg, except for fluoride, since the potentials of zero charge become shifted as the concentrations are increased, e.g., in NaCl, KBr and KI.

The degree of anion adsorption is also a function of electrode surface charge and undergoes an inflexion at moderate positive charges.

1.2.2.e) Optical Studies of Bromide Adsorption at Pt

A more direct approach for study of halide ion adsorption

at electrodes is by means of optical reflectivity measurements including analysis of the state of polarization of light reflected from electrodes (ellipsometry). A number of works [25, 37-43] have addressed this matter and include optical studies on Br^- ion adsorption at Pt [37], Ag [38] and Au [39].

Halide ion adsorption on Pt electrodes was studied using ellipsometry by Chiu and Genshaw [40] where the main effect is a diminution of the phase-shift parameter Δ. However, ellipsometry is not as sensitive as voltammetric techniques; thus Br^- adsorption is already detectable from 10^{-6} M Br^- solutions by the latter method but only at concentrations > 10^{-3} M in ellipsometry. However, Barrett and Parsons [41] measured the relative reflectance changes, $\Delta R/R_{\parallel}$, caused by Cl^- and Br^- adsorption at Pt and showed that lowering of the reflectance was detectable, in their experiments, even with 10^{-5} M solutions of bromide. They stated that the increase in coverage of adsorbed Br^- ions with increasing anodic potential could be determined from the lowering of the relative reflectance ratio, $\Delta R/R_{\parallel}$, for light polarized parallel ($\parallel$) to the plane of incidence, caused by the adsorption of Br^- ions from the solution.

Gottesfeld and Reichman [42] used combined ellipsometric and reflectometric measurements to follow halide anion adsorption at very low concentrations at Pt. Two effects were involved: a) the change of optical constants increased with coverage, θ_{Br^-}, by the adsorbed Br^- anion at constant potential; this causes an increase in the refractive index of the solution

region of the double-layer and thus of the complex dielectric constant of the surface metal atom layer due to the increase in excess positive charge. These two contributions were estimated in terms of $(\partial\Delta/\partial\theta_{Br^-})_v$ for constant potential. b) The change of electric field across the interphase due to the film of adsorbed bromide ions at constant coverage can also result in a shift of the optical constants of both the metal surface layer and the layer of the specifically adsorbed ions themselves (polarization effect). These effects were considered in terms of $(\partial\Delta/\partial V_{\theta_{Br^-}})$ for constant Br^- adsorption (θ_{Br^-}). This derivative has a negative sign due to Br^- ion coverage. Interpretations were given in terms of a model in which field-induced charge-transfer arises from the adsorbed layer to the metallic substrate causing a decrease of the effective film thickness and its refractive index, as well as its extinction coefficient.

The specific adsorption of Br^- ions was also studied on a gold electrode by Anderson and Hanson [43] in the presence of an excess of non-specifically adsorbed supporting electrolyte, NaF, by the reflectance technique, accompanied by cyclic-voltammetry measurements.

Ellipsometry measurements by Breiter [25] (1962) showed that a concentration of 8×10^{-4} M Br^- leads to considerable adsorption of Br^- ion at a Pt electrode, resulting in a decrease of the phase parameter Δ with increasing potential in the "double-layer" potential region. The observed decrease in Δ, which also accompanies oxide formation, was found to be shifted

to higher anodic potentials in the presence of Br^- ion. This observation is consistent with the cyclic-voltammetry behaviour which reveals [25] competitive adsorption between electrodeposition of OH and O at Pt, and Br^- chemisorption.

1.2.3. Anodic Reactions Involving Br^- and Br_2 Formation

1.2.3.a) Introduction

The electrochemical behaviour of the bromide/bromine system in aqueous and nonaqueous solvents has attracted the attention of various workers, e.g., Breiter [23,25,27], Conway [11,26,44], Biegler [45], Yeager [46] and Bagotskii [24,31], etc. For example, cyclic voltammetric and ellipsometric studies of processes involving bromide in aqueous medium ($HClO_4$) have been made, but few reports describe the voltammetric behaviour of Br^-/Br_2 in nonaqueous media such as CH_3CN [47] where competitive surface oxide formation does not arise in dry solutions. The conclusions are, however, mainly qualitative in character and few publications on quantitative aspects of the kinetics of the electrode reactions involving Br^- and Br_3^- have appeared [48,49].

1.2.3.b) Aqueous Solutions

The earliest reliable data on anodic bromine formation kinetics seems to be that obtained by Chang and Wick [50] in 1935 at Hg and Ir using the conventional polarization measurement procedure for evaluation of Tafel relations. They reported systematic studies on the Br_2/Br^- reaction for which the overall reaction at the Br_2/Br^- electrode was $2Br^- \rightleftharpoons Br_2 + 2e$.

They observed only small overpotentials at the Hg electrode even at appreciable current-densities, i.e., the process occurs with relatively little kinetic retardation compared e.g. with H_2 evolution at Hg. However, the overpotential is appreciable at Ir electrodes and its variation with current density obeys the Tafel equation, as confirmed by the work of Loschkarew and Esin [51] in 1938. Chang and Wick [50] obtained the following data for the exchange current-densities, i_0, and transfer coefficients, α for anodic Br_2 formation from 1 M KBr:

$$i_0 = 3 \times 10^{-3} \text{ A cm}^{-2}, \ \alpha = 0.6$$

(α increased with temperature to 1.07 at 353 K.)

Cooper and Parsons [52], in a more modern approach (1970), studied the kinetics of the bromide/bromine electrode reaction at Pt in aqueous sulphuric acid by means of impedance measurements. The frequency response does not follow the behaviour expected for a Randles circuit [53] (Fig. 3); however, the addition of an adsorption capacity across the diffusional (Warburg) impedance W then seems to give a more satisfactory equivalent circuit. Study of the concentration dependence of the exchange current suggested that the rate-controlling step [52] is $Br^- \rightleftharpoons Br^{\cdot} + e$ (Fig. 4).

Various authors have reported work on adsorption of Br^- at a platinum electrode in aqueous medium as discussed earlier. The current/voltage curves obtained by Yeager [46] with aqueous solutions containing lithium bromide show two waves, starting at an initial potential close to 0.85 ± 0.03 V, referred to the

Ag/AgBr electrode. The origin of the two waves is probably connected with oxide film formation together with Br_2 formation.

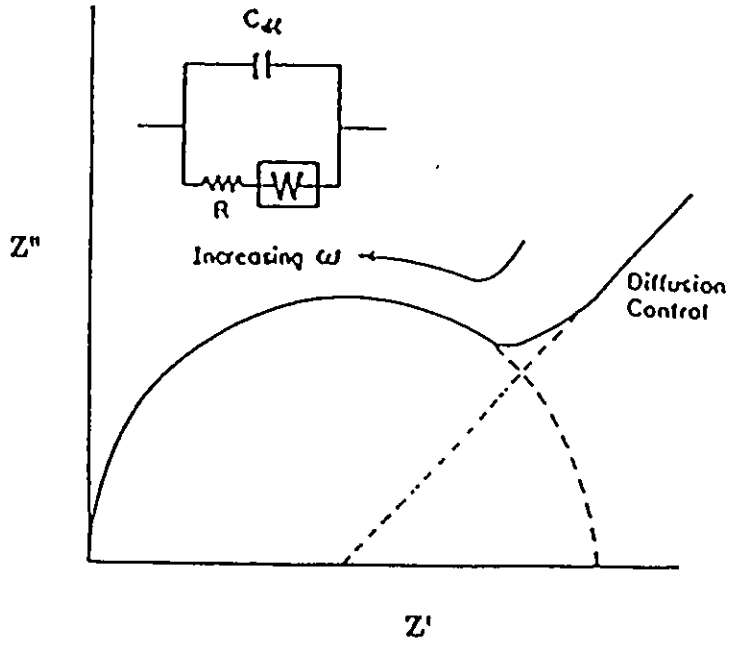

Fig. 3. Randles circuit and corresponding complex-plane plot

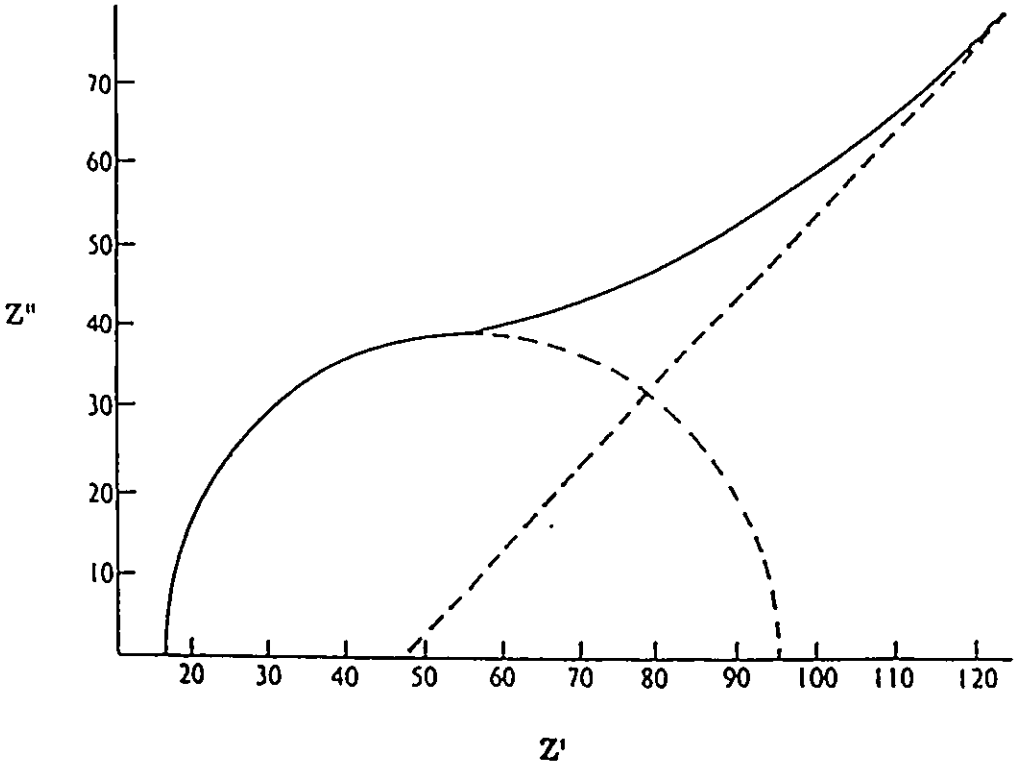

Fig. 4. Results (at low η) for the Br_2/Br^- system [51]

1.2.3.c) Nonaqueous Solutions

Interest in study of the Br_2 formation from non-aqueous aprotic media arises because competitive anodic oxide-film formation at the electrode surface does not occur, at least if the non-aqueous solution is sufficiently dry. However, even traces of water can lead to monolayer oxide film formation at Pt.

Iwasita and Giordano [47] (1969) studied the kinetics of the bromine-tribromide redox processes on Pt electrodes in anhydrous acetonitrile solutions using a Pt disk working electrode rotated at 200—2000 rpm. They found that both the anodic and cathodic current/voltage behaviour was characterized by two well-defined waves which they attributed to the existence and stability of the tribromide ion (Fig. 5). They stated that the bromide ion, in acetonitrile as solvent, can be oxidized to Br_3^- and to Br_2 in two steps. The experimental results indicate that the first and second anodic steps are

$$3Br^- \rightarrow Br_3^- + 2e \qquad \text{I}$$

$$2Br_3^- \rightarrow 3Br_2 + 2e \qquad \text{II}$$

Both waves exhibited some degree of irreversibility. On the basis of the experimental data, the above two reaction mechanisms were advanced. Iwasita and Giodano also found a third wave in the anodic current/voltage plot. A first hypothesis argued that the reagent of the third wave was an intermediate in the Br_2 formation reaction and that the formation of this Br_3^- (I) as the reagent in step (II) is competitive vis

à vis the presence of Br^- as the reagent in step (I). The intermediate species, supposed by many authors, are bromine atoms adsorbed on the platinum; such species are, of course, formed both in aqueous and nonaqueous media. The reaction mechanism for the third process would be:

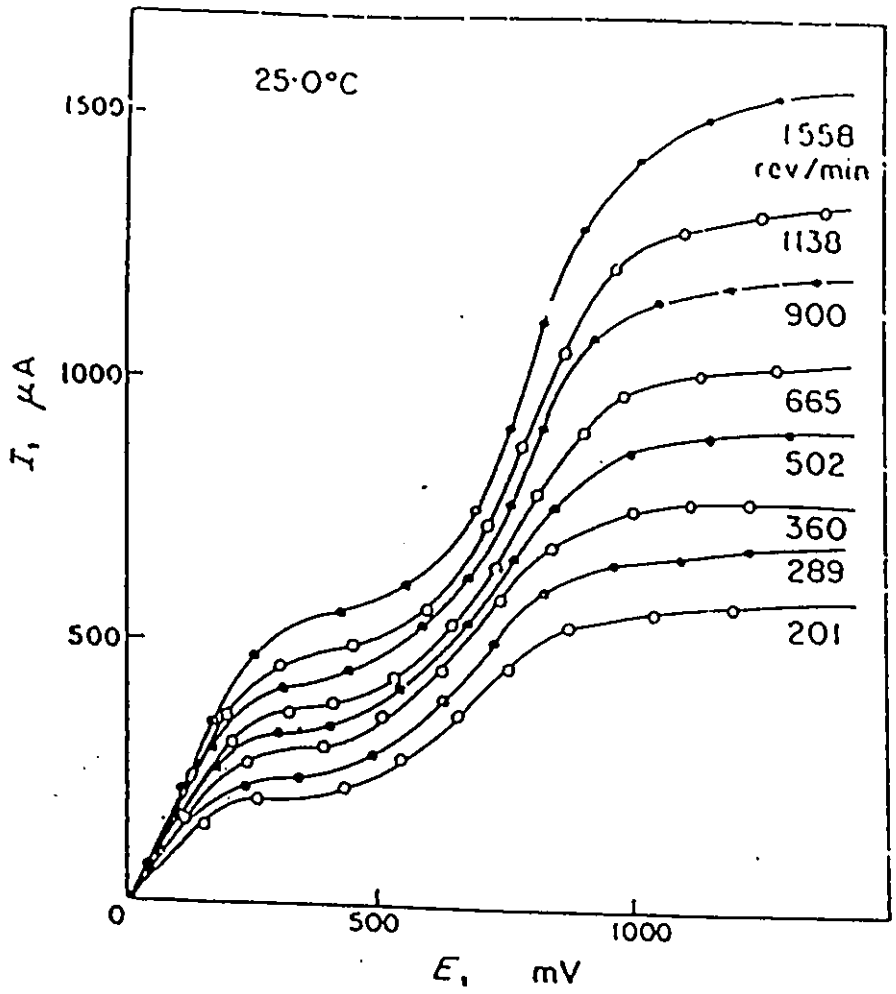

Fig. 5. Anode current/voltage curves in CH_3CN, C_{Br^-}, 0.0139 M [47]

$$Br_3^- + S \rightarrow Br_2 + S/Br^{\cdot} + e \qquad (a)$$

where S is a surface site on the electrode, followed by

$$S/Br^{\cdot} \rightarrow \tfrac{1}{2}Br_2 + S \qquad (b)$$

Either (a) or (b) arises as the third step, competitive with reaction II (p.33).

Two mechanisms of the bromine-tribromide-bromide system at the Pt electrode in CH_3OH were therefore assumed to be as follows:

Mechanism A

$$Br^- + S \rightleftharpoons S/Br^{\cdot} + e \qquad 1$$

$$S/Br^{\cdot} + S/Br^{\cdot} \rightleftharpoons Br_2 + 2S \qquad 2$$

$$Br_2 + Br^- \rightleftharpoons Br_3^- \qquad 3$$

Mechanism B

$$Br^- + S \rightleftharpoons S/Br^{\cdot} + e \qquad 1$$

$$S/Br^{\cdot} + Br^- \rightleftharpoons Br_2 + S + e \qquad 2$$

$$Br_2 + Br^- \rightleftharpoons Br_3^- \qquad 3$$

where S stands again for a surface site and $S/Br^{\cdot}$ represents a bromine atom adsorbed on the surface site.

Iwasita and Giordano [47] suggested, based on their kinetic data, that the reaction mechanism A is preferred.

The second hypothesis B supposed that the reagent of the third process is just the "Br^- species" adsorbed on the platinum surface and the competitive reactions are again Br_3^- and Br_2 formation. However, note that Br^- and I^- chemisorption occurs at Pt with appreciable charge transfer, so it is not the fully charged Br^- that is the anode reagent (see chapter 5).

Thermodynamic considerations of the experimental findings,

i.e. the anodic unreactivity of Br_2 and the quasi-reversible behaviour of the second electrode reaction B—2, strengthen the above second hypothesis B. However, in the presence of Br^- ions, the mechanism predicts the Br_2 and S/Br^- potential values, and consequently does not require that the supposed equilibrium $S/Br^- \rightleftharpoons \frac{1}{2}Br_2 + S$ be fast. Therefore, the mechanism B, these authors concluded, should be rejected.

In the case of acetonitrile solutions, Iwasita and Giodano also found, when bromide ions and bromine are present, that two types of current/voltage curve arises [47], depending on the Br^-/Br_2 concentration ratio. With excess of bromine, only one anodic wave appears while the cathodic wave remains the same. When bromide ions are in excess, the anodic curves remain the same, while the cathodic curves show only one wave.

Since the stability constant for process $Br^- + Br_2 \rightleftharpoons Br_3^-$ is large enough, viz, $K_{f(Br_3^-)} = 16$ (aqueous [54]), $K_{f(Br_3^-)} = 10^7$ (nonaqueous [55]), the observed limiting current must be related to the Br_3^- reacting species involved in reaction step II (p.33).

When the concentration ratio of bromine to bromide ion is greater than one, the tribromide concentration would correspond approximately to the initial bromide concentration; when the concentration ratio is less than one, the tribromide ion concentration can be taken as the initial bromine concentration.

1.2.4. Electroanalytical Aspects of the Br_2 Reaction

Measurement of currents associated with electro-oxidation

of Br^- to Br_2 affords a procedure for electro-analytical determination of Br^- concentrations.

Laitinen and Kolthoff [56] suggested the use of the rotating platinum electrode for the amperometric determination of bromine, since with this electrode there is a proportionality between diffusion-current and concentration, at constant ionic strength. El Wakkad et al [57] reported a single anodic wave, corresponding to the oxidation process $2Br^- \rightarrow Br_2 + 2e$, which is obtained at a smooth platinum electrode in a 5×10^{-4} M bromide solution in 1 M $HClO_4$. Its half-wave potential is 0.970 V and is independent of pH of the solution at constant Br^- concentration; therefore, a decrease in the pH of the solution may cause the oxidation wave of bromide to bromine to overlap the wave for evolution of O_2 from water. At bromide concentrations of 5×10^{-4} M, the masking of the former wave by the latter takes place at pH-values greater than 8. The process involving Br^- appears to be completely reversible in 1 M $HClO_4$, independent of the state of the electrode. The main diffusion limiting current is proportional to the bromide (ion) concentration. It is clear that at a sufficiently high i_0 for the charge transfer and desorptive reactions, a diffusion-step must become rate-determining.

Voltammetric determination of iodide and bromide at the rotating pyrolytic graphite (R.P.G.) electrode has been studied by Dryhurst and Elving [58]. A typical method for determining bromide in the presence of chloride on a microscale is the well-

known procedure of van der Meulen [59]. Bromide gives only one analytically useful anodic wave at the R.P.G. electrode.

Chapter 2. OBJECTIVES OF THE PRESENT WORK

The overview of previous work on the adsorption and electrochemical reactions of bromide ions, given in chapter 1, shows that the adsorption of Br^- ion and its reactions at Pt has attracted considerable attention [12,21,23,25—27,45—47,60,61]. However, substantial further work is needed to characterize and interpret anodic Br_2 formation kinetics in relation to Br^- adsorption, complexation with Br_2 and interference with Pt surface oxide formation, and especially the role of chemisorbed $Br^{\cdot}$ and $Br_3^{\cdot}$ intermediates.

The aims of the present work have therefore been to determine mechanisms of the Br^-/Br_2 system, particularly its anodic reaction kinetics as bromide ion becomes adsorbed and bromine is formed. Also, since stable tribromide ion exists, it is suggested that an adsorbed $Br_3^{\cdot}$ intermediate, in addition to $Br^{\cdot}$, must also be taken into consideration in the overall reaction mechanisms that are involved, depending on relative concentrations of Br^- ion and molecular Br_2.

The standard reversible potential is 1.09 V vs. NHE, so that significant current-densities for Br_2 formation on noble metals can usually arise prior to O_2 formation, the standard

reversible potential for which is 1.23 V vs. NHE. In this respect, the reaction differs from Cl_2 evolution which proceeds normally *above* the thermodynamic potential for O_2 evolution and well into the range of potentials over which Pt surface oxide formation takes place. The electrochemical Br_2 formation reaction is found to proceed under most conditions (i.e. except from dilute Br^- solutions) at the electrode *metal* surface. Therefore, the electrode kinetic behaviour of the bromine formation reaction, and the role and identity of adsorbed intermediates involved, are of major interest in the fields of electrocatalysis and electrosorption, especially at halide metals.

The present research project involves examination of the effects of Br^- ion concentration on the anodic Br_2 formation reaction, the reversibility and stability of oxide films in the presence of Br^- ion, on the Pt electrode at which the reaction takes place, and steady and non-steady-state measurements of anodic Br_2 formation on the Pt RDE together with effects associated with $Br^{\cdot}$ and $Br_3^{\cdot}$ adsorption.

Adsorption in an electrocatalytic reaction involves coverage both by the reactant species (here $Br^{\cdot}$ or $Br_3^{\cdot}$) *and* by the kinetically-involved intermediate(s), and depends on the material nature of, and the overpotential at, the electrode. The coverage by chemisorbed species normally appears explicitly in the expression for the reaction rates, and needs to be experimentally evaluated, where possible, in a proper kinetic

study of the electrocatalysis involved.

The principal objective has been to study the role of chemisorbed bromine species (Br^- ion and the intermediates $Br^\cdot$ or $Br_3^\cdot$) in the electrocatalytic reaction steps, to examine how their behaviour at electrode surfaces can be experimentally deduced by electrochemical and physicochemical means, and to investigate and characterize the kinetics and mechanisms involved in the anodic Br_2 formation reaction, taking into account the above factors, hitherto little examined in the case of anodic Br_2 formation.

The following three major types of electrode processes need to be distinguished in the present work:

1) Processes without adsorption of the reacting bromide species (unlikely here);
2) Processes with chemisorption of the reacting bromide species;
3) Processes with potential-dependent adsorption of reacting bromine intermediate species.

For each of these types, the following cases need to be considered:

a) No specific adsorption of supporting electrolyte ions;
b) Adsorption of supporting electrolyte ions involving ionic specific adsorption or physical adsorption of an uncharged substance (not involved here, except for the solvent H_2O molecules and possibly the reaction product, molecular Br_2).
c) Chemisorption of a species not participating directly in the

electrode process (not involved in the Br^-/Br_2 reaction case here), and

d) Adsorption or blocking of the surface by a reaction product, here Br_2 molecules or a thin liquid film of Br_2.

Attention will be also given to the following factors which can influence and complicate the reaction kinetics of Br_2 formation and the interaction of Br^- and Br_3^- with the electrode:

(a) the state of oxide film formation at the anode (Pt) at which Br^- discharge and Br_2 formation are occurring;

(b) competitive formation of the oxide film at Pt vis à vis Br^- deposition and Br^- adsorption;

(c) role of mass-transport of Br^- ion in its discharge and of Br_2 molecules away from the electrode in relation to anode current-density values; and

(d) adsorption or blocking of the electrode surface by Br_2 molecules formed in the reaction (as in c above) and their diffusion or hydrodynamic transfer away from the electrode, e.g. at a rotated disc electrode.

Chapter 3. EXPERIMENTAL

3.1. Electrochemical Systems Examined

Experiments on the Br_2 formation reaction in the present work have been mainly conducted in:

a) aqueous HBr (10^{-8}, 10^{-7}, 10^{-6}, 10^{-5}, 10^{-4}, 10^{-3} and 10^{-2} M) in $HClO_4$;

b) aqueous NaBr (0.5, 1, 1.5, 2, 2.5, 3 and 5 M) in $HClO_4$;

c) nonaqueous $CoBr_2$, $(CH_3)_4NBr$, $(C_2H_5)_4NBr$ and $(C_3H_7)_4NBr$ in CH_3CN; and

d) nonaqueous KBr in trifluoroacetic acid (TFA).

3.2. Cell

Studies of the bromine formation reaction were made in an all-glass 3-compartment cell with three electrodes, the working and counter electrodes and an appropriate reference electrode, Ag/AgBr. The electrical circuit, connected to the cell for steady-state polarization and potential relaxation measurements, is as shown in Fig. 6.

Concentrated sulphuric acid was used as a cleaning agent for soaking electrodes and the cell (often overnight), and double-distilled water was used for rinsing and solution preparation.

In order to be meaningful, potential measurements must be made relative to a stable reference electrode. This reference electrode takes the form of an electrochemical half-cell placed either directly in the solution examined or in a connecting but separate cell compartment, as in the present work. In this way, electrolytic contact with the test solution is made.

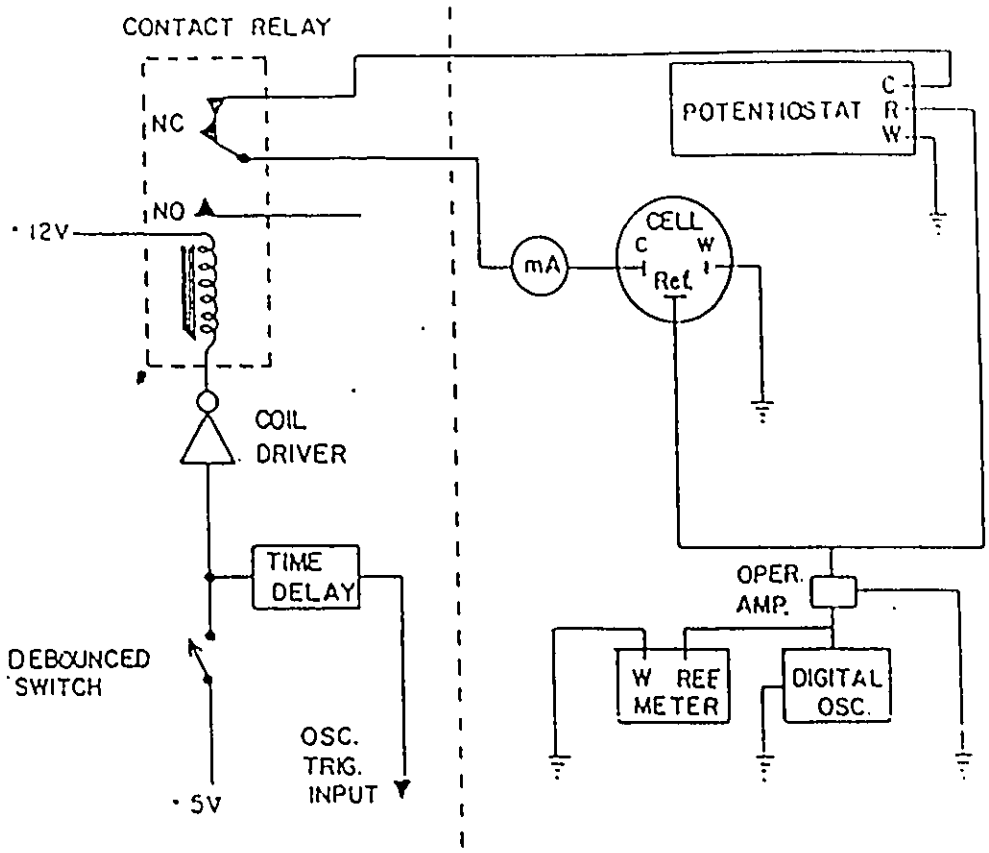

Fig. 6. Electrical circuit connected to the cell for steady-state polarization and potential relaxation measurements

3.3. Electrodes

3.3.1. Working Electrodes

3.3.1.a) Introduction

A Pt wire electrode or a platinum rotating disc electrode (Pt RDE) was used as the working electrode (WE) in the kinetic and adsorption studies.

Because of the corrosive nature of the electrochemical oxidative process involving Br_2 formation, platinum was chosen as

the preferred working electrode material for all experiments on the anodic bromine formation processes and because some previous works in the literature had been carried out at this metal. Platinum foil, wire or gauze can be used as an electrode and its physical form has no significance; however, it is desirable to make electrodes sufficiently large to maximize sensitivity of measurements.

There are normally two types of working electrodes that can be used:

a. stationary electrodes such as are employed in a quiet solution or in an externally stirred solution, as well as in flowing electrolyte; and
b. rotated disc electrodes (RDE) used at moderate or high rotation rates in order to provide high mass-transport rates of Br^- or Br_2 to or from (respectively) the electrode disc surface (see 3.3.1c below).

3.3.1.b) Pt Wire

At least one electrode design involved the incorporation of a Pt/Ag weld into the metal-glass seal. For making the seal, the easiest procedure is to use soft-glass tubing to mount the Pt wire; then, after careful annealing, the seal will be stable and vacuum-tight.

3.3.1.c) Pt RDE

In order to control and maximize mass-transport effects associated with Br_2 removal from the surface region of active electrodes, a number of experiments were conducted at a Pt disc

electrode rotated at 1600, 3600 and 6400, r.p.m., as well as at lower rates and 0 rpm (without rotation) for comparison.

The purposes of the experiments at a Pt RDE were:

1. To be able to control reactant mass-transfer to the electrode when Br^- diffusion control may be operative at low reactant Br^- concentration and/or with fast reaction kinetics.
2. To distinguish whether the approach to a limiting current density, i, is activation or diffusion-controlled.
3. To spin away a product of the reaction, e.g., Br_2, the reaction product in the present work, in the anodic bromine formation reaction.

Rotated electrodes allow controlled mass-transport conditions to be achieved when diffusion processes are involved at an electrode at which current-potential curve determinations are to be made. Under some conditions, diffusion control can be eliminated at sufficiently high rotation rates as the diffusion-layer thickness diminishes in proportion to the square-root of angular rotation velocity. However, with rapid, quasi-reversible systems, the rotated-disc electrode may supply insufficiently high-enough mass-transport rates that the electrochemical system shows mixed charge and mass-transfer control. Therefore, the reversible potential, E_r values may shift due to increasing irreversibility as increasing rotation rates allowed greater diffusion currents to pass with systems which are on the borderline of reversibility.

Usually a range of rotation rates is employed from 0 rpm (normal static condition) up to a maximum of 10,000 rpm. Quite often the required information can be achieved over a range 0 to ca. 5000 rpm especially as rates as high as 10,000 rpm may entail mechanical and hydrodynamic difficulties.

3.3.2 Counter Electrode

A platinized platinum gauze was used as the counter electrode (CE) in the cyclic voltammetry experiments.

In other types of experiments, a Pt counter electrode made from a platinum foil of thickness around 0.004 cm or more, and 1 cm^2 in area, was usually employed. The most convenient size of the electrode is ca. 2 × 0.5 cm^2, so that it is easy to insert the electrode into the electrode vessels. The foil is welded to a platinum wire which is sealed into a glass mounting tube, which serves as a physical support and provides electrical contact by means of a silver wire in the tube.

3.4. Reference Electrodes

The choice of an appropriate redox couple for use in a reference half-cell is limited. A suitable couple must be reversible, stable and unreactive in relation to any other components of the system in which it is used. The mercury-mercury(I) and the silver-silver(I) couples are very often used because electron transfer between the two oxidation states in both these cases is very rapid. Also, the components of these

two couples are neither strong oxidants nor strong reductants; hence, they are stable under most ordinary conditions.

An Ag/AgBr electrode was used as the reference electrode (RE) in the present work, both in aqueous and non-aqueous (acetonitrile) solutions.

For this electrode, an AgBr film is generated by anodic oxidation of Ag at an Ag metal electrode from a ~0.1 M KBr solution, sometimes made up with addition of some HBr. A somewhat low current density, 0.25 mA cm^{-2}, and a long period of electrolysis, ~40 min, are found most suitable for the preparation of the AgBr electrode. The colour of the fresh electrode varies from tan to yellow. The electrode is generally somewhat less stable than the corresponding chlorine/chloride electrode, but is capable ideally of ±0.2 mV reproducibility.

3.5. Solutions and Salts Used

3.5.1. Aqueous

Since the effects of specifically adsorbed Cl^-, Br^- and I^- ions are found to be detectable at Pt already at very low concentrations, it is useful to mention that some standard concentrated reagents, normally used for preparing supporting electrolyte solutions, can contain significant traces of halide ions (such as Cl^- in concentrated H_2SO_4 and particularly $HClO_4$), although traces of bromide ion are normally much less. In the present work, 0.1 M $HClO_4$ was used for most of the experiments.

Perchloric acid was chosen as the supporting electrolyte, mainly because the ClO_4^- ion is less specifically adsorbed at Pt than HSO_4^- in aqueous H_2SO_4 solutions. Also, cold and dilute aqueous solutions of perchloric acid are quite stable thermally and its reactions as an oxidizing agent are slow. However, at concentrations above 60%, the acid, is unstable and dangerous.

$HClO_4$ and HBr were the BDH high-purity reagents. NaBr and KBr, used as electrolytes, were the ACS analytical grade materials. The NaBr solutions in 0.1 M $HClO_4$ electrolyte were prepared from 0.1 to 5.0 M (0.1, 0.5, 1.0, 1.5, 3.0 and 5.0 M) Br^-. A micrometer pipette was employed to prepare HBr solutions in $HClO_4$ electrolyte at concentrations from 10^{-8} to 10^{-2} M (10^{-8}, 10^{-7}, 10^{-6}, 10^{-5}, 10^{-4}, 10^{-3}, 10^{-2}) Br^-.

3.5.2. Nonaqueous

$CoBr_2$, $(CH_3)_4NBr$, $(C_2H_5)_4NBr$, $(C_3H_7)_4NBr$, used as electrolytes, were the ACS analytical grade materials. Anhydrous CF_3COOH, used as a solvent in some experiments, was supplied by Aldrich Chemical Company.

Acetonitrile (BDH high purity reagent) was used as the aprotic solvent in certain comparative experiments in the present work. Its properties are very different from those of water (Table 3). However, the choice of acetonitrile as the nonaqueous solvent was because of its low chemical reactivity with Br_2 and the high positive potentials that can be attained without its anodic decomposition.

The anhydrous $CoBr_2$ had a green colour. Its saturated solution in CH_3CN was prepared by initially making up hot saturated solutions, allowing equilibration to room temperature for 6 hours, during which, the solutions were shaken periodically. It was interesting to see that the green anhydrous $CoBr_2$ turned sky-blue after it became solvated by CH_3CN. If the $CoBr_2$ crystals turns pink, there must be absorbed moisture.

TABLE 3. Comparison of Properties of CH_3CN and Water [62]

Structural formula	T_f (°C)	T_b (°C)	ϵ (at 25°C)
CH_3CN	-45.7	81.6	36.2
H_2O	0	100	79.0

As the solubility of NaBr in water is higher in cold water than that of most other bromide salts (Table 4), NaBr was favoured for the experiments involved in most of the work.

TABLE 4. Solubility of Some Bromide Compounds Employed

Inorganic	in cold H_2O	in hot H_2O
$CoBr_2$	66.7 g/100ml	68.1 g/100 ml
RbBr	98.0 g/100 ml	205 g/100 ml
NaBr	116 g/100 ml	121 g/100 ml
KBr	53.5 g/100 ml	102 g/100 ml

The saturated calomel electrode has often been used as the reference electrode in work involving nonaqueous solvents with

which Hg_2Cl_2 or Hg does not react. Also, Hg_2Cl_2 must not undergo any disproportionation. A soluble chloride must be found to replace the normally used KCl which has a limited range of solubility in most nonaqueous solvents. The slow diffusion of some water into the nonaqueous solution will occur and introduce undesirable effects in most cases. However, AgBr formed on an Ag wire is quite suitable for direct use in non-aqueous solutions containing Br^- ion and was the preferred reference electrode also for this part of the work.

3.6. Gas for Bubbling

Both aqueous and nonaqueous bromide ion solutions were bubbled with high-purity nitrogen gas that was passed through a gas purification line of the type used in our laboratory over the past 30 years (cf. refs. [1] and [26]) to eliminate aerial oxygen from the solutions. Because of the adsorption competition between bromine and oxygen at Pt electrodes, a solution without dissolved oxygen is preferred for the experiments on the anodic bromine formation reaction.

3.7. Measurement Techniques

3.7.1. Introduction

The following methods were applied in the experiments:

A. Steady-state Tafel polarization measurements (η vs. log i)— method for evaluation of the overall kinetics of the Br_2 generation process;

B. Non-steady state measurements — for adsorption information;

a) Cyclic Voltammetry — for evaluation of competitive adsorption of Br^- vis à vis oxide film formation;

b) Transient Techniques — recording of potential relaxation-transients, following interruption of current, for investigation of role of adsorbed intermediates;

c) Frequency Response — a.c. impedance measurements over a range of frequencies for evaluation of role of adsorbed intermediates and participation of tribromide species.

Developments in experimental technique since the end of the 1940's have made it possible to study electrode processes such as bromine formation more effectively than were the hydrogen and oxygen evolution reactions in earlier work, prior to that time. Special techniques are, however, required for the study of fast processes, because mass transport limitation (i.e. diffusion) to the electrode can become rate-controlling soon after the electrode processes start. Such conditions, if significant, conceal the role of the actual reaction mechanism in determining the overall rate of the process at the electrode.

Some of these difficulties can be overcome as a result of Levich's work (from the 1940's) concerning the effect of diffusion on the kinetics of electrode processes studied with rotated disc electrodes.

Similarly, important contributions to the study of kinetics and mechanisms of reaction can be made by means of impedance measurements using alternating current, a procedure introduced by Dolin, Ershler and Frumkin (1940) and applied by them to the

hydrogen evolution reaction at Pt.

3.7.2. Cyclic Voltammetry

From linear potential sweep modulation of the electrode potential, with recording of the response current, detailed information can be found on anion adsorption effects, and competitive oxide film formation and reduction processes. Also, from voltammetry with superimposed alternating voltage [61], the impedance can be obtained as a function of potential and is usually sensitive to pretreatment of the electrode surface and to contamination by impurities adsorbable on noble metal electrodes.

3.7.3. Tafel Relation Measurements

From Tafel measurements (η vs log i plots), the overall kinetics can be determined and whether they are activation (recombination or discharge) or diffusion controlled.

3.7.4. Potential Relaxation Measurements

Potential-relaxation curves can be recorded on open-circuit following interruption of the polarizing current of the electrode reaction, and their analysis enables the potential dependence of the pseudocapacitance associated with adsorbed intermediates in the reaction to be evaluated as well as (over short times) the double-layer capacitance. The time-scale of transients digitally recorded on a Nicolet oscilloscope was from μs to 10's of s.

3.7.5. A.C. Impedance Measurements

A.c. impedance measurements also provide complementary information on the evaluation of the kinetics of electrode processes and the interfacial capacitance of the electrode, as employed by Dolin, Ershler and Frumkin (1940) based on earlier experiments by Proskurmin and Frumkin (1937). These methods were further developed (from 1947 onwards) by Ershler, Randles, etc. and later by Sluyters and Sluyters, and by Armstrong, as well as by Bai and Conway more recently in this laboratory.

3.7.6. Procedures for Pt Electrode Pretreatments

Production of "fresh" electrode surfaces and "pre-oxidized" Pt surfaces were conducted according to a procedure described by Conway and Gu [63]. The "fresh", i.e. "freshly reduced" Pt electrodes were prepared in concentrated H_2SO_4, washed in distilled and pyrodistilled water and then subjected to potential cycling in cyclic voltammetry in order to check the cleanliness of their surface prior to their use in the Br_2 formation experiments. Any oxide species on the Pt surface were reduced by controlling the cycling potential range between 0.6 and 0.9 V (vs RHE), with the sweep programme being terminated in a negative-going potential sweep at 0.05 V, RHE.

The "pre-oxidized" Pt electrodes were prepared by pre-oxidizing their surfaces in Br^--free 0.1 M aqueous $HClO_4$ at 298 K at a potential of 1.6 V, RHE, for one hour with gradual 10 mV steps initially (see Fig. 7), that is, after previous potential

cycling in cyclic voltammetry, the potential was anodically increased by about 10 mV per second from 0.9 V to 1.6 V (vs RHE) and then the electrodes were held at 1.6 V (vs RHE).

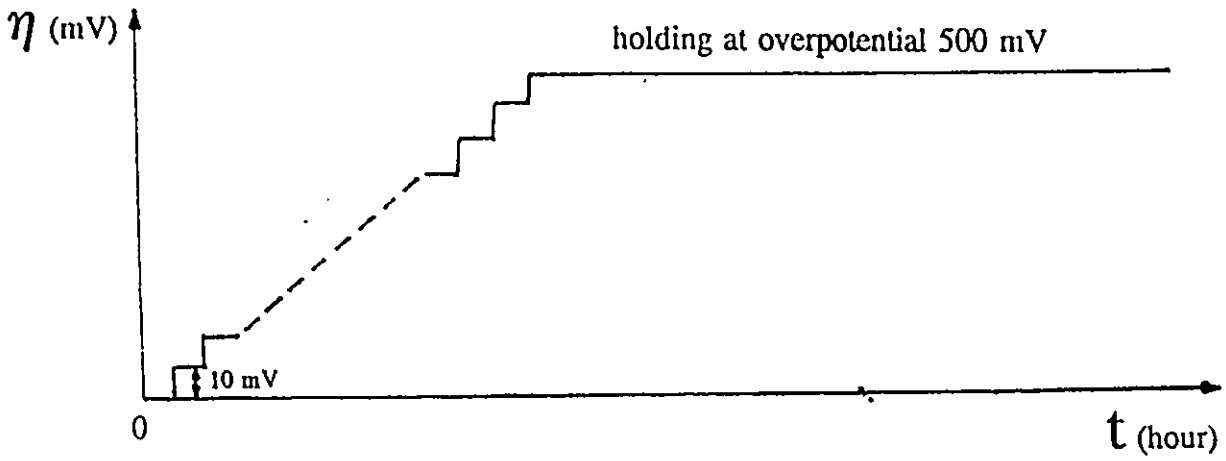

Fig. 7. Procedure for pre-oxidation of the Pt electrodes

The pre-oxidized electrode, thus prepared, was then transferred to the main experimental cell containing Br^- ion for the kinetic experiments of various kinds. Independent experiments in previous work showed that pre-formed oxide films on Pt could be thus transferred without loss of the oxide film.

3.8. Instrumentation Required for the Measurements

3.8.1. Cyclic Voltammetry

The apparatus employed for the cyclic voltammetry experiments was: a potentiostat (HA-301, Hokuto Denko Ltd), a function generator (PAR Model 175, Universal Programmer) which provides the required potential or current programming, a

digital oscilloscope (Nicolet 2090 or 310), a computer (HP 9000 series 200/300 or Zegna) and an HP Plotter (or HP laserjet III printer).

3.8.2. Tafel Relation Measurements

The apparatus used for recording Tafel plots was: a KEPCO Programmer, a KEITHLEY 195A Digital Multimeter, an HP computer 9000 (217) and an HP Plotter. Tafel relations and their shapes (since they were not linear) were determined for the bromine formation reaction by carrying out polarization studies under potentiostatic conditions over an appropriate range of controlled potentials and corresponding currents. Each curve was based on ca. 50~100 points.

3.8.3. Potential Relaxation Measurements

The apparatus employed for the recording of potential relaxation transients was: a potentiostat (HA-301, Hokuto Denko Ltd), a digital oscilloscope (Nicolet 2090 or 310), a computer (HP 9000 series 200/300 or Zegna) and an HP plotter (or an HP laserjet III printer). The potential-time transients were initiated by interruption of previously passing steady currents by means of a micro-switch with a triggering arrangement.

3.8.4. A.C. Impedance Measurements

The apparatus used for the a.c. impedance measurements was: a Solartron Schlumberger 1286 Electrochemical Interface or an EG & G Princeton Applied Research—Potentiostat/Galvanostat, Model 273, a Solartron Schlumberger 1250 (or 1255 HF) frequency-

response analyzer, an HP computer 9000 (216) or a Zegna computer and an HP 7470A/Color Pro plotter.

3.9. Brief Discussion of Measurement Reliability and Precision

Neither the significance of the double layer-capacitance nor the presence of a charging current in non-steady-state electrochemical experiments can be neglected so, in such experiments, "double-layer charging" corrections have to be applied. Also, the experimental results obtained by the above instrumental procedures have certain margins of error, either intrinsic or random, that can usually be reasonably estimated.

Due to Br_2 and Br_3^- formation, the Br^- concentration can become changed, but only to a small extent, from its initial value. In addition, the Ag/AgBr reference electrode requires a constant bromide concentration for provision of an accurate reference potential. Potentials of the Ag/AgBr reference electrodes used were checked periodically against the RHE.

The conditions under which the maximum precision in the experimental results could be achieved were carefully monitored to avoid erroneous readings. The instrumentation was operated within its known range of accuracy, at settings for which a given error or uncertainty in measurements would cause the least uncertainty in results. Instruments were kept in good calibrated condition to attain optimum precision, with percentage uncertainty on the order of better than 0.1% of total respective scales.

3.10. iR-Drop Correction

It is normally desirable to employ a three-electrode system which serves to complete the electrochemical measurement system. The potential of the working electrode is measured with respect to a reference half-cell, the third electrode of the system.

When the potential of an electrode of interest is measured against a nonpolarizable reference electrode during the passage of current, an iR_s potential drop will normally be unavoidably included in the measured potential, proportional to the polarizing current passing, where R_s is the solution resistance between the working electrode and the tip of the reference electrode probe. On open-circuit (i = 0) the potential of the electrode is an equilibrium value, E_{eq} (volts vs. reference electrode) or a stationary one. By applying an external potential of magnitude E_{appl} with a power supply, a current is forced through the cell and the potential of the electrode will shift to a new value E (volts vs. reference electrode). The relation of E to $E_{appl.}$ is:

$$E_{appl} = E + iR_s = E_{eq} + \eta + iR_s \qquad (9)$$

where η is the current-dependent overpotential.

The term iR_s is the ohmic potential drop (colloquially, the "iR-drop") in the solution between the tip of the Luggin reference probe and the working electrode; however, it should not be regarded as a form of overpotential, since it is a

characteristic of the bulk solution and the geometry of the cell and not of the electrode reaction. Its contribution to a measured electrode potential can be minimized or compensated for by proper cell design, instrumentation and/or calculation.

It is important to note that it is not always possible to eliminate all the iR_u drop by means of a three-electrode cell with Luggin capillary connection to the reference electrode. Although the tip of the reference electrode is designed for very close placement to the working electrode surface by means of a fine capillary tip, the so-called Luggin-Haber capillary, some small uncompensated solution resistance usually remains.

The exact potential profile in an actual cell depends on the electrode shapes, geometry, solution conductance, etc. The solution between the electrodes can be thought of as a potentiometer. For the reference electrode, placed anywhere but exactly at the electrode surface, some fraction of the overall iR_s (also called iR_u, which is the "uncompensated" solution resistance) will be included in the measured potential.

The uncompensated potential drop can usually be taken into account in steady-state measurements, e.g., by measurement of R_u with point-by-point computer correction, at any given i, of the measured potentials, or by an analogue compensator.

In the present work, iR_u drop correction was applied to all the measurements at appropriate current-densities. iR_u can be determined conveniently from open-circuit potential decay transients, recorded on an oscilloscope, following interruption

of current. Upon interruption of a polarizing current, the rate of decline of potential, -dE/dt, is determined by the interfacial capacitance, C_{dl}, and the previously passing current (see 4.2.3).

3.11. Data Collection and Processing by Means of Computers and Digital Oscilloscopes

The intensive development of digital computers from the 1960's to the present time has provided inexpensive digital devices of wide variety which have found many applications in electrochemical instrumentation. These range from the use of logic circuits for timing and control in hybrid analog–digital circuitry, to the use of minicomputers for on-line control of experiments, data acquisition and data analysis or processing. Such systems were used in the present work, employing IBM PC clones.

In the case of the potential transient experiments, data collection and recording over 6 to 7 decades of time was effected by means of two Nicolet digital oscilloscopes in tandem, For the a.c. impedance spectroscopy, the Solartron provides a digital analysis of the real and imaginary components of the impedance vector. Subsequent fitting of the data to equivalent-circuit or kinetic models is conducted by means of computers, e.g. employing so-called "Z-plot" software and some in-house software developed in our laboratory by Dr. L. Bai.

Chapter 4. ELECTROCHEMICAL KINETICS AND THE ROLE OF ADSORBED INTERMEDIATES

4.1. General Aspects

It has been emphasised earlier that the Br_2 formation reaction involves adsorption of at least one intermediate, $Br^{\cdot}$, and possibly a second, $Br_3^{\cdot}$. The potential-dependence of coverage by these species will hence be important in considering the electrode-kinetics of the overall reaction.

It will therefore be desirable, with regard to discussion and interpretation of the results to be presented in chapter 5, to give first the theoretical basis of treatments of electrode kinetics, potential relaxation and a.c. impedance methods employed in much of this work in so far as they apply to a reaction involving adsorbed intermediates. The following sections outline the general concepts and principal equations that are involved.

An electrochemical multi-step reaction generally occurs via the following consecutive steps which constitute its "mechanism":

1. Mass-transfer (diffusion) from the bulk of the solution to the layer in contact with the electrode, replacing those ions/molecules that have just undergone chemical change in the electrode process;

2. Adsorption of ions or molecules in the region of the interfacial double-layer;
3. Dehydration of the ion, coupled with electron transfer and adsorption of a discharged intermediate, giving rise to:
4. Adsorption of the primary product(s) of the electrochemical process on the metal;
5. Desorption of the primary product;
6. Departure of the overall product(s) from the surface of the metal by diffusion or in a further polarized charge-transfer step (in certain cases), or gas bubble formation or migration to growth centres, in the case of solid phase formation;
7. In most cases, removal of the final product occurs by diffusion into the bulk of the electrode, e.g., Br_2 going into the solution as Br_3^- or dissolved Br_2.

The adsorption behaviour of kinetically-involved intermediate species[2], in a multi-step electrode reaction may be treated in terms of either:

(1) the "quasi-equilibrium hypothesis" in which all steps prior to the rate-determining one in the reaction sequence are regarded as being almost in equilibrium. This condition arises if the rate constant of the rate-determining step is

[2]Here the case of intermediates that are formed in an *adsorbed* state is considered; however, many complex, multi-step organic electrochemical reactions involve intermediates that pass into solution, e.g. radical anions or cations, and subsequently undergo further heterogeneous reactions at the electrode or homogeneous ones in solution. This is not, it is believed, the case in the reaction of Br_2 formation treated in this thesis.

at least ten times smaller than those for the antecedent steps in both directions; or

(2) the "steady-state method" in which the rate of change of concentration of intermediates with time is equated to zero. This second approach is preferred but, for some mechanisms, e.g., recombination, the expressions are cumbersome so that numerical computing is required in order to derive the theoretically predicted behaviour. Limiting cases for (2) are equivalent to those derivable on the basis of the assumption in (1).

4.2. Tafel Relations and Coverage by an Intermediate: Steady-State Relations

4.2.1. Introduction

It is well known that most electrochemical reactions (except one-electron ionic redox processes) proceed by at least two consecutive steps, and may involve alternative pathways in some cases, as in the case of Br_2 generation in the present work. The rate-determining step is the step whose rate constant is the smallest of those in the series of consecutive reactions in multi-step process. In alternative pathways, the rate-determining step arises in the pathway associated with the largest velocity. Since the electrochemical rate constants of various steps depend on potential, a rate-determining step at one potential may not necessarily be kinetically limiting at

another potential.

As mentioned in chapter 1, among the halide → halogen reactions, the electrochemical kinetics and mechanisms of the bromide/bromine system sometimes behave more like the chloride/chlorine, and other times more like the iodide/iodine kinetics.

The kinetics of the Br^-/Br_2 reaction formally follow the same kinetic equations as those for cathodic H_2 or anodic Cl_2 evolution. Thus (cf. 1.1.4.), a discharge step producing a chemisorbed intermediate (here $Br^\cdot$) is followed by one of two alternative $Br^\cdot$ desorption steps: an electrochemical, and thus potential dependent one — step **IIb**, as in chapter 5, or a chemical catalytic recombinative one — step **IIa**, as in chapter 5. The latter step, since it involves no electron transfer, is not directly potential dependent. However, the coverage, $\theta_{Br^\cdot}$, of the intermediate *is* potential-dependent and, when a Langmuir-type isotherm applies, $\theta_{Br^\cdot}$ is given by

$$\frac{\theta_{Br^\cdot}}{1 - \theta_{Br^\cdot}} = KC\exp\frac{\eta F}{RT} \qquad (10)$$

or for a Frumkin-type one

$$\frac{\theta_{Br^\cdot}}{1 - \theta_{Br^\cdot}} \exp(g\theta_{Br^\cdot}) = KC\exp\frac{\eta F}{RT} \qquad (11)$$

based on ref. [27] and ref. [64]. The overall recombination rate or equivalent current-density, i, is then potential dependent up to a limiting rate corresponding to $\theta_{Br^\cdot} \rightarrow 1$, i.e.,

full occupation of available surface sites by the intermediate $Br^{\cdot}$.

In both equations (10) and (11), the isotherms arise from the assumption of quasi-equilibrium in the discharge step **I** producing adsorbed $Br^{\cdot}$; in this way, the above relations are Nerstian equations (in exponential form) for the coverage fraction $\theta_{Br^{\cdot}}$ as a function of potential for the condition that adsorption of $Br^{\cdot}$ and its desorption in step **I** (see chapter 5) are virtually at equilibrium, a following step being rate-controlling.

Then the overall rate equations for the Br_2 formation reactions are easily written for the cases of step **I**, **IIa** or **IIb** being rate-controlling. In the latter two cases, the *faster* of the two alternative desorption steps will dominate the overall kinetics when the rate constants for either **IIa** or **IIb** are smaller than that of step **I**.

Then for step **IIb** being rate-controlling

$$i_{2b} = 2Fk_{2b}C_{Br^{\cdot}}\theta_{Br^{\cdot}}\exp(\beta\eta F/RT) \qquad (12)$$

where $C_{Br^{\cdot}}$ is the bulk concentration of $Br^{\cdot}$ in solution and k_{2b} is an electrochemical rate constant for $\eta = 0$ and containing any double-layer potential terms for the potential profile at the electrode interface and for the local concentration of $Br^{\cdot}$ at the inner Helmholtz plane (Grahame [36], 1947).

Substitution of $\theta_{Br^{\cdot}}$ (Langmuir condition) here, from eqn. (10), gives the overall kinetic equation

$$i_{2b} = 2Fk_{2b}C_{Br^{\cdot}} - \frac{K_1 C_{Br^-} \exp(\eta F/RT)}{1 + K_1 C_{Br^-} \exp(\eta F/RT)} \exp\frac{\beta \eta F}{RT} \qquad (13)$$

where K_1 is the quasi-equilibrium constant for step **I** at $\eta = 0$.

Two well-known cases arise from this equation for conditions:

(a) where η is relatively small ($K_1 C_{Br^-} \exp \eta F/RT \ll 1$), so that

$$d \ln i_{2b}/d\eta = (1 + \beta)F/RT \qquad (14)$$

or

(b) when η is large ($K_1 C_{Br^-} \exp \eta F/RT \gg 1$), so that

$$d \ln i_{2b}/d\eta = \beta F/RT \qquad (15)$$

These are the inverse Naperian Tafel slopes for these conditions, with step **IIb** rate-determining and much faster than step **IIa**.

For step **IIa** being rate-determining,

$$i_{2a} = 2Fk_{2a}\theta^2_{Br^{\cdot}} \qquad (16)$$

Then substituting again for $\theta_{Br^{\cdot}}$ in terms of its potential dependence (eqn. 10), the inverse Tafel slope derivatives are

$$d \ln i_{2a}/d\eta = 2F/RT \qquad (17)$$

for small η ($\theta_{Br^{\cdot}} \ll 1$) and

$$d \ln i_{2a}/d\eta \rightarrow 0 \quad (d\eta/d \ln i_{2a} \rightarrow \infty) \qquad (18)$$

for large η with $\theta_{Br^{\cdot}} \rightarrow 1$.

Corresponding forms of these relations are easily obtainable if a Frumkin-type isotherm (eqn. 11) represents the electrochemical adsorption of $Br^{\cdot}$ at coverages where significant lateral interactions arise, usually for $\theta_{Br^{\cdot}} >$ ca. 20 %. Note

that in a square, "(100)" type lattice, adsorbate species are already diagonal nearest neighbours at $\theta = 0.5$.

In the case of step I being rate-determining, it is usually justifiable to assume that $\theta_{Br} \ll 1$, i.e., $1 - \theta_{Br} \rightarrow 1$ so that d ln $i_1/d\eta$ is simply $\beta F/RT$, the same value as for step **IIb** at high θ_{Br}, assuming the barrier-symmetry factors for steps **I** and **IIb** are approximately the same, which may not always be the case.

Finally, it can be noted that the limiting cases deducible by means of the "quasi-equilibrium hypothesis" may be obtained more generally by means of the steady-state method, with introduction of appropriate limiting conditions.

It is seen that for multi-step reactions involving an adsorbed intermediate, the overall kinetic behaviour of the process *is importantly determined by the potential-dependence of the coverage θ by the intermediate*, expressed by some adsorption isotherm such as eqn. (10) or (11). In general, when θ is dependent on some function of potential, a Tafel slope for the process will have a lower value than:

a) that for initial discharge control, or

b) that for full coverage where θ is no longer dependent on potential.

For a reaction scheme involving n charge-transfer events (at quasi-equilibrium) prior to the rate-determining step (for most electrode reactions $n \neq 3$), the limiting values of the Tafel slopes work out to be

$$b' = RT/(n + \beta)F \quad (i.e., \ \alpha = n + \beta)$$

or

$$b' = RT/nF \quad (i.e. \ \alpha = n)$$

depending on whether or not charge-transfer is involved in the final rate-controlling step. "Chemically-controlled" rate-determining steps have Tafel slopes determined by even fractions of RT/F, while those that involve a charge-transfer process in the rate-controlling step have slopes that are odd fractions of RT/F, depending on the values of n and β.

The experimental evaluation of the potential dependence of coverage θ by the electroactive intermediates in the reaction is important for relation to reaction mechanisms and determines the Tafel slope b of the process representing the dependence of ln i on the overpotential η. For desorption of an electroactive adsorbed intermediate at potential-dependent coverage θ, e.g. by the electrochemical pathway, **IIb**, the reciprocal of the Tafel slope can be expressed by:

$$1/b' = d \ln i/d\eta = d \ln \theta/d\eta + \beta F/RT \qquad (19)$$

The first term on the right side of the equation can be recognized as an "adsorption factor" and the second term as the "charge-transfer factor". When $d \ln \theta/d\eta$ is significant, for an appreciable and potential-dependent θ, b' is « $RT/\beta F$. This situation corresponds to "good electrocatalysis", i.e., when the process exhibits a relatively large rate of increase of ln i with η.

The determination of b', through b'^{-1} in the equation above

in terms of chemisorption effects has been treated by Conway et al [65—67], who have stressed that the term d ln $\theta/d\eta$ is as important as i_0 in characterizing good electrocatalysis especially at relatively high current-densities in practical electrolytic processes.

It is important for aspects of the present experimental work to note that the derivative of θ with respect to η gives an expression for this potential-dependence

$$d \ln \theta/d\eta \equiv (1/\theta)(d\theta/d\eta) \qquad (20)$$

which is, in fact, proportional to the adsorption pseudocapacitance, C_ϕ (eqn. 21), which is a quantity experimentally accessible from potential-relaxation or a.c. impedance measurements as described in sections 3.7.4 and 3.7.5.

As noted elsewhere (4.2.3)

$$C_\phi = q_1 d\theta/d\eta \qquad (21)$$

where q_1 is the charge required for deposition or desorption of a monolayer of the adsorbed intermediate.

Returning to the Tafel slope for an electrochemically-controlled desorption step such as **IIb**, it follows that d ln $i/d\eta$, the reciprocal of the Tafel slope, is given by eqn. 19, and since

$$d \ln \theta/d\eta = \frac{1}{\theta}\frac{d\theta}{d\eta} = \frac{1}{\theta} C_\phi/q_1 \qquad (22)$$

then

$$\frac{1}{b} = d \ln i/d\eta = \frac{1}{\theta} C_\phi / q_1 + \beta F/RT \qquad (23)$$

which shows how the adsorption pseudocapacitance can be seen to be involved in determining the Tafel slope.

4.2.2. Applications to the Br_2 Formation Reaction

The case of the Br_2 formation reaction provides an example of an overall electrode reaction that involves at least two steps with two or more parallel pathways involving, as noted on p.62, an adsorbed intermediate (see reaction schemes as in chapter 5), as for the H_2 and Cl_2 evolution processes.

The chemisorption of bromide ions and the kinetics of their anodic discharge to form bromine molecules depend both on the strength of adsorption and coverage by the bromide ion itself, and of the discharged $Br^{\cdot}$ intermediate. In the present work, an important aspect has been the study of how the adsorbed bromide anion affects the state of thin oxide film formation at the Pt anode surface which, in turn, influences its electrocatalytic properties for discharge/adsorption of $Br^{\cdot}$ and for Br_2 formation.

In addition, the coverage by the $Br^{\cdot}$ intermediate has been quantitatively evaluated in the present work as a function of η (see section 5.1) in relation to the kinetics of the overall reaction and the pseudocapacitance C_ϕ (eqn. 21).

4.2.3. Potential Dependence of Current and Coverage by an Intermediate, Non-Steady-State Relations: Potential Relaxation Transients

Here we consider the case of overpotential relaxation in

time, t, following interruption of a prior steady-state density of current, i. As is shown below, analysis of the resulting transient $\eta(t)$ leads to information on the capacitance of the electrode interphase, as determined in the present work.

In order to derive the time-dependence $\eta(t)$ (i.e. the potential-relaxation transient) of (over)potential, η, following interruption of a previous polarization current-density, i, the equation for self-discharge of the interfacial capacitance and the potential dependence of i (Tafel relation) are combined.

On interruption of a polarizing current, the rate of decline of overpotential, $-d\eta/dt$, is determined (eqn. 24) (at that moment) by the interfacial capacitance C and the current immediately previously passing, determined by the kinetics of the reaction:

$$i = -C(d\eta/dt)_{t=0} \qquad (24)$$

The current at any $\eta(t)$ during the transient is then assumed to be equal to the value of the steady-state current, i_{ss}, which would have been passing at the same η as determined by the Tafel relation for the electrode process. If the prior steady-state current is i_{ss} and obeys the Tafel equation, and C is assumed to be independent of potential, the potential relaxation relation (eqn. 24) becomes

$$i_{ss} = i_0 \exp(\beta F\eta/RT) = -Cd\eta/dt \qquad (25)$$

The above equation may be integrated, giving

$$\eta(t) = (RT/\beta F)[\ln(\beta F i_0/CRT) - \ln (t + \tau)] \qquad (26)$$

where τ is an integration constant:

$$\tau = RTC/\beta F i_0' \exp(\beta F \eta_0/RT) \qquad (27)$$

where β is the charge-transfer symmetry coefficient and i_0 the exchange current-density. η_0 is the initial overpotential at time t = 0, when $i = i_{ss}$.

Thus, from eqn. (26), the potential relaxation $\eta(t)$ is *logarithmic* in modified time $(t + \tau)$ provided C is independent of potential. However, in many cases it is not. It is seen that the slope $-d\eta/d \log(t + \tau)$ is the same as the Tafel slope.

A corresponding relation involving $-d\eta/dt$ follows directly by taking logarithms of eqn. (25), viz.

$$\ln i'_0/C + \beta\eta F/RT = \ln[-d\eta/dt] \qquad (28)$$

or

$$\eta = -(RT/\beta F)\ln[i_0/C] + (RT/\beta F)\ln[-d\eta/dt] \qquad (29)$$

which is seen has the same slope as the Tafel equation for the kinetic process involved.

From the above it is seen that plots of both η <u>vs</u> log $(t+\tau)$ and η <u>vs</u> log $(-d\eta/dt)$ are useful for characterizing the electrode process and obtaining the interfacial capacitance behaviour through C.

For the condition that a single relaxation time is observed in a corresponding impedance measurement, the new potential relaxation treatment has been demonstrated in other work from this laboratory [68] to provide a quantitative evaluation of the electrode's interfacial double-layer capacitance by determination of the *initial* rate of decay of potential, $(d\eta/dt)_{t=0}$, determined immediately following the opening of the

circuit (eqn. 24).

Because θ is a function of overpotential, $\theta = f(\eta)$, a different kind of capacity quantity can be defined, as in eqn. (30)—see below. This adsorption pseudocapacity cannot exist at an ideal polarized electrode which exhibits only an electrostatic double-layer capacity. The prefix "pseudo" is used because C_ϕ refers to a leaky capacitor at which some chemisorbed species is faradaically discharged; in the case of UPD processes, no continuous faradaic reaction takes place. The pseudocapacity is proportional to the rate of change of coverage with potential, as in eqn. (21).

Under Langmuir conditions for θ_{Br^-}, C_ϕ follows from the electrochemical Langmuir adsorption isotherm (eqn. 10) as

$$C_\phi = \frac{(q_1 F/RT)[K_1 C_{Br^-}\exp(F\eta/RT)]}{[1 + K_1 C_{Br^-}\exp(F\eta/RT)]^2} \qquad (30)$$

where $K \equiv K_1$ and $C \equiv C_{Br^-}$.

C_ϕ can also be expressed as a function of coverage by

$$C_\phi = (q_1 F/RT)[\theta(1 - \theta)] \qquad (31)$$

using eqn. (10); from eqn. (31) it is seen that C_ϕ is a maximum when $\theta = 0.5$.

In the case where a Frumkin type isotherm applies, θ cannot be written as an explicit function of overpotential η, but C_ϕ can, however, be expressed as a function of θ as

$$C_\phi = (q_1 F/RT)[\theta(1-\theta)]/(1 + g\theta) \qquad (32)$$

From the relation $C_\phi = q_1 d\theta/d\eta$, $q_1 \int d\theta = \int C_\phi(\eta)\, d\eta$; therefore,

$$\theta_{Br\cdot} = (1/q_1) \int C_\phi d\eta + \theta_0 \qquad (33)$$

where θ_0 is an initial coverage at $\eta = 0$, i.e., the surface coverage at equilibrium.

The C_ϕ vs η (or E) relation can be experimentally obtained using the potential-relaxation method; therefore the integration of the C_ϕ vs η (or E) relation can be made numerically, and $\theta_{Br\cdot}$ can be evaluated as a $f(\eta)$ (relative to $\theta_{Br\cdot,\eta=0}$, $\equiv \theta_0$).

From the overall $\eta(t)$ transient, C_ϕ can be derived from the behaviour at longer times (> ca. 10 ms). This is because the double-layer discharge normally has a much shorter relaxation time (μs to 100's μs) than the pseudocapacitance (10's ms to s). This corresponds to the usually observable distinction in frequency-domain response (see section 4.4) of these two types of interfacial capacitance.

4.3. Cyclic Voltammetry Studies of Electrode Processes

In the cyclic voltammetry technique, the rate of an electrode process is modulated in a repetitive way by linear variation of the potential, E, in time, in both the anodic and cathodic directions and the corresponding currents are recorded as a function of the varying potential. A kind of "electrochemical spectroscopy" of the processes that can occur over the scanned potential range results. Two kinds of information result from application of this procedure at an electrode interface: a) information on electrochemically formed, adsorbed species in the underpotential deposition region

and b) kinetic information on the electrode processes involved.

Kinetic information can be derived as follows:

a) by analyzing the forms of the resulting i vs E profiles;

b) by relating potentials of current peaks to log [sweep-rate], which leads, in certain cases, to a Tafel-like linear plot for an irreversible process, thus characterizing its kinetics; and

c) by means of computer-based numerical simulations.

When an adsorbed species is generated electrochemically on a surface such as Pt in the absence of a continuous faradaic process (as in the cases of UPD of H or O species at Pt), cyclic voltammetry provides a sensitive way of deriving the coverages by the electrosorbed species and their adsorption in various sub-monolayer states, as a function of electrode potential. Thence the electrochemical adsorption isotherm for such species can be evaluated.

It should be noted, however, that the coverages by electrosorbed species (such as $Br^{\cdot}$ in the present work) arising in most *continuous* faradaic reaction proceeding at finite overpotentials and corresponding appreciable net current-densities, *cannot* be evaluated by means of cyclic voltammetry. The reason for this is that the non-steady current contribution arising from changes of coverage by the electroactive adsorbed intermediate(s) with changing η, e.g. $Br^{\cdot}$ in the Br_2 formation reaction, are much smaller (10^5 ~ 10^3 times) than the overall faradaic currents arising from the reaction itself. For this

reason, only other types of experimental procedures are applicable, viz. non-steady-state methods, e.g., pulse, current-interruption and impedance spectroscopy are required, as mentioned earlier in 3.7.

However, cyclic voltammetry as applied in the present work, provides useful information on: a) the competition between Br^- chemisorption and electrosorption of OH/O species in Pt surface oxidation and, related to that, b) the conditions for onset of continuous faradaic Br_2 formation.

4.4. Frequency Response of the Reaction: A.C. Impedance Spectroscopy

4.4.1. General

Two principal types of results that arise from application of a.c. techniques to the study of electrode processes are:

1. description of the electrical behaviour of the system in terms of impedance parameters, which can be interpreted in terms of physico-chemical phenomena and kinetics (rate constants) of the reactions; and
2. provision of an electrical description of the system which enables comparison to be made between the behaviour of a model "equivalent circuit" with that observed experimentally, e.g., with respect to frequency-response of the impedance components of the system and of the overall network. The required simulations of the frequency response

can be carried out relatively easily by means of PC's.

Regarding the methodology of a.c. studies on electrode interfaces and electrode processes, the key early contributions were made by Frumkin, Dolin and Ershler [95] and by Randles [20] in proposing his "equivalent circuit", which combines the elements of charge-transfer, diffusion, double-layer capacitance and electrolyte conductivity (solution resistance). The work of Randles is to be considered as the seminal contribution in the treatment of frequency—response of electrode processes. An important and complementary approach is that of Timmer, Sluyters-Rehbach and Sluyters [69] who showed how the impedance of an electrode process could be treated in terms of real (Z') and imaginary (Z") components, with one being plotted against the other in a "complex-plane" or Argand diagram, for various frequencies. This approach often enables the solution resistance, the (potential-dependent) Faradaic resistance and the double-layer capacitance to be identified from a single plot of Z" vs Z', or a series of plots for different potentials. Also, in appropriate cases, the impedance contribution from the adsorption pseudocapacitance can be separately identified, and its frequency response characterized.

4.4.2. Equivalent-Circuit Representation of Electrode Processes

The response of adsorbed electroactive species in a.c. impedance measurements is taken into account by inclusion in the equivalent circuit representing the electrode reaction [67], of an "adsorption capacitance" component in parallel with an

adsorption resistance (when or if diffusion is involved, a Warburg impedance W is in place of R_2 in Fig. 9) and in series with a faradaic charge-transfer resistance together with the double-layer capacitance. The resulting equivalent circuit (Fig. 9) then differs from the simple one (Fig. 8) representing a faradaic charge-transfer process, characterized by a reaction resistance R_1, not involving potential-dependence of coverage (i.e. C_p) by an intermediate.

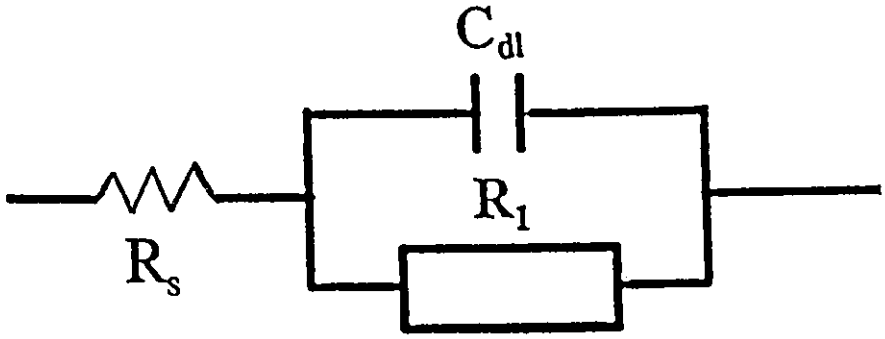

Fig. 8. Simple equivalent circuit

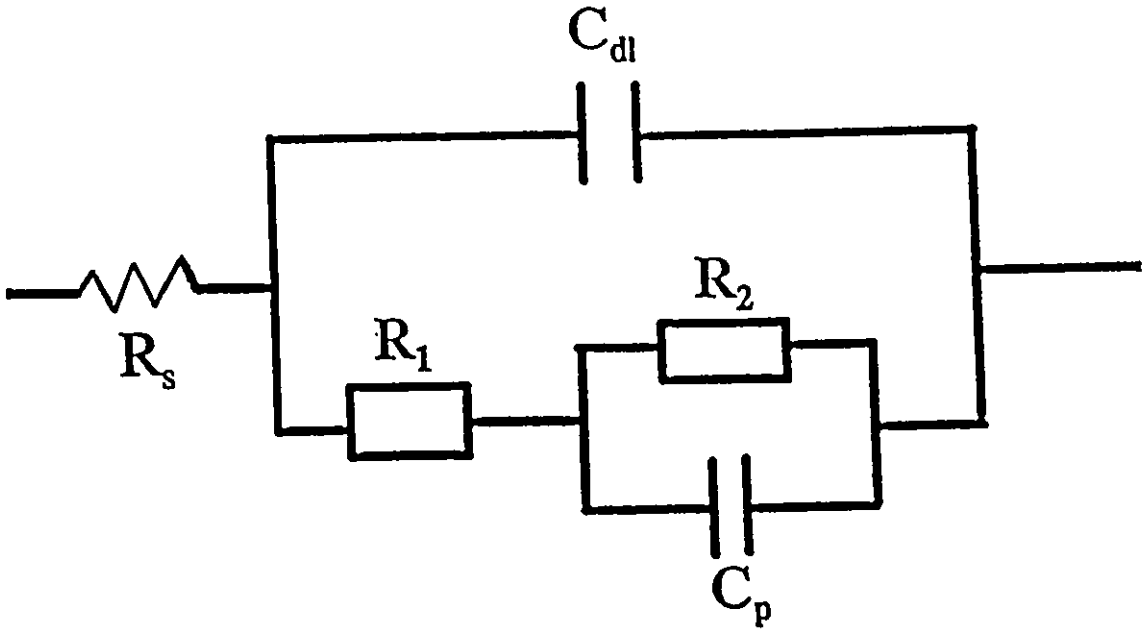

Fig. 9. Armstrong's equivalent circuit involving a pseudocapacitance, written as C_p

A solution resistance R_s also usually arises in series with the faradaic impedance and depends on cell geometry and on the nature and conductance of the electrolytes present; it may be sufficiently small that it can be neglected (< 1 Ω), but its value depends on electrolyte concentration and temperature.

4.4.3. Influence of Frequency

In order to provide a basis for interpretation of the impedance results for the Br_2 formation reaction to be described in chapter 5, we outline here the main principles of impedance analysis that are used in the treatment of the results.

Determination of the frequency response of an electrode reaction over a wide range of frequencies is the principal objective of a.c. impedance measurements. The frequency response can be represented in three complementary ways: a) in complex-plane plots of the imaginary (Z") vs the real (Z') component of the impedance vector, Z, for a series of angular frequencies, ω; b) as phase-angle, ϕ ($\tan \phi = -Z''/Z'$), plots as a function of ω or $\log \omega$ and c) as Bode plots of $Z=[(Z'')^2+(Z')^2]^{1/2}$ vs $\log \omega$.

The frequency response is interpreted in terms of either (or both) the behaviour of equivalent circuits written to represent the functioning of the electrode process or kinetic modelling in terms of rate equations [70,71].

In the simplest case (Fig. 8), the interfacial process is described by only a faradaic resistance (R_t) and a double-layer capacitance. The complex-plane plot (Z" vs Z') is then a single

semicircle over the instrumentally accessible frequency range, 0.01 to 65,000 Hz, depending on the values of the circuit elements.

In the case of Armstrong's equivalent circuit (Fig. 9), a two semicircle complex-plane plot will arise again over the accessible frequency range 0.01 to 65,000 Hz, and again depending on the values of the circuit element components.

4.4.4. Low- and High-Frequency Limit Behaviour

It is always useful to examine the frequency-response behaviour of equivalent circuits for limiting frequency conditions, $\omega \rightarrow 0$ or $\omega \rightarrow \infty$, as applied in chapter 5. The limiting behaviour of equivalent circuits at $\omega \rightarrow 0$ or $\omega \rightarrow \infty$ is determined principally by the behaviour of capacitive elements, usually C_{dl}. The impedance of C_{dl} is simply $Z = 1/j\omega C_{dl}$ which approaches ∞ for $\omega \rightarrow 0$, or zero for $\omega \rightarrow \infty$. Hence, for the simple equivalent circuit in Fig. 8, $Z \rightarrow R_s + R_1$, for $\omega \rightarrow 0$ (purely ohmic) while for $\omega \rightarrow \infty$, R_1 is "shorted-out" by $Z_c \rightarrow 0$, so $Z \rightarrow R_s$. Hence, in the complex-plane plot, intercepts of $Z' = R_s$ and $Z' = R_s + R_1$ appear on the Z' axis at ∞ and 0 ω, respectively. The characteristic frequency of the top point of the semicircle is $\omega = 1/C_{dl}R_1$.

In the case of the equivalent circuit of Fig. 9, for $\omega \rightarrow \infty$ Z' is simply the sum $R_s + R_1 + R_2$. Two semicircles arise, determined by the values of the two C's, and the two other intercepts that arise on the Z' axis correspond to $Z' = R_s$ ($\omega \rightarrow$

∞) and $Z' = R_s + R_1$ at an intermediate value of ω.

These principles apply to the experimental frequency response curves obtained in the present work, as shown in chapter 5.

In the case of a diffusion-controlled process, characterized by the presence of a so-called Warburg "CR" element W in the equivalent circuit (e.g. cf. Fig. 3, p.31), the complex-plane plot becomes a straight line of slope 45° at low frequencies, following a single semicircle, or part thereof, for the simple equivalent circuit case (with W), as was illustrated by Cooper and Parsons' results in Fig. 4. Thus, as frequency rises, the charge-transfer resistance R_1 together with R_s and the C_{dl} become the more important elements determining the impedance.

In general, if diffusion is a significant rate-limiting process in the kinetics of the overall reaction at the electrode, in the lower-frequency region, the Warburg impedance will become important (Fig. 3—p.31 and Fig. 4—p.32) and determine the frequency response.

At relatively high frequencies, the Warburg and the double-layer impedances become unimportant in determining Z in relation to R_1 or $R_1 + R_s$, as described above.

4.4.5. Application to Real Systems as for the Br_2 Formation Reaction

Actual plots of impedance behaviour (see chapter 5) are the combinations of the features of the limiting cases for both lower and higher frequency regions. The frequency response of the electrochemical interface, and the reaction going on across

it, is conveniently represented in terms of the three types of plots mentioned in 4.4.2:

a) the complex-plane plot of Z" vs Z' over a range of frequencies, with intercepts at $\omega \rightarrow 0$ and $\omega \rightarrow \infty$;

b) the Bode plot of $|Z|$ vs $\log \omega$ and

c) the phase angle plot vs $\log \omega$.

The determining parameters are the values of the charge-transfer resistance R_1 and its relation to any Warburg impedance when/if diffusion is significant, the double-layer capacitance and any adsorption pseudocapacitance. If the electrochemical reaction is kinetically rather sluggish, it will exhibit a large R_1, and then will usually display only a very limited-frequency region, or none, over which mass-transfer is the significant factor characterized by a Warburg impedance element. Note that R_1, the faradaic resistance, is exponentially potential-dependent, with negative argument, corresponding to an inverse Tafel relation (small η, large R_1) so that the diameters of Z" vs Z' semicircles diminish with increasing η.

Chapter 5. RESULTS AND DISCUSSION

5.1. Cyclic Voltammetry for Characterizing the General Features of the Bromine Reaction, as a Function of Potential

5.1.1. Introduction: Competitive Adsorption Between Halide Ions and Oxide Film Species at Pt, and the States of Oxidized Pt Surfaces

According to Conway [44] and Devanathan [72], the strength of chemisorption of an halide X^- to a metal is inversely related to the bond strength of H to the halogen, i.e. to the halogen's electronegativity.

The chemisorption of halide ions from aqueous solutions has been extensively studied at Hg where anion adsorption can be quantitatively examined as a function of potential (or surface charge, q_M) and concentration without the complications of competition with surface oxidation processes that arise at noble metals. Also the Hg surface presents an ideal liquid one but probably with short-range (111)-type hexagonal arrangements of surface atoms. Thus the Hg surface is in many ways an ideal "reference" one and has been so regarded in many works in the literature.

One of the important ways in which halide ion adsorption is manifested at Hg is through the shift, $\Delta E(pzc)$, of the potential of zero charge ($q_M = 0$) by such ions at a given concentration,

e.g. 0.1 M. The work at Hg has given some general basis for understanding the factors determining anion adsorption at other metals, e.g. Pt, as in the present work.

Generally, the strength of chemisorption is determined by: a) the donicity of the lone electron pairs on the anion and its polarizability; b) the Gibbs energy of hydration of the anion and its dependence on charge-density of the anion; c) the deformability of the anion's hydration shell and the associated increase of its Gibbs energy and d) the electron affinity (equivalent to the negative of the work function) of the electrode metal and some complex image interactions.

It is of interest to show empirically (Fig. 10) the relationship between $\Delta E(pzc)$ values for Cl^-, Br^- and I^- (at Hg) [96,97] and the respective individual ionic hydration energies [98] and also, for the common axis of abscissae, the plot against the nucleophilicity component in Edwards' scale of donicities [98,99]. While the pzc data are for Hg and the anion surface-excess data are also available for that metal, the trends and their nucleophilicities of adsorbability of halide ions with hydration energies are similar and the order of adsorbabilities is similar at Pt (cf. refs.[31,100]).

The adsorptivity being related to the hydration of X^- (Table 5), will be weaker, energywise, for the smaller ions of the more electronegative halogens. Solvation is thus an important factor in anion adsorption in addition to chemisorptive charge-transfer but the relation between adsorption of anions and their

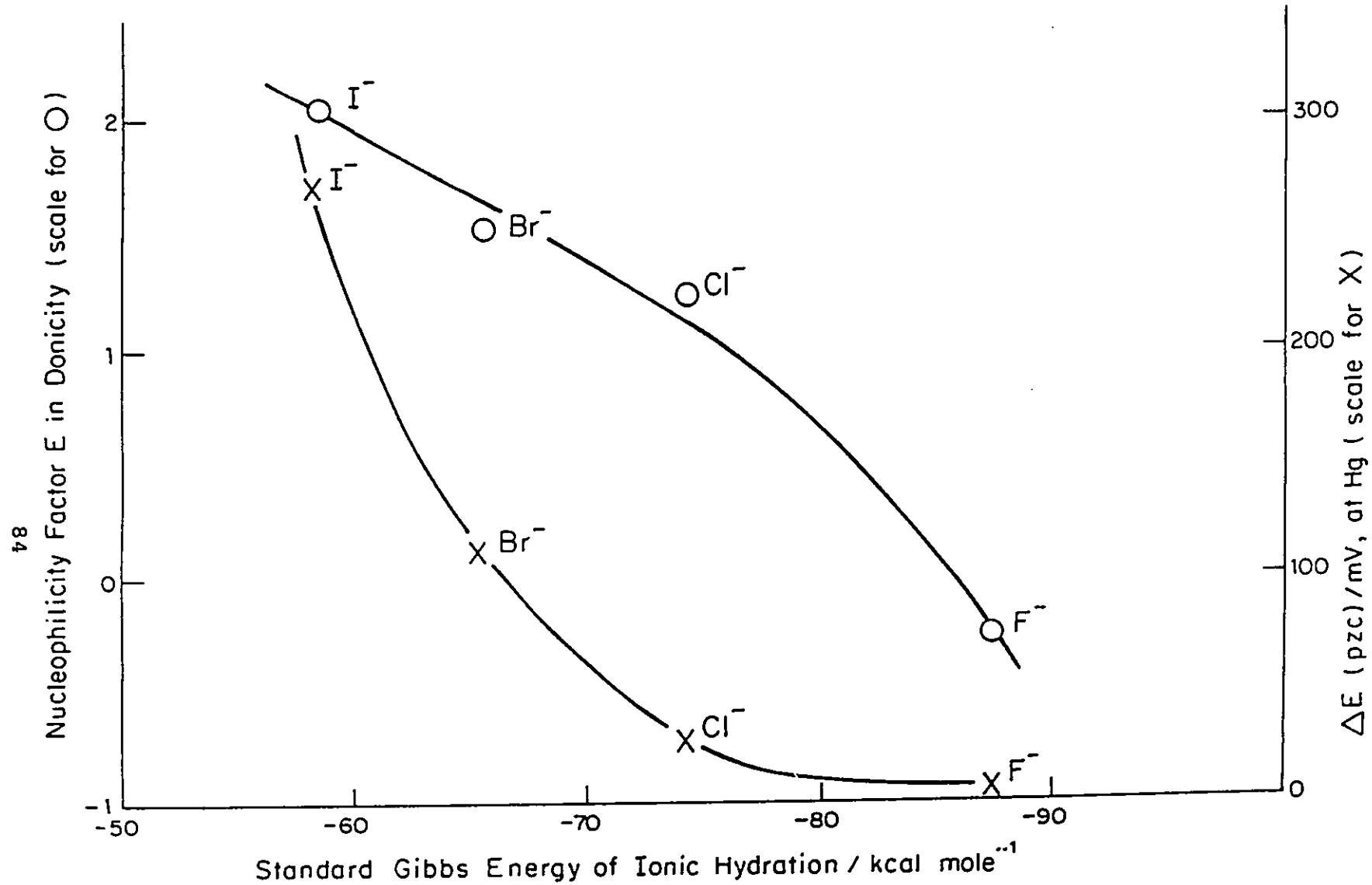

Fig. 10. Hierarchy of strengths of adsorption of anions at the Hg electrode in aqueous solution in terms of changes of potential of zero charge ΔE(pzc) at 0.1 M (based on data from refs. [96] and [97]) in relation to the nucleophilicity (Edwards' scale, ref. [98] of the respective anion

hydration is a complex one [73]: it probably depends not only on the overall first coordination-shell energy but on the energy required for *deformation* of the hydration shell in order to allow a lone-pair orbital to be accessible for interaction with the metal surface, giving rise to the chemisorption.

In a general sense, hydrated anion chemisorption is analogous to ligand exchange; a coordinated hydration H_2O molecule at the anion becomes replaced by coordination to a surface metal atom involving electron-pair overlap with surface orbitals. The larger halide ions therefore tend to be more strongly adsorbed at Pt due to:

a) their greater donicity [72] and polarizability, coupled with

b) their weaker hydration.

Both these effects depend on ionic radii which increase appreciably from F^- to I^- while the hydration energies decrease (Table 5).

TABLE 5. Crystallographic Halide Ion Radii (nm) and Hydration Energies ΔH_h (kJ mol^{-1})

F^-	0.136 nm	-435 kJ mol^{-1}
Cl^-	0.181 nm	-364 kJ mol^{-1}
Br^-	0.195 nm	-330 kJ mol^{-1}
I^-	0.210 nm	-284 kJ mol^{-1}

ΔH_h values based on enthalpy of hydration of H^+ of -1095±25 kJ mol^{-1}

The adsorption of halide ions at noble metal anodes has to be understood in terms of the spontaneous tendency of the metal

surface to become covered with an oxide film, initially a sub-monolayer, over a range of potentials common with that for the anion adsorption. Thus, the state of the anode surface as an interface for the Br_2 formation reaction is of primary importance in electroanalysis of the reaction, both in the step of Br^- (or Br_3^-) discharge and in the final step of Br_2 generation.

Not only do the competitively adsorbed OH and O species occupy sites on the Pt surface that would otherwise be available for Br^- adsorption but they also will change the electronic work function of the Pt, diminishing it. This will have the effect of decreasing the electron affinity of the surface for the lone-pair orbitals of Br^- thus tending to lower its chemisorption energy.

Much previous work in the formation and reduction of the oxide films on Pt has appeared in earlier literature, e.g. refs. [61,73—76]. In much of that work, attention has centered on the difference between the initially formed, quasi-2-dimensional film of OH and/or O species at Pt and the subsequently formed thicker, quasi-bulk films that can be generated at high positive potentials after long times of polarization [77]. Kozlowska and Conway et al. [78] demonstrated important differences between the properties of the reversibly formed sub-monolayer of OH and more extended states of the film that are irreversibly formed and reduced. In terms of a surface-chemical model, they proposed 2-d structures, identified as "Pt_4OH", "Pt_2OH", "PtOH" but not to be regarded as stoichiometric compounds. To attain

the OH monolayer stage, a total charge q_0 = 220 μC cm^{-2} is consumed. Following these initial, 2-d stages of oxidation, viz.

$$4Pt + H_2O \rightarrow Pt_4/OH + H^+ + e, \text{ etc,} \qquad (34)$$

over a broad region beyond 1.1 V E_H, "PtO" species arise after further oxidation by processes such as:

$$Pt/OH \rightarrow Pt/O + H^+ + e \qquad (35)$$

and

$$Pt/O \rightarrow O/Pt \text{ (place exchange)} \qquad (36)$$

The properties of three distinct states in the formation of surface oxide below ~0.8 V vs SCE have been distinguished and explained [61,78], designated as the PtO_{ads} region in the summarizing Fig. 11. In this region, the surface reactions are fairly reversible, in contrast to those above +0.8 V vs SCE, designated as the "PtO_2" region (Fig. 11).

More recently, it has been shown by Birss et al. [79,80] that the initial compact layer can be formed and removed independently of the presence of an overlying, thicker hydrous oxide which is formed and reduced only in an highly irreversible manner.

Under strongly oxidizing conditions, at potentials > ca. 2.0 V RHE and over long periods of anodization, thicker films of the type characterized by Shibata [81] are formed. Two states of such films have been characterized: an "α"-oxide, PtO, which is reducible over a broad potential range and is formed only up to a limited amount [82]; and a "β"-oxide, PtO_2, which is reduced

over a narrower potential range, but extending into the H desorption region. The conductivity of these two types of oxides has been measured by Shibata [81], the β-film being less conducting than the α.

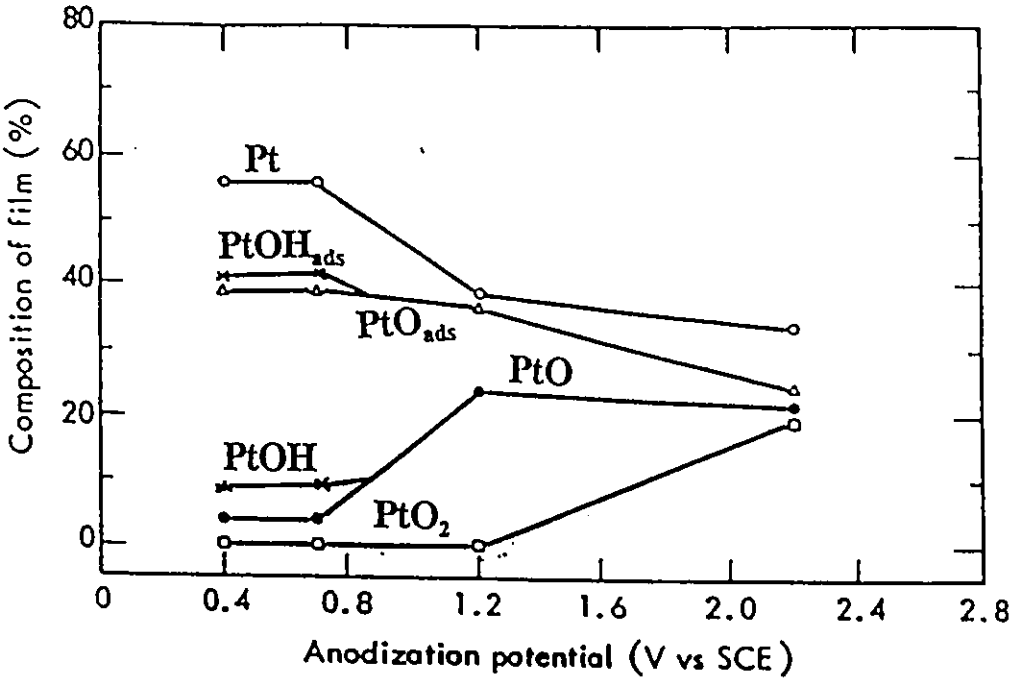

Fig. 11. Distribution of Pt, and supposed PtOH, PtO and PtO_2 species on a platinum electrode surface after anodization in 1 M $HClO_4$ (based on the work of Breiter [61]; note that the assignment for free "Pt" sites up to 2.1 V must be in error.)

Only in the case of the anodically "preoxidized" surfaces of Pt, also investigated in the present work (see 3.7.6 and later in this chapter), are the above types of thick films involved. In these cases the films grow logarithmically in time [83] according to the relation:

$$Q_t = A \log (t + t_0) \qquad (37)$$

where $t \gg t_0$ for the main region of logarithmic growth and t_0 is

an integration constant of the differential kinetic equation for growth and A depends on anodization potential.

5.1.2. Bromine Formation in Aqueous Solutions in Relation to Competitive Adsorption of Br^- Ion vis à vis Oxide Film Formation

Electrochemical methods based on cyclic voltammetry are specially suitable for the study of electroactive monolayers because of their sensitivity, and also for characterizing the general features of a process in terms of its current vs potential behaviour, with changing potential.

We first show results which provide information on extents of chemisorption of Br^- ion in relation to the state of the Pt anode surface at which Br^- discharge and recombination to form Br_2 occur, in particular, the development of co-deposited Pt surface oxide to extents dependent on Br^- concentration and electrode potential. Such results are most conveniently obtained by means of cyclic voltammetry which, as will be seen below, enables both the onset of Br_2 formation to be identified and the mutual effects of Br^- adsorption and surface oxide film formation to be evaluated. Thus, in the case of the bromine reaction, Br^- discharge and Br_2 formation arise competitively with Pt surface oxidation processes (5.1.3).

In aqueous solutions at Pt, increasing concentrations of bromide ion lead to a series of characteristic cyclic voltammograms (CV's). Figs. 12—18 show a succession of such voltammograms obtained at the platinum electrode for a series of

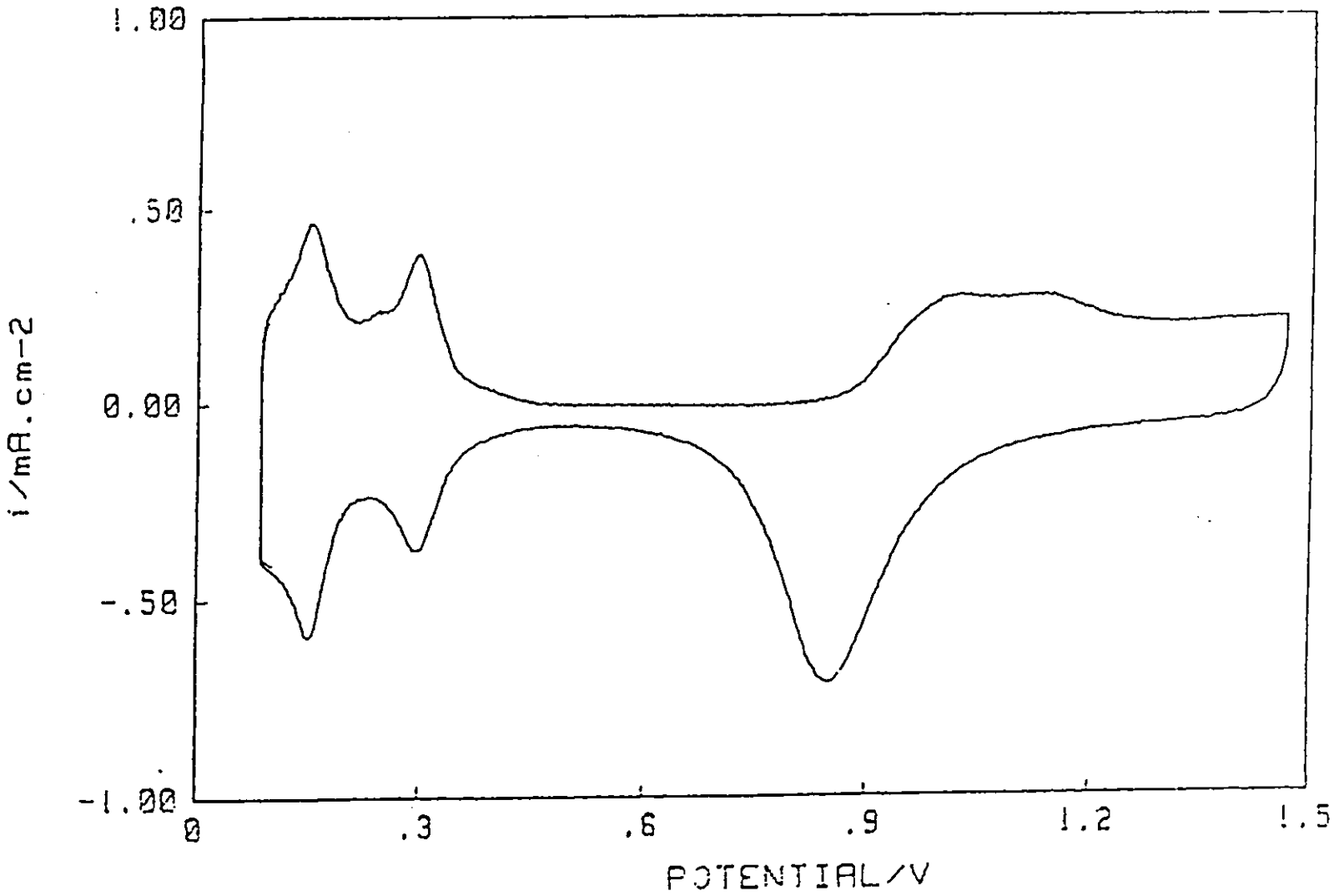

Fig. 12. CV of 0.1 M $HClO_4$ at Pt

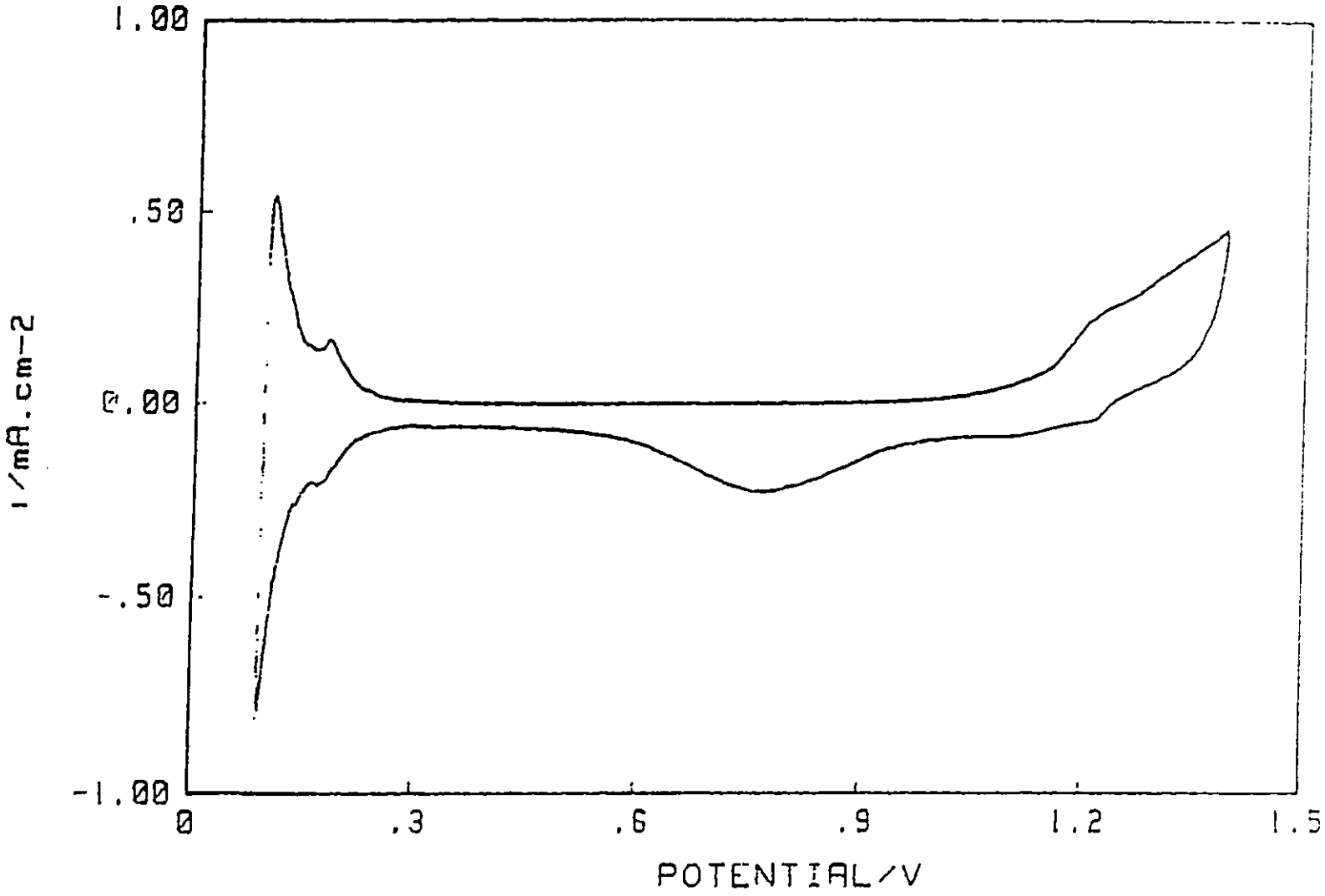

Fig. 13. CV of 10^{-6} M HBr in 0.1 M $HClO_4$ at Pt

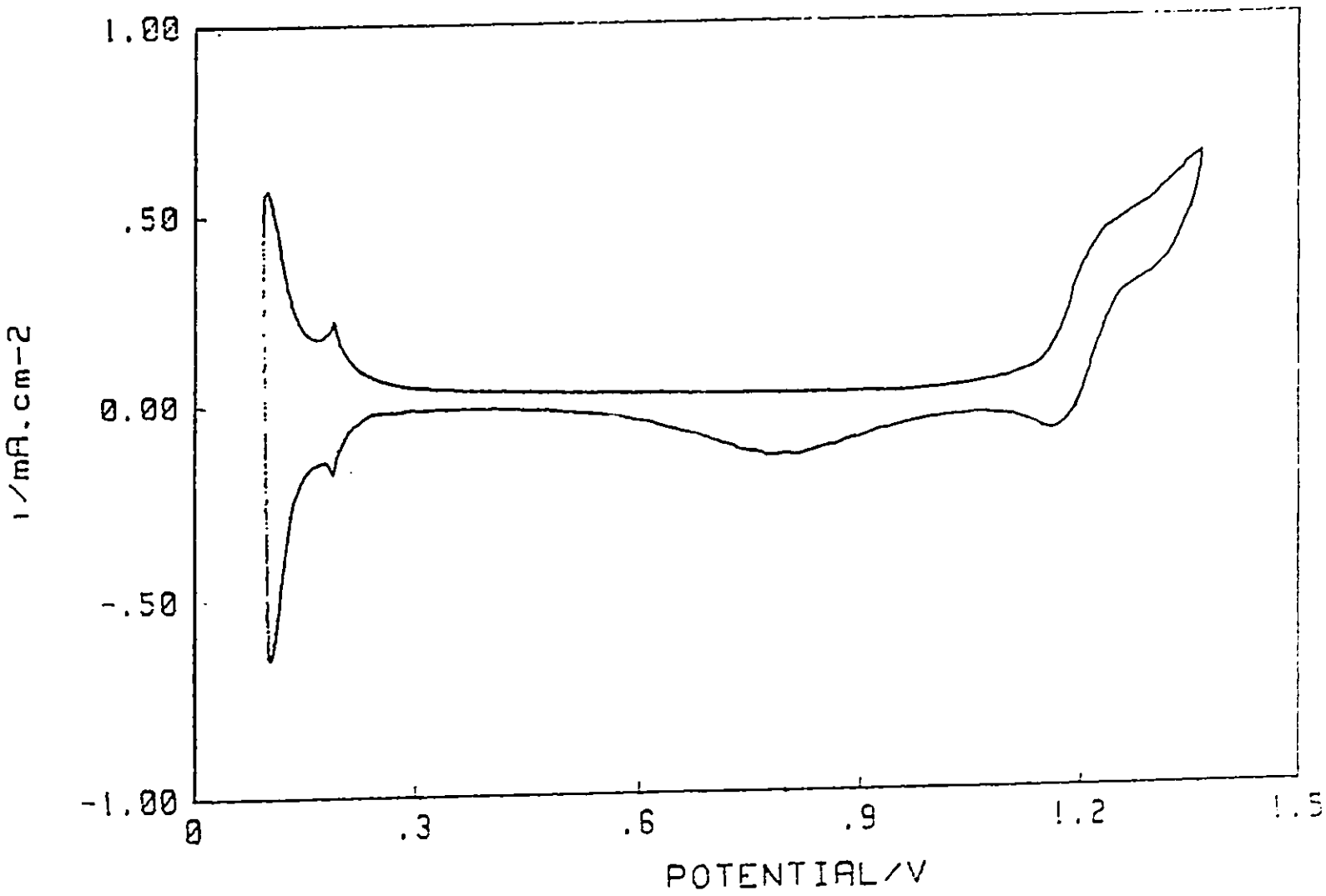

Fig. 14. CV of 10^{-5} M HBr in 0.1 M $HClO_4$ at Pt

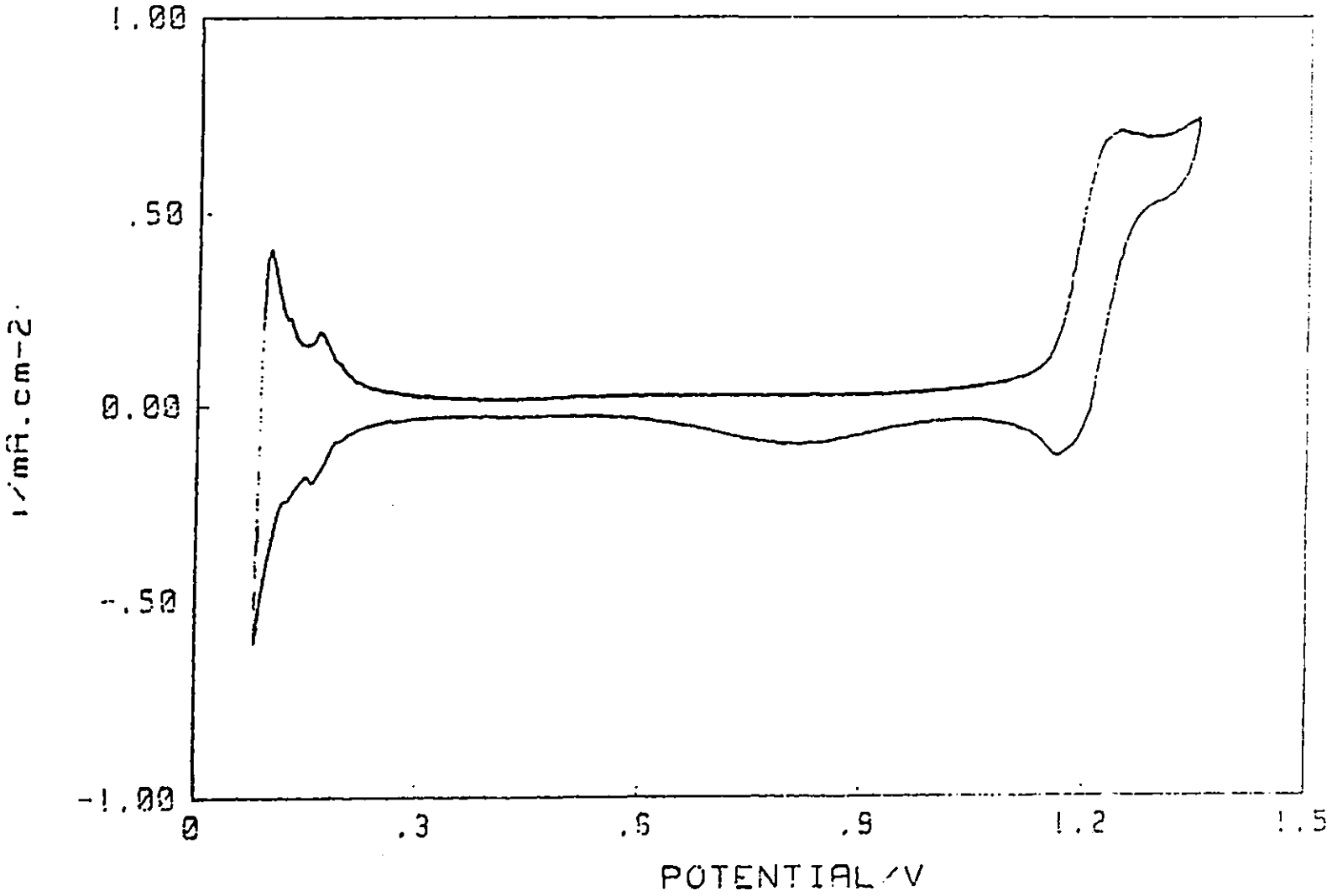

Fig. 15. CV of 10^{-4} M HBr in 0.1 M $HClO_4$ at Pt

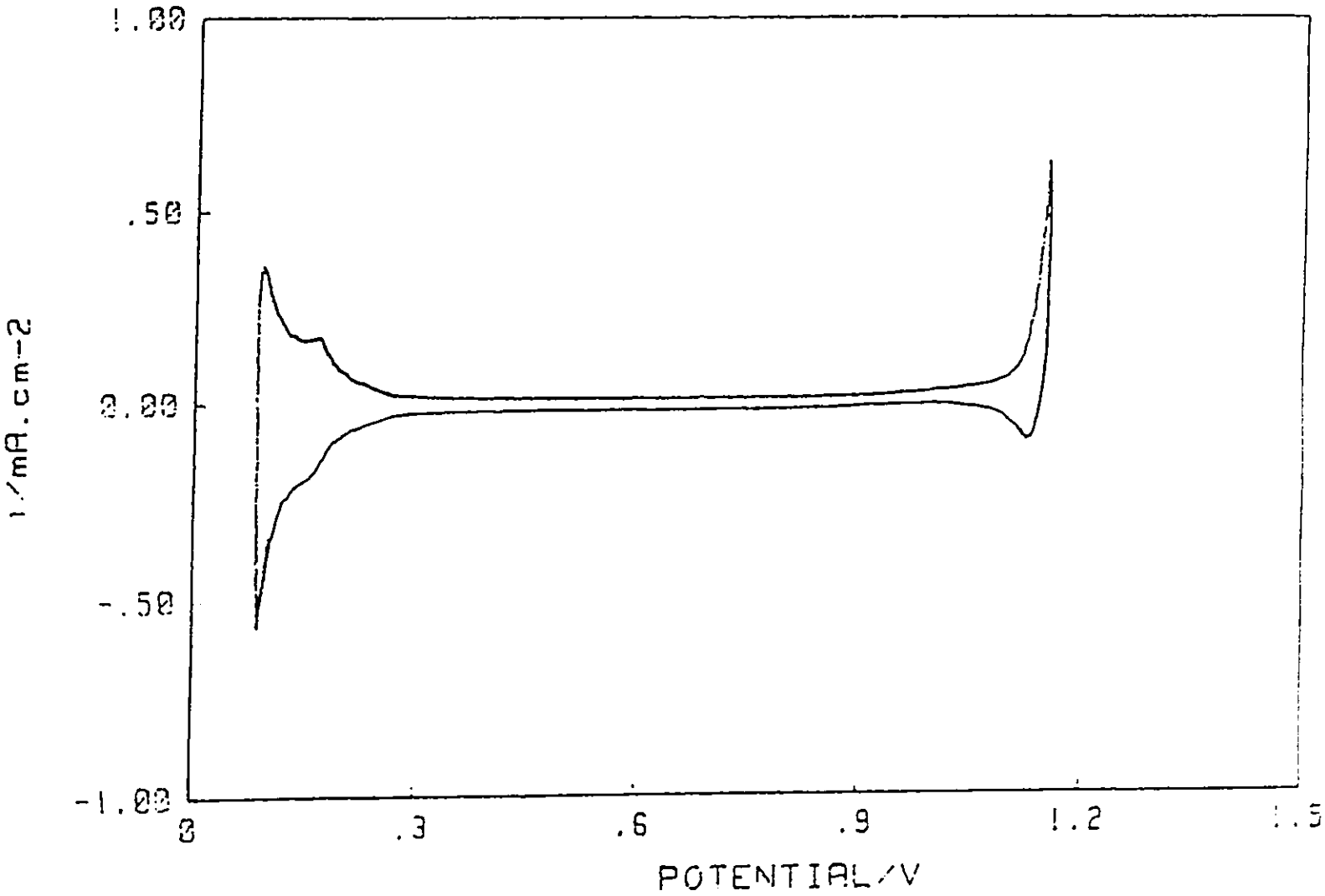

Fig. 16. CV of 10^{-3} M HBr in 0.1 M $HClO_4$ at Pt

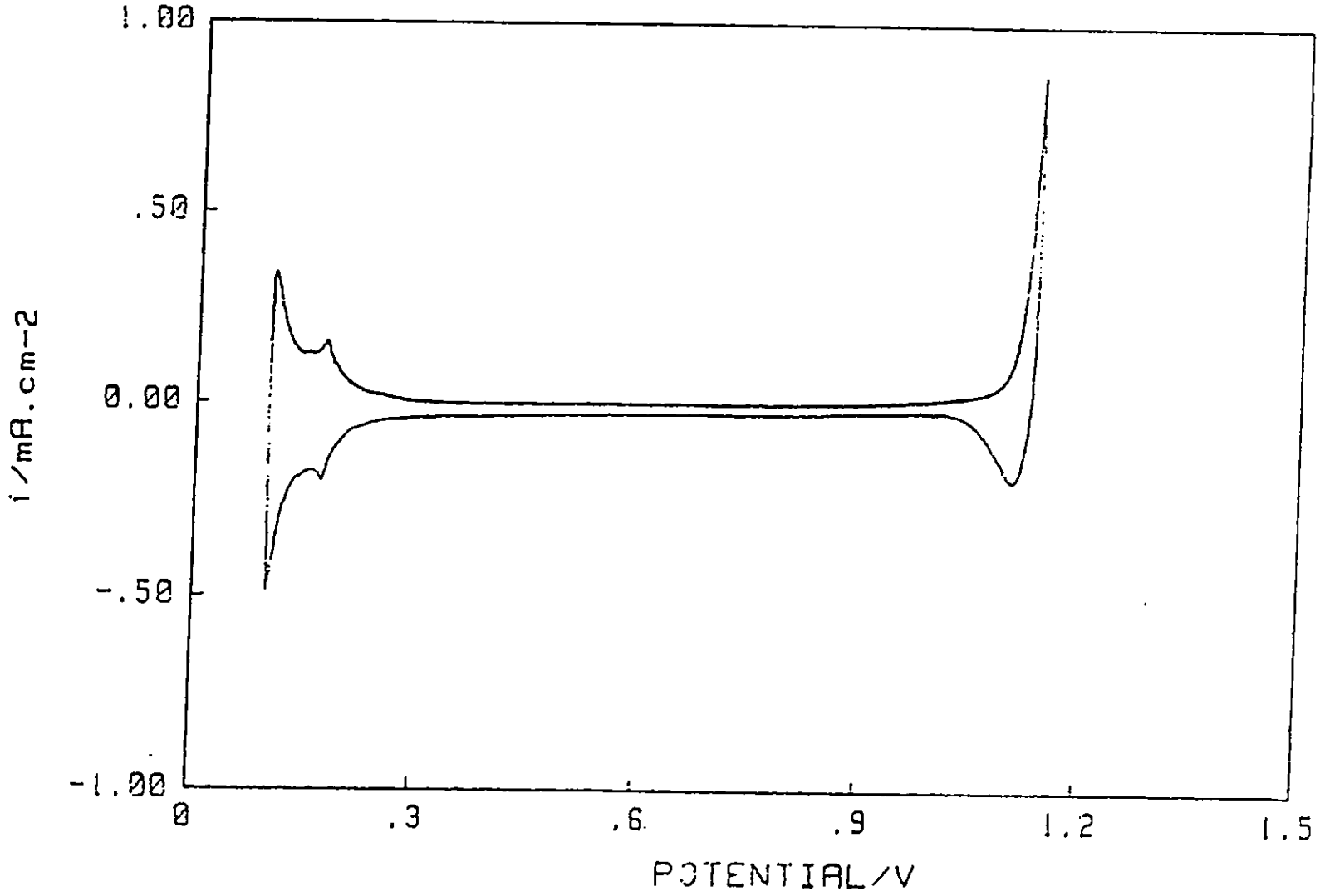

Fig. 17. CV of 10^{-2} M HBr in 0.1 M $HClO_4$ at Pt

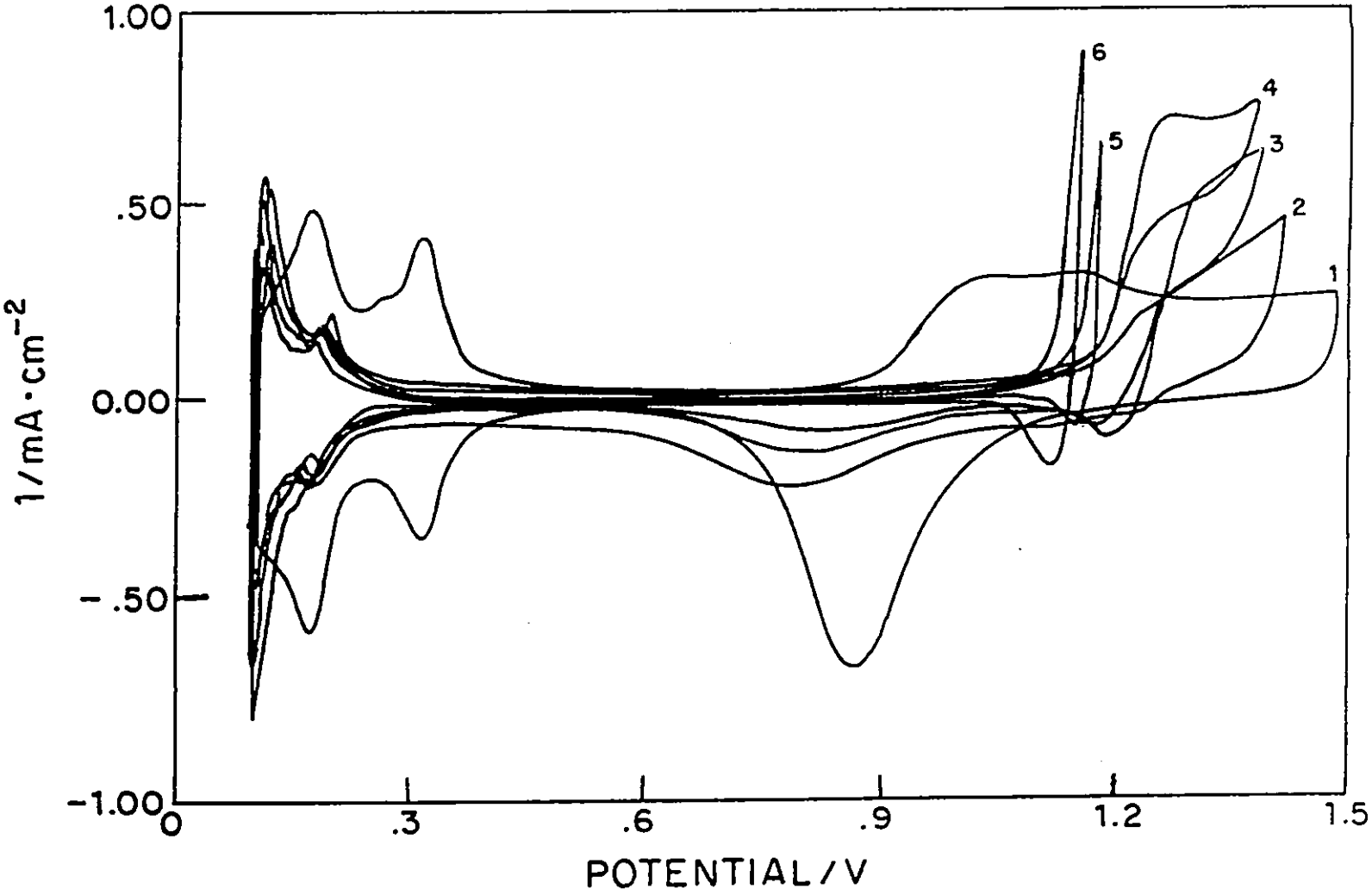

Fig. 18. Six superimposed CV's of 0.1 M $HClO_4$ and 10^{-6}, 10^{-5}, 10^{-4}, 10^{-3}, 10^{-2} M HBr in 0.1 M $HClO_4$ at Pt, for comparison

increasing Br^- concentrations in a supporting electrolyte of aq. 0.1 M $HClO_4$. These diagrams should be compared serially in the order which they are shown in the following pages, with the final comparison being shown in Fig. 18, where the series of curves are superimposed. The individual curves (Figs. 12—18) are shown here to provide a detailed record of the response currents over the surface oxide formation and reduction potential regions that are observed in the multi-curve, overlap diagram, Fig. 18, which unavoidably obscures some of the details of individual curves, e.g. at potentials above 1.05 V.

The curve of Fig. 12 is for Pt in 0.1 M $HClO_4$ in the absence of Br^- ion. Already with 10^{-6} M Br^- present (Fig. 13), it is seen that the CV has become quite different from Fig. 12 but surface oxide formation and reduction regions are still distinguishable over the respective potential ranges 1.1—1.4 V and 1.0—0.5 V, vs Ag/AgBr, and some component of anodic current for Br_2 formation is already discernable. This is more easily seen in Fig. 14 and following diagrams where eventually it becomes the principal anodic current component and virtually no surface oxide film formation or reduction currents arise (Figs. 16, 17).

Figs. 14 and 15, with the inflections in the curves at ca. 1.25 V, are interesting intermediate situations where the anodic Br_2 formation currents are clearly becoming added to, or modifying, the oxide formation currents (1.1 to 1.35 V) over the same potential range before the latter are eventually diminished towards zero at higher Br^- concentrations (Figs. 16, 17). In

dilute solutions, Br_2 formation is less favoured because its exchange current is diminished in some power of Br^- ion concentration determined by the transfer coefficient of the reaction. In addition, at sufficiently high current-densities, the reaction will become diffusion-controlled; then O_2 evolution from discharge of water will accompany the reaction.

Surface oxidation current profiles in the cyclic voltammetry i vs E curves for Pt are progressively diminished with successive additions of Br^- ions from 10^{-6} to 10^{-2} M, while at the higher anodic potentials, currents for Br_2 formation arise. The oxide coverage which can be developed is determined by competitive co-adsorption of Br^- at Pt, initially on the oxide-free anode metal surface, at potentials lower than that required for onset of oxide film formation. It is seen that blocking of oxide-film formation by Br^- arises over a broader potential range than that with Cl^-, and without the selectivity exhibited by Cl^- when the latter ion initially blocks the Pt/OH region up to 1.05 V in preference to the Pt/O region (cf. Fig. 19).

From previous work by Conway and Novak (1980) on the competitive blocking of surface formation at Pt by Cl^- ion [26], it was shown that the adsorbed "Cl" species retains much (ca. 50%) of its charge [26], giving a competitive isotherm linearly extended on a log[Cl^-] scale (Fig. 20) due to strong lateral interaction effects, whereas it is found here that adsorbed "Br" behaves more like a neutral atom; I^- is similar [26]. The previously obtained data for Cl^- and I^- [26] are shown for

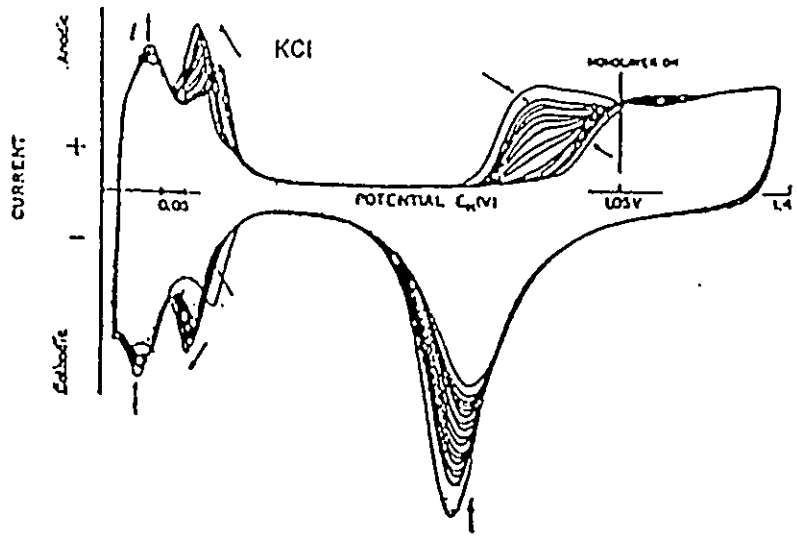

Fig. 19. Series of cyclic voltammetry i vs. E profiles for the Pt electrode in 0.1 M H_2SO_4 (298 K) at 25 mV s^{-1} with successive additions of chloride ion from 10^{-7} to 10^{-4} M (arrows show directions of changes due to Cl^- addition) [26]

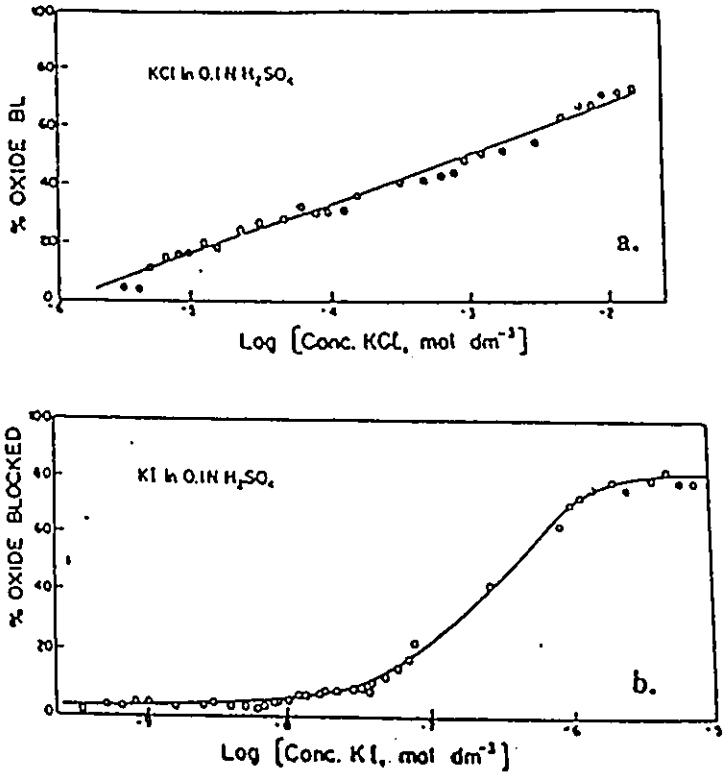

Fig. 20. Competitive adsorption isotherms for % surface oxide blocked at Pt (to 1.2 V) as a function of log [halide] a) Cl^- and b) I^- at 298 K [26]

convenience here, in Figs. 19 and 20, rather than in the "overview" section in chapter 1. The data for Cl^- adsorption are based on the series of voltammograms in Fig. 19 from ref. [26].

Blocking of the initial stages of Pt surface oxidation also increases the irreversibility of oxide formation on the Pt electrode because of the adsorption of halide ion, X^-.

In Figs. 14—17 is also seen, in each cathodic curve around 1.1 V, a peak for reduction of Br_2 formed in the previous anodic half-cycle. This also serves to identify the onset (already seen in Fig. 13) of anodic Br_2 formation. That the cathodic peak around 1.1 V is due to Br_2 reduction is confirmed by its substantial attenuation by electrode rotation which spins away anodically generated Br_2 before it has a chance to be reduced at the electrode surface.

5.1.3. Isotherms for Competitive Adsorption of Br^- Ion and Electrosorbed OH and O Species at Pt

The cyclic voltammograms in Figs. 12—18 demonstrate the progressive competition between Br^- ion adsorption and the desorption of OH/O species generated in the initial stages of surface oxidation of the Pt electrode, as Br^- concentration is increased.

The surface oxide formation processes were represented formally by the eqns. 34—36; for convenience of the reader, they are repeated here:

$$4Pt + H_2O \rightarrow Pt_4/OH + H^+ + e, \text{ etc.} \qquad (38)$$

$$Pt/OH \rightarrow Pt/O + H^+ + e \qquad (39)$$

$$Pt/O \rightarrow O/Pt \text{ (place exchange)} \qquad (40)$$

and, at sufficiently high potentials,

$$2Pt/O \rightarrow 2Pt + O_2 \qquad (41)$$

In earlier work [26], the effects of Cl^- and I^- on Pt surface oxidation were studied from very low concentrations upwards. The results [26] for Cl^- ion are strikingly different from those for I^-, as shown in Figs. 20a, b where the isotherms for competitive oxide blocking at Pt by Cl^- and I^- are plotted comparatively; because of the linear *logarithmic* behaviour in Fig. 20a it was clear that Cl^- ion blocking follows a Frumkin-type isotherm (cf. eqn. 11)

$$\frac{\theta}{1-\theta} = KC\exp(\eta F/RT)\exp(-g\theta) \qquad (42)$$

requiring a substantial value of the repulsive interaction term, $g\theta$, giving rise to a linear *logarithmic* isotherm. The isotherm for Cl^- showed that the *log* form for Cl^- is not due to heterogeneity (Temkin isotherm) but rather to strong repulsive effects in the ad-layer (Frumkin effect). Such behaviour arises because, for halide ions, adsorption occurs with partial charge transfer:

$$X^- + Pt \rightarrow PtX^{\cdot}_{ads}{}^{(1-\gamma)} + \gamma e \qquad (43)$$

where γ for Cl^- is <u>ca</u>. 0.5 while for I^- it is close to 1 [26]. The γ value for adsorbed Br^- intermediate is larger than 0.5 but was estimated as ≥ 0.9 in the present work (see below).

Fig. 21a shows the adsorption behaviour of Br^- derived from CV's recorded in the present work, plotted as a competitive isotherm of % oxide blocked by Br^- ion and the log of Br^- ion concentration over four decades of concentration. Note the very different shape of this isotherm compared with that for Cl^- at Pt (Fig. 20a) derived in a previous paper [26]; such a comparison suggests that the adsorption takes place with a substantially larger degree of charge-transfer (cf. eqn. 43) compared with Cl^- at Pt.

These results suggest that the state of adsorbed Br^- is much more atomic than ionic, i.e., the electrosorption valency is estimated, from the present results, to be near 0.9, while, for Cl^-, it is ca. 0.5, with the ion retaining, after adsorption, a substantial fraction of its charge. This is consistent with the known properties of Br^- and I^- (especially I^-) in charge-transfer complexation. A similar conclusion for adsorption of I^- at Pt was reached by Lane and Hubbard [84] from charge-potential measurements.

The above conclusion for Br^- adsorption is important for considering the kinetics of, and electrocatalysis in, Br_2 generation and the comparison of such behaviour with that at pre-oxidized electrodes (see 3.7.6 and below) at which donative chemisorption of anions is much less favoured.

It is of interest to compare the form of Fig. 21a with that expected for a Langmuir isotherm function. Fig. 21b shows the expected coverage of an adsorbed species as a function of the

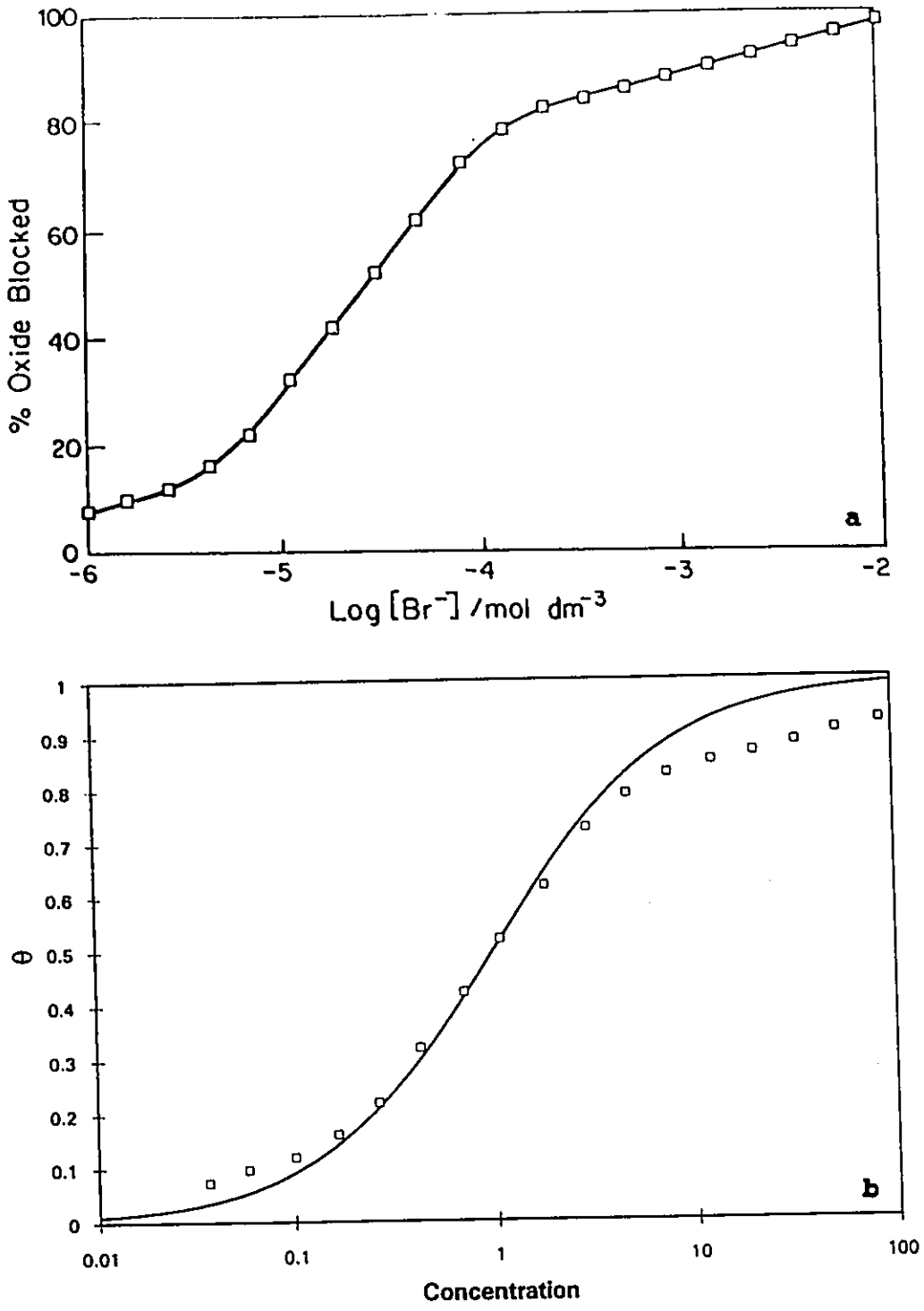

Fig. 21. Competitive adsorption isotherm for % surface oxide blocked at Pt as a function of log [Br^-] a) experimental data; b) Comparison with the Langmuir isotherm function, normalized for coincidence at θ = 0.5 (solid line); □, points from experimental data shown in upper graph (a)

log of concentration of the adsorbate for an arbitrary value (for convenience, 1) of the Langmuir adsorption constant K in $\theta/1-\theta = Kc$. The comparison between the experimental data of Fig. 21a and the theoretical form of the Langmuir isotherm is facilitated by arbitrarily setting the datum for 50% blocking at the $\theta = 0.5$ point on the theoretical curve (solid line in Fig. 21b).

It is seen that up log C ≈ 0.8, the experimental data (Fig. 21b) are fitted rather well by the Langmuir isotherm function and only beyond the above concentration (log C ≈ 0.8) do the experimental data deviate, in fact in a manner approaching a linear log C form. This corresponds, probably, to onset of significant lateral interactions arising at relatively high surface concentrations in a way similar to that arising (Fig. 21a) over the *whole* concentration range for Cl^- adsorption at Pt for which γ (eqn. 43) is smaller. In fact, for most of the competitive adsorption curve for Br^- (Fig. 21a), γ must be as large as ca. 0.9 up to log $[Br^-] = 0.8$ (Fig. 21b).

The large qualitative, as well as quantitative, difference in the competitive adsorption behaviour of Cl^- and Br^- vs surface oxide formation at noble metals, indicates an appreciable difference in electrosorptive affinity of Cl^- and Br^- for Pt in the two-dimensional lattice of co-adsorbed OH + O species that are involved in the initial stages of oxide film formation [78] (see below).

5.1.4. Onset of Br_2 Formation at Pt

As was noted above, the sharp current rise at about 1.13 V (see Fig. 17) towards the positive end of the anodic sweep arises on account of bromine formation, the onset potential for which follows the Nernst relation (see chapter 1)

$$E = 1.016 - 0.059 \log a_{HBr}\ (aq) \ \underline{vs}\ Ag/AgBr$$

for the reaction:

$$2Br^-_{(aq.)} \rightleftharpoons Br_{2(aq.)} + 2e \qquad (44)$$

Hence bromine formation commences, thermodynamically, at $E = 1.016 - 0.059 \log 10^{-2} = 1.13$ V for $a_{HBr} = 10^{-2}$ M.

The curves of Fig. 16 and 17 for Pt exhibit the most distinct sharply rising current beyond ca. 1.15 V which is to be attributed to onset of bromine formation over the most positive anodic potential region, as measured in 10^{-2} M and 10^{-3} M HBr (with 0.1 M $HClO_4$). The more concentrated is the bromide solution, the sharper is the anodic current increase in the positive potential range of the cyclic voltammogram, as may be expected since there is less inhibiting effect of the co-deposited OH or O species. In dilute solutions, the sharply rising current profiles are distorted (Figs. 13—15), with shoulders arising due to background currents for simultaneous competitive oxide film formation and, at the highest potentials (>1.23 V), eventually and possibly to some co-evolution of O_2.

From the cyclic voltammograms for appreciable Br^- concentrations (10^{-3}, 10^{-2} M, Figs. 16 and 17), it is seen that

virtually *no* co-deposition of OH and O Pt surface oxide species takes place, as indicated by the lack of an "oxide reduction" current peak on the return cathodic sweep of the kind that clearly arises when the cyclic voltammetry is performed in more dilute bromide solutions, e.g. see Figs. 13 and 14.

This effect arises for two reasons:

a) in the stronger Br^- solutions, the competitive blocking by formation of the oxide species is much less, as seen from Figures 16 or 17;

b) in the stronger Br^- solutions, the onset of appreciable Br_2 formation currents arises for thermodynamic reasons at lower Br^-/Br_2 thermodynamic potentials (cf. eqn. 44) at which less oxide coverage would, in any case, be present.

An important conclusion is then that for anodic Br_2 formation, the process takes place virtually on an oxide-free surface when Br^- concentrations are greater than ca. 10^{-3} M, as seen, e.g., from the comparative curves of Fig. 18. Only on a surface *separately* pre-oxidized in aqueous $HClO_4$, can the process take place on an oxide-film covered electrode, as shown in Fig. 22 for an oxide film of ca. 3 equivalent monolayers of "PtO".

Since study of the anodic Br_2 formation mechanism is one of the purposes of the present research, $[Br^-] \gg 10^{-3}$ M is the preferred minimum concentration, but concentrations of 10^{-1} M have, in fact, been employed in most experiments.

Fig. 15 shows the CV for 10^{-4} M HBr at Pt in 0.1 M $HClO_4$; the onset of bromine formation again corresponds to the steep rise

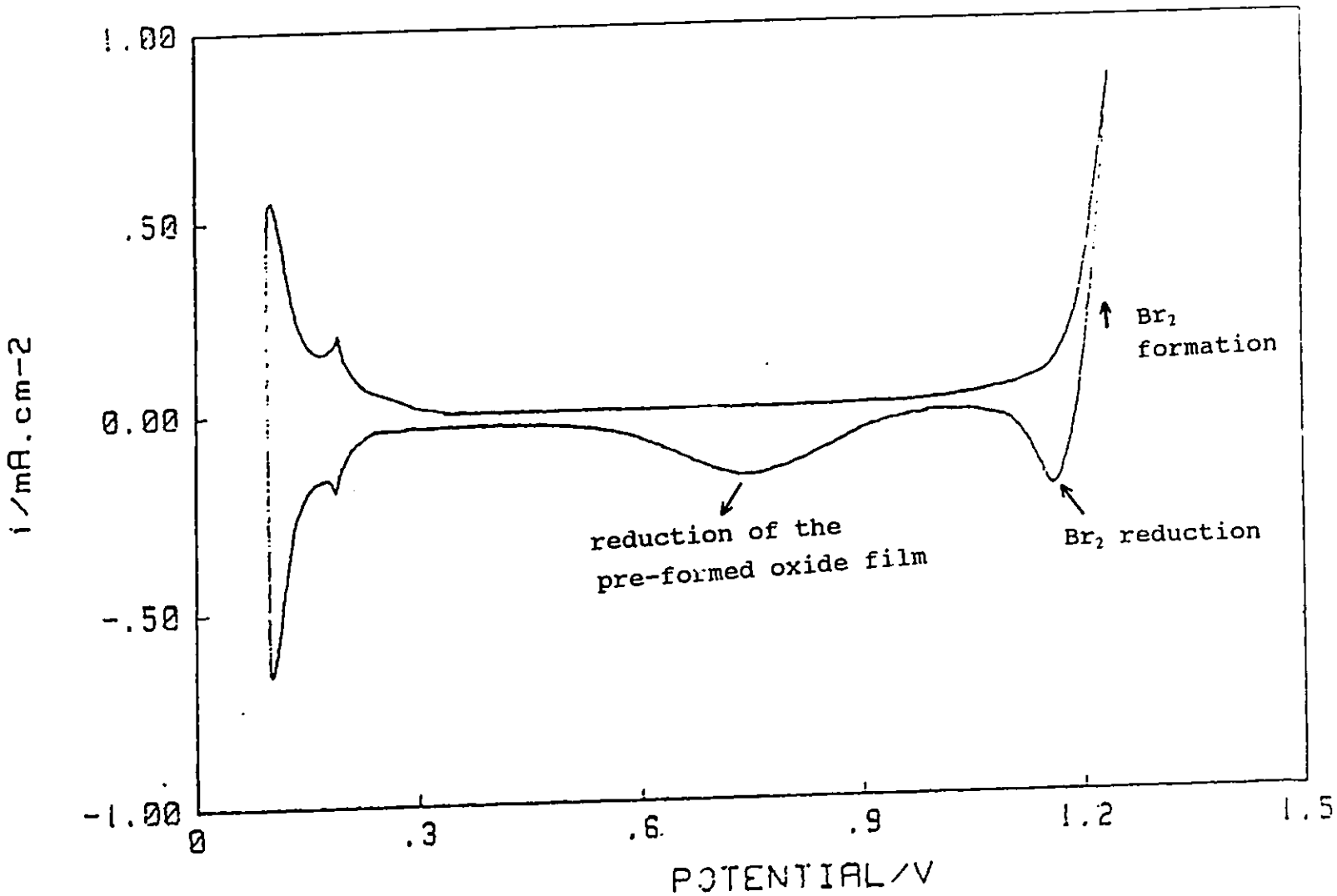

Fig. 22. CV of 10^{-6} M HBr in 0.1 M $HClO_4$ at a preoxidized (~3 oxide monolayers) Pt electrode

of the current-density at the positive end of the sweep; Figs. 16 and 17 show the CV's for 10^{-2} M and 10^{-3} M HBr in 0.1 M $HClO_4$; the potential range for H adsorption becomes narrowed with increasing concentration of Br^-, in this case because of competitive adsorption between H and adsorbed Br^- as known in the earlier work by Breiter [23]. Fig. 14 shows the CV for 10^{-5} M HBr in 0.1 M $HClO_4$ while Fig. 13 records that for 10^{-6} M HBr in 0.1 M $HClO_4$.

In dilute Br^- solutions or at high current-densities where onset of diffusion control could arise, parallel anodic O_2 evolution could set in. The concentration of Br^- that would correspond to a Br^-/Br_2 reversible potential of +1.23 V (E_{H_2}), i.e. equal to the potential that O_2 would (thermodynamically) just begin to be evolved in parallel with Br_2 formation, can be calculated from the Nernst equation:

$$1.23 = 1.087 - 0.059 \log [Br^-]$$

Hence

$$[Br^-] = 0.00377 \text{ M} = 3.77 \times 10^{-3} \text{ M},$$

neglecting activity coefficient effects.

In fact, the CV results for Pt in 0.1 M $HClO_4$ with the addition of HBr at concentrations from 10^{-3} to 10^{-2} M, or beyond, show, as mentioned earlier, virtually no oxide film formation; this, and the Nernst potential factor, makes it possible to establish bromine formation *before* O_2 evolution sets in, unlike the situation with Cl^-/Cl_2. The oxygen evolution potential is

then higher than that for bromine formation, as well as the catalytic surface for O_2 evolution being changed, so that bromine formation sets in earlier than oxygen evolution and bromide adsorption blocks the stages of Pt surface oxide film formation that are involved in electrocatalysis of the O_2 evolution reaction.

The related results of Breiter [27] showed some indications of a small degree of surface oxidation in the more concentrated bromide solutions such as in 10^{-2} and 10^{-3} M HBr, possibly because of the use of more concentrated $HClO_4$ (1 M).

5.1.5. Onset of Br_2 Formation at Other Noble Metals

It was also of interest to examine, comparatively, the onset of Br_2 formation at other noble metals, the surface oxidation characteristics for which are known [11,43,68] to be significantly different from those of Pt and thus the role of the oxide films would be different.

Various noble metal or noble-metal-loaded anodes employing Pt, Rh, Ru, Ir, Pd, etc. have often been studied as electrocatalysts for anodic reactions, e.g. Cl_2 evolution. Figs. 23—26 show comparatively the cyclic voltammograms at Rh, Ir and Ru in 0.5 M aq. $HClO_4$; they are different from those for Pt because their surfaces have different affinities for OH or O, and different kinetics of thicker oxide-film growth; also the UPD H adsorption is different.

Figs. 27—31 show CV's for 0.01 M HBr in 0.5 M $HClO_4$

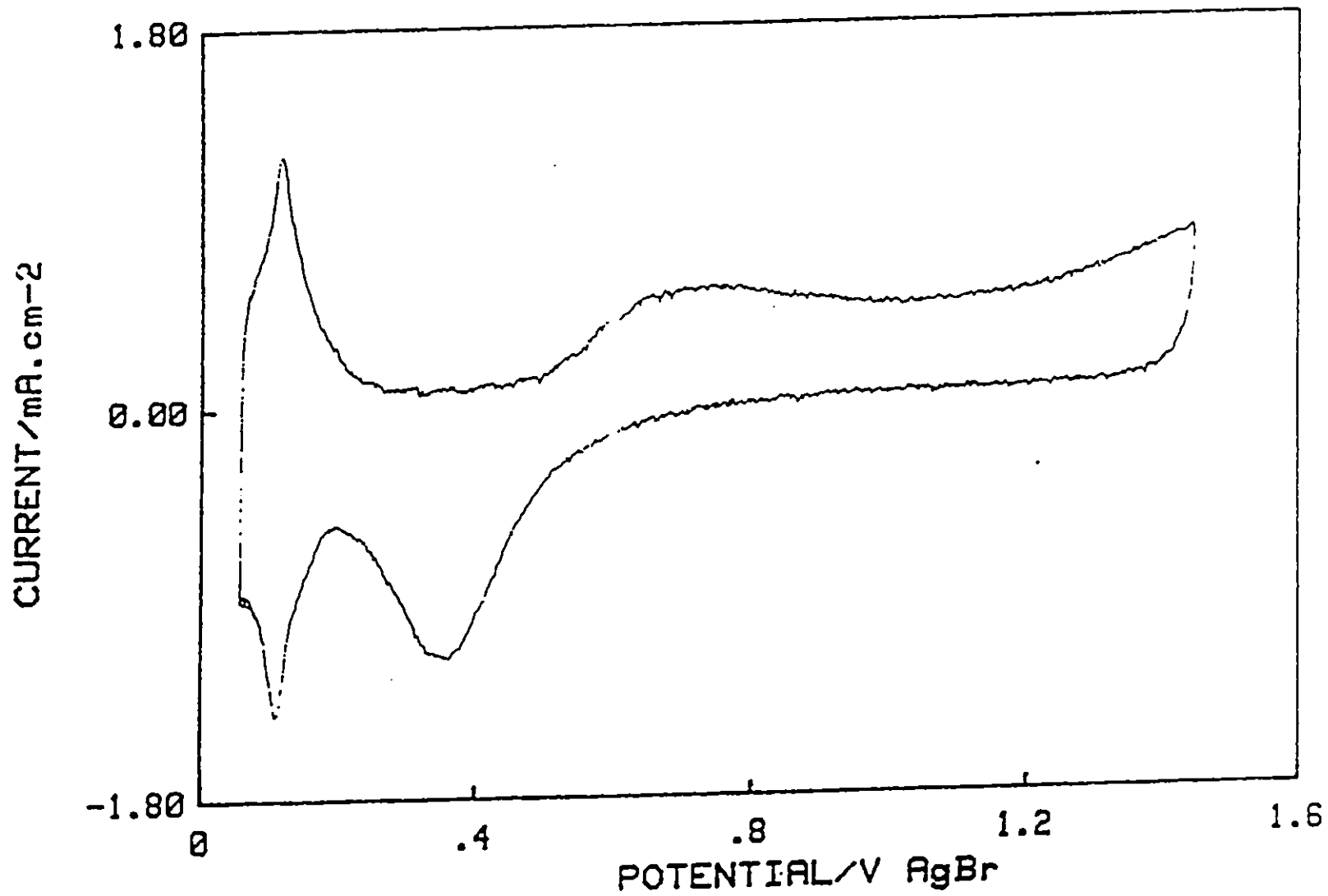

Fig. 23. Cyclic voltammogram for the Rh electrode in 0.5 M $HClO_4$

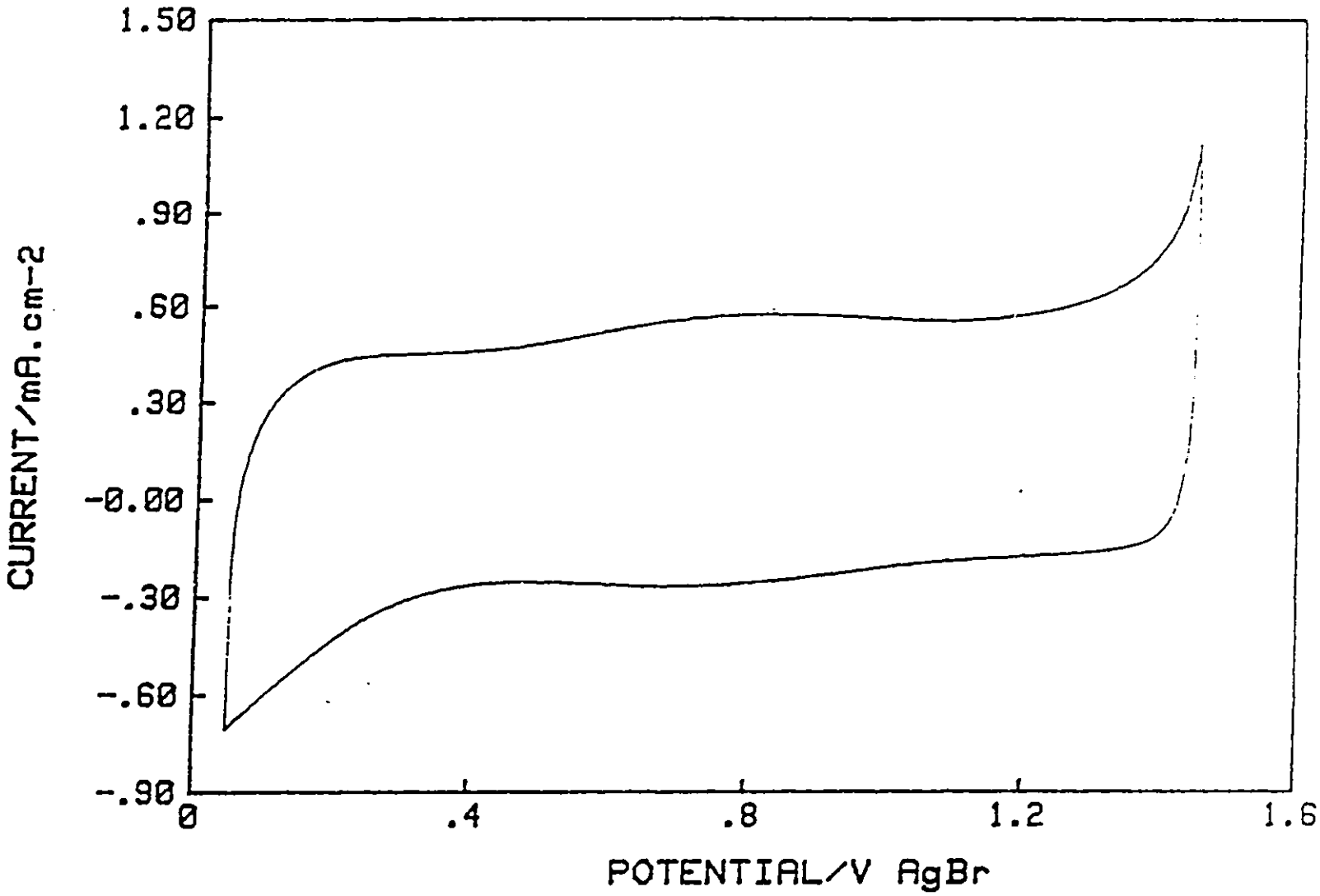

Fig. 24. Cyclic voltammogram for the Ru electrode in 0.5 M $HClO_4$

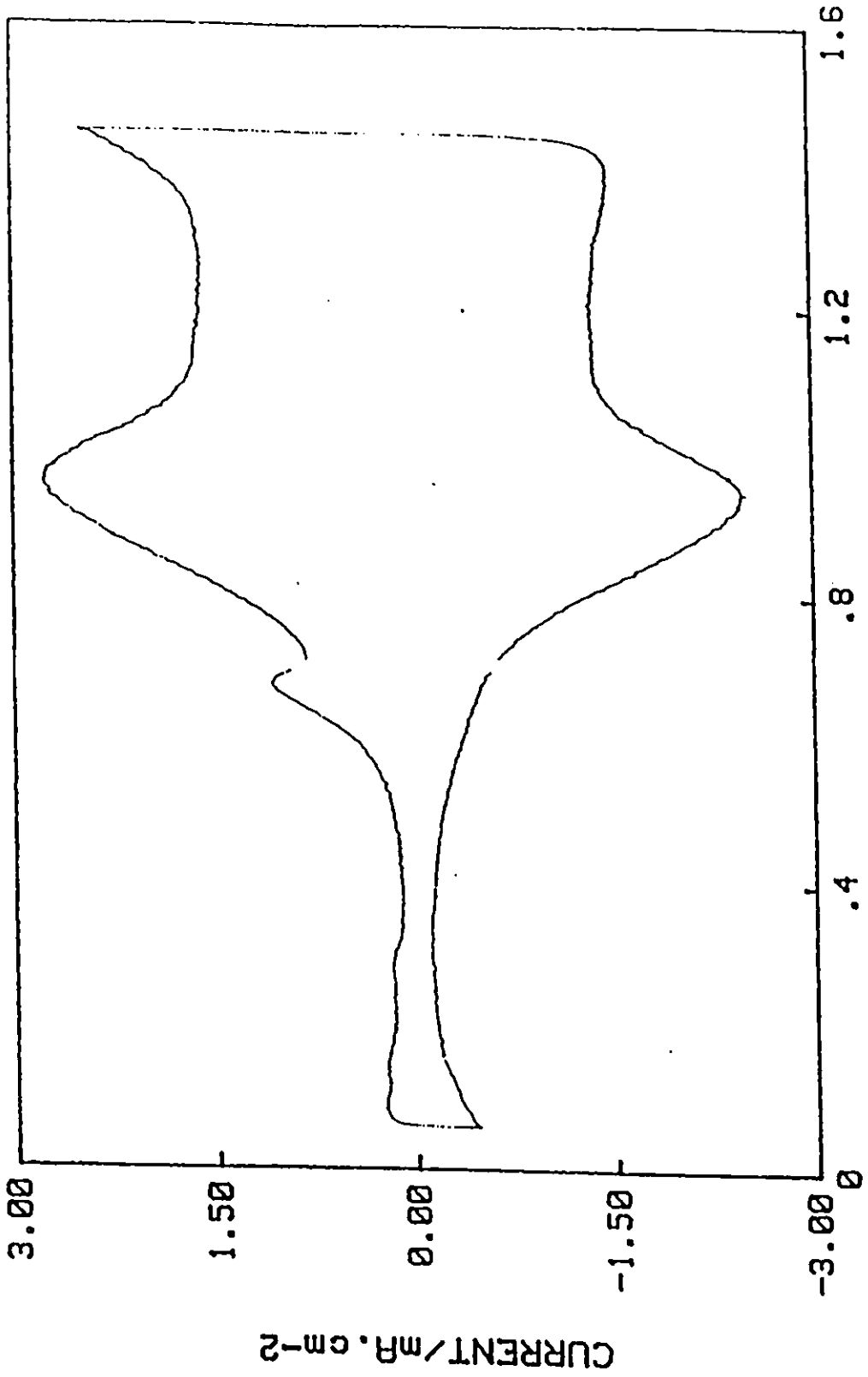

Fig. 25. Cyclic voltammogram for the Ir electrode in 0.5 M $HClO_4$

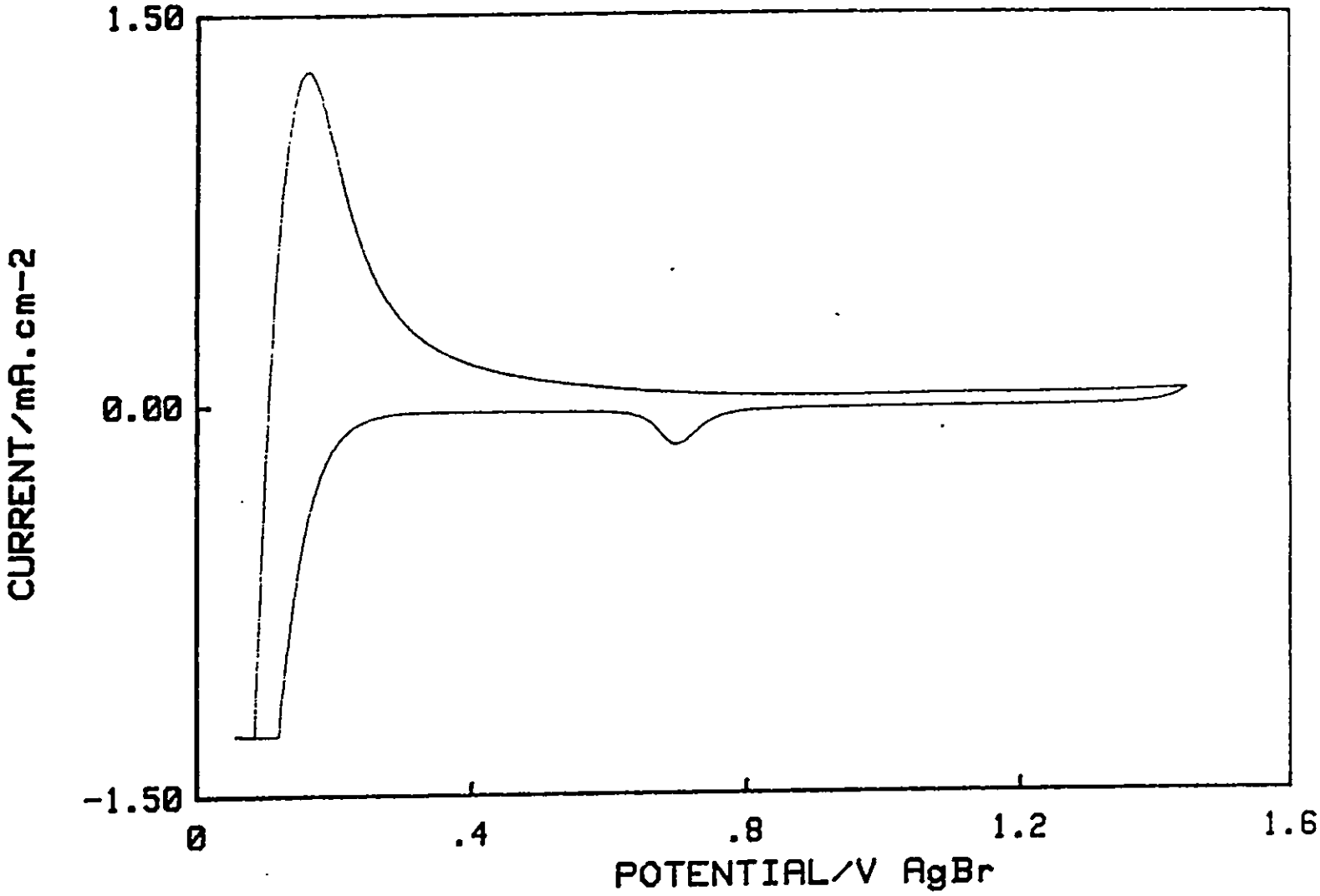

Fig. 26. Cyclic voltammogram for the Pd electrode in 0.5 M $HClO_4$ (the origin of the cathodic current peak is unclear, no observed oxidation may due to the impurity of Pd)

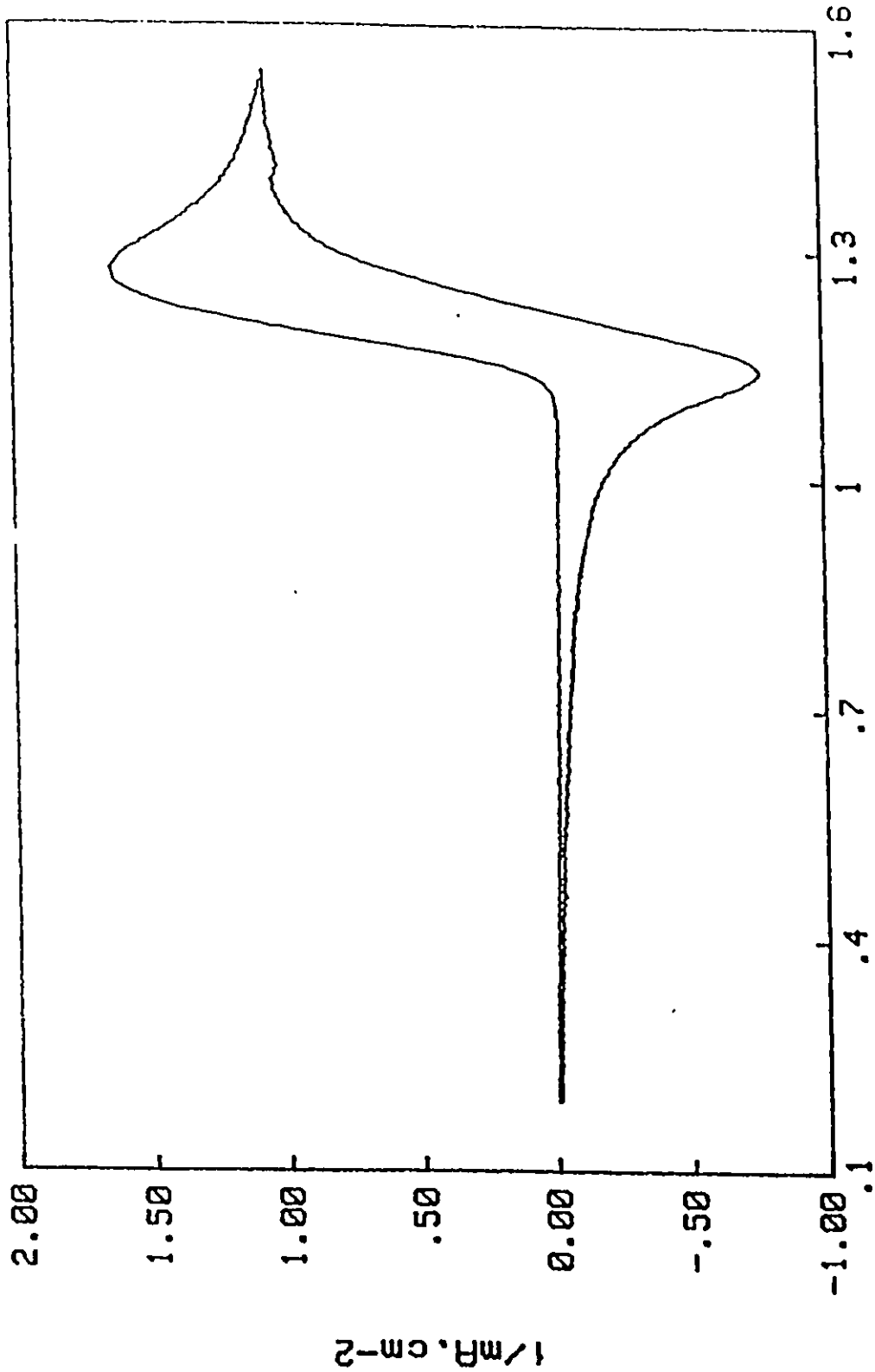

Fig. 27. CV of 0.01 M HBr in 0.5 M $HClO_4$ at Rh

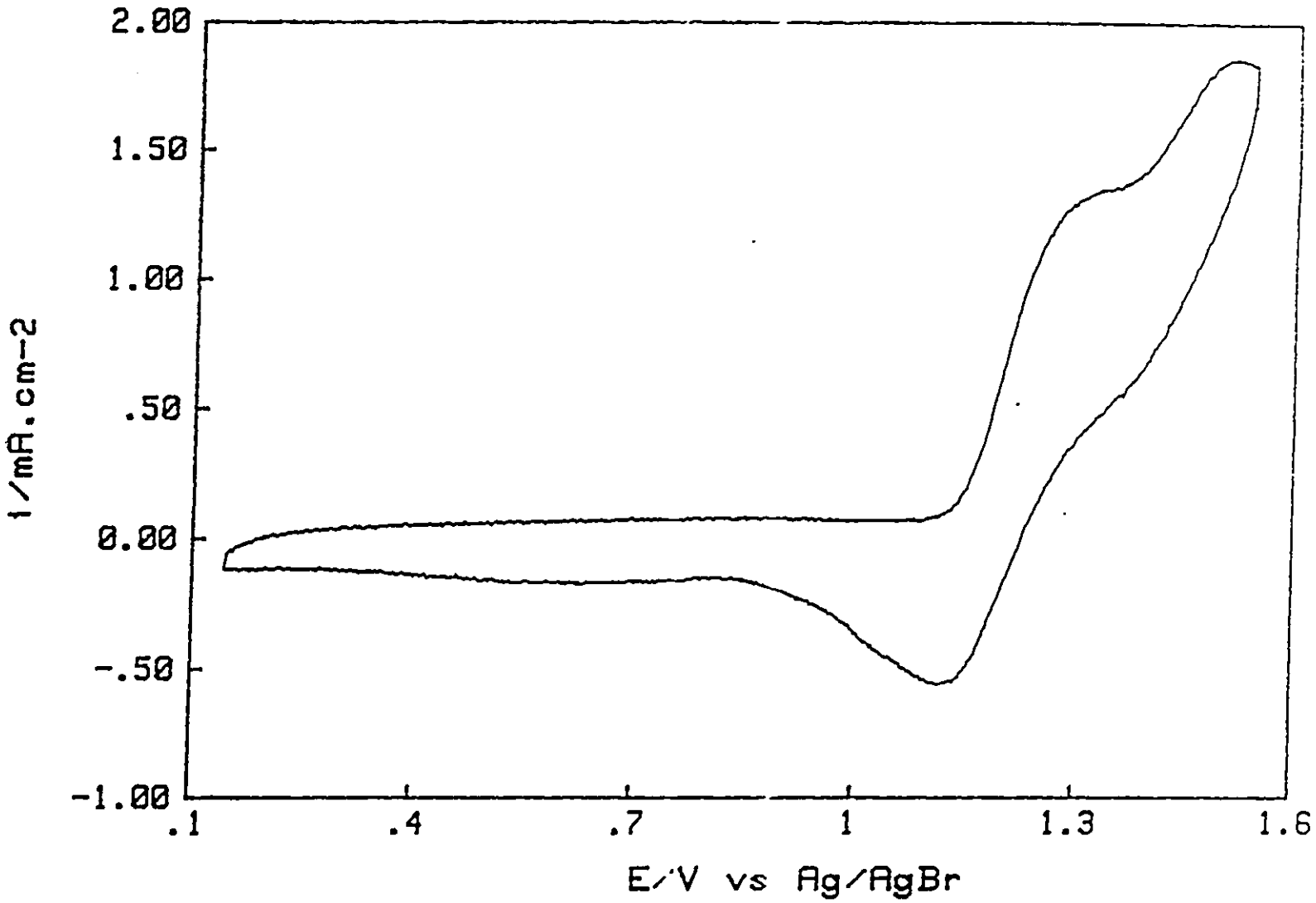

Fig. 28. CV of 0.01 M HBr in 0.5 M $HClO_4$ at Ru

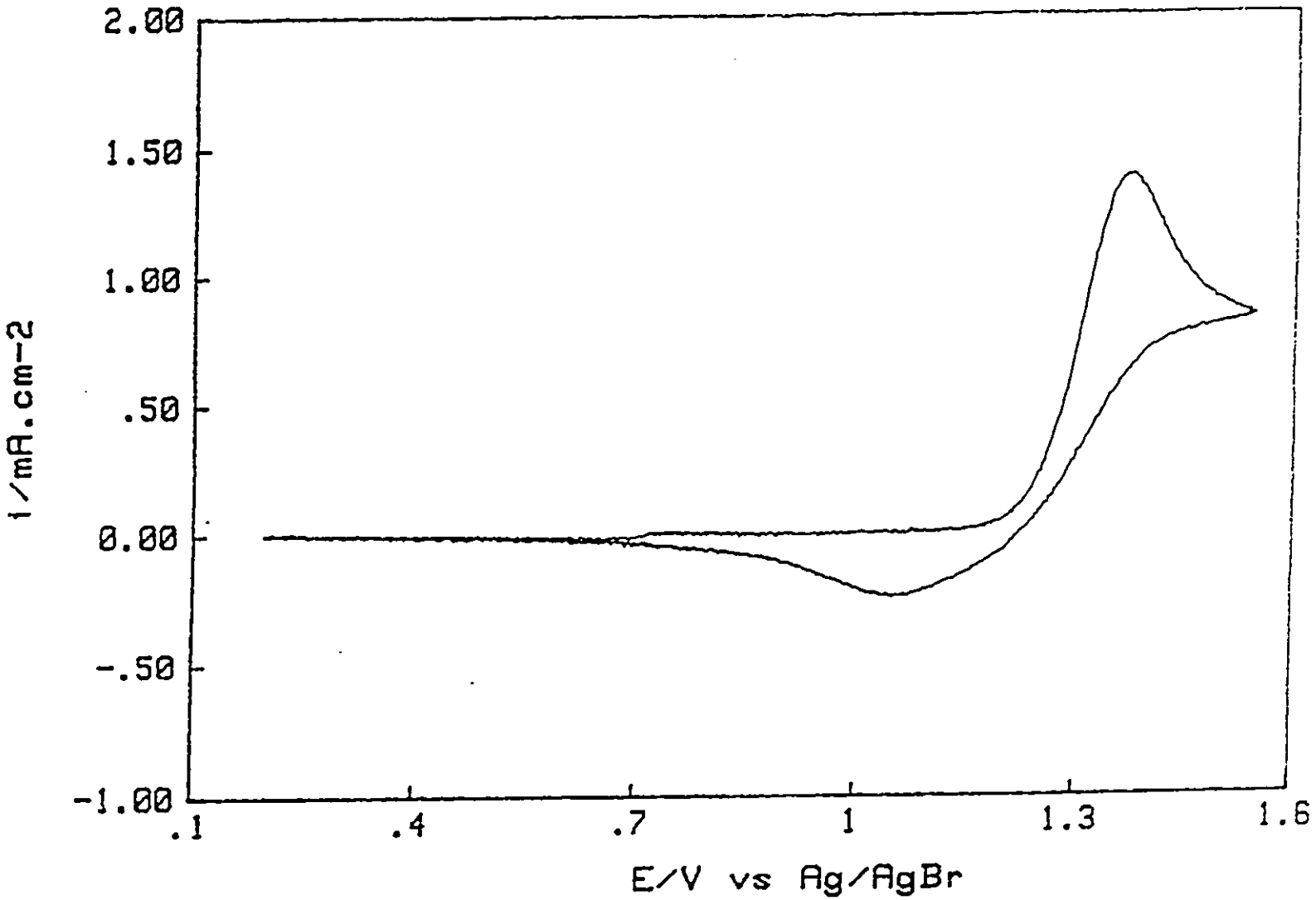

Fig. 29. CV of 0.01 M HBr in 0.5 M $HClO_4$ at Ir

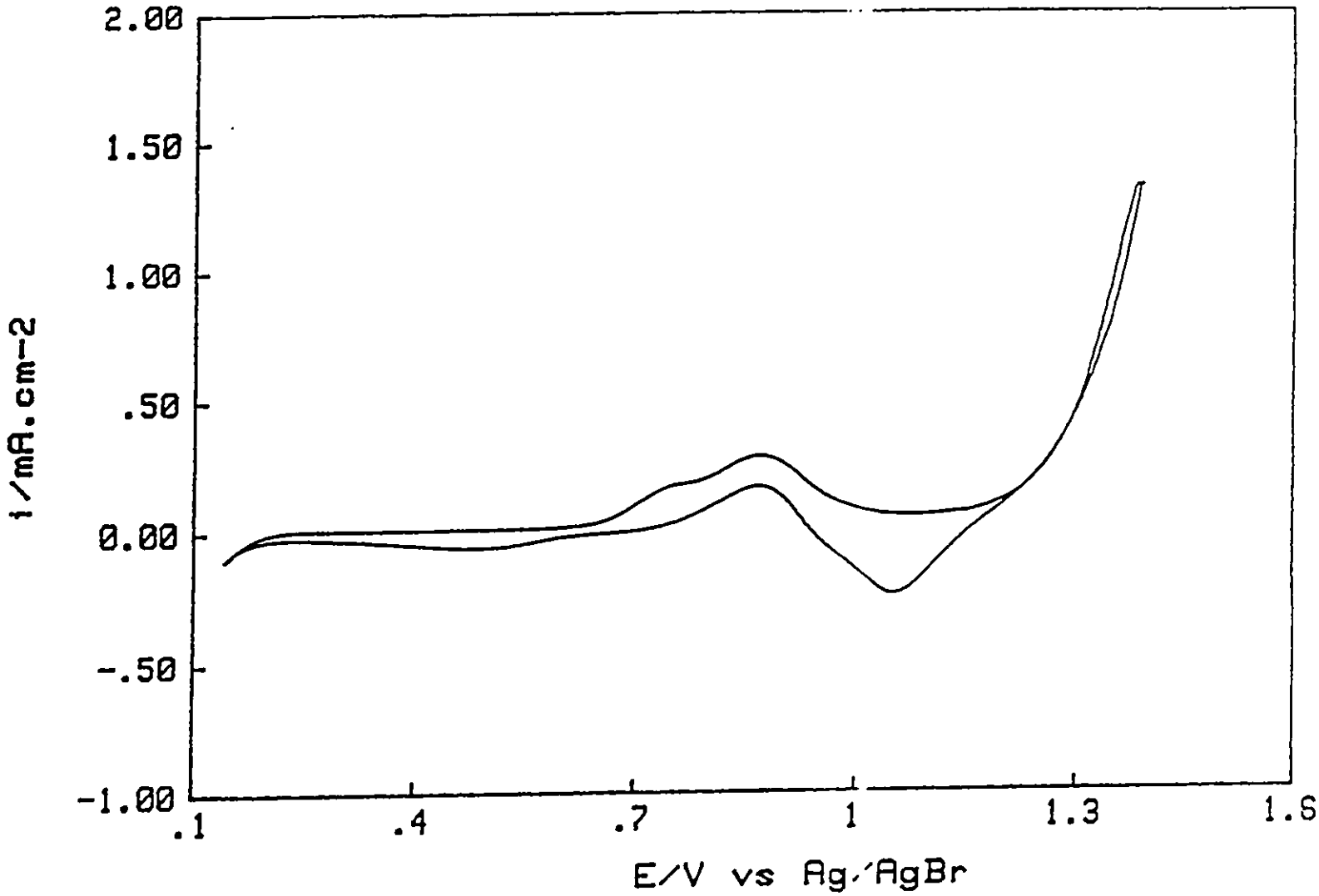

Fig. 30. CV of 0.01 M HBr in 0.5 M $HClO_4$ at Pd (the origins of anodic current peak both on the anodic and cathodic sweep profiles are unclear)

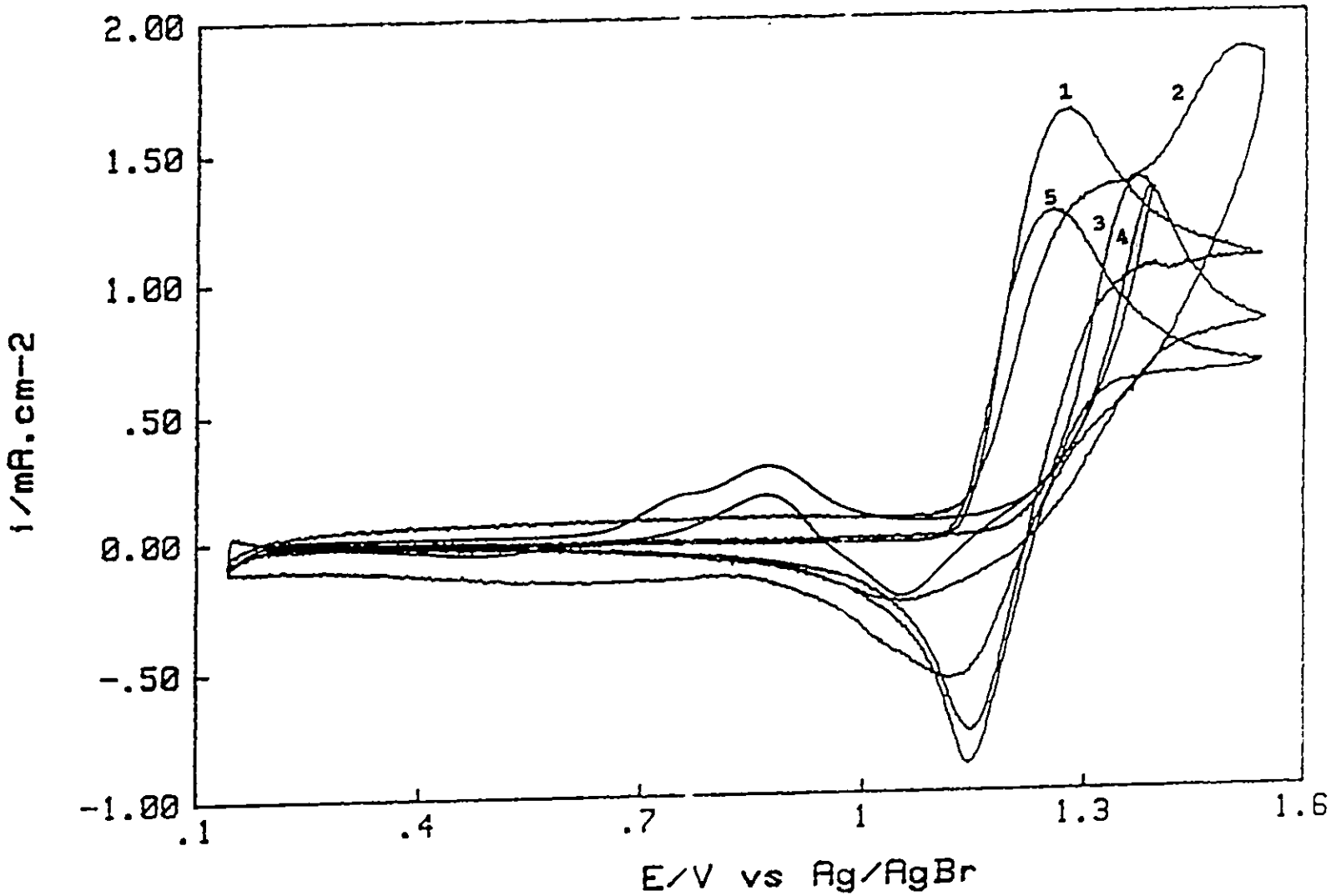

Fig. 31. Comparison of CV's for 0.01 M HBr in 0.5 M $HClO_4$ at Rh (1), Ru (2), Ir (3), Pd (4) and Pt (5)

comparatively at Rh, Ru, Ir, Pd and Pt electrodes. The overall comparison (Fig. 31) shows that Br_2 formation arises rather similarly at Pt, Ir and Rh, with a broad anodic peak around 1.13 V vs AgBr/Ag. However, at the Ru electrode, a shoulder appears on the CV like that at Pt, associated probably with oxide film formation coupled with Br_2 formation. Note that at Ru surface-oxide film formation commences at substantially lower potentials than at Pt and film thickening is more facile. At the Pd electrode, more extensive Br_2 formation arises during the experimental observations and a sharper current rise than that at Pt or Ir appears in the CV. Also, there is an anodic current peak both on the anodic and cathodic sweep profiles at Pd, the origins of which are unclear but will be further checked in continuing follow-up work.

The cathodic peak currents on the cathodic sweeps, in the case of these four metals (Rh, Ru, Ir and Pd), that arise immediately below the rising currents for Br_2 formation (see Fig. 31) are probably associated with reduction of Br_2 formed on the prior anodic sweeps, as was also seen in the results for Pt at appreciable Br^- concentrations (Figs. 15—17).

The influence of bromide ion adsorption on the surface oxidation behaviour of these electrodes is analogous to that at Pt but a certain degree of specificity of the effect with respect to the identity of the substrate metal is observed, as may be expected. This specificity arises jointly from (a) the potential at which oxide film formation begins; (b) the

electrosorption isotherm for sub-monolayer oxide film development and (c) from the properties of the metal surface for Br^- adsorption. The resulting state of the surface thus depends, in part, on the surface and bulk properties of the substrate noble metal electrode, and the species in solution, as well as on the electronic (donicity, polarizability) and hydration properties of the bromide ions themselves that become adsorbed, as has been emphasized earlier.

5.1.6. Thermodynamics of Trihalide Complex-Ion Equilibria in Various Solutions of Br

In the reaction schemes (see section 5.2), the possibility of discharge from the Br_3^- ion, in parallel with that from Br^-, was recognized. Behaviour of the resulting adsorbed Br^- and Br_3^- intermediates in electrocatalysis of the anodic Br_2 formation at Pt is one of the aspects of the Br_2 formation reaction studied in the present work.

The results of Iwasita and Giordano [47] show, because of the stability of Br_3^-, that it is more difficult to reduce $Br3^-$ than Br_2. Possible reactions involved in the n-electron $Br_2/Br^-/Br_3^-$ couples, when Br_3^- ion as a co-reactant is taken into account, are:

$$Br_2 + Br^- \rightleftharpoons Br_3^- \qquad (n = 0) \qquad (45)$$

$$3Br^- \rightleftharpoons Br_3^- + 2e \qquad (n = 2) \qquad (46)$$

$$2Br_3^- \rightleftharpoons 3Br_2 + 2e \qquad (n = 2) \qquad (47)$$

The theoretical 0.059/n value for both the X_3^-/X^- and X_2/X_3^-

couples is 0.030 V dec^{-1}. The larger-than-predicted values obtained [47] for 0.059/n in nearly all cases for X_3^-/X^- and X_2/X_3^- couples in different solvents suggested, therefore, that the electrode reactions were "irreversible".

The formation constants of the I_3^-, Br_3^- and Cl_3^- ions in *aqueous* medium are $10^{2.9}$, $10^{1.2}$ (Table 6), and $10^{-0.7}$, respectively. Because the acid strength, in the Lewis sense, of the three halogens is in the order $Cl_2 > Br_2 > I_2$ and the base strength order of the three halide ions is $Cl^- > Br^- > I^-$, the order of the stability constants [85] of the trihalides at first glance appears to be incorrect. Water, however, is a stronger acid than Cl_2 and a stronger base than Cl^-; therefore, the hydration energy of both X^- and X_2 increases from the triiodide system to the trichloride system. This is mostly an ion-*size* effect. Accordingly, the stability of the trihalides decreases in the order triiodide > tribromide > trichloride.

The above tribromide formation constants, in particular that for Br_3^- enables the concentrations of Br_3^- species to be calculated for a series of Br^- and Br_2 concentrations, as shown in Table 6. These data are, of course, important for consideration of the kinetics of Br_2 formation in relation to the speciation of the reactant ion and that of the intermediate.

Aprotic solvents such as acetonitrile, nitromethane and acetone are appreciably less acidic or less basic than water. The solvation energy of the halogens in such solvents, in the Lewis acid-base sense, and especially of the monomeric halide

ions is much less than in water, so that the stability of the trihalides is hence greatly increased. In fact, it is possible for the formation constants of the trihalides then to show the expected order, $K_{f(Cl_3^-)} > K_{f(Br_3^-)} > K_{f(I_3^-)}$.

TABLE 6. Estimated Concentrations of $[Br_3^-]$ for Various Br^-/Br_2 Concentrations ($K_f = 10^{1.2}$ M)

$[Br^-]$	$[Br_2]$	$[Br_3^-]$
0.5	6.2×10^{-5}	5.0×10^{-4}
1.0	1.2×10^{-4}	2.0×10^{-3}
1.5	1.9×10^{-4}	4.5×10^{-3}
2.5	3.1×10^{-4}	1.2×10^{-2}
3.0	3.7×10^{-4}	1.8×10^{-2}
5.0	6.2×10^{-4}	5.0×10^{-2}

Voltammetric evaluation of the stability of trichloride, tribromide and triiodide ions in nitromethane, acetone and acetonitrile were studied by Adžić, Yeager and Cahan [46]: in aprotic solvents, the order of stability of the trihalides is $Cl_3^- > Br_3^- > I_3^-$, the reverse of that in water.

5.2. Steady-State Kinetic Behaviour of the Br^-/Br_2 Formation Reaction; Tafel Relations

5.2.1. Elementary Reaction Steps in Overall Mechanisms

First we outline the possible reaction steps in several mechanisms and present the relevant kinetic equations and electrosorption relations for the reaction intermediates.

An overall electrode reaction is generally composed of a series of partial reactions except in the case of a simple electron-transfer redox process involving stable ions. In at least one of these partial reactions, charge carriers (electrons and/or ions) are transferred across the electrical double-layer at a phase boundary corresponding to a "charge-transfer" reaction. The rate of such a process is determined by the potential difference across the double-layer or some component region of it, e.g. the Helmholtz layer. A "chemical reaction" is different, being a reaction the rate of which depends on only the concentrations of the components or adsorbed reactants and intermediates (in electrolytic processes), and its rate constant is independent of the potential.

Elementary steps in the bromine formation reaction involve discharge of Br^- ion at the metal (M) surface or at surface oxide sites (see below), followed by recombination or electrochemical desorption of the $M/Br^{\cdot}$ species to form Br_2, where / represents the surface at which the species is adsorbed.

The possible principal reactions, e.g. at a noble metal[3] surface such as Pt, are

$$Br^- + Pt \rightleftharpoons Pt/Br^{\cdot} + e \qquad \text{I}$$

$$2Pt/Br^{\cdot} \rightleftharpoons 2Pt + Br_2 \qquad \text{IIa}$$

[3]Anodic Br_2 formation is practically observable only at C and the noble metals, and some unreactive oxides, e.g. RuO_2. At base metals, anodization in the presence of Br^- results either in metal dissolution or "MBr" salt formation at the metal surface, e.g. as for Ag. The results referred to earlier at Hg [50] are puzzling in this respect since Hg_2Br_2 would be expected to be the first product.

or

$$Pt/Br^{\cdot} + Br^{-} \rightleftharpoons Pt + Br_2 + e \qquad \textbf{IIb}$$

Steps **I**, or **IIa** and **IIb** are analogous to respective steps in H_2 or Cl_2 evolution, as noted earlier.

In the case of bromine, other steps involving trimeric species Br_3^- (see section 5.1.6) can be involved, e.g.

$$Br_2 + Br^{-} \rightleftharpoons Br_3^{-} \qquad \textbf{III}$$

which can also be discharged, in parallel with that of Br^-:

$$Br_3^{-} + Pt \rightleftharpoons Pt/Br_3^{\cdot} + e \qquad \textbf{IVa}$$

or

$$Br_3^{-} + Pt \rightleftharpoons Pt/Br^{\cdot} + Br_2 + e \qquad \textbf{IVb}$$

$$2Pt/Br_3^{\cdot} \rightleftharpoons 2Pt + 3Br_2 \qquad \textbf{Va}$$

or

$$Pt/Br_3^{\cdot} + Br^{-} \rightleftharpoons Pt + 2Br_2 + e \qquad \textbf{Vb}$$

According to Llopis and Vàzques [86], the rates of formation of Br_2 and Br_3^- are comparable; the total rate, v_3, for step **III** is then

$$v_3 = k_3[Br^-][Br_2] - k_{-3}[Br_3^-] \qquad (48)$$

For a fresh bromide solution at the beginning of an electrochemical experiment, $[Br_2] = 0$, $[Br_3^-] = 0$, then $v_3 = 0$, $v_4 = 0$, $v_5 = 0$. Therefore, the first two steps are initially the predominant reactions.

5.2.2. Discharge and Chemisorption Involving the Already Chemisorbed $Br^{(1-\delta)-}$ Species

It was shown in section 5.1 that the primary reactant, Br^-,

normally exists in a chemisorbed state at the Pt electrode having suffered an appreciable degree of spontaneous charge-transfer in the adsorption process (eqn. 43).

An interesting situation arises in such a situation when electrosorption of an intermediate, here $Br^{\cdot}$ (step I), originates from an anion already chemisorbed with partial (δe) transfer of its electronic charge. This case has not, it is believed, been previously considered and is relevant to the mechanisms of Br_2 formation considered in the present work.

At a freshly reduced Pt electrode, the reactant species, in its adsorbed state, is $Br^{(1-\delta)-}$ (see eqn. 43) and its discharge, in the first step of the overall reaction supposedly to $Br^{\cdot}$, will therefore involve transfer of $(1-\delta)e$ of charge. It would appear that the argument of the Tafel exponent will then be $\beta(1-\delta)FV/RT$ for that process. However, process I implies an equilibrium between Br^- and $Br^{(1-\delta)-}$ (adsorbed), so that the surface concentration of $Br^{(1-\delta)-}$ should vary with potential according to a function involving $\exp(\delta FV/RT)$. The overall Tafel slope for discharge of Br^- would then be $b=\exp(\delta FV/RT)\cdot\exp[\beta(1-\delta)FV/RT]$, i.e. $\exp[\beta+\delta(1-\beta)FV/RT]$, corresponding to a Tafel slope value of $2RT/(1+\delta)F$ if $\beta \approx \frac{1}{2}$, which is $<2RT/F$ for the regular discharge case with β taken as $\frac{1}{2}$.

Such Tafel slopes would not experimentally be observed in the present case since they are obscured by the recombination step being rate-controlling (see below). However, the pre-rate-controlling reaction (43) is involved implicitly in the quasi-

equilibrium step **I** so that $\theta_{Br^{\cdot}}$ is related to Br^- ion concentration through the term $\exp(\delta FV/RT)$ for $Br^{(1-\delta)-}$ chemisorption combined with the term $\exp[\beta(1-\delta)FV/RT]$ for the electrosorption, i.e. discharge, of $Br^{\cdot}$ from $Br^{(1-\delta)-}$, i.e. the *regular* exponent for the step of electrosorption of $Br^{\cdot}$ from Br^-, $\exp(1VF/RT)$, is recovered as might be intuitively expected for the *overall* quasi-equilibrium process **I**.

5.2.3. Kinetic Equations for the Multi-Step Process and the Role of Intermediates

Kinetic equations for the anodic Br_2 formation reaction take into account the rates of Br^- or Br_3^- discharge in relation to the rates of formation of Br_2 from the adsorbed intermediate, $Br^{\cdot}$ or $Br_3^{\cdot}$. When one of the Br_2-molecule forming steps is rate-controlling, the potential-dependence of the coverage by the adsorbed, discharged intermediate (cf. section 5.2.2) is one of the factors determining the rate of the overall reaction and its potential dependence.

As in the hydrogen or chlorine evolution processes, if step **IIa** is sufficiently faster than the alternative desorption reaction **IIb**, it is referred to as the "Volmer-Tafel" pathway while if step **IIa** is much slower than **IIb**, it is referred to as the "Volmer-Heyrovsky" pathway. Either of the reaction steps **IIa** and **IIb** can have small rate constants compared with those of step **I** and are then referred to as "rate-determining", depending on which reaction has the smaller rate constant compared with

that of step **I**, but then the predominant pathway is determined by which step, **IIa** or **IIb**, is the faster. In the steady-state, no step should be referred to as "slow", a frequently erroneous usage.

The steady-state kinetic equations for a multi-step electrode reaction take into account: a) the potential dependence of the rate-constant of the charge-transfer desorption step, if this is rate-controlling together with b) the potential dependence of coverage by the electro-active intermediate that is involved (here $Br^{\cdot}$ or $Br_3^{\cdot}$, steps **IIa**, **b** or **IVa**, **b**) or, if the recombination steps **IIa** or **Va**, are rate-controlling, only the potential dependence of coverage by $Br^{\cdot}$ or $Br_3^{\cdot}$. Alternatively, c) if the rate constants of the various desorption steps are substantially greater than that for the discharge step **I**, then only the potential-dependence of that charge-transfer rate constant determines the electrode kinetics.

The potential-dependence of coverage by adsorbed reaction intermediates ($Br^{\cdot}$ or $Br_3^{\cdot}$ here) is usually dealt with in terms of a Langmuir-type [87] electrosorption isotherm (or if lateral interaction effects are significant, by a Frumkin-type isotherm, as explained in section 5.1.3). The electrosorption isotherm for coverage by the intermediate is usually derived by means of the approximation (for desorption-controlled kinetics) that the pre-rate-determining step(s) is (are) almost in equilibrium (so-called "quasi-equilibrium" approach) and that the Langmuir-type isotherm is applicable, at least at relatively low coverages.

Assuming the fractional surface coverage by the $Br^{\cdot}$ intermediate (step I), $\theta_{Br^{\cdot}}$, is proportional to the surface concentration of discharged $Br^{\cdot}$ intermediates from step I, and the free-site fraction $(1 - \theta_{Br^{\cdot}})$ (regarded as "reactant" in the adsorption step I) is proportional to the concentration of free sites on the surface, then, an electrochemical Langmuir isotherm can be deduced from the kinetic equations for step I and its reverse, viz.

$$i_1 = Fk_1C_{Br^-}(1 - \theta_{Br^{\cdot}})\exp(\beta\eta F/RT) \qquad (49)$$

$$i_{-1} = Fk_{-1}\theta_{Br^{\cdot}}\exp[-(1 - \beta)\eta F/RT] \qquad (50)$$

If quasi-equilibrium is assumed, the forward and backward currents can be virtually equated, i.e., $i_1 \approx i_{-1}$. Then an electrochemical adsorption isotherm relating the fractional surface coverage $\theta_{Br^{\cdot}}$ to the potential difference across the interphase or the overpotential η can be written, as in eqn. 10, as

$$\theta_{Br^{\cdot}}/(1 - \theta_{Br^{\cdot}}) = K_1C_{Br^-}\exp(\eta F/RT) \qquad (51)$$

where, $K_1 = k_1/k_{-1}$. If interaction effects are significant, K_1 is substituted by $K_{0,1}\exp[-g\theta_{Br^{\cdot}}]$ where g is an interaction parameter (Frumkin isotherm, eqn. 11).

For the case of the Volmer-Tafel pathway, i.e. step **IIa** being the rate-determining but preferred step, with $Br^{\cdot}$ recombination arising from discharged $Br^{\cdot}$ atoms, the rate of the overall reaction will be given by

$$i_{2a} = 2Fk_{2a}\theta_{Br^{\cdot}}^2 \qquad (52)$$

At sufficiently low coverages, $1 - \theta_{Br^{\cdot}} \approx 1$

$$\theta_{Br\cdot} = K_1 C_{Br\cdot} \exp(\eta F/RT) \ll 1$$

i.e, coverage becomes a simple exponential function of η and the rate equation then becomes

$$i_{2a} = 2Fk_{2a}K_1^2 C_{Br\cdot}^2 \exp(2\eta F/RT) \qquad (53)$$

At 298K, a Tafel slope b ≈ 29 mV/dec will arise (Fig. 31) for such a condition. As $\theta_{Br\cdot} \geq 0.1$, however, the η vs log i plot will depart from linearity (see Fig. 31) because then

$$\theta_{Br\cdot} = [K_1 C_{Br\cdot} \exp(\eta F/RT)]/[1 + K_1 C_{Br\cdot} \exp(\eta F/RT)] \qquad (54)$$

and correspondingly

$$i_{2a} = 2Fk_{2a}\{[K_1 C_{Br\cdot} \exp(\eta F/RT)]/[1 + K_1 C_{Br\cdot} \exp(\eta F/RT)]\}^2 \qquad (55)$$

Eqn. 55 enables a special equation to be written as a basis for testing applicability of recombination-controlled kinetics to experimental kinetic data. Thus, eqn. 55 can be rearranged to

$$\exp(\eta F/RT)]/i_{2a}^{1/2} = (2Fk_{2a})^{-1/2}[(K_1 C_{Br\cdot})^{-1} + \exp(\eta F/RT)] \qquad (56)$$

Then if $[\exp(\eta F/RT)]/i_{2a}^{1/2}$ is plotted vs $\exp(\eta F/RT)$ and is linear, this will indicate that the reaction is recombination-controlled. The slope of such a relation will be $(2Fk_{2a})^{-1/2}$ while its intercept will be $(2Fk_{2a})^{-1/2}(K_1 C_{Br\cdot})^{-1}$, from which k_{2a} and K_1 can be evaluated (see Fig. 37 in 5.2.5).

As $\theta_{Br\cdot}$ approaches unity (full coverage), an activation-determined limiting current-density $i_{2a} = 2Fk_{2a}$ will arise (Fig. 32a, in the log i region 1 to 2, log θ region 0 to 1) which is independent of overpotential and any mass-transfer in solution. In regard to the latter point, it should be noted that limiting currents may also arise for quite different reasons if

diffusion-controlled conditions are attained. Below log i = ca. 10^0, (Fig. 32) a Tafel slope of 2.3RT/2F (29 mV at 298 K) arises (eqn. 53) that is characteristic of the recombination type of mechanism.

It is to be noted that if an already appreciable coverage by the Br˙ intermediate arises at the reversible potential of the Br^-/Br_2 reaction, determined by the electrochemical equilibrium constant K_1 of step I, a physically possible situation for a sufficiently large K_1 value at $\eta = 0$, then the Tafel relation shown in Fig. 32a will rise from the $\eta \to 0$ origin at a larger θ_{Br} than for the arbitrary situation chosen for the calculation of the curve in Fig. 32a. For example if K_1 is such that say θ_{Br} (η=0) is around at least 0.001 ~ 0.01, then *no* linear region of Tafel slope 0.029 V will be observable. In fact, near the reversible potential, the Tafel line will curve in asymptotically to the axis of abscissae (in the usual way) without the low-slope linear region being manifested (Fig. 32b), because of the increasing participation of the back-reaction as $\eta \to 0$.

This seems to be the explanation of the Tafel curve behaviour observed in a number of the experimental relations shown (Figs. 34—36, etc., see below) in the present work.

For the case of a Tafel relation having a slope of $RT/\beta F$, $\equiv 2RT/F$ for $\beta = 0.5$, for a discharge-controlled step, the back reaction correction for currents near the reversible potential is through the well known factor originating from the Butler-

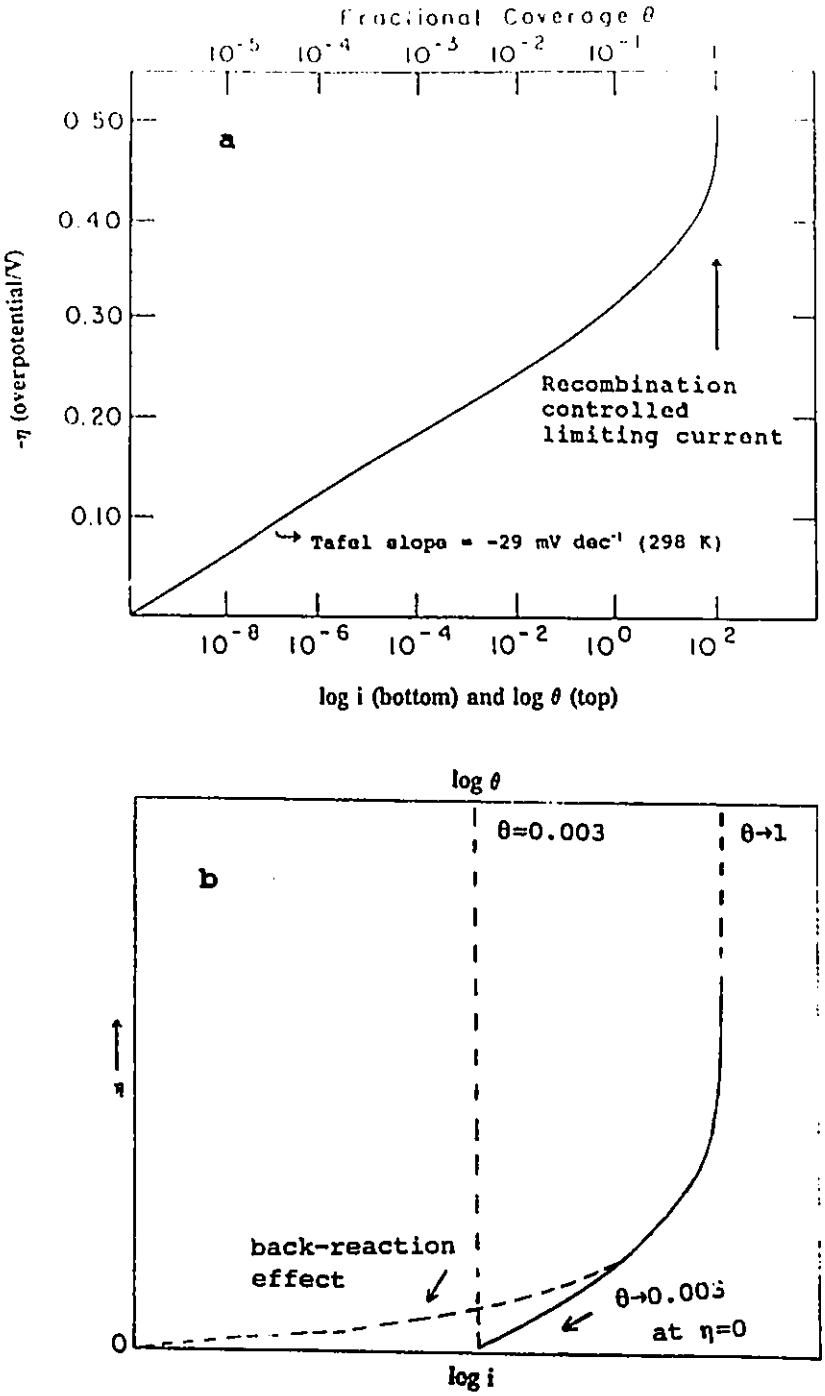

Fig. 32. a) η vs log i Tafel plot and the generalized variation of θ with η (eqns. 52 and 53) according to Langmuir adsorption with the recombination step rate-controlling

b) η vs log i Tafel plot when significant coverage by the intermediate already arises near the reversible potential and the back-reaction current component is also significant

Volmer equation, viz.

$$i_a = i/1-\exp(-\eta F/RT) \qquad (57)$$

where i_a is the actual anodic current component (relevant to the anodic reaction kinetics) and i the net measured currents. However, for a recombination-controlled current, as in Br_2 formation, the equivalent of the Butler-Volmer equation is

$$i = i_a - |i_c| = 2Fk_2\theta^2_{Br^\cdot} - 2Fk_{-2}(1 - \theta_{Br^\cdot})^2 \qquad (58)$$

This relation can be written in terms of the coverage, $\theta_{Br^\cdot,e}$, at the equilibrium potential:

$$i = i_0\theta^2_{Br^\cdot}/\theta^2_{Br^\cdot,e} - i_0(1 - \theta^2_{Br^\cdot})/(1 - \theta^2_{Br^\cdot,e})^2 \qquad (59)$$

so that the actual anodic current component is

$$i_a = i/[1 - \frac{(1 - \theta_{Br^\cdot})^2}{\theta^2_{Br^\cdot}} \cdot \frac{\theta^2_{Br^\cdot,e}}{1 - \theta^2_{Br^\cdot,e}}] \qquad (60)$$

Introduction of the (Langmuir) isotherm for $Br^\cdot$ electrosorption

$$[\frac{\theta_{Br^\cdot}}{1 - \theta_{Br^\cdot}}]_\eta = \frac{\theta_{Br^\cdot,e}}{1 - \theta_{Br^\cdot,e}} \cdot \exp[\frac{\eta F}{RT}] \qquad (61)$$

allows the required anodic current component to be derived as:

$$i_a = i/1-\exp[-\frac{2\eta F}{RT}] \qquad (62)$$

which differs from the correction result for the ion-discharge case shown above with exponent $-\eta F/RT$.

Hence, as the recombination-determined Tafel relation approaches $\eta = 0$ at low polarization, the recombination-controlled anodic current, i_a, for Br_2 formation must be

calculated from the measured net i values with the above correction factor applied. For small η values, $d\eta/d \ln i$ is < RT/2F and not constant.

In Fig. 33, an example (cf. Table 7, 8 and Fig. 34) is shown from which it is seen that an almost linear relation arises down towards $\eta = 0$ rather than the continuous curvature of the experimental net-current relations. Significantly, its Tafel slope is near 30 mV dec^{-1}. Although there are some deviations of the corrected points from the line, there do not exceed the reliability of the η measurements which are 1-2 mV at the low η's here; note the time scale for η.

TABLE 7. Calculated Values for the Correction of i for the Back-Reaction Effect

η/V	.003	.005	.007	.001	.013	.017	.020	.025	.03
1-exp(-2ηF/RT)	.208	.323	.420	.541	.637	.734	.789	.857	.903

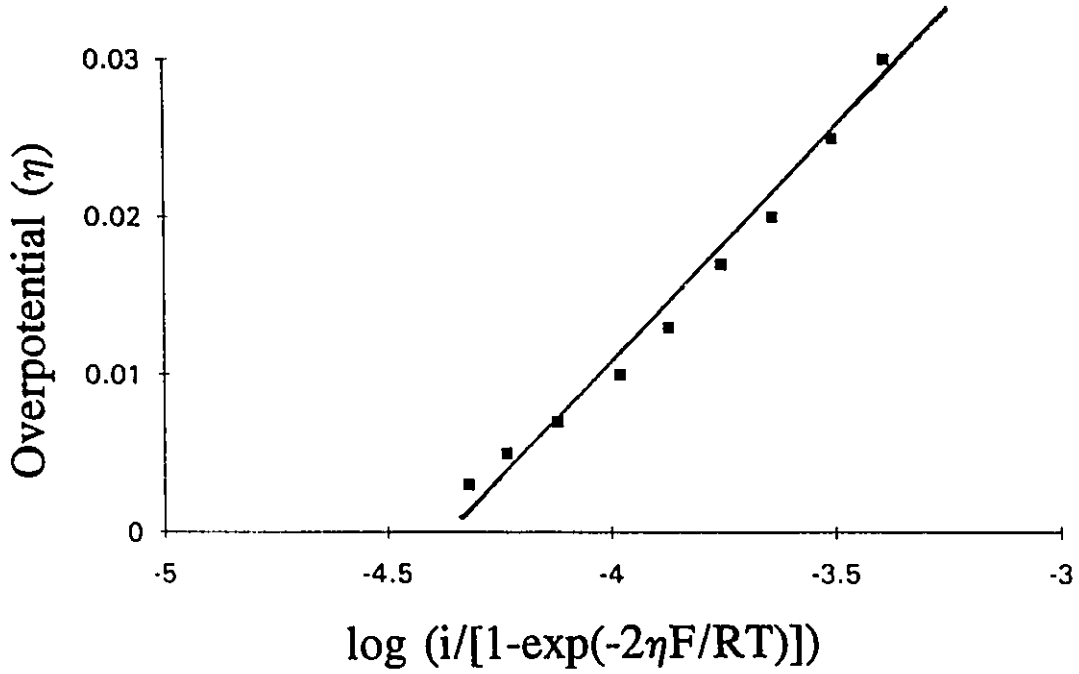

Fig. 33. Correction for the back-reaction effect, e.g. for the Tafel-plot results for Pt in 3 M NaBr/0.1 M $HClO_4$ at η = 0.003, 0.005, 0.007, 0.01, 0.013, 0.017, 0.02, 0.025 and 0.03 V (cf. Fig. 34)

Another modification of the recombination test equation can be made which is best applicable to relatively high θ_{Br} values. Thus rearranging eqn. 55 in a different way, the kinetic behaviour can then be examined more sensitively for high θ_{Br} conditions; the resulting equation is

$$i_{2a}^{-½} = (2Fk_{2a})^{-½} + (2Fk_{2a})^{-½}(K_1C_{Br^-})^{-1}\exp(-\eta F/RT) \qquad (63)$$

This also again enables both k_{2a} and K_1 to be evaluated (see Fig. 36], this time from the slope and intercept of the plot of $i_{2a}^{-½}$ vs $\exp(-\eta F/RT)$. This procedure and that involving eqn. 56 was developed by Conway and Novak [88] as a new method to test the applicability of the "recombination-controlled" mechanism and to evaluate it quantitatively for coupling of steps I and **IIa**.

The Temkin isotherm in the quasi-equilibrium approach has also been used to examine further the "Volmer-Tafel" type mechanism, especially by workers of the Russian School. Both interactions and heterogeneity effects usually arise at a real surface. The latter effects are taken into account by introducing a coverage-dependent adsorption energy in the configurational partition function in the approach used by Temkin [64]. For immobile adsorption, heterogeneity is not detectable by coverage-dependent heat of adsorption because sites of varying energy are filled randomly and the measured heat of adsorption is hence an average value. However, significant lateral interaction effects will still lead to a coverage-dependent adsorption energy for different reasons

arising from close-neighbour configurations (Frumkin isotherm), the probability of which increases with $\theta_{Br\cdot}$.

The basic assumption underlying the Temkin isotherm is that a varying energy of adsorption arises on account of heterogeneity so that the surface is regarded as being made up of patches. At each patch, the Langmuir isotherm is supposed [87] to hold independently, with a local standard Gibbs energy or heat of adsorption, depending on the patch distribution, and decreases linearly with coverage:

$$\Delta G^\circ_{Br\cdot} = \Delta G^\circ_{Br\cdot} + r\theta_{Br\cdot} \qquad (64)$$

$\Delta G^\circ_{Br\cdot}$ does not, however, always vary linearly with $\theta_{Br\cdot}$. To modify the equation, the θ term in the exponent can be raised to a power n, i.e., $\Delta G^\circ_{Br\cdot} = \Delta G^\circ_{Br\cdot} + r\theta^n_{Br\cdot}$; then eqn. 64 is a special case for n = 1.

5.2.4. Kinetic Equations for the Case of Significant Interaction Effects

The equations for i_1, i_{-1} and i_{2a} or i_{2b} can be rewritten as follows, if an interaction term, $g\theta_{Br\cdot}$, is taken into account:

$$i_1 = Fk_1C_{Br\cdot}(1 - \theta_{Br\cdot})\exp(-\beta g\theta_{Br\cdot})\exp(\beta\eta F/RT) \qquad (65a)$$

$$i_{-1} = Fk_{-1}\theta_{Br\cdot}\exp[(1 - \beta)g\theta_{Br\cdot}]\exp[-(1 - \beta)\eta F/RT] \qquad (65b)$$

and

$$i_{2a} = 2Fk_{2a}\theta_{Br\cdot}^2\exp(2g\theta_{Br\cdot}) \qquad (66a)$$

or

$$i_{2b} = 2Fk_{2b}\theta_{Br\cdot}\exp(-\beta' g\theta_{Br\cdot})\exp(\beta'\eta F/RT) \qquad (66b)$$

For the case of step I being in quasi-equilibrium, i.e., $i_1 = i_{-1}$,

$$[\theta_{Br\cdot}/(1 - \theta_{Br\cdot})]\exp(g\theta_{Br\cdot}) = K_1C_{Br\cdot}\exp(\eta F/RT) \qquad (67)$$

This is a Frumkin-type isotherm (cf. eqn. 11). The isotherm comparison in Fig. 21 showed that g is quite small for bromide adsorption up to ca. 70% coverage. The Langmuir isotherm emerges as a special case for g = 0. For intermediate values of coverage, $0.2 < \theta_{Br\cdot} < 0.8$, and if an appreciable value of g applies, the exponential term in the equation would predominate; then taking logarithms of both sides of eqn. 67 and noting then that $\ln [\theta_{Br\cdot}/(1 - \theta_{Br\cdot})] \approx 0$ because $\theta_{Br\cdot} \approx 1 - \theta_{Br\cdot}$, so that $\theta_{Br\cdot}/(1 - \theta_{Br\cdot}) \approx 1$, then

$$\theta_{Br\cdot} = [\ln K_1 C_{Br^-}]/g + \eta F/gRT \qquad (68)$$

This is equivalent to the Temkin isotherm, i.e., $\theta_{Br\cdot}$ would be linearly dependent on the overpotential η and logarithmically dependent on the concentration, C_{Br^-}, as for Cl^-. However, the physical significance of eqn. (68) is quite different from that of Temkin's isotherm and the analysis of the experimental isotherm for Br^- at Pt shows that g is, in fact quite small.

From eqn. (67), $\theta_{Br\cdot}$ can be written implicitly as

$$\theta_{Br\cdot} = \frac{K_1 C_{Br^-} \exp(\eta F/RT)}{\exp(g\theta_{Br\cdot}) + K_1 C_{Br^-} \exp(\eta F/RT)} \qquad (69)$$

If i_1, i_{-1}, i_{2a} are combined, the total current can be obtained as

$$i = 2Fk_2 \left[\frac{K_1 C_{Br^-} \exp(\eta F/RT)}{\exp(g\theta_{Br\cdot}) + K_1 C_{Br^-} \exp(\eta F/RT)}\right]^2 \exp(2g\theta_{Br\cdot}) \qquad (70)$$

which can be rearranged as

$$\exp(\eta F/RT)/i^{1/2} = (2Fk_{2a})^{-1/2} [(K_1 C_{Br^-})^{-1} + \exp(-g\theta_{Br\cdot}) \exp(\eta F/RT)] \qquad (71a)$$

or

$$i^{-1/2} = (2Fk_{2a})^{-1/2}[(K_1C_{Br^-})^{-1}\exp(-\eta F/RT) + \exp(-g\theta_{Br^\cdot})] \quad (71b)$$

The initial Naperian Tafel slope at low overpotential, for conditions when $\theta_{Br^\cdot}$ is small, remains RT/2F but the limiting current-density, i.e. for $\theta_{Br^\cdot} \rightarrow 1$, now interestingly should depend on the lateral interaction parameter g as well as k_2.

The *steady-state* treatment includes the pathways of recombination and electrochemical desorption, and the reverse direction of discharge. In the steady-state, the surface concentration, related to $\theta_{Br^\cdot}$ of adsorbed $Br^\cdot$, is independent of time, i.e., $d\theta_{Br^\cdot}/dt = i_1 - i_{-1} - i_{2a} - i_{2b} = 0$. In the case where the Langmuir isotherm applies

$$i_1 = Fk_1C_{Br^-}(1 - \theta_{Br^\cdot})\exp(\beta\eta F/RT) = k_{-1}'(1 - \theta_{Br^\cdot}) \quad (72)$$

$$i_{-1} = Fk_{-1}\theta_{Br^\cdot}\exp[-(1 - \beta)\eta F/RT] = k_{-1}'\theta_{Br^\cdot} \quad (73)$$

$$i_{2a} = 2Fk_{2a}\theta_{Br^\cdot}^2 = k_2'\theta_{Br^\cdot}^2 \quad (74a)$$

$$i_{2b} = Fk_{2b}\theta_{Br^\cdot}\exp(\beta'\eta F/RT) = k_{2b}'\theta_{Br^\cdot} \quad (74b)$$

β and β' are symmetry factors for the charge-transfer steps of **IIa** and **IIb**. Therefore, $Br^\cdot$ coverage is now given, in the steady-state case, from

$$k_1'(1 - \theta_{Br^\cdot}) - k_{-1}'\theta_{Br^\cdot} - k_{2a}'\theta_{Br^\cdot}^2 - k_{2b}'\theta_{Br^\cdot} = 0 \quad (75)$$

so that

$$\theta_{Br^\cdot} = \frac{-(k_1' + k_{-1}' + k_{2b}') + [(k_1' + k_{-1}' + k_{2b}')^2 + 4k_1'k_{2a}']^{1/2}}{2k_{2a}'} \quad (76)$$

Under some conditions, the current can be contributed by *both* pathways, i.e. for steps **IIa** and **IIb** in parallel; then

$$i = i_{2a} + i_{2b} = k_{2a}'\theta_{Br}{}^{2} + k_{2b}'\theta_{Br} \quad (77)$$

so that "mixed control" of the kinetics can arise with corresponding more complex potential dependence than for the individual cases treated above. This type of situation usually has been emphasized as rare or coincidental but in the papers of Enyo [89,90], for the analogous case of cathodic H_2 evolution, such a possibility has been taken into serious consideration.

5.2.5. Kinetic Behaviour at Fresh Pt (and Pt RDE) Electrode Surfaces

In section 5.1 it was shown experimentally that Br^- ion adsorption is determined in an important way by its concentration (chemical potential) in relation to competitive, potential-dependent, electrosorption of the surface oxide species (eqns. 38 and 39) at Pt and also other noble metals. Hence, the state of oxidation of the Pt anode surface can be important for Br_2 formation, as it is for Cl_2. Accordingly two kinds of kinetic experiments were conducted: one at "freshly reduced" Pt surfaces and the other at controlled "pre-oxidized" ones. The results of experiments under the first set of conditions are described in the present section, those under the second set of conditions in section 5.2.6.

In order to characterize the steady-state kinetics of the Br_2 formation reaction, steady-state polarization curves for the Br_2 formation reaction were measured potentiostatically at a temperature of 298 K. The resulting behaviour at freshly reduced Pt surfaces is shown in Fig. 34 for various

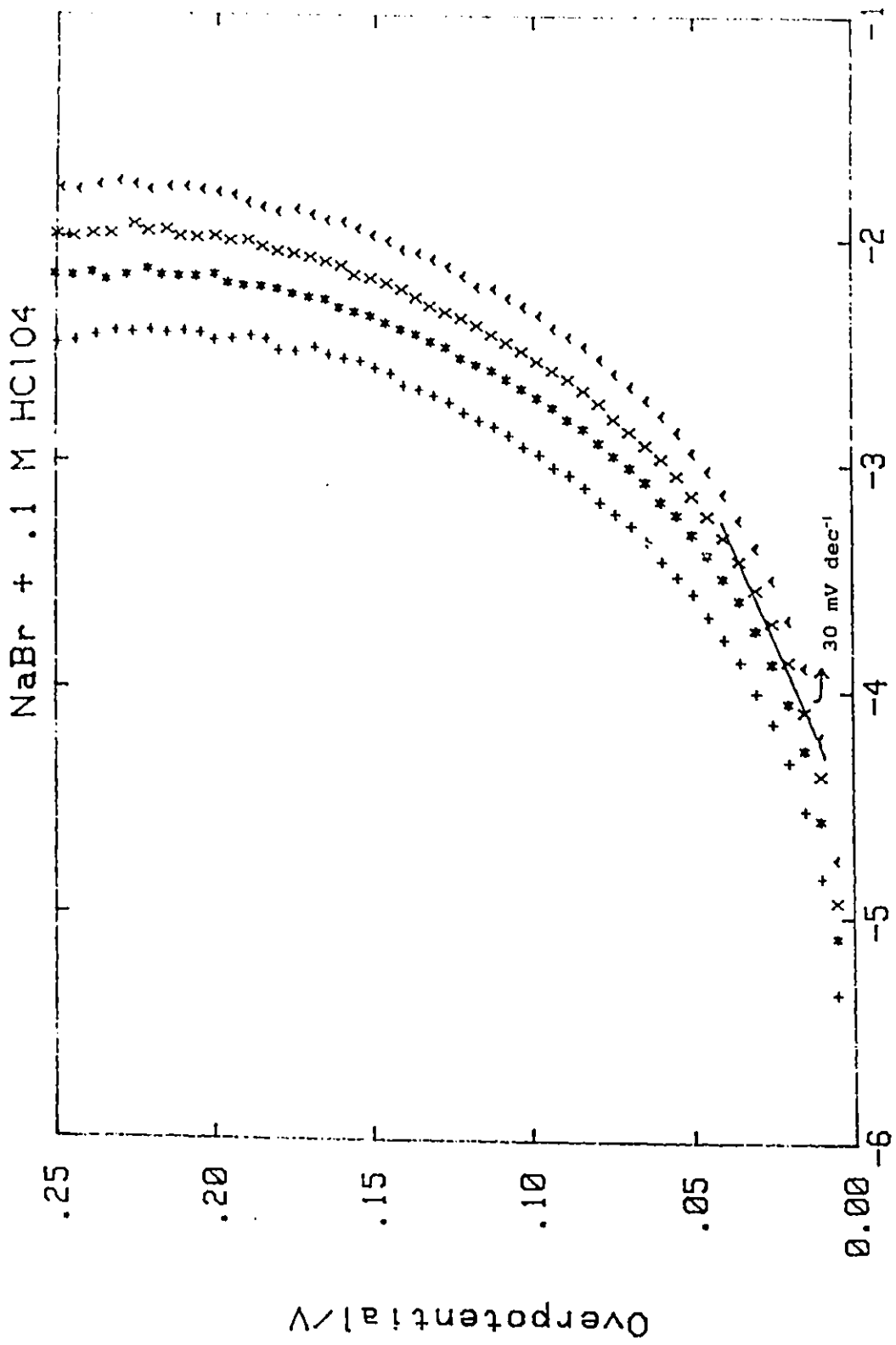

Fig. 34. Tafel plots for 1.0 M (+), 1.5 M (*), 3 M (×) and 5 M (^) NaBr in 0.1 M $HClO_4$

concentrations of Br^- up to 5 M. The concentrations of NaBr in 0.1 M $HClO_4$ from left to right are 1.0 M, 1.5 M, 3.0 M, and 5.0 M. Tafel plots (Fig. 34) showed the Tafel slopes to approach 30 mV dec^{-1} but only over a restricted range of η's in the lower overpotential region. However, continuous curvature in the approach to the reversible potential arises; this is where the back-reaction becomes significant and thus obscures a clear linear low-slope region with b = 30 mV dec^{-1}. However, as shown in section 5.2.4, corrections can be made to the net measured currents for the participation of the back-reaction at low η's as illustrated in the example plotted in Fig. 33.

IR drop corrections were also made with R values being < 7 Ω. The iR-corrected Tafel relations above the low overpotential region all seem to be non-linear, with apparent approaches to limiting currents in the -1.5 to -0.8 decade of i. The directly measured Tafel relations remain curved after "iR" correction, as exhibited in Figs. 34, 35 and 36. The significant conclusion then follows that the curved Tafel relations observed here cannot be due to the influence of uncompensated resistance effects in the measurement system [70] which can give rise, on a log scale, to an apparent rise towards a limiting current.

The approach to limiting currents in the iR-corrected curves could, however, arise here trivially on account of:

a) mass-transport limitation involving Br^- diffusion and/or

b) inhibition due to Br_2 accumulation at the electrode surface.

Both of these effects can be eliminated or diminished by

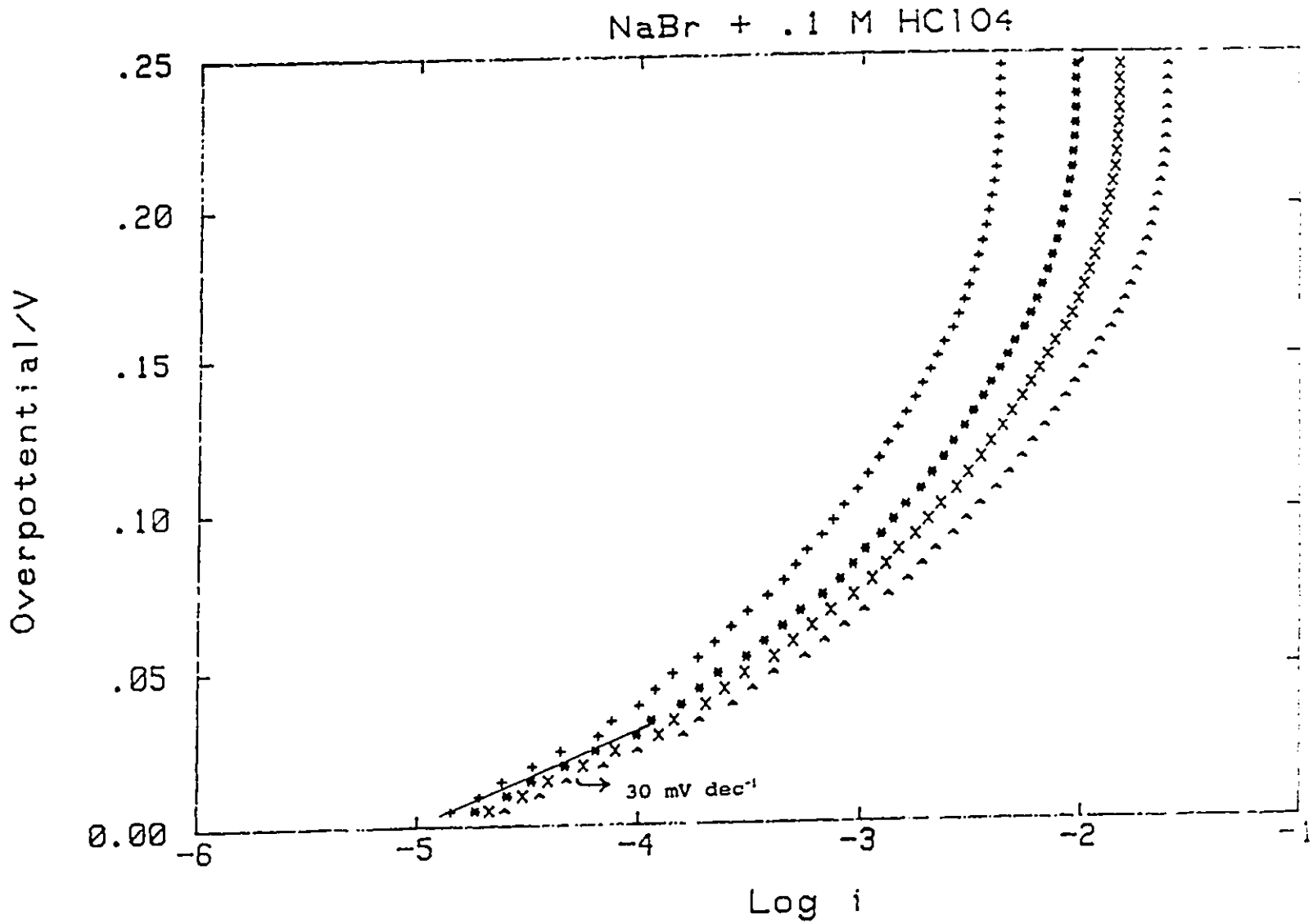

Fig. 35. Tafel plots of 1 M NaBr/0.1 M $HClO_4$ at Pt RDE with rotation rates of 240 (+), 480 (*), 720 (×) and 960 (^) rpm

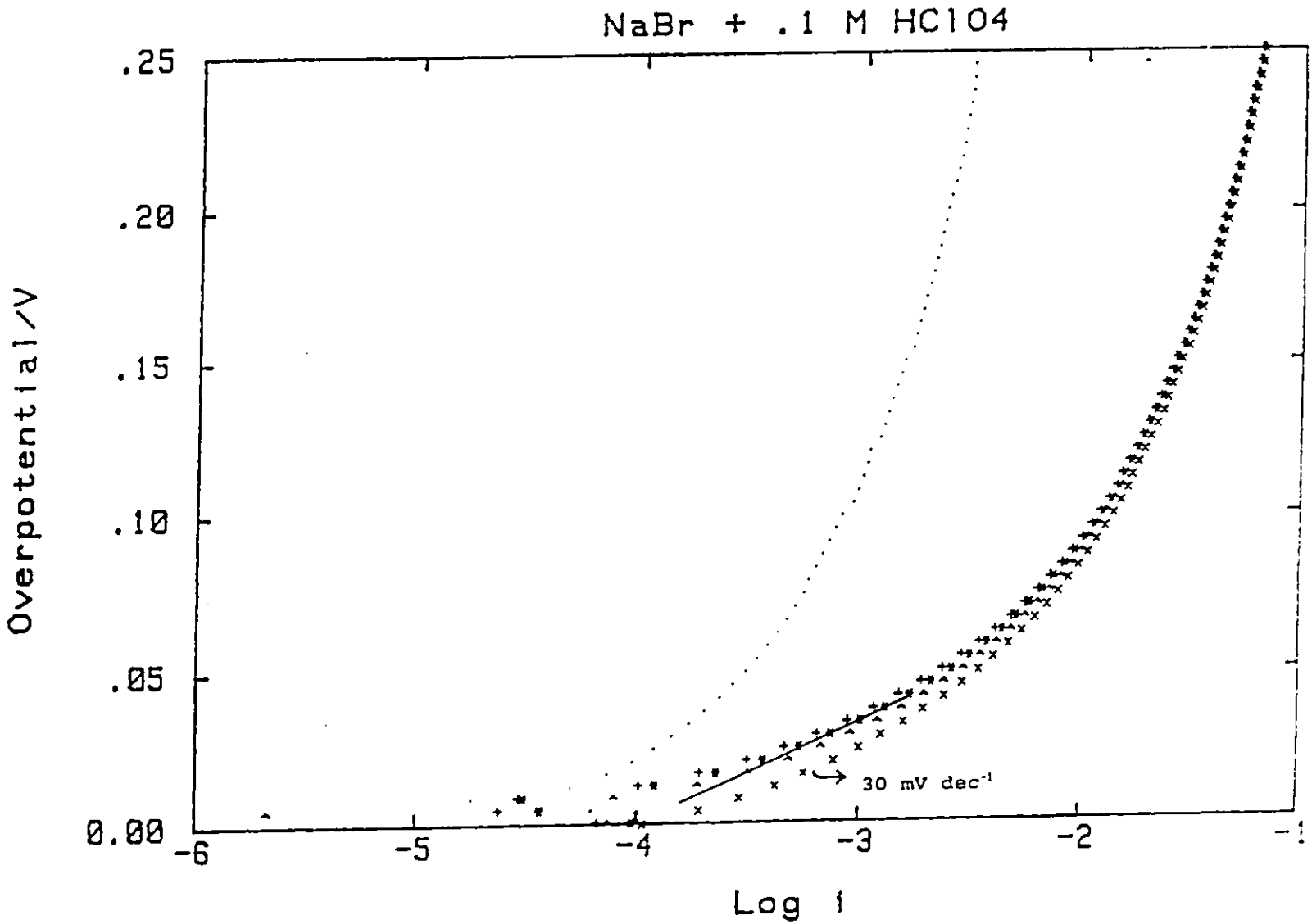

Fig. 36. Comparison of Tafel plots without rotation (·) and with rotation rates of 1200 (+), 2400 (*), 3600 (^) and 4800 (×) rpm at Pt RDE in 1 M Br^- solution

use of a rotating disk electrode. A set of experiments using a rotating platinum disk was therefore carried out in sodium bromide in 0.1 M $HClO_4$ supporting electrolyte solution at rotation rates 0 to 4800 rpm. Results for 240, 480, 720 and 960 rpm are shown in Fig. 35 and for 0, 1200, 2400, 3600 and 4800 rpm in Fig. 36. All these results have been "iR"-corrected. It is important to observe that the resulting Tafel relations are usually still smooth curves, and for 1200—4800 rpm they reach a common, *rotation-independent*, limiting current-density of ca. 10^{-1} A cm^{-2}. At rotation speeds higher than 5000 rpm, some noise arises sometimes which may be due to unavoidable mechanical disturbance or turbulence of the system.

The Tafel plots thus obtained at the Pt RDE demonstrate clearly that the limiting currents are *independent* of rotation rate in the range 1200 to 4800 rpm but somewhat dependent at the lower rotation rates (see Fig. 35) probably due to slowness of Br_2 removal. The exchange current-density is ca. 10^{-2} A cm^{-2}.

The curved form of these relations, with approaches to limiting currents that do not arise either from "iR" effects *or* diffusion control, suggests that Br_2 formation kinetics, under the present conditions at Pt, are $Br^{\cdot}$-*combination controlled* (Fig. 36). This is supported by the observations of approaches to low Tafel slopes of 28—33 mV dec^{-1} at low overpotentials.

A further critical test is use of the eqn. (56) for testing applicability of recombination control, i.e. by plotting as in Figs. 37a and b, $\exp(\eta F/RT)/i^{1/4}$ vs $\exp(\eta F/RT)$ or, alternatively

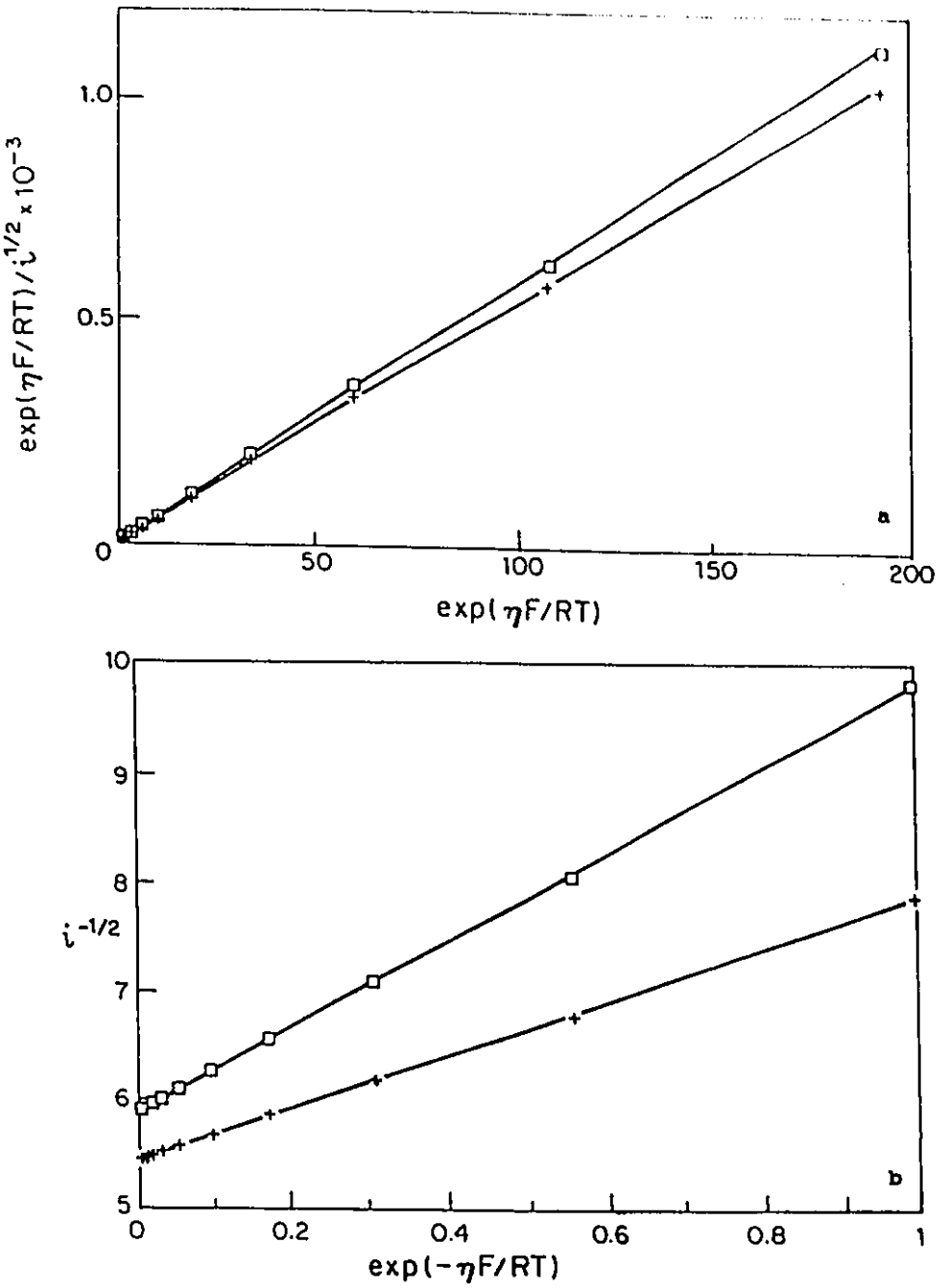

Fig. 37. a) $\exp(\eta F/RT)/i^{1/2}$ vs $\exp(\eta F/RT)$; b) $i^{-1/2}$ vs $\exp(-\eta F/RT)$ based on the Tafel-plot results for 3 M (□) and 5 M (+) Br^- solutions, estimated k_{2a} and K_1 values (cf. eqns. 56 and 63) are: a) 3 M Br^-, $k_{2a} = 4.80\times10^{-7}$ M^{-1} s^{-1}, $K_1 = 1.09$ M^{-1}; 5 M Br^-, $k_{2a} = 5.46\times10^{-7}$ M^{-1} s^{-1}, $K_1 = 0.616$ M^{-1}; b) 3 M Br^-, $k_{2a} = 4.43\times10^{-7}$ M^{-1} s^{-1}, $K_1 = 1.03$ M^{-1}; 5 M Br^-, $k_{2a} = 5.19\times10^{-7}$ M^{-1} s^{-1}, $K_1 = 0.607$ M^{-1}

(eqn. 63) $i^{-\frac{1}{2}}$ vs $\exp(-\eta F/RT)$ using data obtained in experiments performed in 3 M and 5 M Br^- (NaBr in 0.1 M $HClO_4$ at Pt). Figs. 37a and b show the results of such plots: in both figures, straight lines are obtained. Therefore, the major rate-determining reaction is quite clearly indicated as the $Br^\cdot$ recombination step.

Since electrode rotation experiments using a Pt disc showed that the Tafel relations were independent of rotation rate (Fig. 36) except at low rpm, it is also to be concluded that possible effects due to mass-transport of Br^- ion to, or of Br_2 away from the Br_2-forming anode were rendered negligible under the conditions for Fig. 36.

For the purpose of providing quantitative data for the record and for possible future use, the data obtained in aqueous $HClO_4$ solutions are listed in Tables 8 and 9 for reference.

TABLE 8. Experimental Data on Tafel Measurements at Pt for Various Br^- Concentrations

η (V)	i_1(5M Br^-)	i_2(3M Br^-)	i_3(1.5M Br^-)	i_4(1M Br^-)
0.000	1.9×10^{-5}	9.4×10^{-6}	7.1×10^{-6}	2.1×10^{-6}
0.010	2.7×10^{-4}	5.7×10^{-5}	9.6×10^{-6}	7.2×10^{-6}
0.015	3.5×10^{-4}	1.1×10^{-5}	1.0×10^{-5}	9.0×10^{-6}
0.020	0.0043	1.8×10^{-4}	1.7×10^{-4}	1.6×10^{-5}
0.030	0.0057	3.7×10^{-4}	2.1×10^{-4}	3.1×10^{-5}
0.040	0.0071	0.0037	0.0028	0.00049
0.045	0.0086	0.0043	0.0034	0.00064
0.050	0.010	0.0058	0.0046	0.00080

0.060	0.012	0.0073	0.0057	0.0013
0.070	0.013	0.0088	0.0069	0.0019
0.075	0.015	0.010	0.0080	0.0023
0.080	0.017	0.012	0.0096	0.0026
0.090	0.019	0.014	0.011	0.0035
0.100	0.022	0.016	0.013	0.0046
0.105	0.024	0.018	0.015	0.0053
0.110	0.026	0.020	0.017	0.0074
0.120	0.028	0.022	0.019	0.0091
0.130	0.030	0.025	0.022	0.011
0.135	0.033	0.027	0.025	0.013
0.140	0.035	0.029	0.027	0.016
0.150	0.039	0.032	0.030	0.018
0.160	0.043	0.035	0.032	0.020
0.165	0.046	0.039	0.035	0.023
0.170	0.048	0.042	0.038	0.026
0.180	0.051	0.045	0.041	0.028
0.190	0.053	0.048	0.044	0.031
0.195	0.056	0.051	0.047	0.034
0.200	0.058	0.054	0.051	0.037
0.210	0.063	0.057	0.054	0.040
0.220	0.067	0.060	0.058	0.043
0.225	0.070	0.064	0.062	0.047
0.230	0.072	0.067	0.064	0.050
0.240	0.075	0.070	0.067	0.052
0.250	0.078	0.074	0.072	0.056

TABLE 9. Experimental Data from Tafel Measurements in 0.5 M NaBr (columns 2 and 3) and 0.1 M NaBr (columns 4 and 5)

η (V)	i_1 (A cm^{-2})	log i_1	i_2 (A cm^{-2})	log i_2
0.000	2.31×10^{-5}	-4.636	5.67×10^{-6}	-4.245
0.015	0.000105	-3.979	9.27×10^{-5}	-4.033
0.030	0.000278	-3.556	0.000268	-3.572
0.045	0.000584	-3.233	0.000630	-3.201
0.060	0.00121	-2.919	0.00130	-2.885
0.075	0.00206	-2.687	0.00223	-2.652
0.900	0.00310	-2.509	0.00347	-2.460
0.105	0.00482	-2.317	0.00504	-2.298
0.120	0.00685	-2.164	0.00706	-2.119
0.135	0.00924	-2.035	0.00948	-2.023
0.150	0.0121	-1.918	0.0122	-1.914
0.160	0.0159	-1.800	0.0152	-1.819
0.170	0.0193	-1.715	0.0194	-1.713
0.180	0.0229	-1.640	0.0230	-1.638
0.190	0.0272	-1.566	0.0268	-1.571
0.200	0.0313	-1.505	0.0310	-1.509
0.210	0.0355	-1.449	0.0351	-1.455
0.220	0.0401	-1.397	0.0395	-1.404
0.230	0.0454	-1.343	0.0448	-1.349
0.240	0.0501	-1.301	0.0492	-1.308
0.250	0.0549	-1.260	0.0541	-1.267

5.2.6. Role of the Presence of an Oxide Film at Pt

In the aqueous medium, in the absence of competitive adsorption by Br^- ion, an oxide film would be expected to develop at Pt over the range of potentials for Br_2 formation up to

appreciable rates, as seen in Fig. 13. When Br^- concentrations are low, it has been remarked that an ascent towards a limiting current [90] could be due to inhibition by increasing coverage of codeposited OH and O species with increasing potential, as well as possibly to onset of diffusion limitation. Inhibition in that manner, however, is not the reason for the behaviour observed in the present work since:

(a) similar behaviour is found for Br_2 formation at Pt from a completely anhydrous, non-aqueous solvent, CF_3COOH (see below, section 5.3 and Fig. 39), in the complete absence of water and oxide films and,

(b) kinetically-controlled limiting currents, with a curved Tafel relation (see below), also arise at *preoxidized*-rotated Pt surfaces where the electrode is already fully covered by an oxide film which changes little during the polarization run with potentials being changed in a *decreasing direction*, under which conditions, oxide coverage remains constant with potential.

Overpotential vs log (current density) curves were determined over the overpotential range 0 to 0.25 V, on an electrode successively pre-oxidized to different states of oxide film formation (Fig. 38). Comparing the behaviour observed with the results obtained at a reduced Pt electrode, Fig. 39 shows that the limiting current for Br_2 formation is reached at lower currents at the preoxidized Pt electrode than at the "freshly reduced" one.

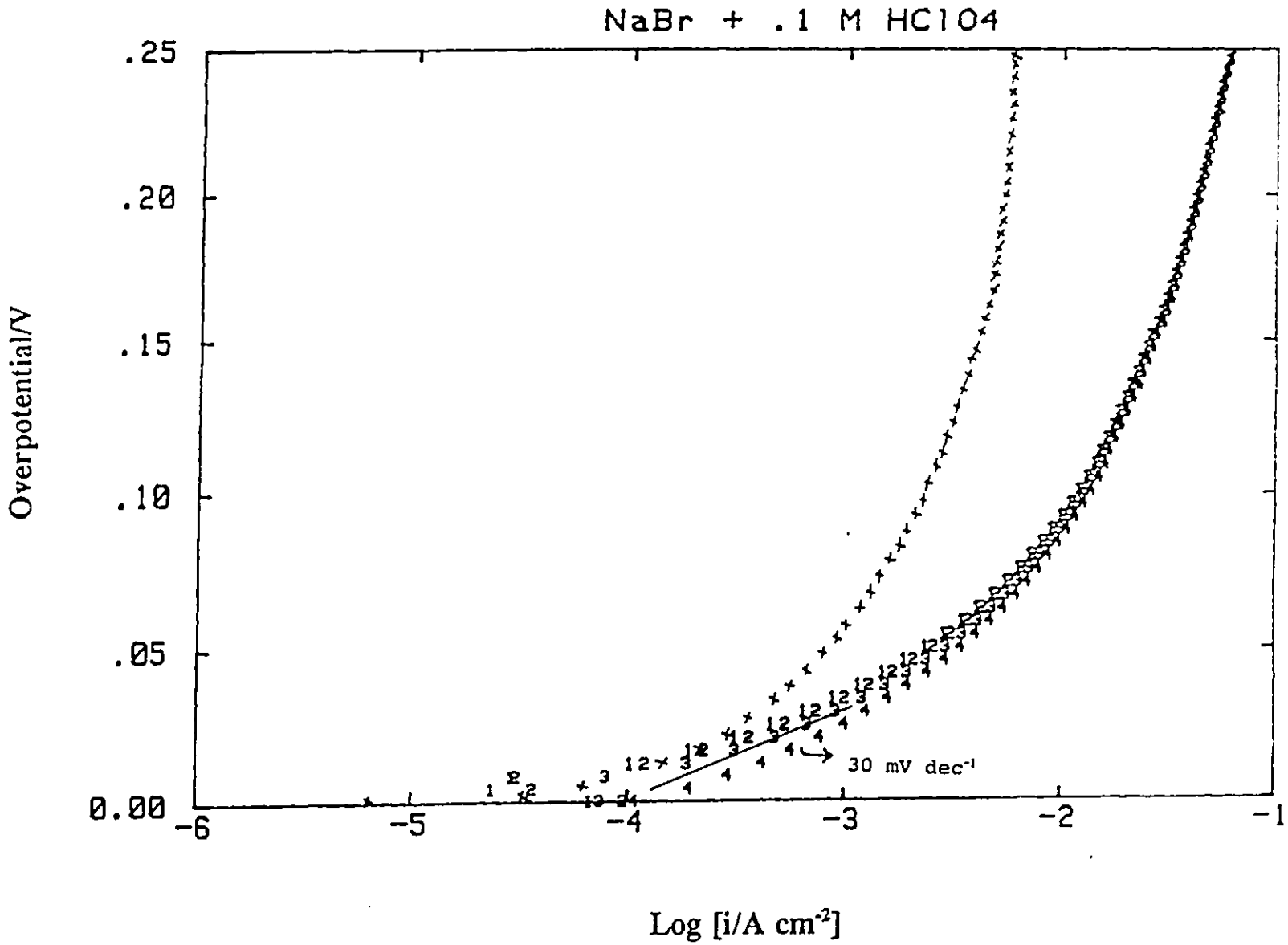

Fig. 38. Comparison of Tafel plots with rotation rates of 1200 (1), 2400 (2), 3600 (3) and 4800 (4) rpm at Pt RDE and 3600 (·) rpm at the preoxidized Pt RDE (preoxidized at overpotential 500 mV for one hour) in 1 M Br^- solution

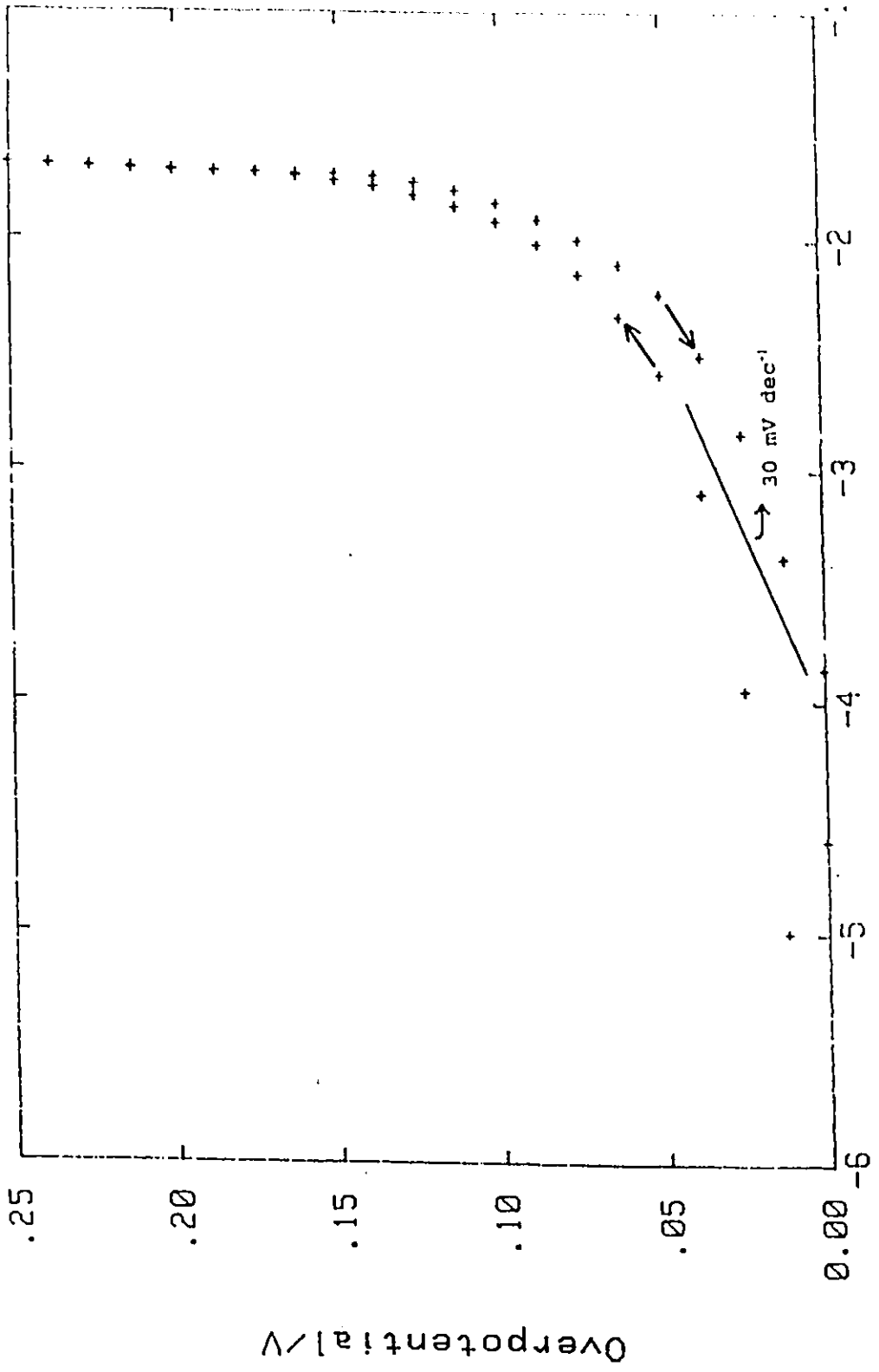

Fig. 39. Tafel plots of KBr in anhydrous TFA at Pt (no oxide film present)

It was found in previous work [23] on the Cl_2 evolution reaction that kinetics of Cl_2 formation could be examined at completely oxide-free Pt surfaces, using anhydrous trifluoroacetic acid (TFA) as solvent.

Figure 39 shows a Tafel plot for Br_2 formation at Pt in 0.1 M KBr in nonaqueous, dry TFA solution for which no oxide film is generated at Pt; again a limiting current is reached but at a lower current-density than that for the aqueous solution case. As for the other cases, it appears that the $Br^{\cdot}$ recombination step again controls the kinetics of Br_2 formation at low potentials (approach to a 29 mV slope) while the second region shows a clear approach to a limiting current, corresponding to the limiting rate of the recombination mechanism proceeding at more or less full coverage by $Br^{\cdot}$ of the sites available for adsorption of $Br^{\cdot}$, taking account of coverage by the organic solvent (TFA) molecules.

5.3. Bromine Formation from Non-Aqueous Solutions

Interest in Br_2 formation from non-aqueous Br^- solutions arises from several directions: a) because the solvation energy of Br^- will be different from that in water, the Gibbs energies of adsorption of Br^- ion should also be different; b) for related reasons, the kinetics of Br_2 formation will be different from those in water; c) the $Br^-/Br_2/Br_3^-$ equilibrium will be different and, finally, d) if the non-aqueous (aprotic) solvent is

sufficiently dry, no competitive oxide-film formation can arise.

For large concentrations, the product Br_2 can become complexed with Br^- according to the process considered earlier:

$$3Br^-_{(nonaq.)} \rightleftharpoons Br_3^-{}_{(nonaq.)} + 2e \qquad (78)$$

or some dissolution of Pt can arise according to:

$$Pt + 4Br^-_{(nonaq.)} \rightleftharpoons PtBr_4^{2-} + 2e \qquad (79)$$

Acetonitrile (CH_3CN) is an excellent solvent for a number of inorganic electrolytes. As an aprotic solvent, CH_3CN shows no self-ionization.

The polar nature of CH_3CN, which has a dipole moment of 3.37 D at 298 K and a dielectric constant of 35.99 (298 K), allows strong ion-solvent interactions to arise leading to good solubilities of a wide range of bromide salts such as $CoBr_2$, $(CH_3)_4NBr$, $(C_2H_5)_4NBr$, or $(C_3H_7)_4NBr$ in it.

Cobalt bromide in CH_3CN has been demonstrated to have a strong ion-solvent interaction [39], hence an appreciable solubility. However, only rather few studies of electrochemical Br_2 formation in this solvent have been reported. The present experimental results on cobalt bromide or $(CH_3)_4NBr$, $(C_2H_5)_4NBr$ and $(C_3H_7)_4NBr$ in anhydrous CH_3CN enable comparative information to be obtained under conditions where interfering OH and H adsorption at Pt are absent, provided that the solutions were sufficiently free from traces of water.

For $CoBr_2$ in CH_3CN, the following complexation processes have, however, to be considered:

$$2CoBr_2 + 6CH_3CN \overset{K_1}{\rightleftharpoons} [CoBr_2 \cdot 3CH_3CN]_2 \overset{K_2}{\rightleftharpoons} Co(CH_3CN)_6^{2+} + CoBr_4^{2-} \quad (80)$$

Taking C_1, C_2 and C_3 as the equilibrium concentrations of $CoBr_2$, $[CoBr_2 \cdot 3CH_3CN]_2$ and $Co(CH_3CN)_6^{2+}$ or $CoBr_4^{2-}$, respectively, with the restriction $C_1 + C_2 + 2C_3 \rightarrow C_0$, the initial stoichiometric concentration of $CoBr_2$, one obtains

$$C_1 = C_0/[1 + 2(K_1K_2)^{1/2}] \quad (81)$$

$$C_2 = K_1 C_0^2/[1 + 2(K_1K_2)^{1/2}] \quad (82)$$

$$C_3 = (K_1K_2)^{1/2}/[1 + 2(K_1K_2)^{1/2}] \quad (83)$$

since $C_1^2 \approx 0$ after extensive complexation and $C_{CH_3CN} \approx$ constant.

Interactions of bromide ions with Pt or other electrodes also arise in nonaqueous Br^- ion solutions such as those of $CoBr_2$, $(CH_3)_4NBr$, $(C_2H_5)_4NBr$ and $(C_3H_7)_4NBr$ in CH_3CN used in the present work. The voltammograms in Figs. 40—43 show one peak and a sharp rise in the anodic sweep current which is observed with an almost opposite peak in the cathodic sweep. The humps that appear in both the anodic and cathodic curves thus correspond to Br^- discharge and Br_2 formation at the sharp rise in the anodic current.

These cyclic voltammograms show only anodic currents for Br_2 formation and cathodic ones for reduction of any Br_2 formed in the anodic sweep. No current components arise for oxide film formation or reduction in these cases, since the solvent is virtually free of water.

Anodic Br_2 formation arises, of course, in the cyclic voltammogram beyond the appropriate reversible potential (Fig.

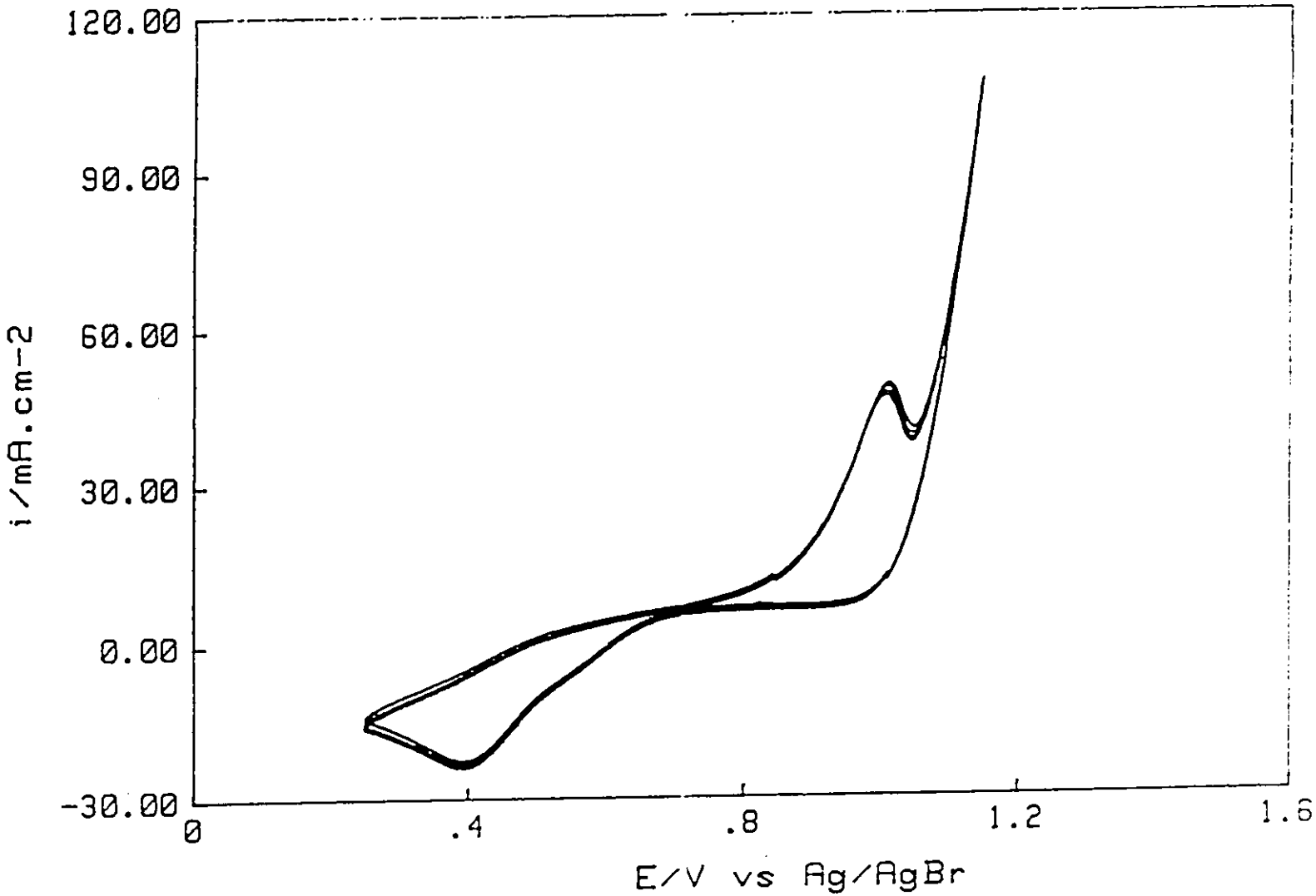

Fig. 40. CV of conc. $CoBr_2$ in CH_3CN, the anodic hump may be due to $CoBr_4^{2-}$ complex ion adsorption

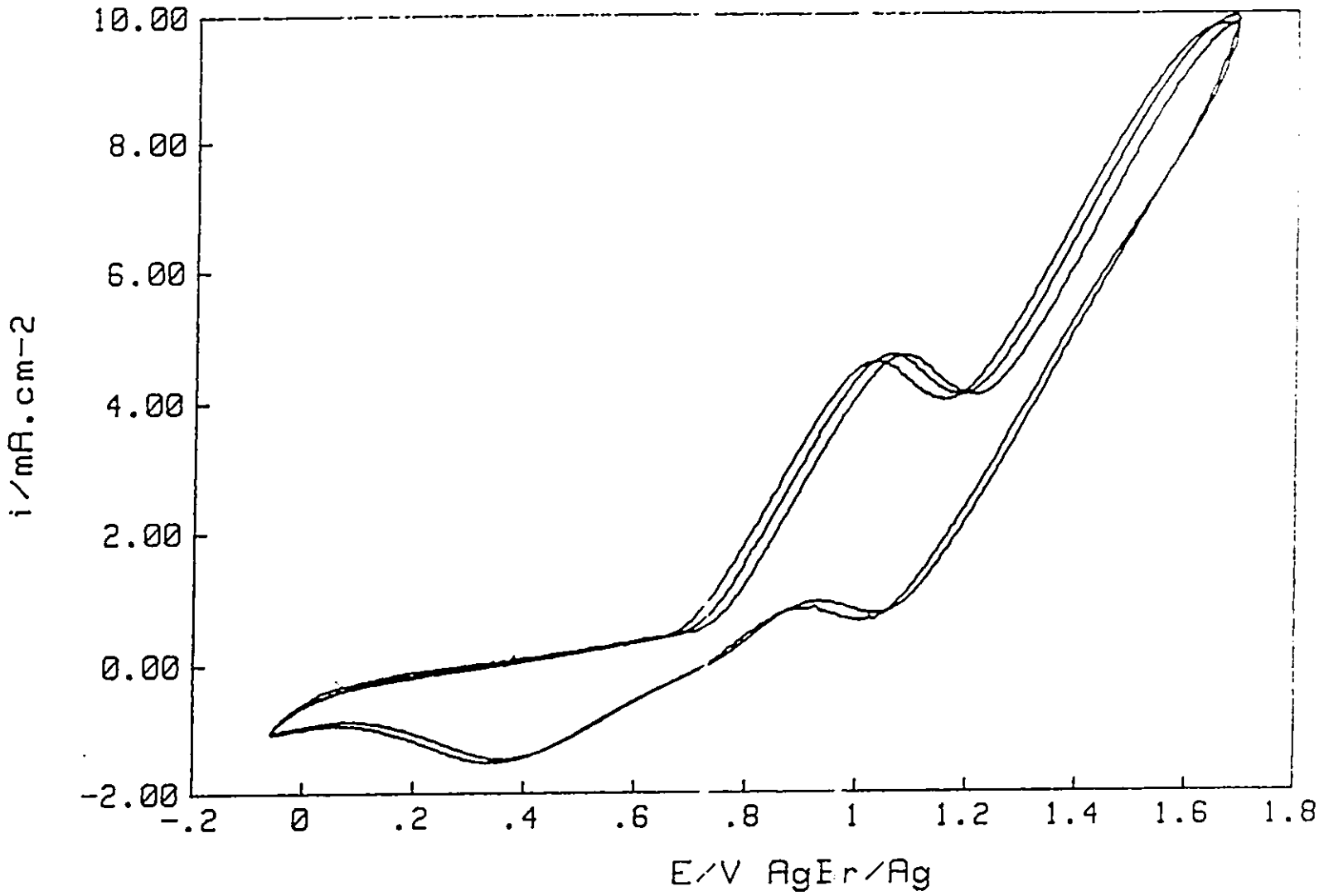

Fig. 41. CV of conc. $(CH_3)_4NBr$ in CH_3CN

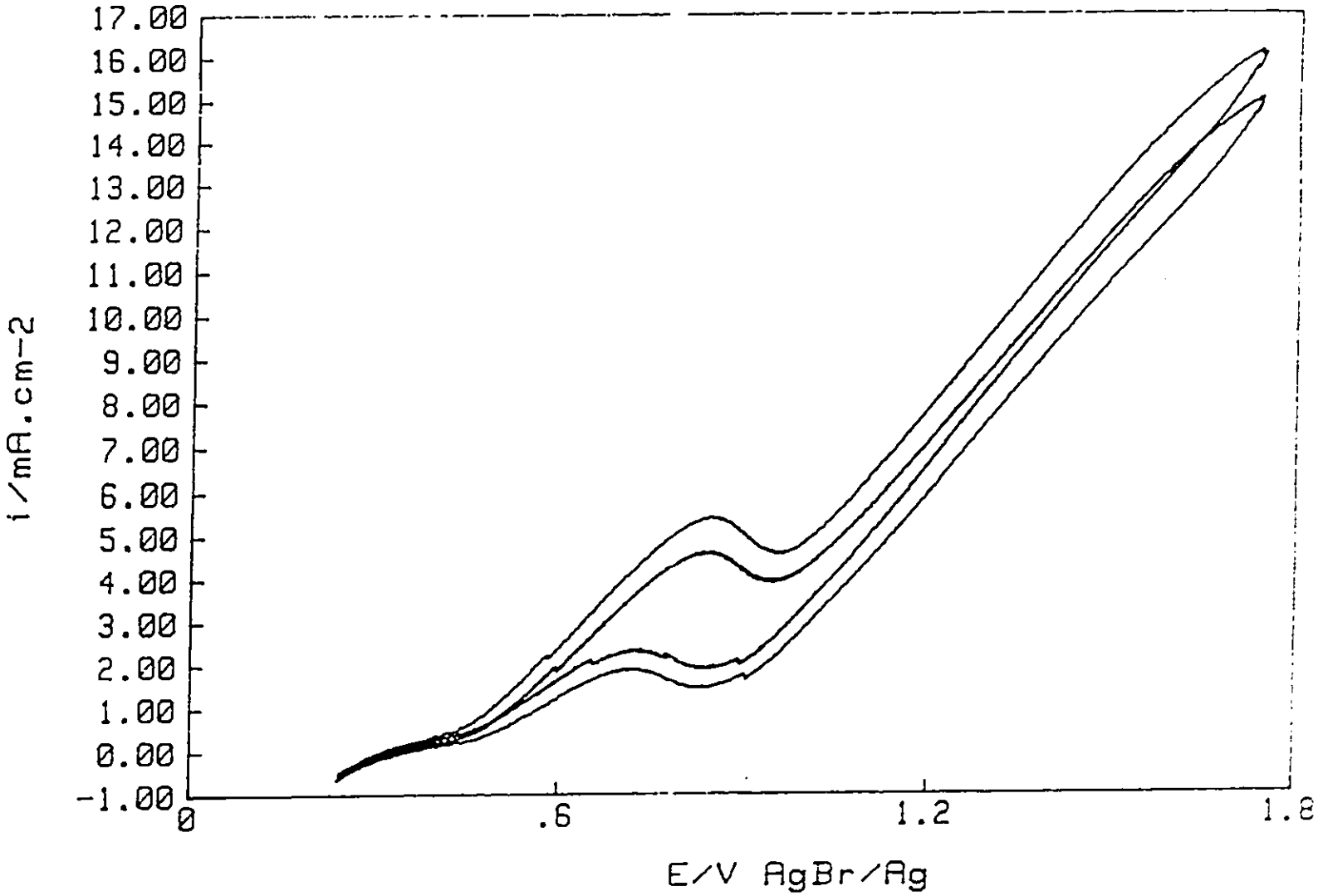

Fig. 42. CV of conc. $(C_2H_5)_4NBr$ in CH_3CN

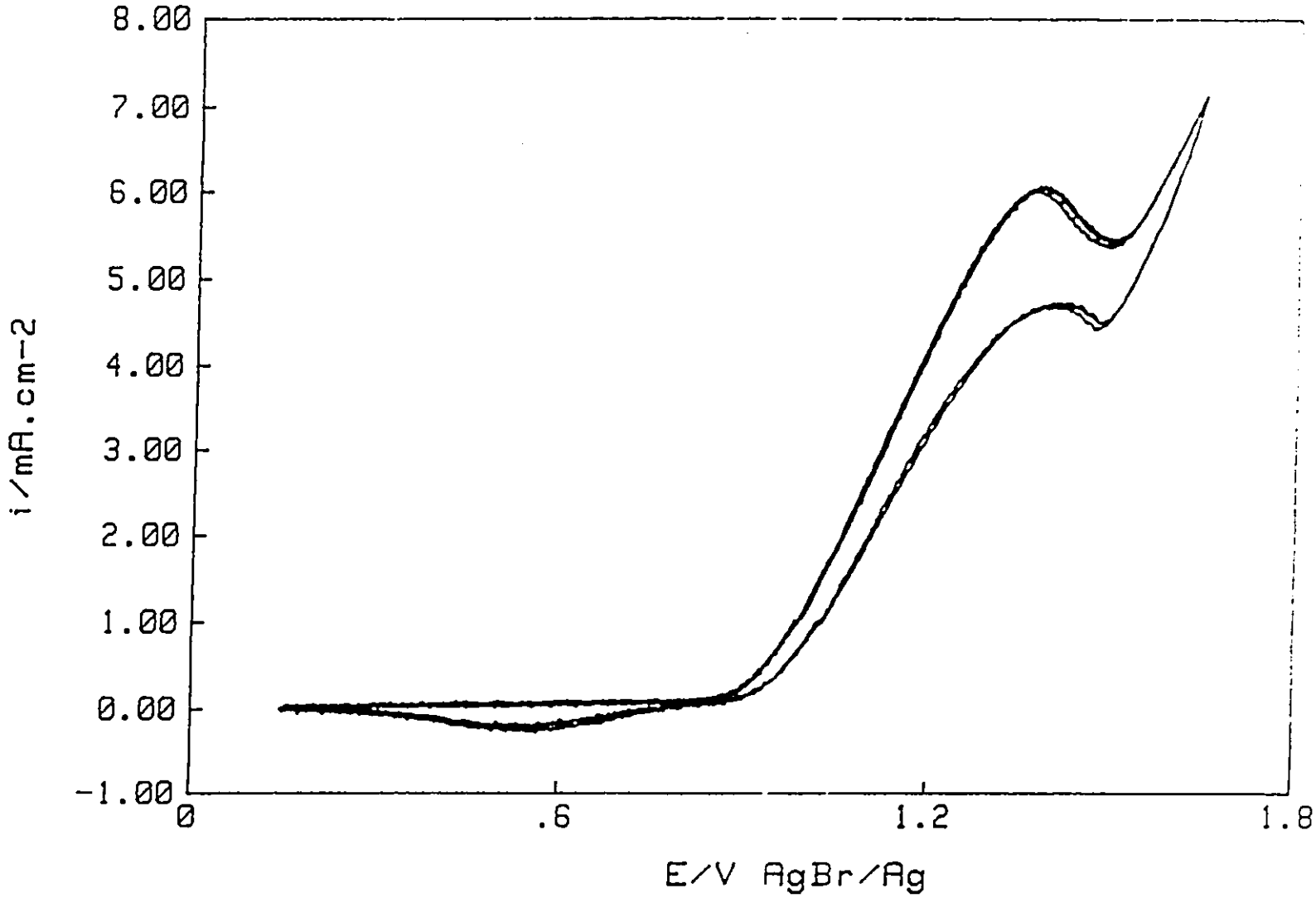

Fig. 43. CV of conc. $(C_3H_7)_4NBr$ in CH_3CN

40); hence, either the bromide ion forms bromine faster than the bromide ion forms the cobalt bromide/acetonitrile complex or, most probably, Br_2 discharge can occur directly from the complex or through its dissociation. When $CoBr_2$ is replaced by $(CH_3)_4NBr$, $(C_2H_5)_4NBr$, or $(C_3H_7)_4NBr$ in CH_3CN, the cyclic voltammograms (Figs. 41—43), show adsorption peaks, probably associated with organic cation adsorption/desorption and sharp current rises for bromine formation. The voltammograms shift very little with increasing cycling time.

Cyclic voltammetry experiments were also conducted in TFA with KBr as electrolyte. Fig. 44 shows the behaviour for 0.1 M KBr in this solution; a sharply curved rise of current occurs beyond ca. 0.9 V (Ag/AgBr) corresponding to Br_2 formation. It is possible for decomposition of TFA itself to arise by the Kolbe reaction involving TFA, viz.

$$CF_3COO^{\cdot} \rightarrow CF_3COO^{\cdot}_{ads} \quad (84)$$

$$CF_3COO^{\cdot}_{ads} \rightarrow CF_3COO^{\cdot} + e \quad (85)$$

$$CF_3COO^{\cdot} \rightarrow CF_3^{\cdot} + CO_2 \quad (86)$$

$$2CF_3^{\cdot} \rightarrow CF_3\text{-}CF_3 \quad (87)$$

but this probably occurs only at much higher potentials; Br_2 formation from discharged $Br^{\cdot}$ will normally be preferred prior to $Br^{\cdot}$ diffusion-control setting in.

Fig. 45 shows, for comparison, the inflected Tafel relations that are observed for Br_2 formation from $(CH_3)_4NBr$, $(C_2H_5)_4NBr$ and $((C_3H_7)_4NBr$ in CH_3CN. They are unlike the smooth curves for Br_2 formation at Pt in the aqueous or TFA

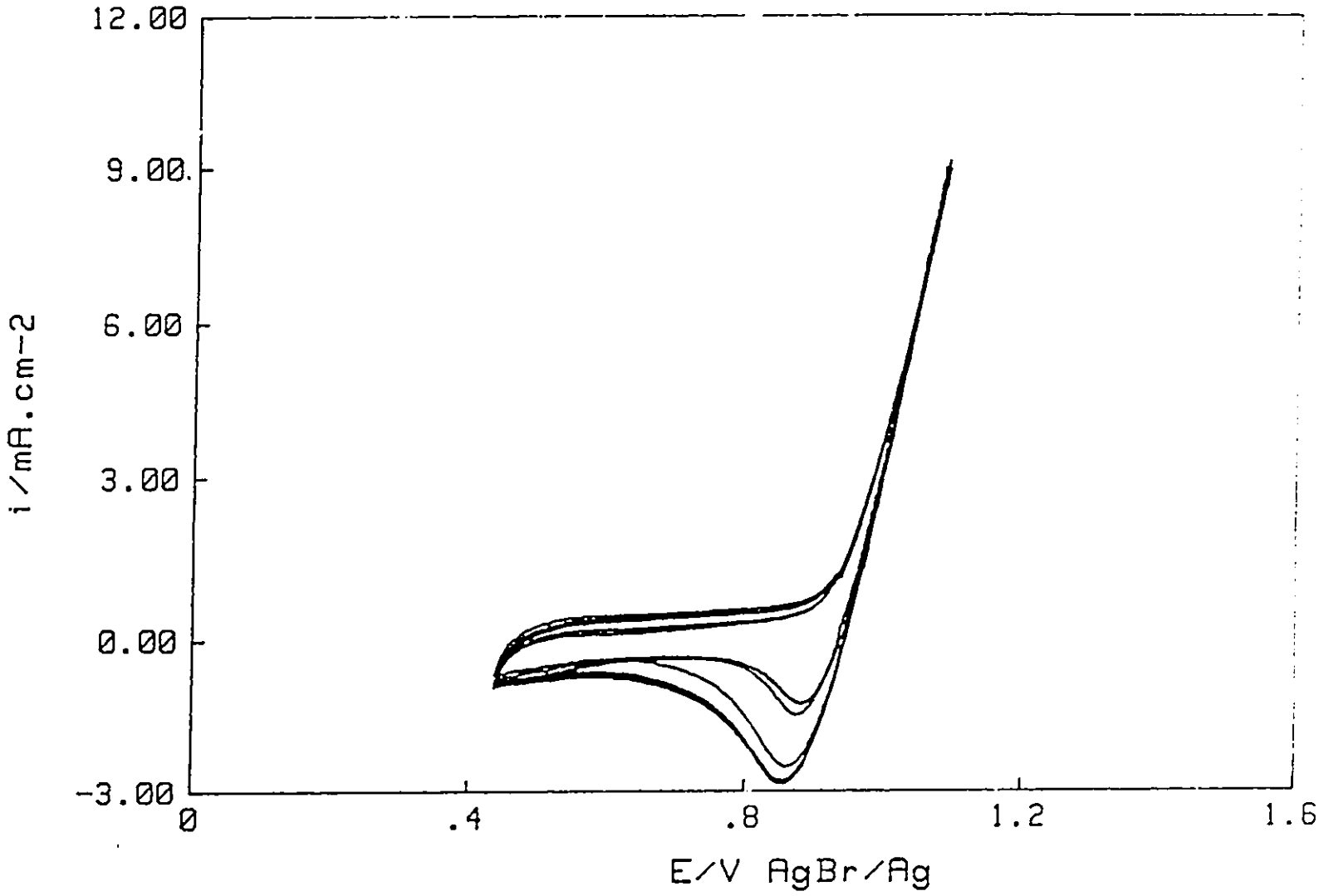

Fig. 44. Cyclic voltammogram of 0.1 M KBr in TFA

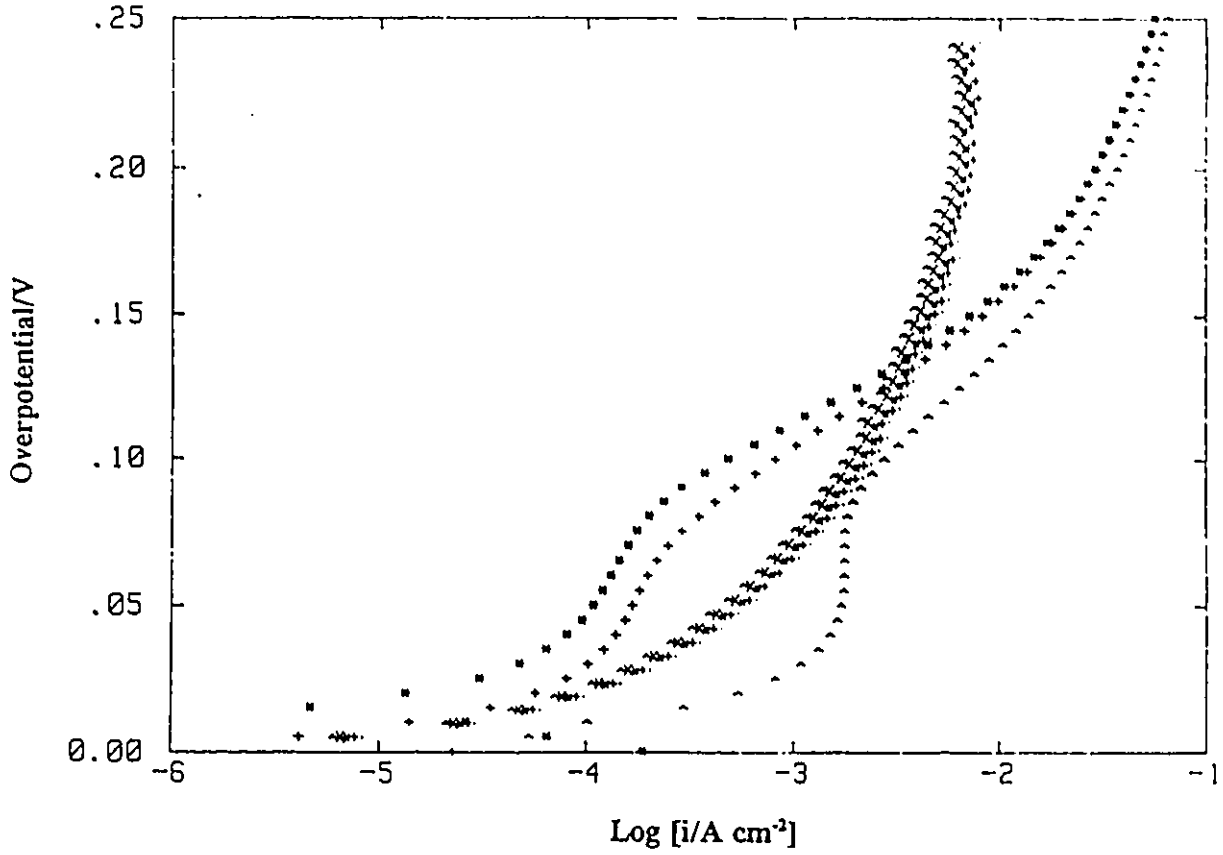

Fig. 45. Tafel plots for Br_2 formation from 0.1 M solutions of $(CH_3)_4NBr$ (*), $(C_2H_5)_4NBr$(+), $(C_3H_7)_4NBr$(^) in CH_3CN at the preoxidized Pt RDE at a rotation rate of 1200 rpm (inflected curves); and comparatively from 1 M NaBr in 0.1 M $HClO_4$ at a Pt RDE (3600 rpm) preoxidized at 1.6 V (RHE) for periods of times as follows: . 1.25 h, + 1.5 h, * 1.75 h, × 2 h, ^ 2.25 h (smooth curves).

solutions and should be considered in two parts: the lower may be due to bromine formation accompanied by adsorption of bromide ions, and the upper part may be due to bromine formation accompanied by adsorption of tribromide; the inflexion which arises between the two parts is not, however, observed in aqueous solutions.

The current densities are, however, small (before the inflexion) compared with those in aqueous medium, and are only in the range 10^{-5} to 10^{-3} A cm^{-2} as is seen from Fig. 45.

The curves of Fig. 45 show that the inflexion behaviour is clearly dependent on the size of the R_4N^+ cation of the electrolyte. It is therefore probably associated with potential-dependent adsorption of the cation and associated changes of the structure of the double-layer and the local concentration of the co-anions, Br^- or Br_3^-, in the double-layer. With increasing positive potential, R_4N^+ cations will tend to be decreasingly adsorbed but this effect will set in at higher potentials the larger is the size of the ion. In fact the inflections in the Tafel relations of Fig. 45 are typical of relatively sudden desorption of a previously adsorbed cation as the electrode potential is increased positively. It seems, at relatively low bromine overpotentials, that the kinetics of Br_2 formation are evidently facilitated by the presence of R_4N^+ ions, the more so the larger they are. This is probably due to enhancement of local Br^- concentration in the double-layer on account of the surface excess of R_4N^+ cations.

The approach to low apparent limiting currents below the inflexion region up to η = 0.10 V cannot, it is believed, be due to onset of recombination control in this case because the approaches to apparent limiting currents over this potential range depend markedly on the size of the R_4N^+ cation. Rather, therefore, the behaviour up to η = 0.10 V should be attributed to a "double-layer" effect associated with onset of desorption of the specifically adsorbed cations. Beyond η = 0.10 V, at more positive potentials, the Tafel curves proceed in a more normal way, approaching a common, true limiting current of ca. $10^{-1.1}$ A cm^{-2}. Comparison with superimposed Tafel curves for the polarization of preoxidized Pt (conditions exhibited) in aqueous NaBr medium (3600 rpm) is shown in Fig. 45.

5.4. Use of the Potential Relaxation Method ("Potential Decay") for Investigation of the Adsorbed Br$^{\cdot}$ Intermediates

An important section of the present work involved application of non-steady-state methods (chapter 4, potential relaxation and impedance spectroscopy), to the investigation of the behaviour and participation of the adsorbed intermediates, Br$^{\cdot}$ and $Br_3^{\cdot}$ (see reaction steps **I** and **IV**), and their relation to the overall mechanisms of the anodic bromine formation reaction.

The principle of the so-called potential relaxation or "potential decay" method as a means for studying electrode processes was first discussed by Butler and Armstrong [91] in

terms of self-discharge of the ionic double-layer capacitance. The mathematical treatment of results from this method was outlined in 3.7.4.

Developments were made subsequently by Morley and Wetmore [92], Anderson and Eyring [93] and later authors, for example, Lukovstev and Temerin [94]; Conway and Bourgault [95] examined the theoretical significance of results obtained from the potential decay method, especially for the case of potential-dependent pseudocapacitance in the O_2-evolution reaction at nickel oxide electrodes, involving OH and O intermediates at the oxide interface.

Open-circuit potential-relaxation measurements were employed to derive the adsorption pseudocapacitance associated with Br$^{\cdot}$ coverage as a function of overpotential in the Br_2 formation reaction at both the reduced and pre-oxidized Pt electrode surfaces. The decay curves are based on at least one thousand points recorded by means of the digital oscilloscope, and provide the following information, according to the analysis given in 4.2.3):

(a) η(t) vs log t plots (Fig. 46); various curves were derived from data recorded from different initial overpotentials (and corresponding currents);

(b) corresponding η(t) vs log ($-d\eta/dt$) plots (Fig. 47);

(c) the capacitance C(η) vs η(t) plots (Figs. 48);

(d) Log C vs η(t) plots (Fig. 49).

As in previous papers [63,65,71], information on the

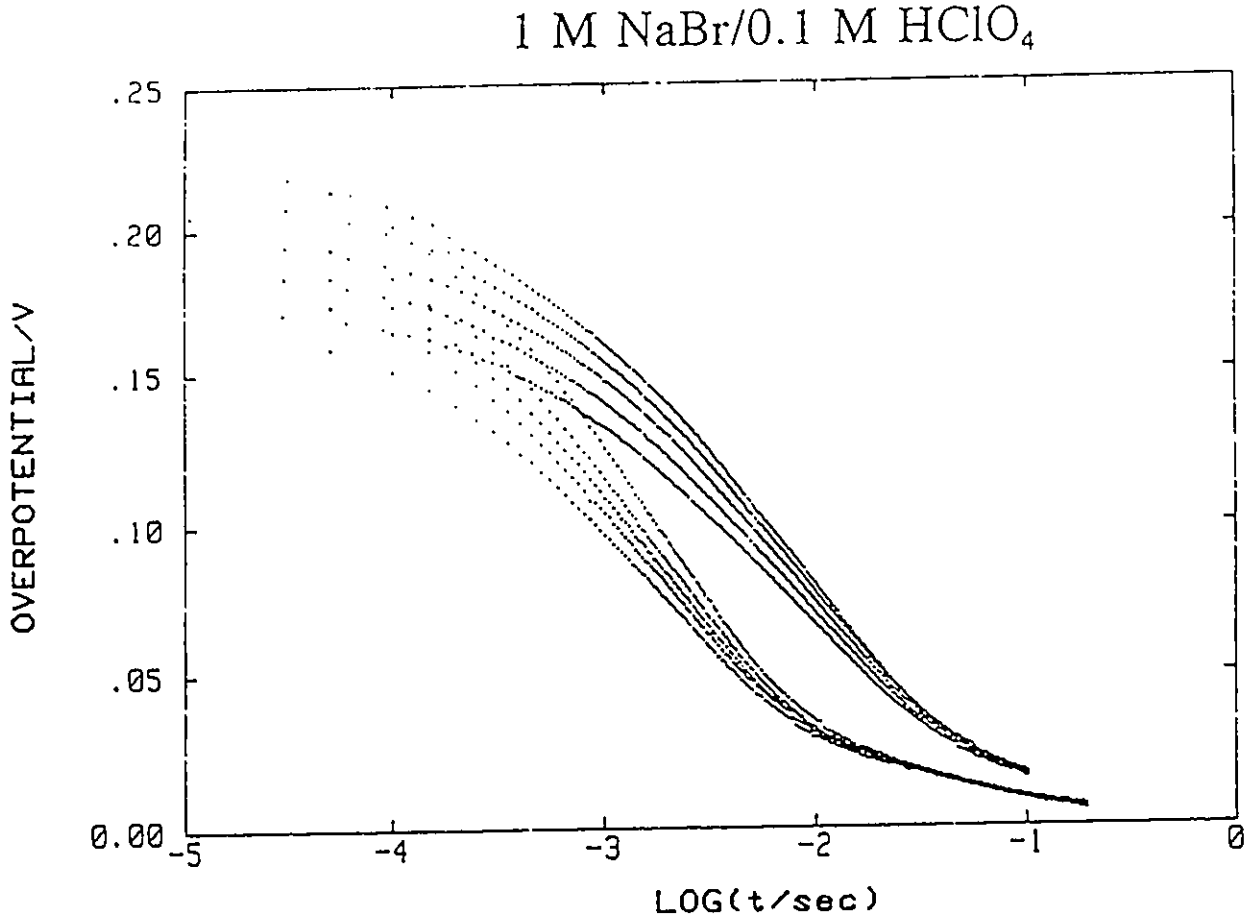

Fig. 46. Potential decay plot (η vs log t), for the Br_2 formation reaction at freshly reduced (top 5 curves) and pre-oxidized (5 curves in the bottom) Pt electrodes in 1 M NaBr in 0.1 M $HClO_4$ (298 K); order of descending initial overpotentials in both series of 5 curves: 0.225, 0.210, 0.195, 0.185, 0.170 V

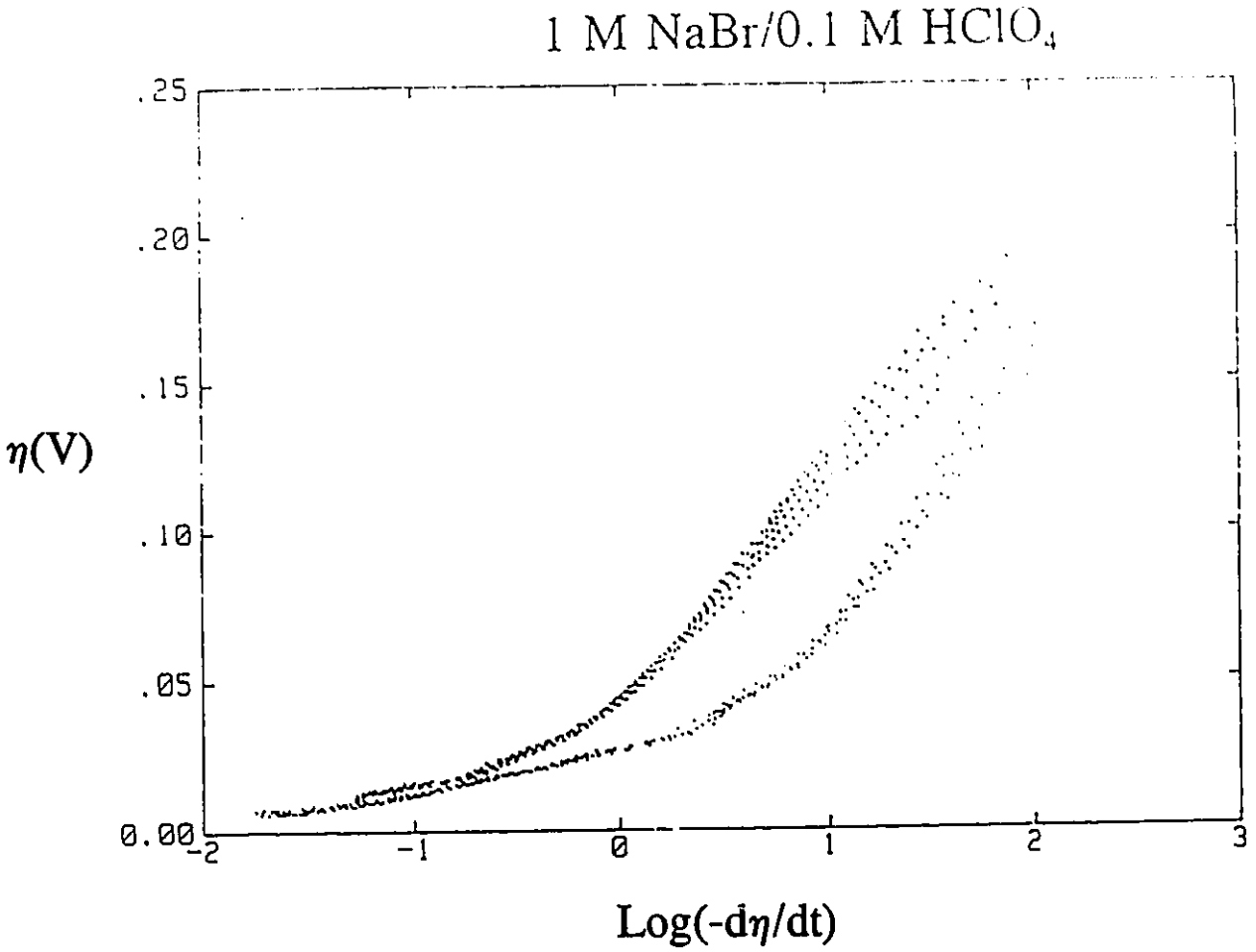

Fig. 47. Potential decay plot [η vs log(-dη/dt)] corresponding to the respective potential relaxation curves in Fig. 46 (left-hand family, freshly reduced surfaces; right-hand family, pre-oxidized — ~ 3 monolayer oxide surfaces)

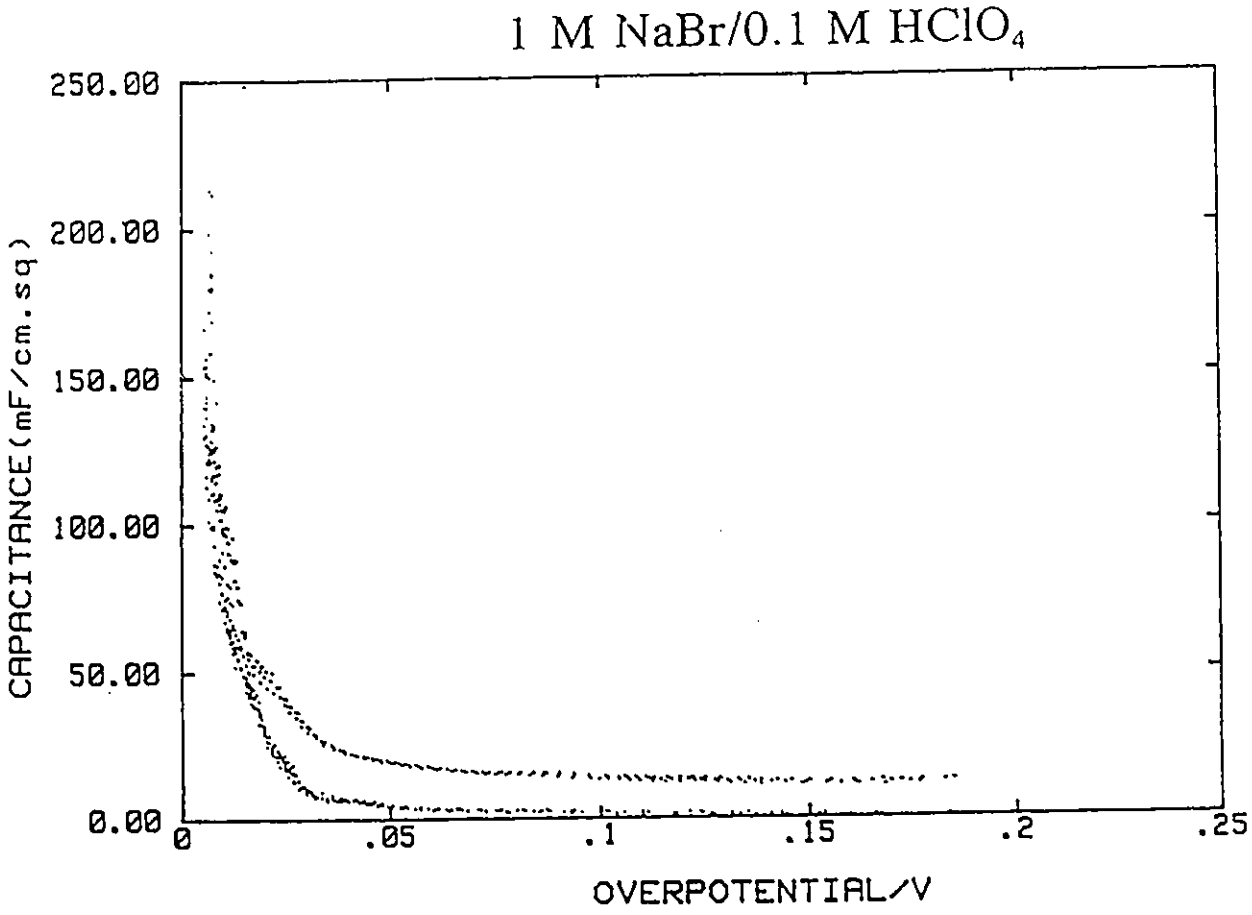

Fig. 48. Interfacial pseudo-capacitance vs η derived from the potential relaxation transients in Fig. 46 (top curves, freshly reduced Pt; curves at the bottom, pre-oxidized Pt)

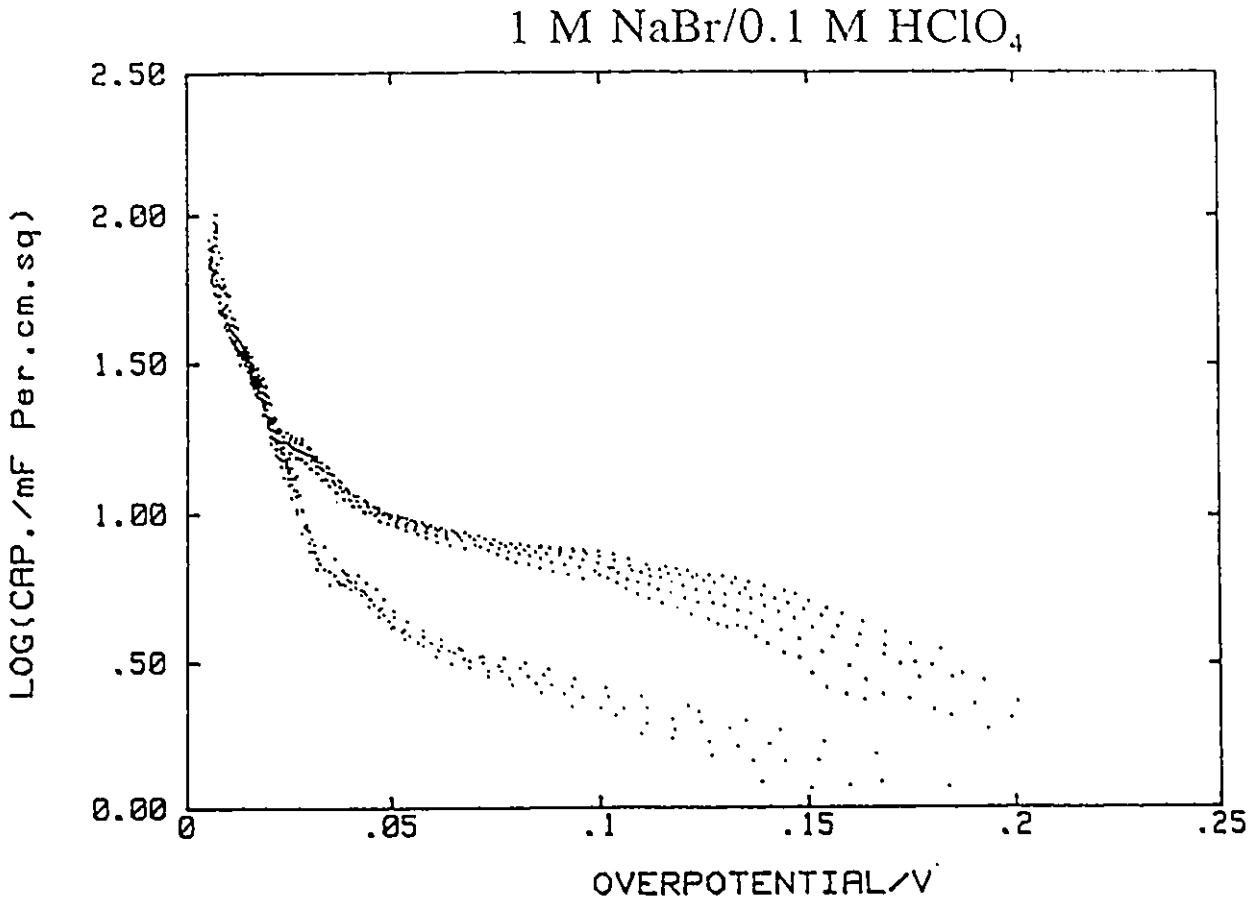

Fig. 49. Log C vs η plots corresponding to the respective curves in Fig. 48 (top curves, freshly reduced Pt; curves at the bottom, pre-oxidized Pt)

pseudocapacitance C_ϕ [= $q_{1,Br^-}(d\theta_{Br^-}/d\eta)$ here] is obtained by processing digitally acquired data from potential relaxation transients, following current interruption, according to eqn. (25) where the r.h.s. is the Tafel function in *exp* form in terms of the exchange current-density, i_0, and the transfer coefficient, α. If C is constant, which is not usually the case for processes involving chemisorption, eqn. (25), $-C(d\eta/dt) = i_0 \exp(\alpha\eta F/RT]$, integrates to a *log* form in $t+\tau$, an integration constant. Correspondingly, a plot can be made according to (cf. eqn. 29)

$$\ln(-d\eta/dt) = \ln i_0/C + \alpha\eta F/RT \qquad (88)$$

which follows a Tafel-like relation in η which is linear if C is constant with potential which, as noted above, is usually not the case experimentally.

Comparisons were made of the potential relaxation transients, taken from various initial overpotentials, at freshly reduced and at pre-oxidized Pt electrodes, as shown in Fig. 46 on the same scales. The relatively flat run-in on the η vs log t curves at short times is well understood [68] and arises on account of the role of the integration constant τ arising in $\eta = a' - b \log(t + \tau)$ (cf. eqn. 26 in chapter 4). Adjusted plots to a fitted single value of τ, are then *linearly* logarithmic in the quantity $t + \tau$. Various curves were recorded from different initial overpotentials and all merge towards a single curve after relatively long times ($t \rightarrow 1$ s), as they should if the same process is occurring at all potentials.

The corresponding plots of η vs $\log(-d\eta/dt)$, according to eqn. (88) are shown in Fig. 47. The fall of potential at the pre-oxidized electrode is more rapid than at the freshly reduced one, corresponding to the Tafel relations at these two surfaces and the differences of capacitance or τ values.

The shapes of the $\eta(t)$ vs $\log(-d\eta/dt)$ plots are similar to those of the η vs $\log i$ (Tafel) plots, some approach to limiting $d\eta/dt$ values being attained at high potentials corresponding to the approaches to limiting currents in the Tafel curves. The slopes of the linear parts of the η vs $\log t$ and η vs $\log(-d\eta/dt)$ plots are equal, but of opposite sign.

The apparent interfacial capacitances derived from the potential relaxation data are shown in Fig. 48 and 49 (on a log scale) as a function of η.

The general forms of these relations for the reduced and pre-oxidized surfaces are surprisingly similar but generally the capacitance values at the preoxidized surfaces are substantially smaller than those at the "reduced" Pt surfaces due presumably to the diminished tendency for chemisorption of $Br^{\cdot}$ or $Br_3^{\cdot}$ at already oxidized surfaces. Large capacitances, which must be due to the $Br^{\cdot}$ pseudocapacitance (values of which are quite large, cf. Table 10 in section 5.5), are observed within about 30 mV of the reversible potential but decline, in the usually observed way [65,67,71], towards the double-layer capacitance at higher overpotentials. No maximum in C is indicated in the way that is exhibited by H or OH pseudocapacitance in the HER or OER

reactions at Pt, Ni or Co. Whether or not a maximum is seen above the reversible potential depends on the ratio k_1/k_{-1} for step I in relation to k_2/k_1 [91].

5.5. Experimental and Simulated A.C. Impedance Behaviour

5.5.1. At the "Reduced" Pt Electrode

Historically, the use of a.c. techniques [91] in electrochemistry has been mainly for impedance measurements of the differential double-layer capacity at polarized electrodes [35]. Typical C_{dl} values, thus found, are in the range 18—40 μF cm^{-2}. However, complementarily, especially in more recent years, impedance studies have been directed towards kinetic-type measurements and electrosorption experiments.

The background and principles of application of a.c. impedance methods to the study of electrode processes have been treated in chapter 4 (section 4.4).

In this section of the present work, impedance spectroscopy measurements have been made on the Br_2 formation reaction at a) the "reduced" Pt electrode and b) at preoxidized ones, as in the other types of experiments conducted and described earlier.

We first show the simpler behaviour observed where single semicircles in complex-plane plots arise, as in Fig. 50 for the "reduced" Pt electrode in 0.9 M/0.1 M HBr for polarization overpotentials of 60, 70, 80, 90 and 100 mV; the solution resistances are all $R_s \approx 5\ \Omega \cdot cm^2$ for NaBr/0.1 M HBr while the

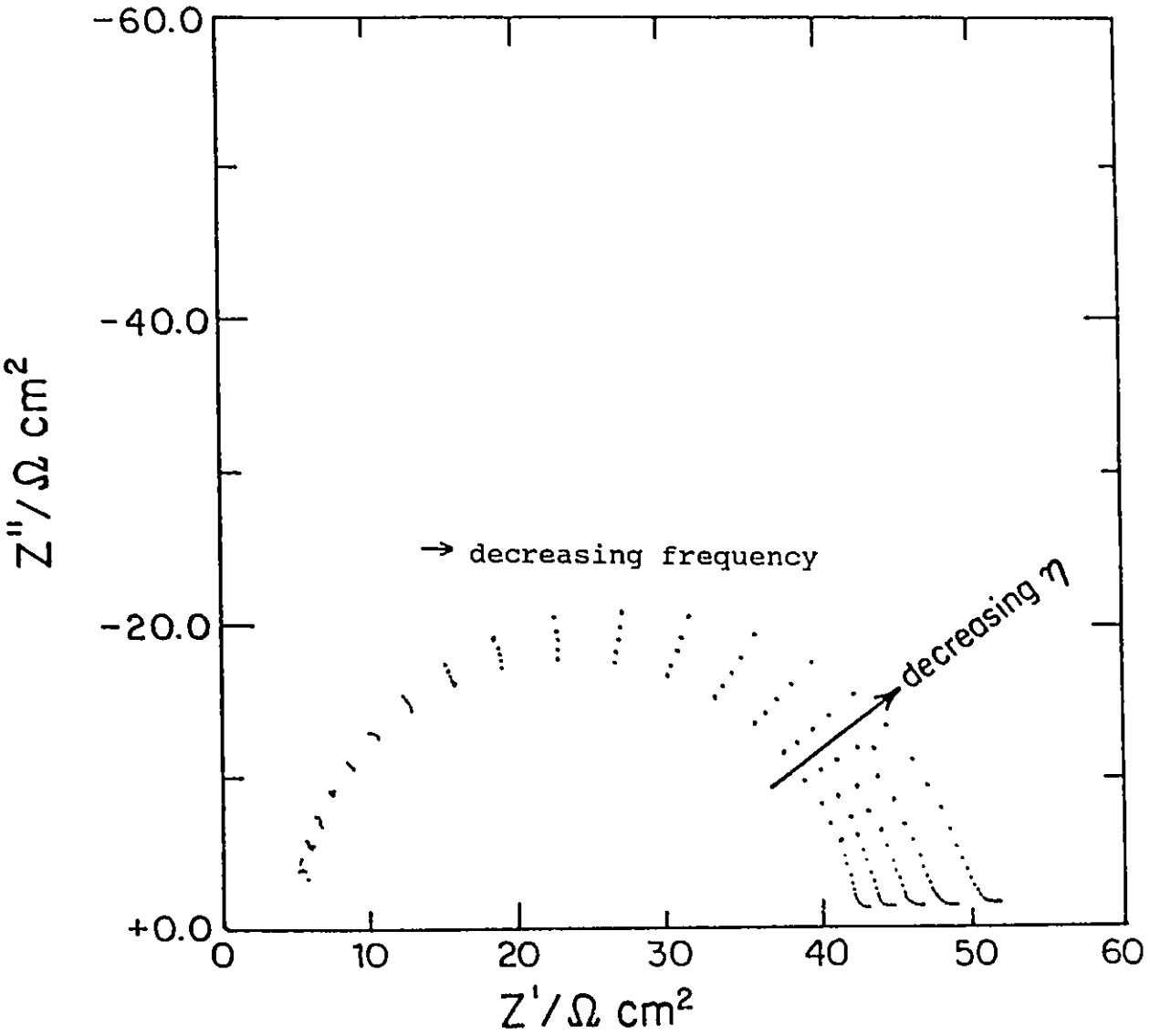

Fig. 50. Complex-plane a.c. impedance plot for the Br_2 reaction from 0.9 M NaBr/0.1 M HBr at Pt showing a series of single semicircles with increasing polarization overpotentials of 60, 70, 80, 90 and 100 mV

charge-transfer resistance depends on the polarization overpotential, as expected. The faradaic resistances (the high to the low-frequency intercepts on the Z' axis of Fig. 50, in relation to Tafel slopes) increase with decreasing η, as expected.

When the polarization is increased to η = 250 mV, but with [Br^-] increased to 2.5 M to avoid onset of diffusion control since the Tafel measurements indicate that substantial d.c. currents then pass, i.e. the a.c. modulation takes place on a substantial continuous d.c. current, two somewhat distorted semicircles (Fig. 51) arise suggesting the role of pseudo-capacitance associated presumably with significant coverage by the $Br^{\cdot}$ intermediate (reaction step **IIb**) being involved in the overall reaction mechanism.

In the possible reaction schemes outlined earlier (section 5.1), steps involving the tribromide ion, Br_3^-, and a corresponding $Br_3^{\cdot}$ intermediate were recognized, conjugate to steps involving the corresponding monomeric species. In regard to participation of the tribromide species, it is interesting that Figs. 52 a and b (for fresh Br^- solutions) show *three* semicircles in the complex-plane plot at polarization overpotentials of 150 and 200 mV, respectively. At such overpotentials, Br_2 formation is occurring at appreciable rates (ca. 7×10^{-2} A cm^{-2}; see Fig. 34), so, with Br_3^- in solution, $Br_3^{\cdot}$ species will tend to be formed *at* the surface,. This suggests that the third semicircle (low frequency end) may be associated

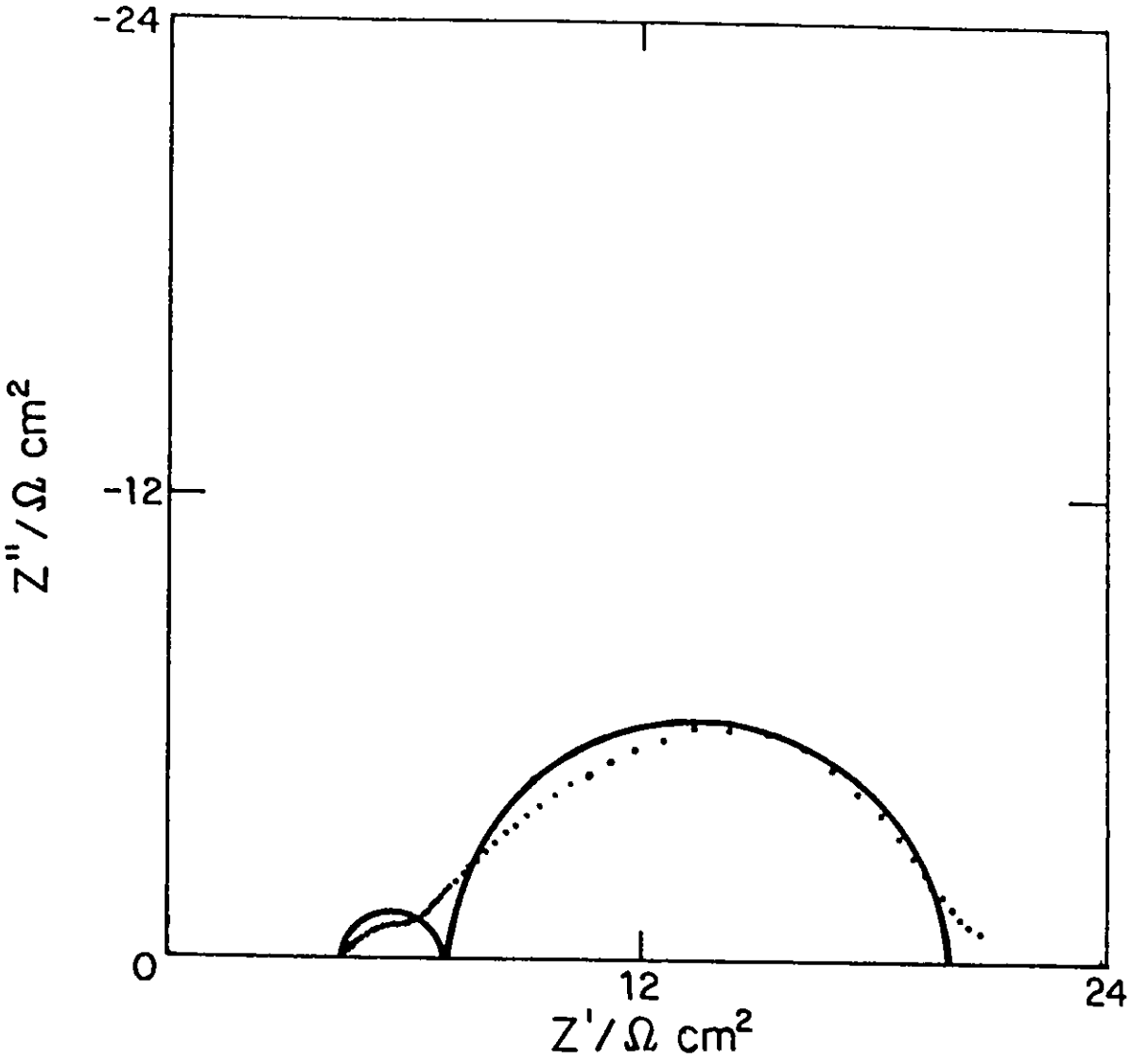

Fig. 51. Complex-plane a.c. impedance plot for the Br_2 reaction from 2.5 M NaBr/0.1 M $HClO_4$ at Pt solution showing two semicircles at a polarization overpotential of 250 mV (solid line—simulation curve)

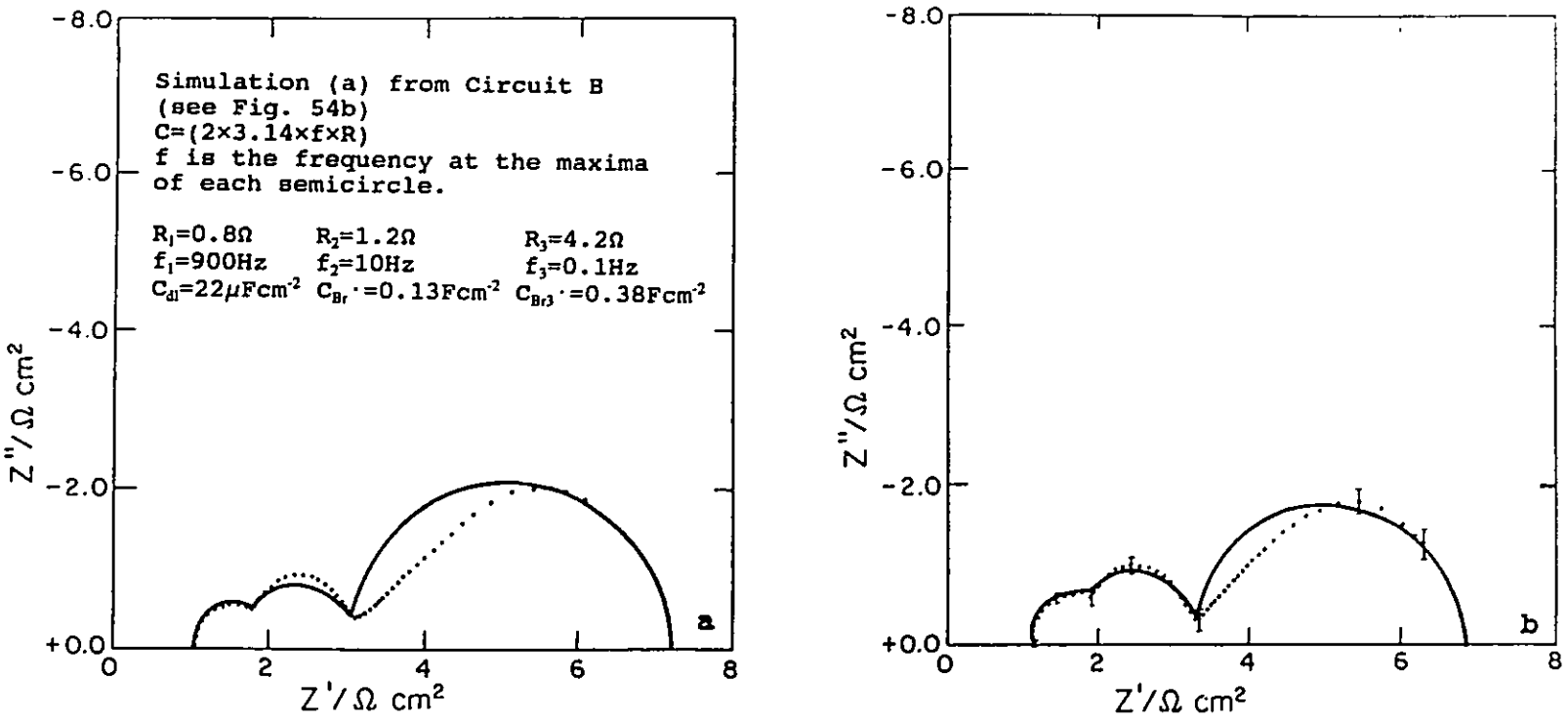

Fig. 52. Complex-plane a.c. impedance plots for the Br_2 reaction from a fresh 2.5 M NaBr in 0.1 M $HClO_4$ at Pt at a polarization overpotential of a) 150 mV and b) 200 mV (solid line—simulation curve)

with involvement of the tribromide species. In fact, the third semicircles in both Figs. 52 a and b start off (towards lower frequencies) with an approximately 45° line that then passes into a r.h.s. part of a semicircle. This suggests participation of a diffusion process. Since the latter cannot be due to Br^- transfer (since it is not seen under other conditions and Figs. 52 a and b are for 2.5 M Br^- solutions), these results suggest that the third semicircles are associated with the production and participation of a "Br_3" species, that is diffusing away from the electrode surface.

A special experiment was conducted to test this hypothesis, as follows. Fresh-solution conditions were set up; then 0.05 M Br_2 was added to give a concentration as Br_3^- of 0.02 M in solution. The impedance spectrum, plotted in the complex-plane then exhibited *three* semicircles, as in Figs. 52 a and b. In fact, the third semicircle was then more fully developed, Fig. 53.

It is significant that in the presence of the added Br_2 the faradaic resistance intercepts (Fig. 53) are larger than for corresponding experiments in the absence of added Br_2. This suggests that Br_2 has an inhibiting effect on Br^- discharge or a self-inhibiting effect in discharge of Br_3^- which results from the presence of Br_2 at the electrode surface.

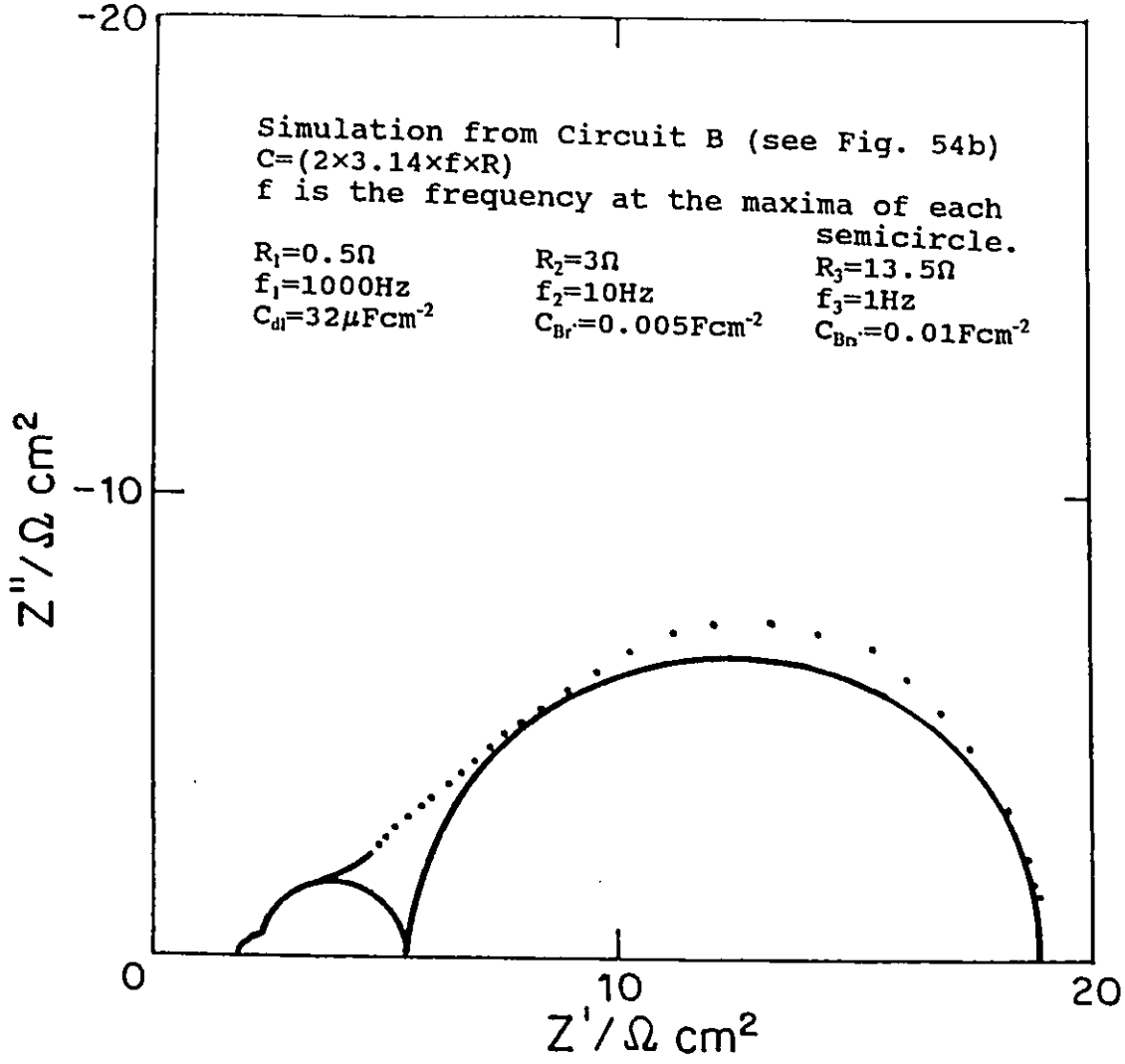

Fig. 53. Complex-plane a.c. impedance plot for the Br_2 reaction from 2.5 M NaBr/0.1 M $HClO_4$ at Pt with addition of 0.05 M Br_2 at a polarization overpotential 150 mV, exhibiting three semicircles, demonstrating that adsorbed $Br_3^{\cdot}$ is involved (solid line—simulation curve)

5.5.2. Equivalent Circuit Simulation of the Kinetics and Mechanism of the Br_2 Formation Reaction, Taking into Account of the Role of $Br^{\cdot}$ and $Br_3^{\cdot}$ Species

It was already mentioned how the electrochemical behaviour of the electrode interface can be represented conveniently by the electrical behaviour of a network of equivalent circuit elements. Figs. 8 and 9 showed the simple equivalent circuit (Fig. 8) and Armstrong's equivalent circuit (Fig. 9), taking into account the additional adsorption capacitance, C_p, related to C_ϕ.

One of the main experimental directions of the present work on bromine formation was to make a.c. impedance measurements in order to characterize the role of the adsorption behaviour of the supposed two intermediates, $Br^{\cdot}$ and $Br_3^{\cdot}$, in the Br_2 formation reaction (step **I** and step **IVa** in 5.1).

The complexity of the possible reaction schemes for Br_2 formation, taking into account participation of both $Br^{\cdot}$ and $Br_3^{\cdot}$ ion reactants, and the role of adsorbed $Br^{\cdot}$ and $Br_3^{\cdot}$ intermediates, leads to some corresponding complications in the equivalent-circuit representation of the electrical response of the reaction.

Two configurations of equivalent circuit were considered for representing the experimental frequency-response behaviour observed experimentally and for general examination of the properties of the circuit by computer simulation.

The first circuit, A (Fig. 54a) represents the Br_2 formation reaction in terms of two *parallel* discharge reactions of Br^- and Br_3^- (faradaic resistances R_1 and R_3), producing respective intermediates $Br^\cdot$ and $Br_3^\cdot$ exhibiting respective pseudocapacitances and resistances (R_2 and R_4) for desorption as Br_2. This sequence implies that some Br_2 has already been formed in solution, giving Br_3^-.

The second circuit, B (Fig. 54b) is based on the supposition that $Br^\cdot$ has to be formed prior to $Br_3^\cdot$, rather than $Br_3^\cdot$ being formed independently from Br_3^- ion, already present and derived from electro-generated Br_2, in a parallel step, as in circuit A. Thus, there corresponds a mechanistic difference between the significance of circuits A and B.

The total impedance of circuit B, including effects associated with the adsorbed $Br^\cdot$ and $Br_3^\cdot$ in Fig. 54b, can be represented by a scheme of reciprocal admittances:

$$Z=\cfrac{1}{\cfrac{1}{R_1+\cfrac{1}{j\omega C_{p_{Br^\cdot}}+\cfrac{1}{R_2+\cfrac{1}{j\omega C_{p_{Br_3^\cdot}}+\cfrac{1}{R_3}}}}}+j\omega C_{dl}} \qquad (89)$$

Let

$$A = 1 - \omega^2[C_{dl}C_{PBr^\cdot}R_1R_2 + C_{dl}(C_{PBr^\cdot}+C_{PBr_3^\cdot})R_1R_3 + (C_{dl} + C_{PBr^\cdot})C_{PBr_3^\cdot}R_2R_3] \qquad (90)$$

and

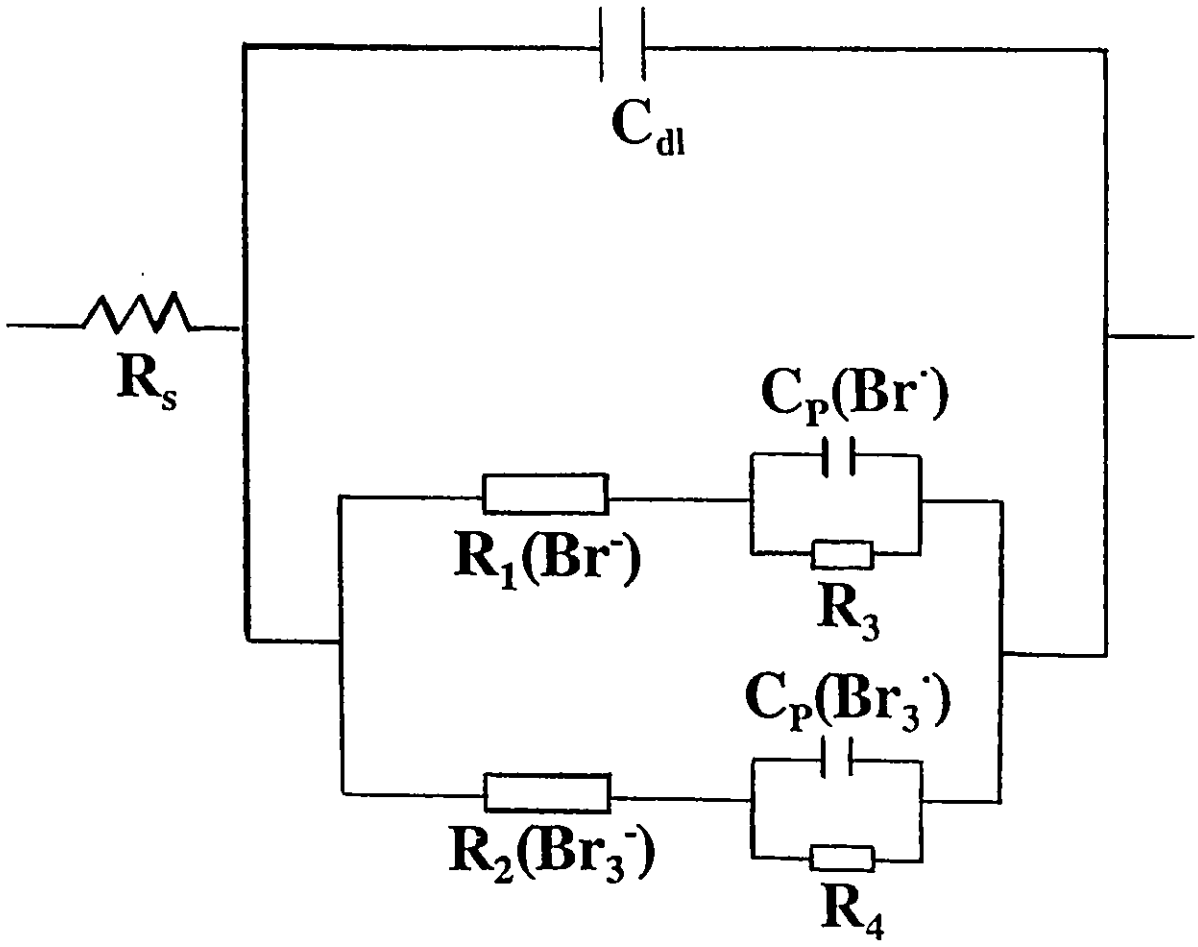

Fig. 54a. Equivalent circuit "A" for *parallel* Br^- and Br_3^- discharge processes

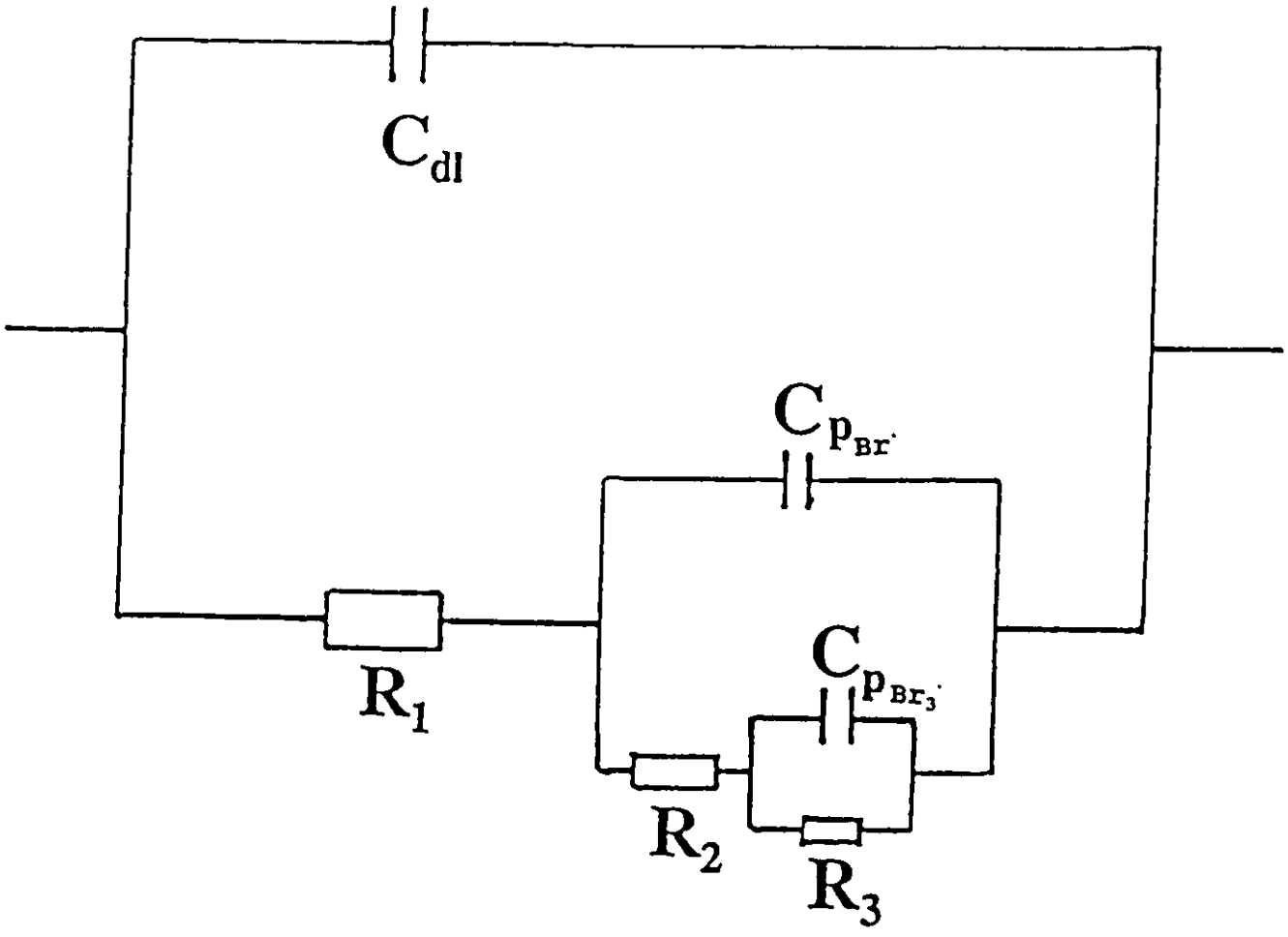

Fig. 54b. New equivalent circuit "B" proposed for the bromine formation process, to include the role of adsorbed $Br^{\cdot}$ and $Br_3^{\cdot}$ intermediates

$$B = \omega[\omega^2 C_{dl} C_{P_{Br^-}} \cdot C_{P_{Br_3^-}} \cdot R_1 R_2 R_3 + C_{dl}(R_1 + R_2 + R_3) + C_{P_{Br^-}} \cdot (R_2 + R_3) + C_{P_{Br_3^-}} \cdot R_3] \quad (91)$$

Then rationalizing eqn. (89), Z' and Z" are

$$Z' = \frac{A(R_1 + R_2 + R_3 - \omega^2 C_{p_{Br^-}} . C_{p_{Br_3^-}} . R_1 R_2 R_3)}{A^2 + B^2} \quad (92)$$

$$Z'' = \frac{B(R_1 + R_2 + R_3 - \omega^2 C_{p_{Br^-}} . C_{p_{Br_3^-}} . R_1 R_2 R_3)}{A^2 + B^2} \quad (93)$$

where

(i) R_1 = the electron-transfer faradaic resistance;

(ii) R_2 = the resistance associated with discharge of the adsorbed $Br^{\cdot}$ intermediate;

(iii) R_3 = the resistance associated with discharge of the adsorbed $Br_3^{\cdot}$ intermediate;

(iv) C_{dl} = the double-layer capacitance, the magnitude of which depends on the area of the electrode and on the electrolytes present (it is normally [62] about 18 μF cm^{-2} in aqueous solution). However, the adsorption-desorption of anions can have a major influence on the magnitude of the double-layer capacitance which may be > 40 μF cm^{-2} for such conditions at positively charged electrode surfaces.

(v) $C_p(Br^{\cdot})$ = the pseudocapacitance associated with adsorption of the $Br^{\cdot}$ intermediate at the electrode;

(vi) $C_p(Br_3^{\cdot})$ = the pseudocapacitance associated with adsorption of the $Br_3^{\cdot}$ intermediate at the electrode.

Simulation values for the C_{dl}, $C_p(Br^{\cdot})$ and $C_p(Br_3^{\cdot})$ components are initially estimated taking $C_{dl} = (2\pi R_1 f_1)^{-1}$, $C_p(Br^{\cdot}) = (2\pi R_2 f_2)^{-1}$, and $C_p(Br_3^{\cdot}) = (2\pi R_3 f_3)^{-1}$, where f_1, f_2 and f_3 are the characteristic frequencies corresponding to the maximum imaginary (Z") component in each semicircle of the resolved complex-plane plot.

A solution resistance R_s also usually arises and depends on cell geometry and on the nature and conductance of the electrolytes present; it may be sufficiently small that it can be neglected (< 5 Ω), but its value depends on electrolyte concentration and temperature. In the present work involving formation of Br_2, it is possible that an additional film resistance due to liquid Br_2 formation at the electrode interface arises but this will be in series with the solution resistance and hence not distinguishable.

While the simple (Fig. 8) and more complex (Armstrong, Fig. 9) equivalent circuits will give rise to a frequency response represented in complex-plane (Z" vs Z') plots by one and two semi-circles, respectively (based on the equivalent circuit B, Fig. 54b, and eqns. 92 and 93) a three semi-circle complex-plane plot can be obtained over a frequency range between 0.01 to 65,000 Hz, for the new equivalent circuit (B) representing the roles of chemisorbed, electroactive $Br^{\cdot}$ and $Br_3^{\cdot}$ species.

In order to make a more extended comparison of the frequency response of the two kinds of equivalent circuits, simulations of the Z" vs Z' relations were made for several sets of C and R values (Table 10). The corresponding frequency-

response behaviours in the form of complex-plane, phase-angle and Bode plots are shown in Figs. 55—59. Three semicircles can be recorded for conditions A_{1s} and B_{1s}, an intermediate case of one recorded and two overlapping for one different value in A_{2s} and A_{3s}, becoming only two semicircles when $C_p(Br^-)$ was 0.3 F (parallel CR combination, Fig. 57), or also when $C_p(Br_3^-)$ = 0.003 F (Fig. 58). Two semicircles arose also for the series circuit shown in Fig. 59.

TABLE 10. C and R Values for Simulations of the Z" vs Z' Relations for Circuits A (Fig. 54a) and B (Fig. 54b)

Conditions	A_{1s}— Fig.55	B_{1s}— Fig.56	A_{2s}— Fig.57	A_{3s}— Fig.58	B_{2s}— Fig.59
C_{dl}/F	2×10^{-5}	2×10^{-5}	2×10^{-5}	2×10^{-5}	2×10^{-5}
$C_p(Br^-)$/F	3.52×10^{-3}	6.733×10^{-3}	0.3	3.52×10^{-3}	0.474
$C_p(Br_3^-)$/F	0.20812	0.58611	0.20812	0.003	0.728
R_1/Ω	4.6145	3.3333	4.6145	4.6145	3.3333
R_2/Ω	12.006	3.8505	12.006	12.006	8.3806
R_3/Ω	13.019	8.2008	13.019	13.019	3.67
R_4/Ω	108.61		108.61	108.61	

It is clear from these simulation calculations that either three or two semicircles can arise with either of the multielement circuits over the frequency range 0.01 to 100,000 rad s^{-1}, depending on the relative values of the reaction C and R components, for a given value of the double-layer capacitance, taken here as 20 μF cm^{-2} for all cases. The phase-angle plots as f(log[frequency]) show corresponding distinguishable peaks at

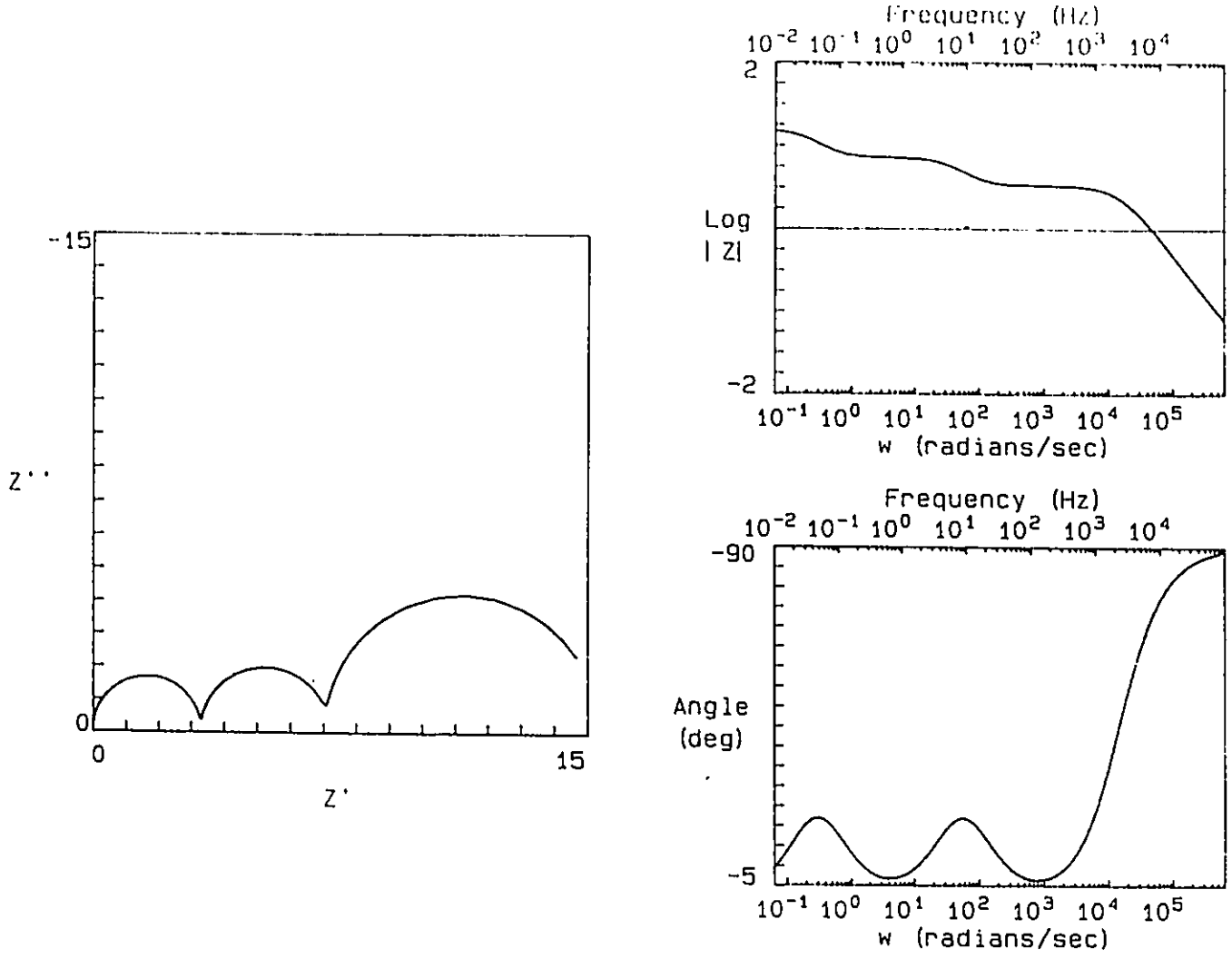

Fig. 55. Simulation of impedance behaviour of equivalent circuit A (Fig. 54a) under conditions A_{1s} (Table 10)

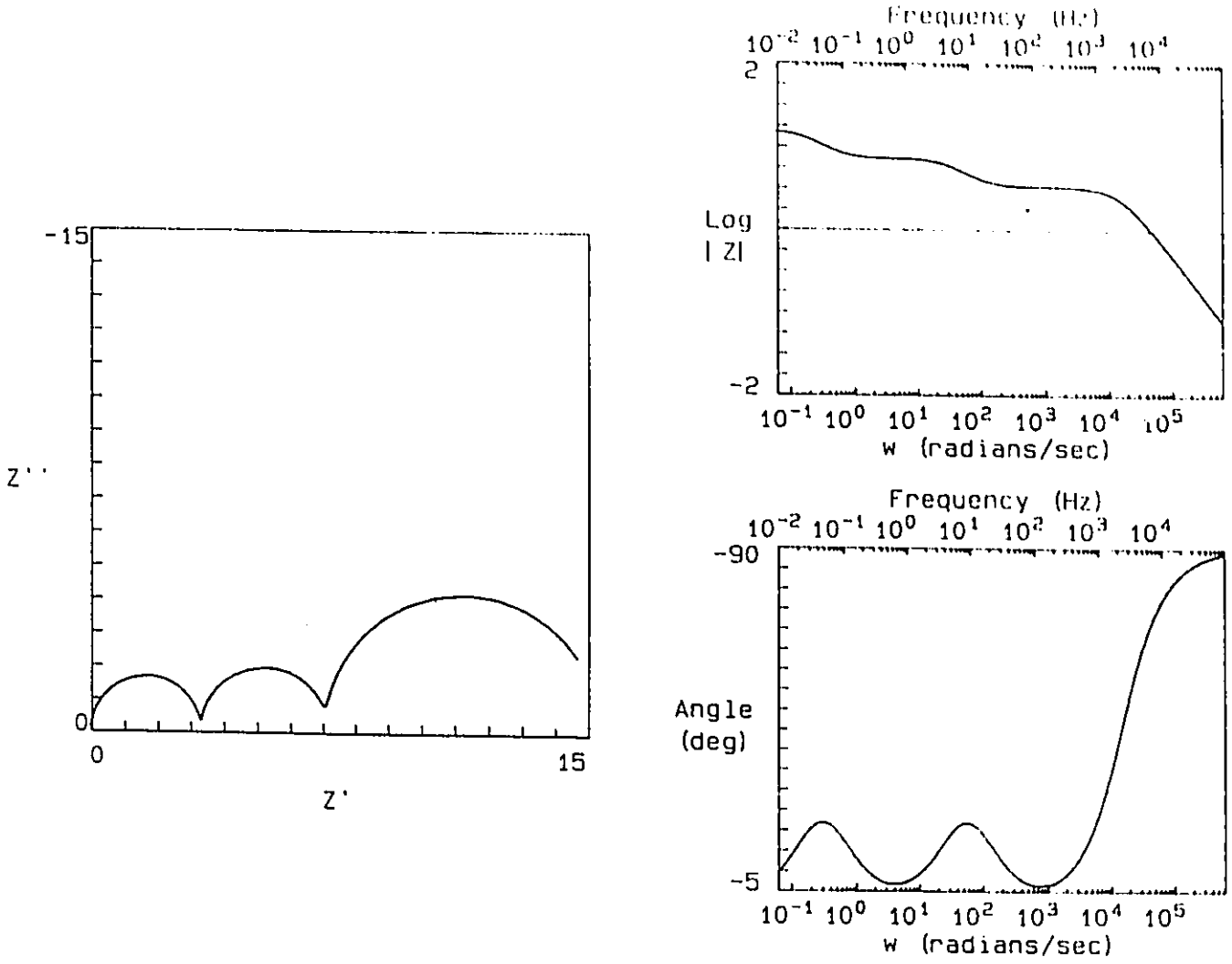

Fig. 56. Simulation of impedance behaviour of equivalent circuit B (Fig. 54b) under conditions B_1, (Table 10)

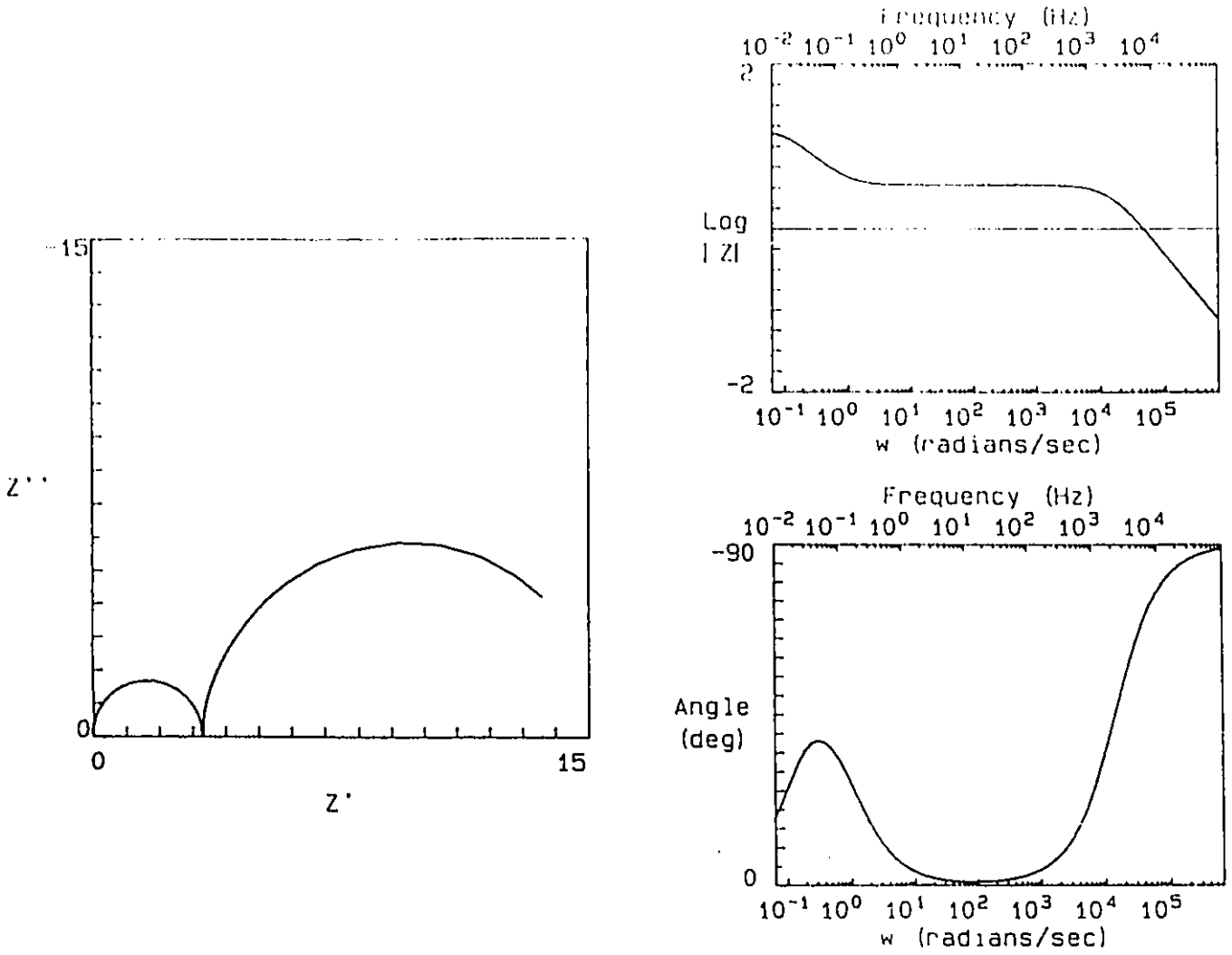

Fig. 57. Simulation of impedance behaviour of equivalent circuit A (Fig. 54a) under conditions A_{2s} (Table 10)

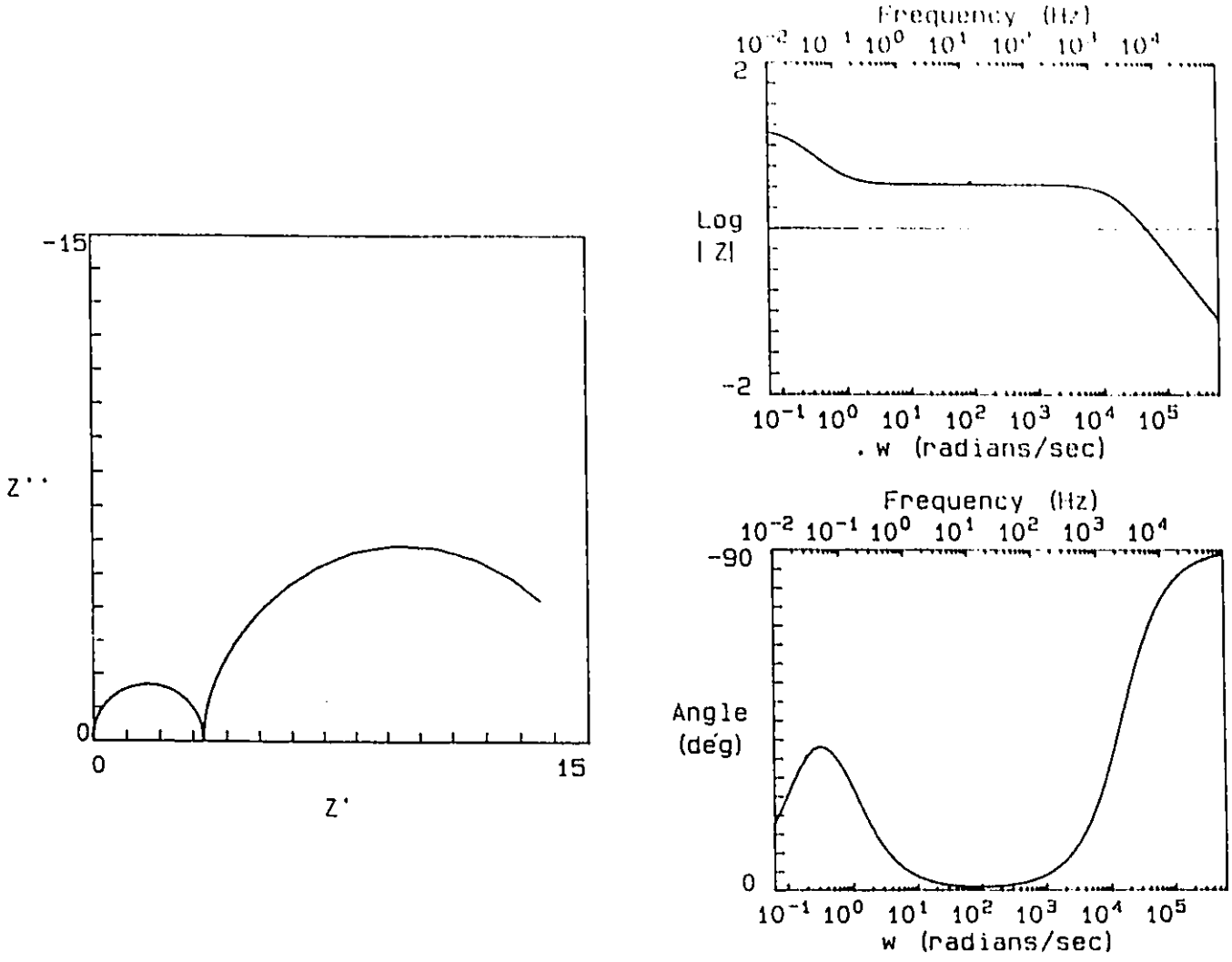

Fig. 58. Simulation of impedance behaviour of equivalent circuit A (Fig. 54a) under conditions A_{3_1} (Table 10)

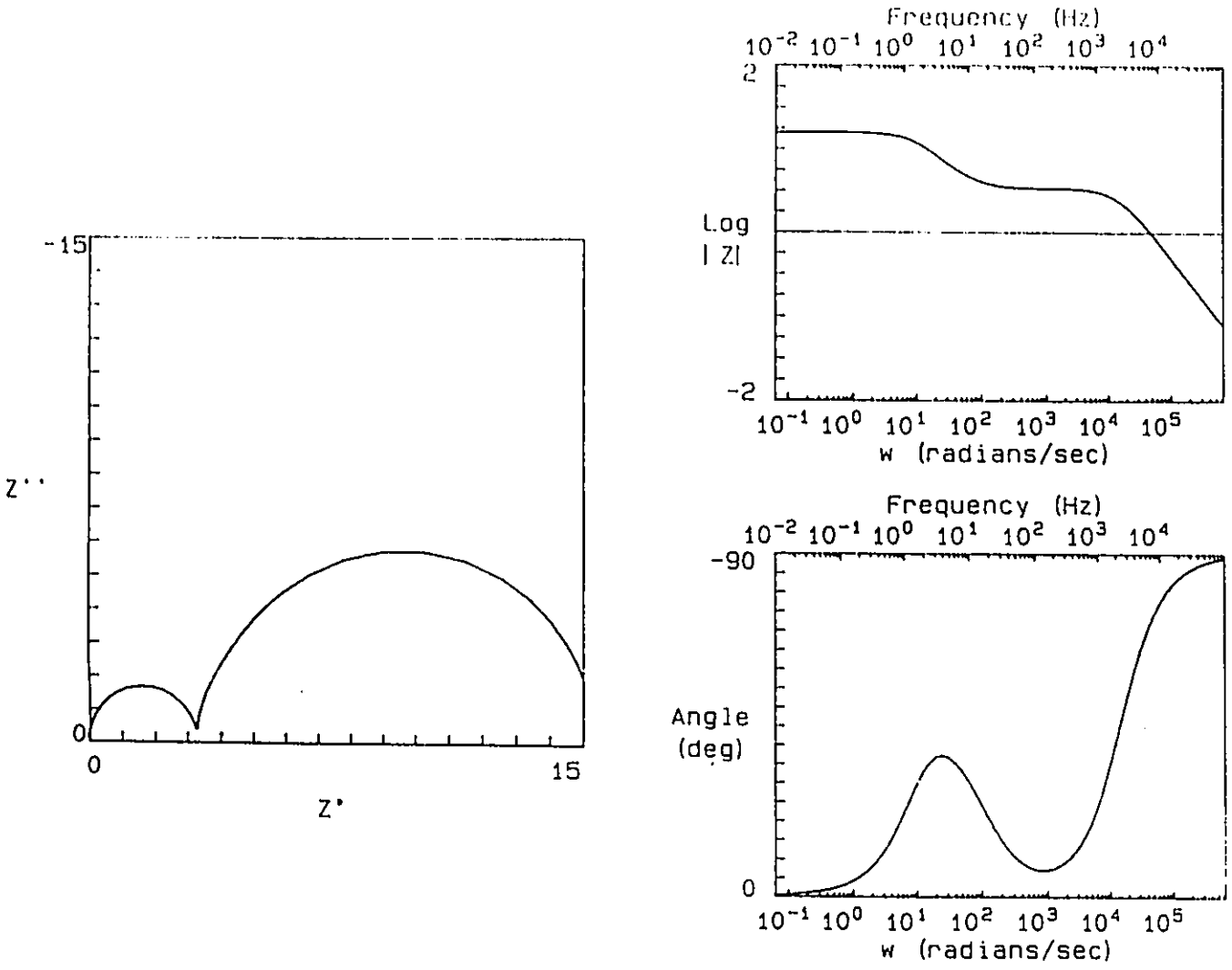

Fig. 59. Simulation of impedance behaviour of equivalent circuit B (Fig. 54b) under conditions B_{2s} (Table 10)

the critical frequencies.

These simulation results therefore help to rationalize the relationship between the several types of complex-plane plots encountered experimentally and presented in Figs. 50, 51 and 52, in particular the origin of two semicircles under some conditions and three under others, depending on overpotential (hence the value of charge-transfer resistance) and/or presence of molecular Br_2 in solution which can change the applicable equivalent circuit, A or B, from that of Fig. 54a to that of Fig. 54b.

The low or zero frequency limit behaviour of circuit A components (assuming zero solution resistance in series) corresponds to the *parallel* combination of $R_1 + R_2$ in series, together with $R_3 + R_4$ also in series. The limiting ($\omega \rightarrow 0$) real component, Z', of the impedance is then given by:

$$\frac{1}{Z'} = \frac{1}{R_1 + R_2} + \frac{1}{R_3 + R_4}$$

$$= \frac{(R_3 + R_4) + (R_1 + R_2)}{(R_1 + R_2)(R_3 + R_4)}$$

$$= \frac{R_1R_3 + R_1R_4 + R_2R_3 + R_2R_4}{\sum_1^4 R} \qquad (94)$$

or

$$Z' = \sum_1^4 R/(R_1R_3 + R_1R_4 + R_2R_3 + R_2R_4) \qquad (95)$$

i.e. Z' is not determined in the zero-frequency limit, by ΣR or successive intercepts of the sums of individual R values (as for circuit B; see below) but by quotients involving products of the different R values, as seen from the equation above.

On the other hand, the zero-frequency limit behaviour for circuit B is seen directly, by inspection, to be:

$$Z' = R_1 + R_2 + R_3 \qquad (96)$$

from which is anticipated three semicircles with respective R intercepts on the Z' axis as frequency decreases, as is in fact indicated from Fig. 55. Here the respective intercepts are equal to the successive sums of the R values, with R_s again assumed to be negligible.

The overall frequency-response behaviour of the two circuits can be evaluated by computer simulation. The results are compared in the series of complex-plane, phase angle and Bode plots shown in Figs. 55—59 for selected and indicated values of the C and R components (Table 10).

It is clear from the simulation calculations, but not immediately obvious, that *both* equivalent circuits can give rise to *three* semicircles in the complex-plane Z" vs Z' plots, as seen from the Figs. 55 and 56. This is an interesting result but not an altogether fortunate one from the point of view of distinguishing the possible mechanisms involving mono-, and tribromide species.

It is to be noted, however, that intuitively, in relation to the physical situation at the electrode, there is a difference to be anticipated between the behaviour of the electrode and the reactions at it when Br_2 has already been formed there and the case of a fresh electrode in a fresh solution where no Br_2 has yet been formed. This is really the essence of the difference between the two representations in circuits A and B of the reaction step sequences.

5.5.3. Role of Diffusion Effects

When diffusional effects are significant they can also be distinguished by the linear relations that then arise between Z' and Z" for various (usually low) frequencies with a phase-angle of 45°, arising from the so-called Warburg impedance component (see section 4.4 and below).

Fig. 60 shows such a plot for the bromine reaction at a low overpotential exhibiting a low-frequency linear tail at ca. 45° to the Z' axis, typical for a process coupled with diffusion which gives rise to a diffusion Warburg impedance, Z_w; however, in the low frequency region, the relation of Z" to Z' departs somewhat from the expected 45° slope so that some participation of an adsorption effect may also be indicated. Note that the behaviour in Fig. 60 is for a low overpotential of only 10 mV. The result here is similar to that of Cooper and Parsons [52] referred to in chapter 1. Since a diffusion process was then indicated, it was of interest to examine the effect of electrode

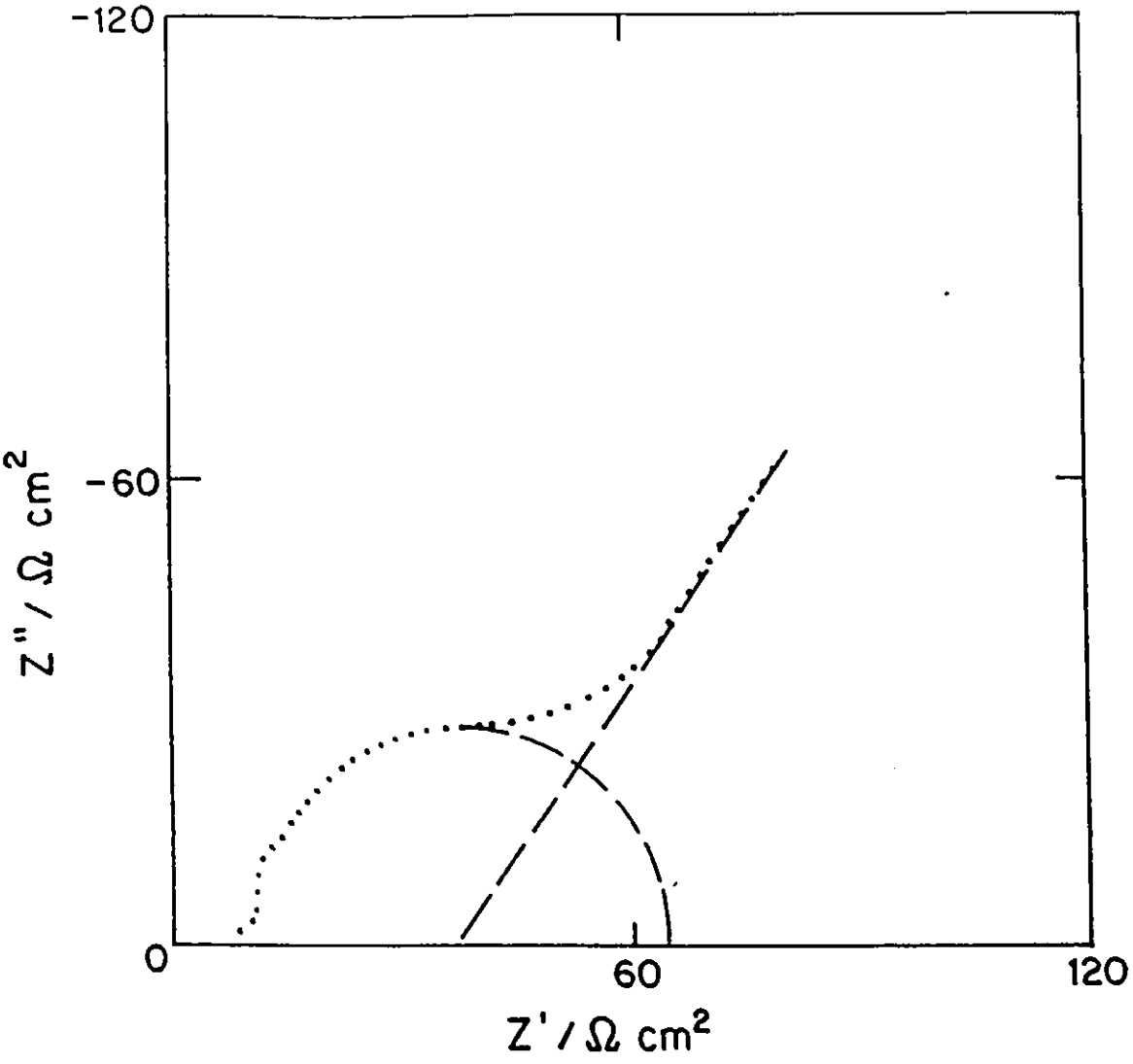

Fig. 60. Complex-plane a.c. impedance plot for the Br_2 reaction from 2.5 M NaBr/0.1 M $HClO_4$ at Pt showing a Warburg diffusion effect accompanied by adsorption at a polarization overpotential of 10 mV.

rotation on the complex-plane plot. This is shown in Fig. 61a for two, low rotation rates at the rotating Pt disc electrode. Up to 240 r.p.m. the two curves shown are almost superimposible and both exhibit long Warburg tails down to low ω's. However, upon increasing the rotation rate to 2400 r.p.m. (Fig. 61b) the tail is *not* observed but the low-frequency Faradaic resistance intercept is about the same as in Fig. 61a. This comparison clearly indicates that whatever diffusion effect is arising, it is eliminated from the frequency response by sufficient mass transport in the solution. Since the limiting currents observed in the d.c. Tafel polarization experiments were not associated with diffusion effects above a rotation rate of ca. 1200 rpm and did not exhibit the dependence on rotation rate characteristic of reactant diffusion, it seems that the effect observed in Figs. 61 a and b should be attributed to diffusion of Br_2 or Br_3^- away from the electrode surface rather than to Br^- diffusing to the electrode.

It is puzzling why diffusion effects are observed only at low overpotentials; thus, no Warburg low-frequency tails are observed for polarizations at higher overpotentials, e.g. 100, 150, 250 mV.

A further set of experiments on the role of diffusion effects related to the supposed role of electrogenerated Br_2, leading to formation of tribromide, species at or near the electrode surface, was conducted at a rotated disc Pt electrode. The effect of added Br_2 at the RDE was also examined. The

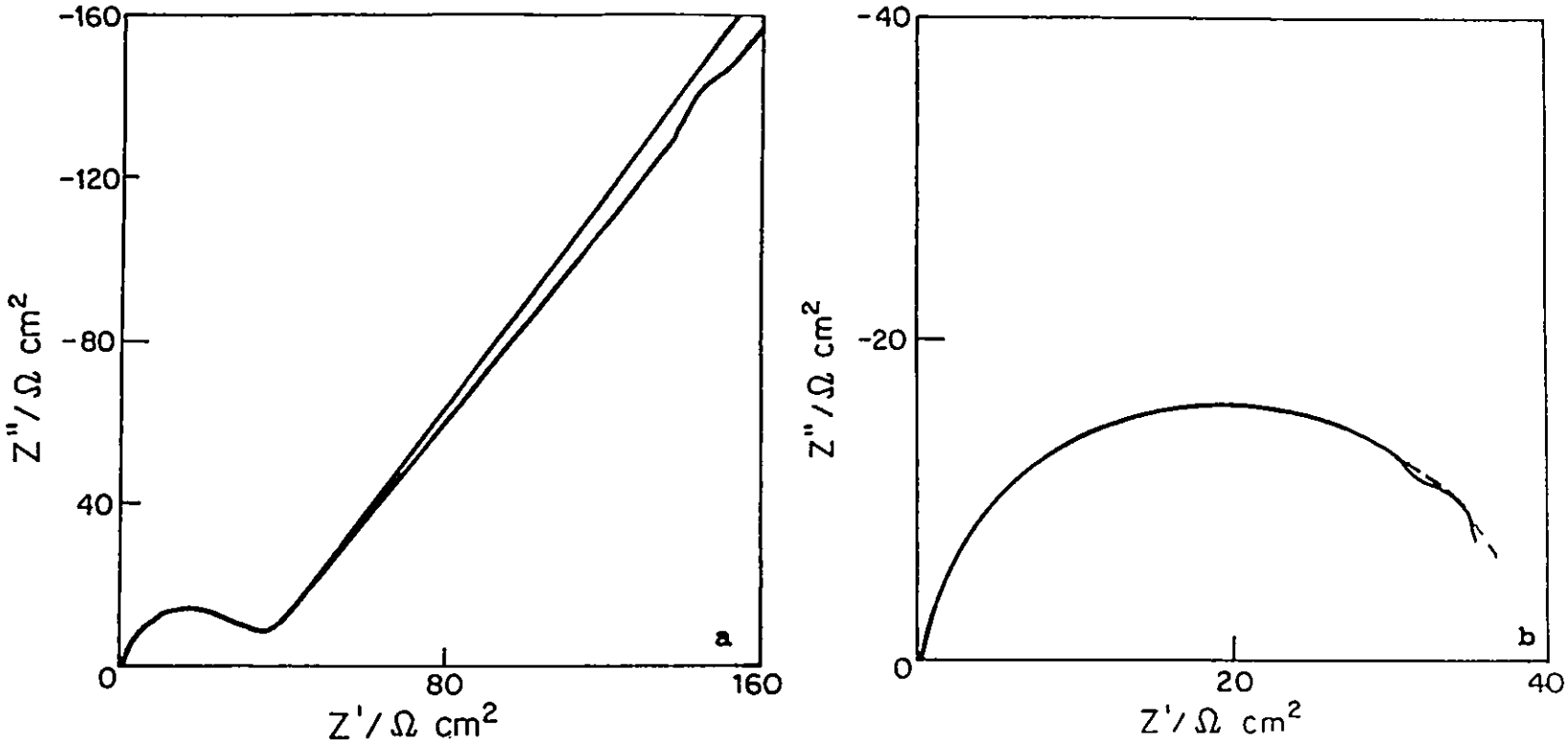

Fig. 61. Complex-plane a.c. impedance plots for the Br_2 reaction from 5 M NaBr/0.1 M $HClO_4$ at Pt RDE at a polarization overpotential of 10 mV showing a) Warburg diffusion effect accompanied by adsorption, for two, low rotation rates (the one above: 120 rpm, the one below: 240 rpm) and b) no Warburg diffusion effect for rotation rate 2400 rpm

electrode was polarized at 150, 200 or 250 mV.

Figs. 62—64 show the complex-plane plots, Z" vs Z', at such a Pt RDE for a rotation rate of 2400 rpm in 5 M NaBr/0.1 M $HClO_4$ (Because of irregularities arising from the mechanical rotation, the quality of these impedance plots is not at all so good as that for the stationary electrodes, shown earlier). It is important to note here that the third semicircle *does not appear* in this case, even for potentials up to 250 mV. This demonstrates, it is suggested, the effective absence of Br_2 or Br_3^- at the electrode as the rotation spins away the electro-generated molecular bromine from the surface of the electrode as soon as it is formed. Even for addition of 0.1 M Br_2 (Fig. 65) to a fresh Br^- solution at the rotated electrode, the third semicircle *does not* appear. However, the fact that two semicircles still arise, demonstrates that Br^- adsorption remains significant and arises in a way dependent on the polarization overpotential (Figs. 62—65), as found also for the stationary electrodes.

These results appear to confirm, at least qualitatively, the conclusions from the complex-plane plots and thus that involvement of tribromide species can be important in the kinetics and surface electrochemistry of the bromine reaction at Pt under certain conditions.

Comparatively, with the anodic Cl_2 reaction, it is to be noted that complex-plane plots of the impedance behaviour of the latter process show only *two* semicircles yet the reaction steps

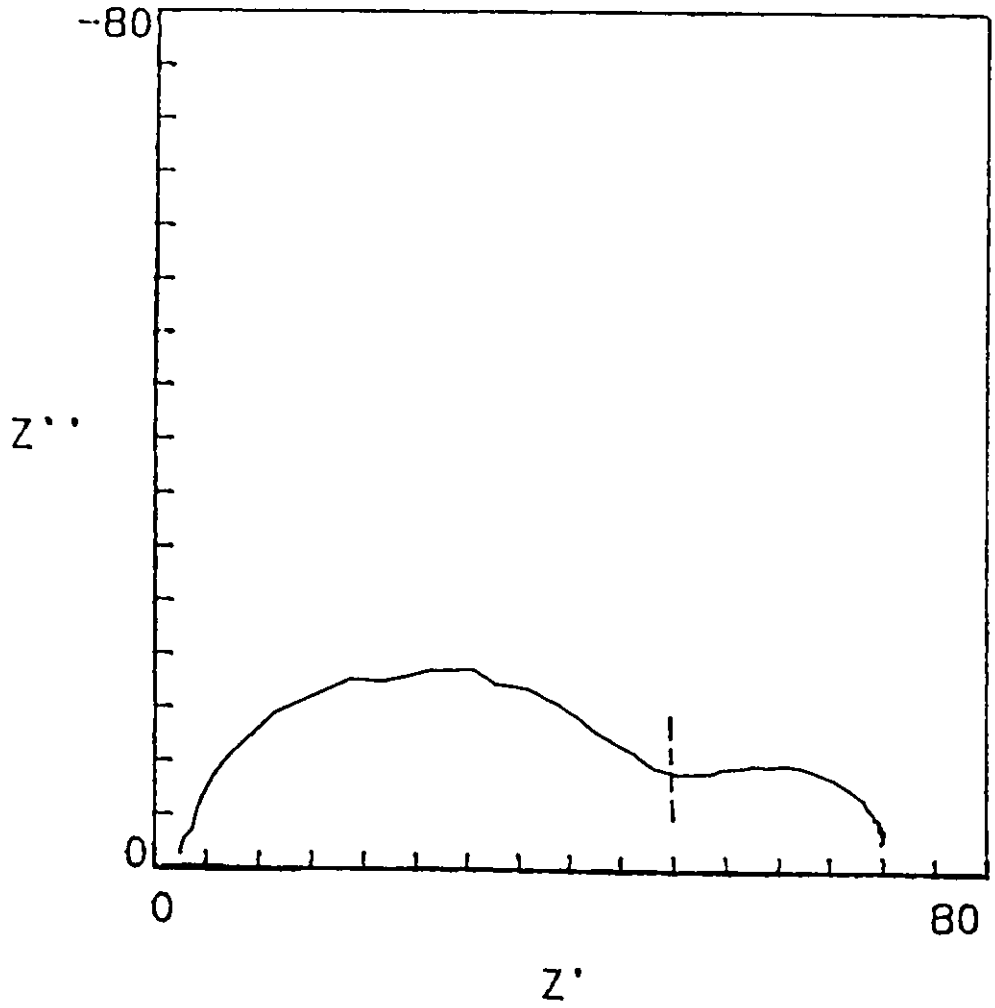

Fig. 62. Complex-plane a.c. impedance plot for Br_2 formation from 5 M fresh NaBr in 0.1 M $HClO_4$ at a polarization overpotential 150 mV at the Pt RDE (rotation rate: 2400 rpm).

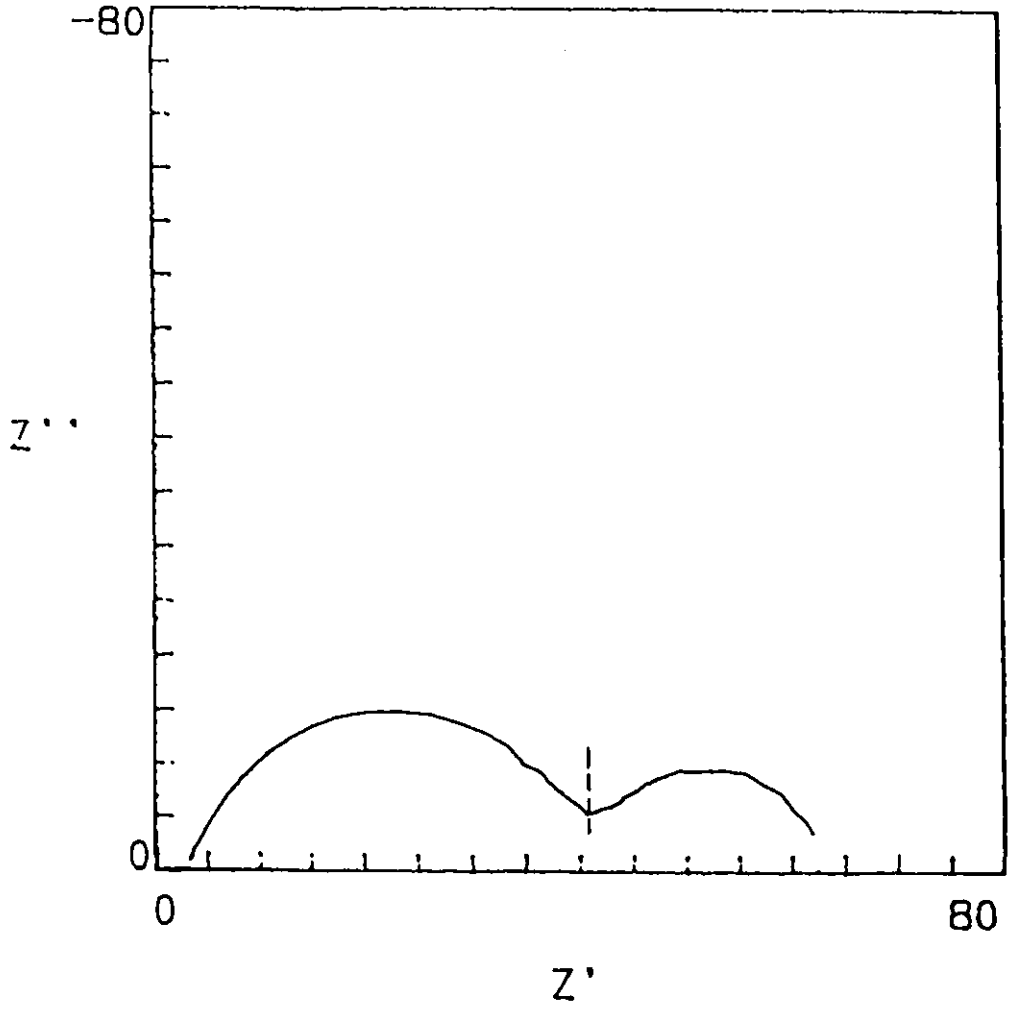

Fig. 63. Complex-plane a.c. impedance plot for Br_2 formation from 5 M fresh NaBr in 0.1 M $HClO_4$ at a polarization overpotential 200 mV at the Pt RDE (rotation rate: 2400 rpm).

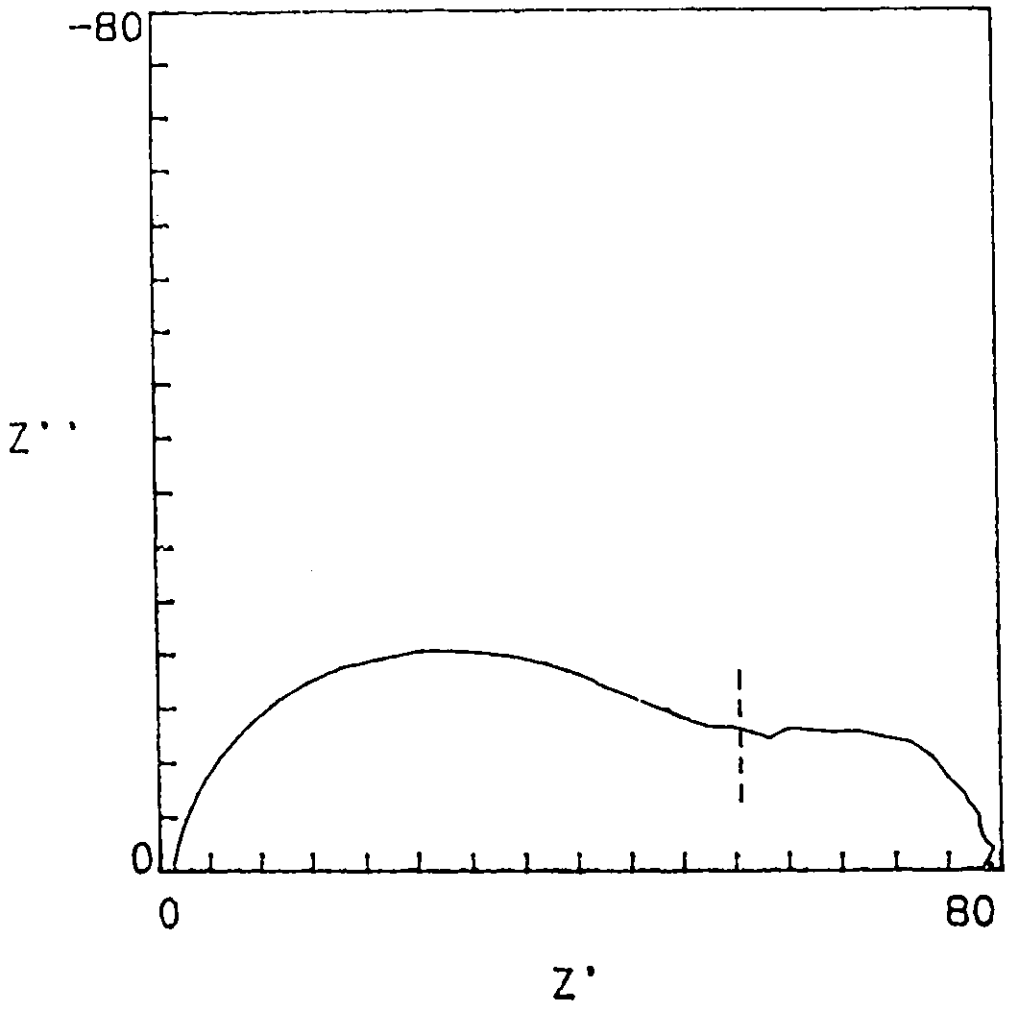

Fig. 64. Complex-plane a.c. impedance plot for Br_2 formation from a 5 M NaBr/0.1 M $HClO_4$ solution at a polarization overpotential 250 mV at the Pt RDE (Rotation rate: 2400 rpm).

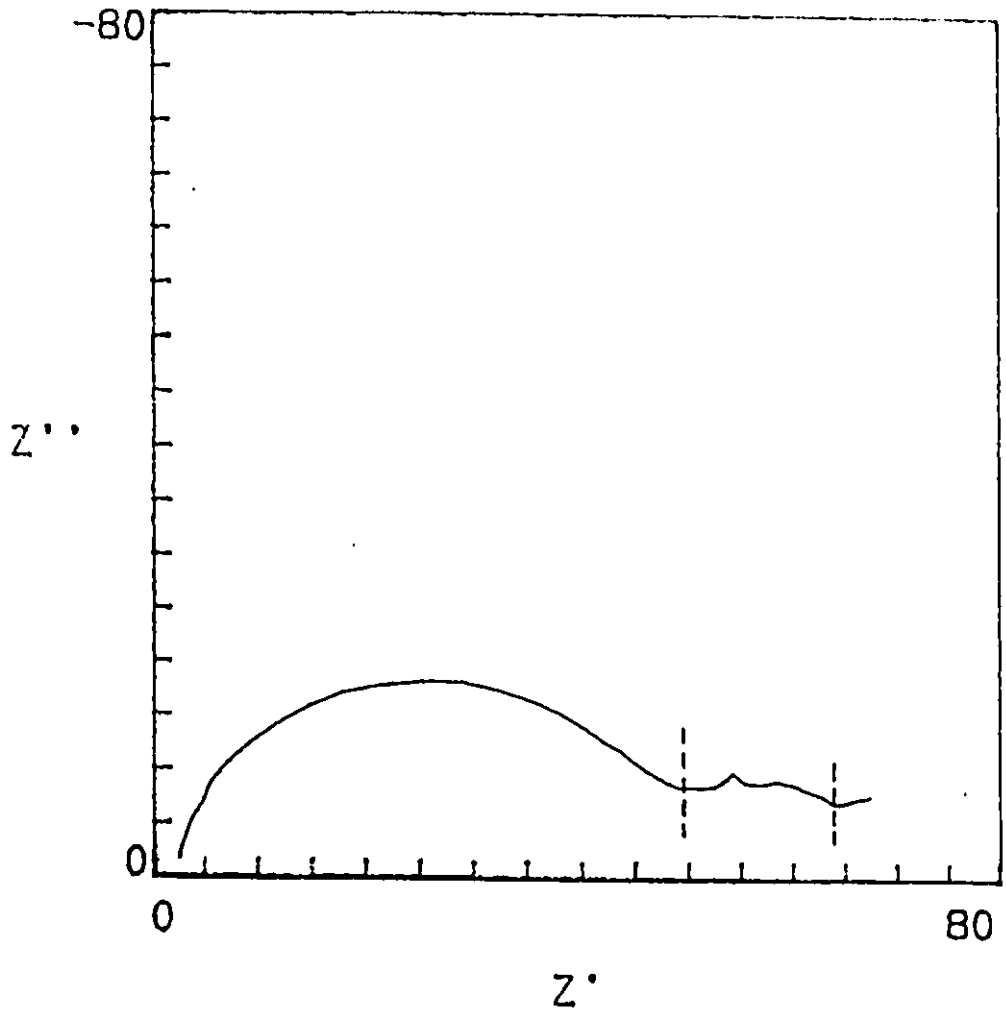

Fig. 65. Complex-plane a.c. impedance plot for Br_2 formation from a 5 M NaBr/0.1 M $HClO_4$ with addition of 0.1 M Br_2 at a polarization overpotential 150 mV at the Pt RDE (Rotation rate: 2400 rpm).

are formally similar to those of the Br_2 reaction but with the important exception that a corresponding Cl_3^- species is not involved under normal conditions. This comparison therefore gives significant indirect supporting evidence for the involvement of "Br_3" species in the case of Br_2 formation as argued from the nature of the impedance results for the latter case.

5.5.4. Simulation of the Impedance Behaviour Involving the Adsorbed Species at Preoxidized Pt Electrodes

Normally, it would be expected that as $i \rightarrow i_{lim}$, $\theta_{Br\cdot} \rightarrow 1$. Actually, the experimental $\theta_{Br\cdot}$ is ≤ 0.1 for experiments involving relatively long times of polarization. This can only be rationalized for the oxide-covered surface if recombination is taking place only on active centres or active areas on the oxide-covered surface that therefore represent a small fraction of the apparent overall available area of the electrode. On the "reduced" electrode, however, apparent $\theta_{Br\cdot}$ values do approach unity. In the presence of some co-deposited OH or O species, lower limits are attained depending on the co-coverage by the competitively formed oxide.

The a.c. results also reveal some important indirect information on the behaviour of the adsorbed species. Figs. 66—68 show the a.c. complex-plane plots, Z" vs Z', for the preoxidized Pt electrode polarized at 150 mV in 2.5 M NaBr/0.1 M $HClO_4$ solutions (Fig. 66—fresh Br^- solution, Fig. 67—used Br^-

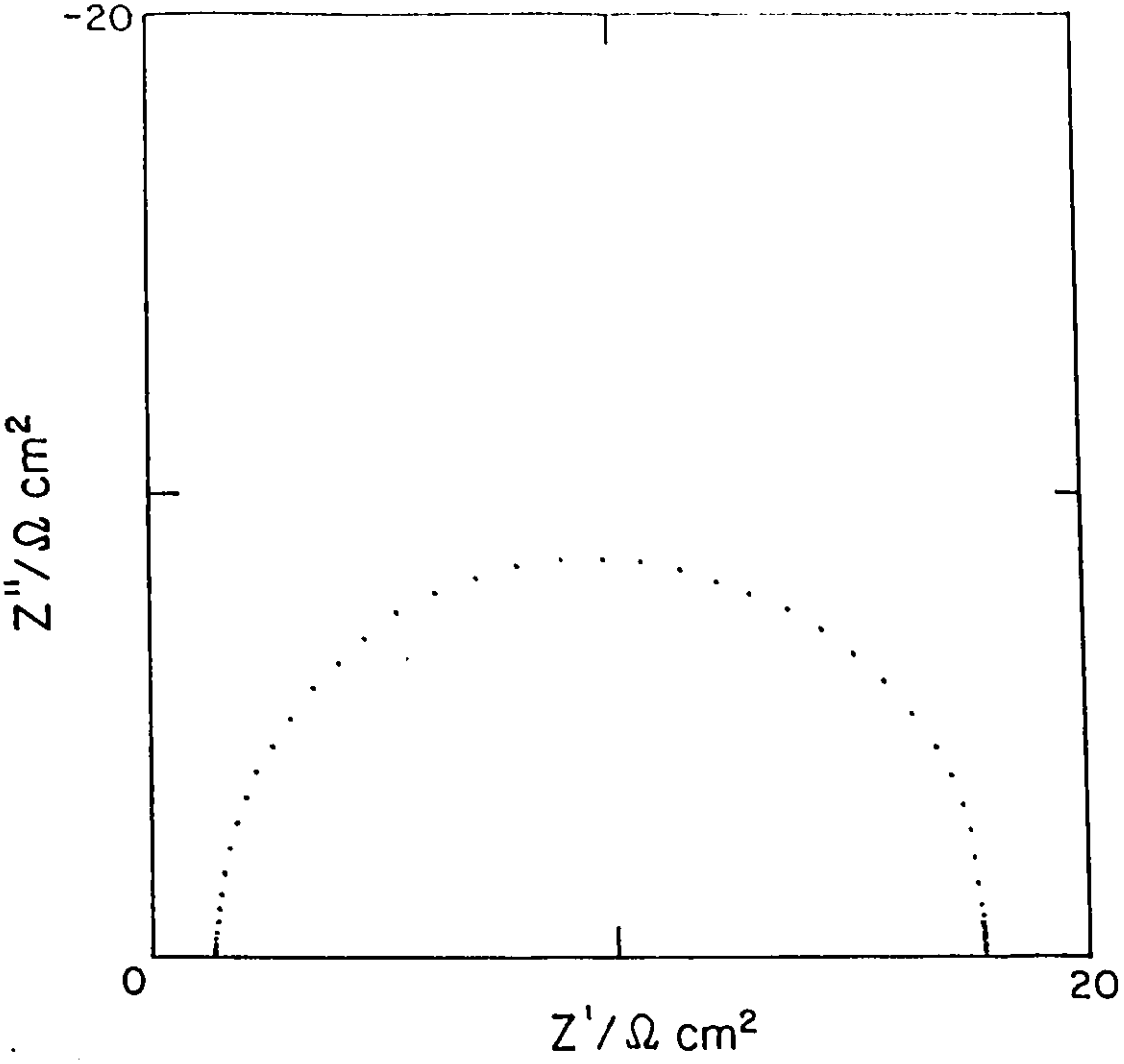

Fig. 66. Complex-plane a.c. impedance plot for Br_2 formation from a 2.5 M (fresh) NaBr in 0.1 M $HClO_4$ at a polarization overpotential 150 mV at the preoxidized Pt electrode.

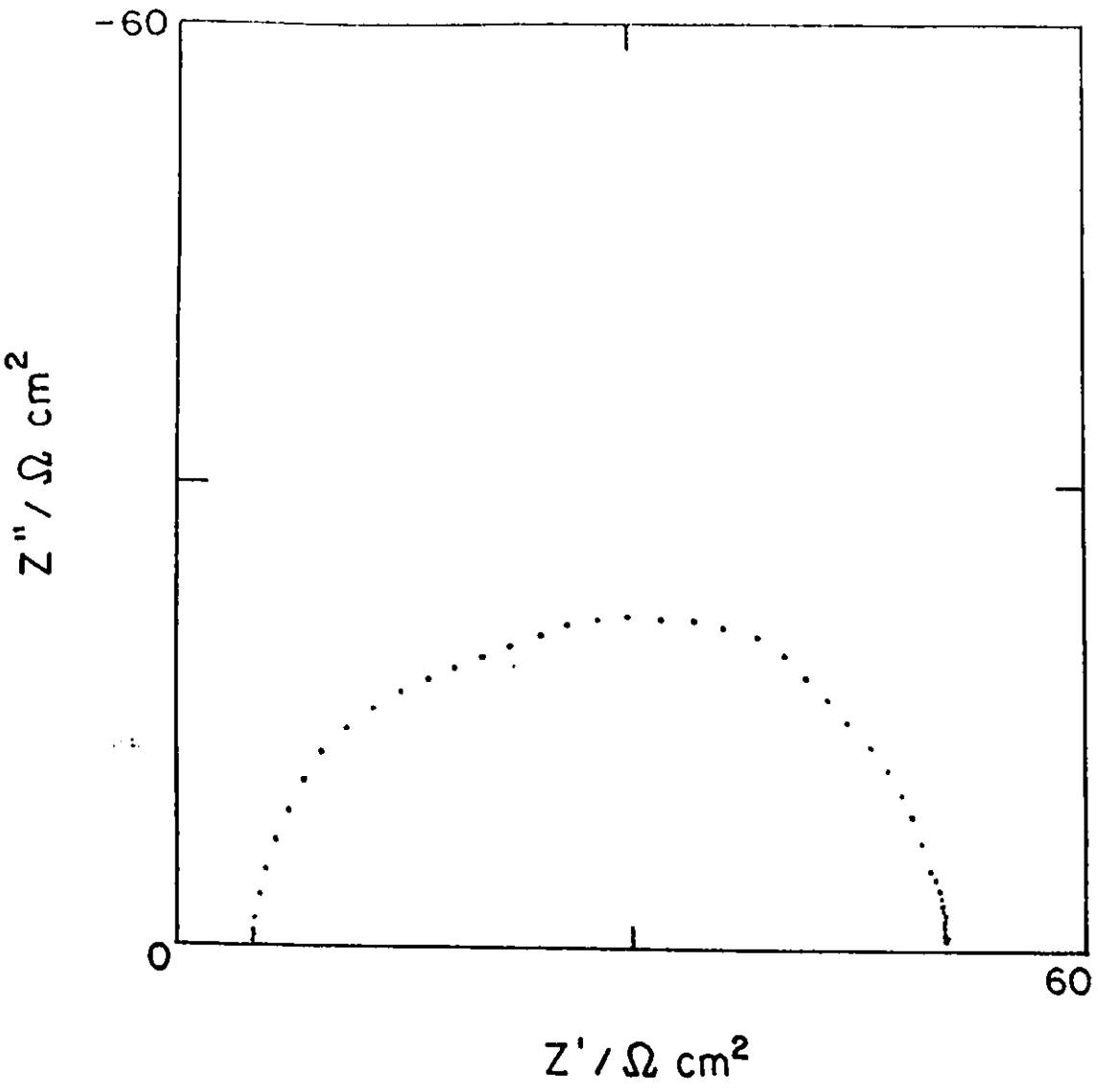

Fig. 67. Complex-plane a.c. impedance plot for Br_2 formation from a 2.5 M (used) NaBr in 0.1 M $HClO_4$ at a polarization overpotential 150 mV at the preoxidized Pt electrode.

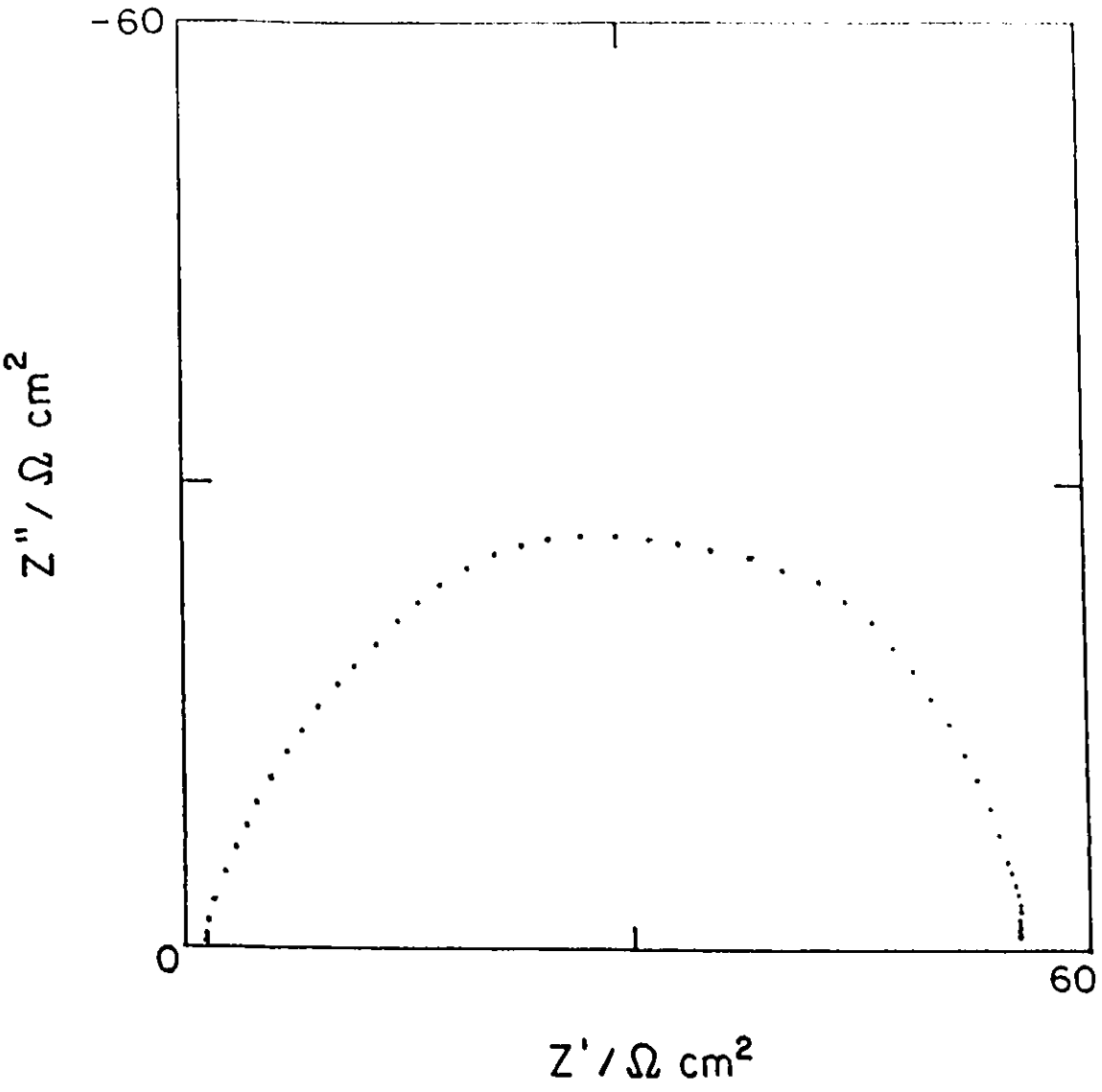

Fig. 68. Complex-plane a.c. impedance plot for Br_2 formation from a 2.5 M NaBr in 0.1 M $HClO_4$ at a polarization overpotential 150 mV at the preoxidized Pt electrode with addition of 0.05 M Br_2.

solution which contains Br_2, Fig. 68—Br_2 was added in 0.05 M Br^- solution). The Br_2 and/or Br_3^- inhibit(s) the reaction step I so that the reaction rate (current) is smaller for the solution with Br_2 initially than that for the fresh Br^- solution. Therefore, the faradaic resistance is increased in Fig. 67 and 68 (cf. Fig. 51 and 53) compared to Fig. 66 (cf. Fig. 52a) at the same polarization overpotential. Only single semicircles were observed at the preoxidized Pt electrodes (Figs. 66—68) indicating that no effects arise (second/third semicircles) due to chemisorption of Br^- or Br_3^- at significant coverages. This again reflects the situation that, at the preoxidized Pt, adsorptive affinities are already satisfied by bonding with OH/O species.

5.6. Conclusions

The study of the kinetics and mechanisms of the anodic bromine formation reaction has indicated the importance of adsorbed Br^- ion and, quantitatively, the role of the adsorbed Br^- intermediate. The latter is predominantly desorbed by the recombination mechanism in the kinetics. Also, it is shown that a tribromide adsorbed intermediate Br_3^- is involved, which explains the origin and significance of the third semicircle in the a.c. impedance complex-plane plots.

The adsorption of both bromide and tribromide, and corresponding intermediates, is shown to be of major

significance in the mechanism of the reaction as indicated by the cyclic voltammetry and the Tafel polarization behaviour, as well as by the potential decay measurements. Even in very dilute aqueous bromide solutions, Br^- adsorption begins significantly to block the otherwise distinguishable stages of surface oxidation at Pt anodes as observed in the cyclic voltammetry experiments, and thus to modify the Pt surface for electrocatalysis and adsorption in the Br_2 generation reaction itself.

The Tafel relations observed under various conditions are curved, with clear approaches towards limiting currents of the type well known to be characteristic of a "recombination-controlled" or a diffusion-limited overall reaction. This conclusion also applies to the results obtained at "pre-oxidized" Pt electrodes where Br^-/OH, O competitive adsorption cannot arise.

By means of experiments at the Pt rotated disc electrode, it is shown that these observed approaches to limiting currents as η is increased are *not* due to onset of diffusion limitation in Br^- transfer to the electrode. They are not due either to "iR" effects at high i values, as all such curved Tafel relations arise *after* "iR" corrections have been made.

In addition to above qualitative indications of "recombination control", the recombination-type (Volmer-Tafel) desorption step is shown to be the principal rate-determining pathway in the overall Br_2 formation reaction on the basis of

observed linearity of special, theoretically based kinetic test equations in $i^{½}$ or $i^{-½}$ for this mechanism, taking account of the potential dependence of coverage by the intermediate. However, it is shown that lack of a clear approach to a linear Tafel relation at low η's having a slope of RT/2F can be due to a) significant $Br^{\cdot}$ coverage already at/near the reversible potential and b) participation of the "back-reaction" at values of η < ca. 30 mV. Quantitative calculations support this interpretation.

The three-semicircle complex-plane plots in some of the a.c. impedance measurements are consistent with two alternative new equivalent circuits (Figs. 54 a and b) suggested in this work. In general, bromide and tribromide adsorption has been found to depend on the applied potential, the durations of the experiments (related to the extents of Br_2 formation), the concentration of the bromide solution, and whether an aqueous or nonaqueous supporting electrolyte is involved. In the beginning of the experiment, bromide adsorption and bromine formation are the two major steps. After more bromine has been formed, the appreciable formation of Br_3^- becomes possible, and then tribromide adsorption becomes significant in the reaction, and tribromide ion and $Br_3^{\cdot}$ become involved significantly in the overall mechanism.

In more concentrated solutions, the adsorption becomes more extensive due to the higher Br^- activity and the reciprocal decrease of water activity but some complications arise in the experimental measurements at lower polarizations. Above ca. 10^{-2}

M and certainly above 0.1 M in Br^-, the Br_2 formation reaction proceeds virtually on an oxide-free surface, so electrocatalysis in the reaction is determined by the underlying oxide-free Pt surface, but one covered extensively by adsorbed Br^- ion, in a partially "charge-transferred" state. The third (low frequency) semicircles become observable in the impedance complex-plane plots when relatively high Br^- concentrations, around 2.5 M (aqueous), are used and Br_2 has been generated significantly during the course of the polarization e.g. during the impedance experiments. When the bromide concentration is taken, however, to 5 M, only two semicircles and/or diffusion (accompanied by bromine adsorption) are found in the experiments at the Pt RDE.

By means of a special extrapolation procedure [67], the potential decay method allows the "true" $\eta_{i=0}$ values to be determined which thereby enables better iR corrections to be made so that the results are more reliable for the purpose of evaluation of the true polarization, free of "iR" error, at various current densities. This extrapolation also allows the derivative, $d\eta/dt$, at $t = 0$ to be reliably determined for the purpose of evaluation of the double-layer capacitance.

In summary, the principal conclusions are:

1) The kinetics of anodic bromine formation reaction are affected in substantial ways by bromide and tribromide adsorption, the differences in behaviour at various bromide concentrations being attributable to the interaction of the bromide and/or tribromide with the Pt electrode surface.

2) As expected, the extent of the Br^- adsorption is related to the bromide ion concentration.

3) The extents of adsorption of $Br^\cdot$ as the principal intermediate in the overall reaction can be evaluated from the potential decay measurements, as a function of overpotential.

4) The $Br^\cdot$ intermediate is desorbed as Br_2 principally by the mechanism of catalytic recombination of $Br^\cdot$ or $Br_3^\cdot$ species.

5) That mechanism is quantitatively proven by the applicability of linear test plots of two kinetic test functions for recombination control, and qualitatively by the observation of approaches to non-diffusion-controlled limiting currents in the already "iR" corrected Tafel plots. Additionally, near the reversible potential, at low η values, Tafel slopes approach the value of RT/2F characteristic of "recombination controlled" kinetics.

6) In a.c. impedance measurements, when the polarization overpotential is decreased, a diffusion process becomes rate-controlling, especially at high bromide concentrations, without rotation of the Pt RDE.

7) As a result of formation of the Br_3^- complex ion, bromine is soluble in bromide electrolytes having sufficiently high concentrations, and such Br_3^- ions can then be involved in the mechanisms.

8) Relations to, and differences from, the analogous Cl_2 evolution reaction are noted; two principal differences are:

a) substantially stronger adsorption of Br^- than Cl^- at Pt, and with greater extent of partial charge-transfer and b) much greater role of the trihalide species (here Br^- and Br_3^-) than in the chloride case.

CONTRIBUTIONS TO ORIGINAL RESEARCH

The electrochemical adsorption behaviour of the bromide anion and the adsorbed Br^- intermediate has been extensively examined in relation to the kinetics and mechanisms of the Br_2 formation reaction at Pt.

The present work demonstrates the importance of a competitive bromide-adsorption blocking effect on the process of formation of surface oxide at Pt, as found using cyclic voltammetry. Thus the effective "electrocatalytic surface" on which Br_2 is formed is shown to depend on the Br^- concentration.

At practical concentrations of reactant Br^-, greater than ca. 0.1 M, the discharge of bromide ion and the process of bromine formation occurs on an almost completely oxide-free surface. However, under such conditions, the surface is covered substantially by chemisorbed bromide ions in an appreciably charge-transferred state.

The reactant Br^- ion is shown to be adsorbed according to almost "Langmuir" behaviour with an extent of partial charge

transfer of ca. 0.9 e, in contrast to the behaviour known for Cl^- at Pt. The chemisorption is strong enough to prevent any measurable co-deposition of OH/O species at Pt above a Br^- concentration of ca. 10^{-2} M.

A new treatment for the kinetics of discharge of an anion already chemisorbed with appreciable charge transfer is given and applied to the case of Br^- discharge in the Br_2-formation reaction.

The kinetics of anodic formation of Br_2 at the platinum electrode has been studied by Tafel measurements, using a rotating Pt electrode to eliminate or minimize diffusion effects, especially involving anodically formed Br_2 transported away from the electrode.

In this and other aspects of the experimental work a digital oscilloscope, main-frame and personal computers, and a plotter have been used for the data acquisition and plotting of graphs, using mainly software developed "in house" for the special purposes of the work, an original contribution arising in this project.

The approaches to limiting currents observed in the Tafel relations are shown to arise neither on account of Br^- diffusion and nor because of uncompensated "iR" drop effects. They therefore are associated kinetically with $Br^{\cdot}$ recombination control as the preferred pathway and rate-controlling step in the overall Br_2 formation process. This is an important conclusion from the results.

The role of such a recombination mechanism has been tested and confirmed by application of two special test-plot procedures which show that the principal pathway for desorption of $Br^{\cdot}$, and resulting Br_2 formation, is the $Br^{\cdot}$ + $Br^{\cdot}$ recombination step. This rate-limiting step is shown to apply to both "reduced" (oxide-free) and "preoxidized" Pt anode surfaces but, at the latter, $Br^{\cdot}$ coverage is smaller. The applicability of the recombination mechanism is also consistent with the approach to a Tafel slope of 29 mV near the reversible potential which is revealed after corrections for the back-reaction current component are properly made.

It is shown that results from complementary a.c. impedance measurements can be represented by two-, and three-semicircle complex-plane plots; the latter demonstrate the role of the stable tribromide ion in the Br_2 formation reaction and the adsorption of both bromide and tribromide species at the electrode.

Two new equivalent circuits are proposed for the simulation of the impedance behaviour in the case of tribromide adsorption, and their properties are comparatively examined. They are shown to satisfactorily represent the experimental results obtained by the a.c. impedance method, including the observation of either two or three semicircles in the complex-plane plots. The role of diffusion of electrogenerated molecular Br_2 from the electrode into solution has also been considered and experimentally examined by means of impedance measurements conducted

comparatively at rotated and stationary Pt electrodes.

The most probable reaction steps for formation of bromine and tribromide, adsorption of bromide and tribromide, etc. are suggested and followed by an electrochemical kinetic and thermodynamic analysis of the data in relation to the experimental results.

REFERENCES

1. B. E. Conway and J. O'M. Bockris, *J. Chem. Phys.*, **26**, 532 (1957).
2. A. J. Bard, Ed., "Electroanalytical Chemistry", (1966-).
3. J. V. Zee and R. E. White, *J. Electrochem. Soc.*, **130**, 2003 (1983).
4. S. L. Chiu, J. R. Selman, *AICHE Symp. Ser.* **83**, 15 (1987).
5. K. Tange, T. Sasaki, K. Kawahara, *Jpn. Kokai Tokyo Koho JP*, **Aug. 15**, 63 (1988).
6. E. Gileadi, E. Kirowa-Eisner and J. Penciner, "Interfacial Electrochemistry", Addison-Wesley Publishing Company, Inc., (1975).
7. W. L. Hsie, M. L. Gopikanth and J. R. Selman, *Electrochim Acta*, **30**, 1371 (1985).
8. J. A. Boon, J. S. Wilkes and J. A. Lanning, *J. Electrochem. Soc.*, **138**, 465 (1991).
9. S. Dallek and R. T. Foley, *J. Electrochem. Soc.*, **123**, 1775

(1976).

10. K. Schwabe, C. Voigt, *Electrochimica Acta*, **14**, 853 (1969).
11. D. M. Novak, B. V. Tilak, B. E. Conway in "Modern Aspects of Electrochemistry", Eds.: J. O'M. Bockris, B. E. Conway, R. E. White, No. 14, (1982).
12. B. E. Conway and D. M. Novak, *J. Electroanalytical Chemistry*, **99**, 133 (1979).
13. R. Woods, *Electroanalytical Chemistry*, **9**, 1 (1976).
14. L. Gierst, "Trans. Symp. Electrode Proc.", Philadelphia, (1959).
15. G. Gouy, *J. Phys.*, **9**, 457 (1910).
16. D.L. Chapman, *Phil. Mag.*, **25**, 475 (1913).
17. O. Stern, *Z. Electrochem.*, **30**, 508 (1924).
18. A. N. Frumkin, *Z. Physik*, **35**, 792 (1926).
19. J. A. V. Butler, *Proc. Roy. Soc.* London, **A122**, 399 (1929).
20. J. E. B. Randles, *Disc. Faraday Soc.*, **1**, 11 (1947).
21. A. Slygin and A. Frumkin, *Acta Physicochim.*, USSR, 3, 791 (1934).
22. J. Lawrence, R. Parsons and R. Payne, *J. Electroanalytical Chemistry*, **16**, 193 (1968).
23. M. W. Breiter, *Electrochimica Acta*, **8**, 925 (1963).
24. V. S. Bagotskii, *Electrokhimiya*, **5**, 1037 (1967).
25. M. W. Breiter, *J. Electrochem. Soc.*, **109**, 549 (1962).
26. B. E. Conway and D. M. Novak, *Croatica Chemica Acta*, **53**, 183 (1980).
27. M. W. Breiter, *Electrochimica Acta*, **8**, 973 (1963).

28. P. Stonehart, *Electrochimica Acta*, **15**, 1853 (1970).

29. A. N. Frumkin, N. A. Balashova and V. E. Kazarinov in the Electrochemical Society Symposium on Electrode Processes of the Theoretical Division, (1966).

30. A. N. Frumkin, V. Sobol and A. Dmitrieva, *J. Electroanalytical Chemistry*, **13**, 179 (1967).

31. V. S. Bagotskii, Y. B. Vasilyév, J. Weber, J. N. Pirtskhalava and B. Knots, *J. Electroanalytical Chemistry*, **27**, 31 (1970).

32. A. Frumkin, *Electrochimica Acta*, **5**, 266 (1961).

33. J. Sobkowski and A. Wieckowski, *J. Electroanalytical Chemistry*, **41**, 373 (1973).

34. D. C. Grahame, M. A. Poth and J. I. Cummings, *J. Am. Chem. Soc.*, **74**, 4422 (1952).

35. M. A. V. Devanathan and P. Peries, *Trans. Faraday Soc.*, **50**, 1236 (1954).

36. D. C. Grahame, *Chem. Rev.*, **41**, 441 (1947).

37. S. Gottesfeld and B. E. Conway, *J. Chem. Soc. Faraday Trans. I*, **11**, 1973 (1974).

38. C. Franke, G. Piazza and D. M. Kolb, *Electrochimica Acta*, **34**, 67 (1989).

39. T. Takamura, K. Takamura and E. Yeager, *J. Electroanalytical Chemistry*, **29**, 279 (1971).

40. Y. C. Chiu and M. A. Genshaw, *J. Phys. Chem.*, **73**, 3571 (1969).

41. A. M. Barrett and R. Parsons, *Symp. Faraday Soc.*, **4**, 72

(1970).

42. S. Gottesfeld and B. Reichman, *J. Electroanalytical Chemistry*, **67**, 1793 (1976).

43. W. J. Anderson and W. H. Hanson, *J. Electroanalytical Chemistry*, **47**, 229 (1973).

44. B. E. Conway, "Theory and Principles of Electrode Processes", (1965).

45. T. Biegler, *J. Electroanalytical Chemistry*, **6**, 365 (1963).

46. R. Adžić, E. Yeager and B. D. Cahan, *J. Electroanalytical Chemistry*, **85**, 267 (1977).

47. T. Iwasita and M. C. Giordano, *Electrochimica Acta*, **14**, 1045 (1969).

48. I. M. Kolthoff and J. F. Coetzee, *J. Amer. Chem. Soc.*, **80**, 5346 (1958).

49. A. I. Popov and D. H. Geske, *J. Amer. Chem. Soc.*, **80**, 5346 (1958).

50. F. T. Chang, H. Wick, *Z. Phys. Chem.*, **A**, **172**, 448 (1935).

51. M. Loschkarew and O. Esin, *Acta Physicochim.*, USSR, **8**, 189 (1938)

52. W. D. Cooper and R. Parsons, *Trans. Faraday Society*, **66**, 1698 (1970).

53. J. E. B. Randles and D. R. Whitehouse, *Trans. Faraday Soc.*, **64**, 1376 (1968).

54. J. Llopis, J. Fernandez-Biange and M. Perez-Fernandez in "Transactions of the Symposium of Electrode Processes", Ed.: E. Yeager, (1961).

55. J. V. Nelson and R. T. Iwamoto, *J. Electroanalytical Chemistry*, **7**, 218 (1964).

56. H. A. Laitinen and I. M. Kolthoff, *J. Phys. Chem.*, **45**, 1079 (1941).

57. S. E. S. El Wakkad, S. E. Khalafalla and A. M. Shams El Din, *Rev. Trav. Chim.*, **76**, 789 (1957).

58. G. Dryhurst and P. J. Elving, *J. Electroanalytical Chemistry*, **12**, 416 (1966).

59. J. H. van der Meulen, *Chem. Weekblad*, **28**, 82 (1931).

60. T. Biegler and Woods, *J. Electroanalytical Chemistry*, **20**, 73 (1969).

61. M. W. Breiter, *J. Electroanalytical Chemistry*, **7**, 38 (1964).

62. G. J. Janz, A. E. Marcinkowsky and H. V. Venkatasetty, *Electrochimica Acta*, **8**, 867 (1963).

63. B. E. Conway and P. Gu, *J. Chem. Soc. Faraday Trans.*, **86**, 923 (1990).

64. M. I. Temkin, *Zh. Fiz. Khim*, **15**, 246 (1941).

65. B. E. Conway, L. Bai and D. F. Tessier, *J. Electroanalytical Chemistry*, **161**, 39 (1984).

66. B. E. Conway and M. Dzieciuch, *Can. J. Chem.*, **41**, 38 (1963).

67. R. D. Armstrong and H. R. Thirsk, *Electrochim. Acta*, **17**, 171 (1972).

68. P. Gu, Ph.D. Thesis, (1990).

69. B. Timmer, M. Sluyters-Rebback and J. H. Sluyters, *J.*

Electroanalytical Chemistry, **18**, 93 (1968).

70. R. D. Armstrong and M. Henderson, *J. Electroanal. Chem. Interfacial Electrochem.*, **39(1)**, 81 (1972).

71. D. A. Harrington and B. E. Conway, *J. Electroanal. Chem.*, **221**, 1 (1987).

72. M. A. V. Devanathan, J. O'M. Bockris and K. Müller, *Proc. Roy. Soc.*, London, **A274**, 55 (1963).

73. S. Trasatti, in: "Electrolysis", Eds.: W. E. O'Grady, P. N. Ross and F. G. Will, The Electrochemical Society, Pennington, N.J. (1982)

74. R. Parsons, *Trans. Faraday Soc.*, **47**, 1332 (1951).

75. R. Parsons and F. R. G. Zobel, *J. Electroanal. Chem.*, **9**, 333 (1965)

76. B. E. Conway and L. Bai, *J. Chem. Soc. Faraday Trans. I*, **81 (8)**, 184 (1985).

77. B. E. Conway and B. V. Tilak, "Advances in Catalysis", Vol. 38, 1991.

78. H. Angerstein-Kozlowska, B. E. Conway and W. B. A. Sharp, *J. Electroanalytical Chemistry*, **43**, 9 (1973).

79. V. I. Birss, H. Elzanowska and S. Gottsfeld, *J. Electroanal. Chem. Interfacial Electrochem.*, **318**, 327 (1991)

80. V. I. Birss and J. Segal, *Proc. Electrochem. Soc.*, 9 (1992)

81. S. Shibata, *Electrochimica Acta*, **22**, 175 (1977).

82. A. K. Vijh and B. E. Conway, *Anal. Chem.*, **224**, 160 (1967).

83. D. Gilroy and B. E. Conway, *Can. J. Chem.*, **46**, 875 (1968).

84. R. F. Lane and A. T. Hubbard, *J. Phys. Chem.*, **79**, 808 (1975).

85. T. W. G. Solomons, "Organic Chemistry", (1983).

86. J. Llopis and M. Vàzques, *Electrochimica Acta*, **6**, 167 (1962).

87. I. Langmuir, *J. Amer. Chem. Soc.*, **38**, 2221 (1916).

88. B. E. Conway and D. M. Novak, *J. Chem. Soc. Faraday Trans I*, **75**, 244 (1979).

89. M. Enyo, "Comprehensive Treatise of Electrochemistry", Vol. 7, Eds.: B. E. Conway, J. O'M. Bockris, B. E. Yeager, S. U. M. Kahn and R. E. White, Plenum Press, N.Y. (1983).

90. T. Yokoyama and M. Enyo, *J. Electroanalytical Chemistry*, **136**, 185 (1982).

91. H. B. Morley and F. E. W. Wetmore, *Can. J. Chem.*, **34**, 359 (1956).

92. T. Anderson and H. Eyring, *J. Phys. Chem.*, **67**, 92 (1963).

93. P. D. Lukovstev and V. I. Temerin, *Tr. Akad. Nauk.* USSR., Otd. Khim. Nauk, 494 (1953).

94. B. E. Conway and P. L. Bourgault, *Can. J. Chem.*, **37**, 292 (1959).

95. A. N. Frumkin, P. Dolin and B. V. Ershler, *Acta Physicochim.* U.S.S.R., **13**, 779 (1940).

96. D. Barclay, *J. Electroanal. Chem.*, **19**, 318 (1968).

97. B. E. Conway, *Chemical Society Reviews*, 253 (1992).

98. B. E. Conway, "Ionic Hydration in Chemistry and Biophysics", Chapter 30, Elsevier Publ. Co., Armsterdam-

Oxford-New York, (1981).

99. J. O. Edwards, *J. Amer. Chem. Soc.*, **76**, 1540 (1954).

100. D. M. Novak and B. E. Conway, *J. Chem. Soc., Faraday Trans., I*, **77**, 2341 (1981).